Characterization and inhibition of NADPH-producing enzymes from the pentose phosphate pathway of *Plasmodium* parasites

Inauguraldissertation

zur Erlangung des Grades

Doktor der Naturwissenschaften

— Dr. rer. nat. —

des Fachbereichs Biologie und Chemie, FB08
der Justus-Liebig-Universität Gießen

vorgelegt von

Kristina Maria Elisabeth Häußler

geboren in Roth

Gießen, Oktober 2018

Die vorliegende Arbeit wurde von März 2015 bis Oktober 2018 an der Professur für Biochemie und Molekularbiologie, Interdisziplinäres Forschungszentrum der Justus-Liebig-Universität Gießen unter Leitung von Prof. Dr. Katja Becker angefertigt. Teile der experimentellen Arbeiten wurden an der University of California San Diego, San Diego, CA, USA und dem Sanford Burnham Prebys Medical Discovery Institute, La Jolla, CA, USA durchgeführt.

Erstgutachterin

Prof. Dr. Katja Becker, Professur für Biochemie und Molekularbiologie, Interdisziplinäres Forschungszentrum, Justus-Liebig-Universität Gießen, Heinrich-Buff-Ring 26-32, 35392 Gießen

Zweitgutachterin

Prof. Dr. Gabriele Klug, Institut für Mikrobiologie und Molekularbiologie, Interdisziplinäres Forschungszentrum, Justus-Liebig-Universität Gießen, Heinrich-Buff-Ring 26-32, 35392 Gießen

Weitere Mitglieder des Prüfungskomitees

Prof. Dr. Christoph Grevelding, Institut für Parasitologie, Biomedizinisches Forschungszentrum Seltersberg, Justus-Liebig-Universität Gießen, Schubertstraße 81, 35392 Gießen

Prof. Dr. Jörg Fahrer, Rudolf-Buchheim-Institut für Pharmakologie, Biomedizinisches Forschungszentrum Seltersberg, Justus-Liebig-Universität Gießen, Schubertstraße 81, 35392 Gießen

Summary

With around half a million deaths per year, malaria is still one of the world's most deadly infectious diseases, mainly caused by two species of *Plasmodium* parasites, *P. falciparum* (*Pf*) and *P. vivax* (*Pv*). Currently, there are antimalarial drugs available; however, increasing resistance of *Plasmodium* strains hampers the fight against the disease. Therefore, new antimalarial drugs urgently need to be developed. During their life cycle, *Plasmodium* parasites are continuously exposed to oxidative stress from different sources. Antioxidative systems that highly depend on the electron donor nicotinamide adenine dinucleotide phosphate (NADPH) are employed to maintain the redox balance. One strategy of new antimalarial drugs is to create a fatal dosage of oxidative stress by disturbing cellular redox homeostasis. For *Plasmodium* parasites, the oxidative pentose phosphate pathway (PPP) is the main source of the critically important NADPH, generated by two enzymes: the bifunctional glucose 6-phosphate dehydrogenase 6-phosphogluconolactonase (GluPho) and the 6-phosphogluconate dehydrogenase (6PGD). *Pf*GluPho has already been shown to be essential for blood stage parasites; since this enzyme shares high similarities with the corresponding enzyme of *P. vivax*, *Pv*GluPho is considered a potential drug target as well. 6PGD contributes to the NADPH supply in the same amounts as GluPho and is already considered a drug target in other organisms such as the parasite *Trypanosoma brucei*. The aim of this thesis was to (further) characterize these enzymes structurally and functionally and to investigate the potential of several small molecules as future antimalarial drug components.

Similar to naturally occurring human glucose 6-phosphate dehydrogenase (G6PD) variants, naturally occurring mutations have been discovered in *Pf*GluPho; however, in contrast to the human host, these mutations as well as the studied naturally occurring phosphorylations do not lead to major changes in the properties of the enzyme and are therefore unlikely to have an impact on the parasites' redox homeostasis; potentially, they grant the parasites with others than kinetic benefits, which need to be further investigated. In addition to *P. falciparum*, recombinant production and characterization of *P. vivax* G6PD, the C-terminal and NADPH-producing part of *Pv*GluPho, are described in this thesis. Notably, *Pv*G6PD has lower activity and higher K_M values for substrate and cofactor than the *P. falciparum* enzyme, indicating that it has some functional disadvantages. Moreover, recombinant hexahistidly-tagged *Pv*G6PD existed in a presumably hexameric oligomerization state, which might represent an artifact. Therefore, full-length *Pv*GluPho ought to be investigated. However, since the recombinant production of *Pv*GluPho is extremely challenging, the characterization of *Pv*G6PD makes this important enzyme in the meantime accessible to drug discovery activities.

Within this thesis, recombinant production and kinetic characterization of *Pf*6PGD are described. In addition, we were able to solve the X-ray structures of native *Pf*6PGD as well as in complex with its substrate 6-phosphogluconate (6PG) or its cofactor $NADP^+$ (the oxidized form of NADPH) at resolutions of 2.8 Å, 1.9 Å, and 2.9 Å, respectively. Knowledge of the three-dimensional structure of an enzyme is helpful during all stages of drug discovery. With its dimeric conformation, each subunit consisting of a cofactor binding domain, a substrate binding domain, and a C-terminal tail threading through the adjacent subunit, the overall structure of *Pf*6PGD is similar to structures of 6PGDs from other species. We could, however, show that a flexible loop bordering the substrate binding site rearranges upon binding 6PG, thereby likely regulating the binding conformation of $NADP^+$; in the absence of 6PG the loop

is open, and $NADP^+$ binds in a flexible waiting position. As soon as 6PG binds, the active site loop adopts a closed conformation. This indicates that cofactor and substrate can bind independently from each other in a sequential binding mechanism, which was supported by kinetic studies. Furthermore, the interaction between the *Plasmodium*-specific residue W104 and the conserved residue W265 was shown to play a role in the interaction between the cofactor and the substrate binding domain of the enzyme.

Moreover, the impact of the two important post-translational modifications *S*-glutathionylation and *S*-nitrosation on *Pf*GluPho, *Pf*G6PD, *Pf*6PGD, and *Pv*G6PD was tested within this thesis. None of the enzymes were prone to *S*-glutathionylation under the conditions tested, but all of them were prone to *S*-nitrosation. The three enzymes catalyzing the G6PD reaction were only moderately inhibited upon incubation with *S*-nitrosoglutathione, while the *Pf*6PGD activity was reversibly inhibited by up to 65%. This might protect the enzyme from irreversible nitrosative damage. The reason for the downregulation of this important pathway upon nitrosative stress needs to be further investigated.

The aim in drug discovery is to identify compounds that specifically and effectively impact their target proteins. All tested compounds had comparable IC_{50} values and mode of inhibition on *Pf*GluPho and *Pv*G6PD. This supports the hypothesis that the two enzymes might be structurally very similar and that it might be possible to develop a drug that effectively treats both *P. falciparum* and *P. vivax* malaria. The most promising tested compound was SBI-0797750 with an inhibitory concentration in the very low nanomolar range. Moreover, inhibition of hG6PD was below 50% at 99 µM as the highest concentration tested; therefore, this compound is highly selective for the plasmodial enzymes. In mode of inhibition studies, SBI-0797750 was determined to compete with the substrate glucose 6-phosphate for the binding site in *Pf*GluPho. Further characterization showed that it acts in cell culture on asexual blood stage parasites as well as on gametocytes in the low nanomolar range; using genetically encoded probes, SBI-0797750 was shown to disturb the cytosolic glutathione homeostasis and significantly increase the cytosolic H_2O_2 concentration, which is most likely caused by the depletion of NADPH. Importantly, it did not adversely affect red blood cells from healthy and G6PD deficient donors. Further characterization of SBI-0797750 with regard to its absorption, distribution, metabolism, excretion, and toxicity is needed. An initial set of *Pf*6PGD inhibitors was identified by screening the MMV Malaria Box; several compounds showed IC_{50} values in the very low micromolar range. Since the three-dimensional structure of the enzyme is now known, this is a promising starting point for structure-based optimization approaches.

Zusammenfassung

Mit etwa einer halben Million Todesopfer pro Jahr ist Malaria bis heute eine der bedeutendsten Infektionskrankheiten. Die meisten Fälle werden durch die zwei Arten der *Plasmodium*-Parasiten *P. falciparum* (*Pf*) und *P. vivax* (*Pv*) verursacht. Derzeit sind Medikamente gegen Malaria verfügbar, jedoch erschwert das vermehrte Auftreten von resistenten Plasmodien eine effektive Bekämpfung der Erkrankung. Die Entwicklung neuer Medikamente ist daher dringend angeraten. Im Laufe ihres Lebenszyklus sind die Parasiten kontinuierlich oxidativem Stress unterschiedlicher Quellen ausgesetzt. Die antioxidativen Systeme, die für den Erhalt der Redoxbalance verantwortlich sind, sind in hohem Maß von dem Elektronendonator Nicotinamidadenindinukleotidphosphat (NADPH) abhängig. Eine Strategie neuer Malariamedikamente ist, eine tödliche Dosis an oxidativem Stress zu erzeugen, indem die zelluläre Redoxhomöostase gestört wird. Für Plasmodien ist der oxidative Pentosephosphatweg (PPP) die Hauptquelle des essentiell wichtigen NADPH. Generiert wird es von zwei Enzymen, der bifunktionellen Glukose-6-Phosphat-Dehydrogenase-6-Phosphogluconolactonase (GluPho) und der 6-Phosphogluconat-Dehydrogenase (6PGD). Für *Pf*GluPho konnte bereits gezeigt werden, dass das Enzym für die Blutstadien der Parasiten essentiell ist. Da es zudem sehr ähnlich zu dem entsprechenden Enzym in *P. vivax* ist, wird angenommen, dass auch *Pv*GluPho ein mögliches Zielmolekül für Medikamente ist. 6PGD trägt zur NADPH-Versorgung im gleichen Maße wie GluPho bei. Darüber hinaus wird es bereits als mögliches Zielmolekül für Medikamente in anderen Organismen wie dem Parasiten *Trypanosoma brucei* angesehen. Ziel der vorliegenden Arbeit war daher die (weitere) strukturelle und funktionelle Charakterisierung dieser Enzyme. Daneben wurde das Potential verschiedener Wirkstoffe als mögliche Bestandteile neuer Malariamedikamente untersucht.

Ähnlich wie natürlich vorkommende Varianten der humanen Glukose-6-Phosphat-Dehydrogenase (G6PD) wurden auch in *Pf*GluPho natürliche Mutationen entdeckt. Im Gegensatz zum menschlichen Wirt bewirken diese wie auch natürlich vorkommende Phosphorylierungen jedoch keine bedeutenden Veränderungen der Eigenschaften des Enzyms und tragen daher vermutlich nicht zur Redoxhomöostase der Parasiten bei. Möglicherweise statten sie die Plasmodien mit anderen, derzeit noch unbekannten Vorteilen aus. Neben *P. falciparum* sind die rekombinante Herstellung und Charakterisierung der *P. vivax* G6PD, des C-terminalen und NADPH-produzierenden Teils der *Pv*GluPho, in dieser Arbeit beschrieben. Interessanterweise hat *Pv*G6PD eine niedrigere Aktivität und höhere K_M-Werte als das *P. falciparum* Enzym, was auf einige funktionelle Nachteile hindeutet. Daneben befand sich rekombinant hergestellte *Pv*G6PD in einem vermutlich hexameren Oligomerisierungszustand, was jedoch artifizieller Natur sein könnte. Daher sollten Oligomerisierung und kinetische Eigenschaften der kompletten *Pv*GluPho untersucht werden. Da sich die rekombinante Produktion von *Pv*GluPho allerdings als extrem herausfordernd darstellt, ermöglicht die Charakterisierung von *Pv*G6PD in der Zwischenzeit die Verfügbarkeit dieses wichtigen Enzyms für die Medikamentenentwicklung.

In dieser Arbeit sind die rekombinante Herstellung und kinetische Charakterisierung der *Pf*6PGD beschrieben. Darüber hinaus ist es uns gelungen, die Röntgenstruktur der nativen *Pf*6PGD mit einer Auflösung von 2,8 Å zu ermitteln, die Strukturen in Komplex mit dem Substrat 6-Phosphogluconat (6PG) oder dem Cofaktor $NADP^+$ (der oxidierten Form von NADPH) hatten eine Auflösung von 1,9 beziehungsweise 2,9 Å. Kenntnisse über die dreidimensionale Struktur von Enzymen sind während aller Phasen der

Medikamentenentwicklung von Nutzen. *Pf*6PGD liegt als Dimer vor, wobei jede Untereinheit aus einer cofaktorbindenden Domäne, einer substratbindenden Domäne, sowie einem C-terminalen Endstück besteht, das durch die benachbarte Untereinheit hindurchragt. Damit ist die *Pf*6PGD-Struktur den Strukturen desselben Enzyms anderer Spezies ähnlich. Wir konnten zeigen, dass eine flexible Schlaufe in der Nähe der Substratbindestelle eine neue Position einnimmt, sobald 6PG gebunden hat. Dabei wird möglicherweise die Bindungsposition von $NADP^+$ reguliert. In Abwesenheit von 6PG ist die Schlaufe offen, während $NADP^+$ in einer flexiblen Warteposition bindet. Sobald 6PG gebunden hat, bewegt sich die Schlaufe und verschließt den Zugang zur Substratbindestelle. Dies deutet darauf hin, dass Cofaktor und Substrat unabhängig voneinander in einem sequentiellen Mechanismus binden können, was durch kinetische Untersuchungen bestätigt wurde. Darüber hinaus wurde gezeigt, dass die Interaktion zwischen dem für *Plasmodium* spezifischen W104 mit dem konservierten W265 die Interaktion der beiden Domänen unterstützt.

Darüber hinaus wurde in dieser Arbeit der Einfluss der zwei wichtigen posttranslationalen Modifikationen *S*-Glutathionylierung und *S*-Nitrosierung auf *Pf*GluPho, *Pf*G6PD, *Pf*6PGD und *Pv*G6PD getestet. Unter den getesteten Bedingungen war keines der Enzyme zugänglich für *S*-Glutathionylierung, jedoch alle für *S*-Nitrosierung. Während die Aktivität von *Pf*GluPho, *Pf*G6PD und *Pv*G6PD nur in sehr geringem Maß durch die Inkubation mit *S*-Nitrosoglutathion verringert wurde, wurde die *Pf*6PGD Aktivität reversibel um bis zu 65 % gehemmt. Möglicherweise können die Enzyme so vor irreversiblen Schäden durch nitrosativen Stress geschützt werden. Weitere Untersuchungen sind erforderlich, um die Ursachen für die Hemmung dieses wichtigen Stoffwechselweges aufzuklären.

Ziel der Medikamentenentwicklung ist die Identifizierung von Wirkstoffen, die spezifisch und effektiv auf Zielmoleküle wirken. Alle getesteten Verbindungen zeigten eine vergleichbare Wirkung auf *Pf*GluPho und *Pv*G6PD. Dies unterstützt die Annahme, dass die zwei Enzyme strukturell sehr ähnlich sind und es möglich ist, einen Wirkstoff zu entwickeln, der gegen beide *Plasmodien*-Arten eingesetzt werden kann. Der vielversprechendste Wirkstoff war SBI-0797750 mit einer mittleren hemmenden Wirkung auf *Pf*GluPho und *Pv*G6PD im sehr niedrigen nanomolaren Bereich. Selbst bei der höchsten getesteten Konzentration von 99 µM war die Hemmung von hG6PD bei unter 50 %, womit der Wirkstoff hochselektiv für plasmodiale Enzyme ist. Hemmstudien zeigten, dass SBI-0797750 mit dem Substrat Glukose-6-Phosphat um die Bindestelle in *Pf*GluPho konkurriert. Des Weiteren konnte gezeigt werden, dass SBI-0797750 in Zellkultur das Wachstum sowohl asexueller Blutstadien als auch von Gametozyten im niedrigen nanomolaren Bereich hemmt. Mithilfe genetisch kodierter Sonden wurde darüber hinaus gezeigt, dass der Compound die zytosolische Glutathionhomöostase stört, während der H_2O_2-Spiegel ansteigt, vermutlich aufgrund des hervorgerufenen NADPH-Mangels. Gleichzeitig konnten keine nachteiligen Veränderungen der Erythrozyten sowohl gesunder als auch G6PD-defizienter Spender festgestellt werden. Weitere Charakterisierung von SBI-0797750 im Hinblick auf Absorption, Verteilung, Metabolismus, Ausscheidung und Toxizität wird benötigt. Daneben konnten durch das Screening der Malariabox erste Inhibitoren der *Pf*6PGD mit einer Wirksamkeit im unteren mikromolaren Bereich identifiziert werden. Da die dreidimensionale Struktur des Enzyms jetzt bekannt ist, stellt dies einen vielversprechenden Ansatzpunkt für strukturbasierte Optimierungsversuche dar.

Publications and Conference Contributions

Publications

Allen SM, Lim EE, Jortzik E, Preuss J, Chua HH, MacRae JI, Rahlfs S, **Haeussler K**, Downton MT, McConville MJ, Becker K, and Ralph SA (2015) *Plasmodium falciparum* glucose-6-phosphate dehydrogenase 6-phosphogluconolactonase is a potential drug target. *FEBS J* 282: 3808-3823.

Haeussler K*, Fritz-Wolf K*, Reichmann M, Rahlfs S, and Becker K (2018) Characterization of *Plasmodium falciparum* 6-phosphogluconate dehydrogenase as an antimalarial drug target. *J Mol Biol* 430: 4049-4067. (* shared first authorship)

Haeussler K, Berneburg I, Jortzik E, Hahn J, Rahbari M, Schulz N, Preuss J, Zapol'skii V, Pinkerton A, Bode L, Kaufmann D, Rahlfs S, and Becker K. Glucose 6-phosphate dehydrogenase 6-phosphogluconolactonase: Characterization of the *Plasmodium vivax* enzyme and inhibitor studies. submitted

Pinkerton A, Bode L, **Haeussler K**, Rahbari M, Buchholz K, Moser M, Rahlfs S, and Becker K. Characterization of a novel selective inhibitor of glucose 6-phosphate dehydrogenase 6-phosphogluconolactonase from *Plasmodium falciparum*. in preparation

Louzada RA, Peyrot F, Bodineau C, Marzaioli V, Egorov M, Becuwe P, Becker K, **Haeussler K**, Seibel P, Marteyn B, Delpech B, Dupont C, Galtier C, Thoison O, Achab MC, Gallard JF, Liu JM, Truan G, Servajean V, Abbas K, Benechie M, Bignon J, Pelissier F, Hue N, El Benna J, Bakala J, Dupuy C, Frapart YM, Dang MC, Duran RV, Iorga B, and Collin P. A superoxide anion dependent prodrug activation inducing cytotoxicity in hypoxia, inhibits tumour growth and tumour angiogenesis. in preparation

Conference Contributions

Haeussler K, Preuss J, Jortzik E, Rahlfs S, Bode L, Pinkerton A, and Becker K. The pentose phosphate pathway of *Plasmodium* parasites as a drug target. 9th Annual Conference of the International Giessen Graduate School for the Life Sciences, Giessen, September 20th – 21st 2016 (Talk)

Haeussler K, Preuss J, Jortzik E, Rahlfs S, Pinkerton A, Bode L, and Becker K. The pentose phosphate pathway of *Plasmodium* parasites as a drug target. 18th Drug Design and Development Seminar of the German Society for Parasitology, Borstel, March 30th – 31st 2017 (Talk)

Haeussler K, Fritz-Wolf K, Rahlfs S, and Becker K. Characterization of *Plasmodium falciparum* 6-phosphogluconate dehydrogenase. 10th Annual Conference of the International Giessen Graduate School for the Life Sciences, Giessen, September 27th – 28th 2017 (Poster, 1st place of Poster Price)

Haeussler K, Fritz-Wolf K, Reichmann M, Rahlfs S, and Becker K. 6-Phosphogluconate dehydrogenase of malaria parasites of a potential drug target. 7th Symposium of the DFG Priority Program 1710, Rauischholzhausen, March 12th – 14th 2018 (Talk)

Haeussler K, Fritz-Wolf K, Reichmann M, Rahlfs S, and Becker K. Structural and functional characterization of *Plasmodium falciparum* 6-phosphogluconate dehydrogenase. 14th Annual BioMalPar Conference on the "Biology and Pathology of the Malaria Parasite", Heidelberg, May 23rd – 25th 2018 (Poster)

Haeussler K, Fritz-Wolf K, Reichmann M, Rahlfs S, and Becker K. Structural and functional characterization of *Plasmodium falciparum* 6-phosphogluconate dehydrogenase. Gordon Research Conference on "Thiol-Based Redox Regulation and Signaling", Castelldefels, Spain, July 15th – 20th 2018 (Poster)

Table of contents

List of figures

List of tables

List of abbreviations

6PG	6-Phosphogluconate
6PGD	6-Phosphogluconate dehydrogenase
6PGL	6-Phosphogluconolactonase
6xHis-tag	Hexahistidly-tag
A	Adenine
ACT	Artemisinin-based combination therapy
Aids	Acquired immunodeficiency syndrome
APS	Ammonium persulfate
ATP	Adenosine triphosphate
bp	Base pairs
BSA	Bovine serum albumin
C	Cytosine
CBIS	Chemical and Biological Information Systems
cDNA	Complementary deoxyribonucleic acid
CEA	Coruleoellagic acid
CRISPR	Clustered regularly interspaced short palindromic repeats
Cys	Cysteine
$_{dd}H_2O$	Double-distilled water
$_{d}H_2O$	Distilled water
DHEA	Dehydroepiandrosterone
DMSO	Dimethyl sulfoxide
DNA	Deoxyribonucleic acid
DTT	Dithiothreitol
E. coli	*Escherichia coli*
EA	Ellagic acid
ED_{50}	Median effective dose
EDTA	Ethylenediaminetetraacetic acid
EMP1	Erythrocyte membrane protein 1
FAC	Final assay concentration
FEA	Flavellagic acid
FPLC	Fast protein liquid chromatography
G	Guanine
G6P	Glucose 6-phosphate
G6PD	Glucose 6-phosphate dehydrogenase
GAPDH	Glyceraldehyde 3-phosphate dehydrogenase
GluPho	Glucose 6-phosphate dehydrogenase 6-phosphogluconolactonase
GLUT	Glucose transporter
Gly-Gly-Gly	Glycyl-glycyl-glycine
GR	Glutathione reductase
GSH	Glutathione (reduced form)
GSSG	Glutathione disulfide (oxidized form)
G*S*T	Glutathione *S*-transferase
h	Human
H6PD	Hexose 6-phosphate dehydrogenase
HEG	Homing endonuclease genes

hGrx1	Human glutaredoxin 1
His	Histidine
HIV	Human immunodeficiency virus
IC_{50}	Median inhibitory concentration
IPTG	Isopropyl-β-D-thiogalactopyranoside
IRS	Indoor residual spraying
ITN	Insecticide-treated mosquito net
kb	Kilobase
kDa	Kilodalton
K_M	Michaelis-Menten constant
LB	Luria-Bertani
Lm	*Leuconostoc mesenteroides*
MB	Methylene blue
MMV	Medicines for Malaria Venture
MOI	Mechanism of inhibition
MPD	2-Methyl-2,4-pentanediol
MPI	Max Planck Institute for Medical Research
mRNA	Messenger ribonucleic acid
$NADP^+$	Nicotinamide adenine dinucleotide phosphate (oxidized form)
NADPH	Nicotinamide adenine dinucleotide phosphate (reduced form)
Ni-NTA	Nickel-nitrilotriacetic acid
NMR	Nuclear magnetic resonance
NOS	Nitric oxide synthase
OD_{600}	Optical density at 600 nm
Orp1	Oxidant receptor peroxidase 1
P.	*Plasmodium*
Pb	*Plasmodium berghei*
PCR	Polymerase chain reaction
PEG	Polyethylene glycol
Pf	*Plasmodium falciparum*
pK_a	Logarithmic acid dissociation constant
PMSF	Phenylmethylsulphonyl fluoride
PPP	Pentose phosphate pathway
Pv	*Plasmodium vivax*
PVDF	Polyvinylidene fluoride
RBC	Red blood cell
RFU	Relative fluorescence unit
RNA	Ribonucleic acid
roGFP2	Oxidation sensitive green fluorescent protein 2
ROS	Reactive oxygen species
rpm	Rounds per minute
RT	Room temperature
SBP	Sanford Burnham Prebys Medical Discovery Institute
SD	Standard deviation
SDS-PAGE	Sodium dodecyl sulfate polyacrylamide gel electrophoresis
SMC	Seasonal malaria chemoprevention
T	Thymine

T.	*Trypanosoma*
TB	Terrific Broth
TBE	Tris-Borat-EDTA buffer
TBS(T)	Tris-buffered saline (with Tween 20)
TCA	Trichloroacetic acid
TEMED	Tetramethylethylenediamine
TEW	Tellurium-centered Anderson–Evans polyoxotungstate $[TeW_6O_{24}]^{6-}$
Tris	Tris(hydroxymethyl)-aminomethan
tRNA	Transfer ribonucleic acid
Trx	Thioredoxin
TrxR	Thioredoxin reductase
U	Unit
V_{max}	Maximum velocity
WHO	World Health Organization

One letter code of amino acids

A	Alanine	M	Methionine
C	Cysteine	N	Asparagine
D	Aspartic acid	P	Proline
E	Glutamic acid	Q	Glutamine
F	Phenylalanine	R	Arginine
G	Glycine	S	Serine
H	Histidine	T	Threonine
I	Isoleucine	V	Valine
K	Lysine	W	Tryptophan
L	Leucine	Y	Tyrosine

1 Introduction

Poverty-related diseases are still a major burden for low-income countries. WHO prioritizes 17 neglected tropical diseases, including Chagas disease, dengue, leishmaniasis, and schistosomiasis, threatening more than one billion people in 149 countries worldwide (WHO, 2015b). These diseases not only significantly deteriorate the health status and life quality of infected people, but also cause a significant economic burden to the country (Hung *et al.*, 2018; WHO, 2015b). The reasons for the high prevalence of infectious diseases in low-income countries are manifold; they include malnutrition, poor sanitation and hygiene, a lack of health infrastructure and health education, and a lack of access to already existing prevention and treatment possibilities (Hotez and Kamath, 2009; WHO, 2015b).

A major health-related burden is caused by the strongly poverty-related "big three" diseases, malaria, HIV/aids, and tuberculosis (Bourzac, 2014; Parola, 2013), nowadays also referred to as the "big four" when hepatitis is included (Chen *et al.*, 2015). In 2017, approximately 940,000 people died due to HIV infection (WHO, 2018a); an estimated 1.3 million HIV-negative and an additional 300,000 HIV-positive people died from tuberculosis (WHO, 2018b); and in 2015, 1.34 million people died from hepatitis according to WHO (WHO, 2017a). The global burden caused by malaria will be discussed below. Fighting these diseases is one of the major challenges of the 21st Century.

1.1 Malaria

Since the beginning of the millennium, there has been remarkable progress in the fight against malaria. In 2000, it caused an estimated 262 million cases and 839,000 deaths. Since then, the use of insecticide-treated mosquito nets increased significantly, and access to appropriate antimalarial drugs improved slightly, averting an estimated 1.2 billion cases of malaria and 6.2 million malaria deaths between 2000 and 2015 (WHO, 2015a). However, in 2016, malaria was still endemic in 91 countries, causing an estimated 216 million cases and 445,000 deaths; 90% of these cases and deaths can be found in Africa (WHO, 2017b). Therefore, malaria is still one of the world's most important infectious diseases.

1.1.1 *Plasmodium* parasites

Malaria is a vector-borne disease caused by the protozoan parasite *Plasmodium* (White *et al.*, 2014). There are more than 120 different *Plasmodium* (*P.*) species; six of them regularly infect human beings. With 207 million and 8.5 million estimated cases in 2016, *P. falciparum* and *P. vivax*, respectively, are the two most important species. *P. falciparum* is mainly distributed in sub-Saharan Africa. It induces high levels of blood stage parasites that invade critical organs and lead to severe anemia, especially in children (Ashley *et al.*, 2018). Due to its usually mild course of infection, *P. vivax* has been underestimated for many years (Cowman *et al.*, 2016). However, *P. vivax* parasites are able to produce dormant liver stages (see below) that can cause relapses months or even years after infection (Ashley *et al.*, 2018), severely affecting the development of children. It has been shown that the course of anemia due to *falciparum* or *vivax* malaria are comparable (Naing *et al.*, 2014). Due to a largely Duffy antigen negative population, *P. vivax* is less common in Africa but more widely distributed in the Americas. In Asia and Oceania, *P. falciparum* and *P. vivax* are equally distributed. The morphologically indistinguishable species *P. malariae*, *P. ovale curtisi*, and *P. ovale wallikeri* are distributed worldwide with low incidence; however, *P. ovale* is mainly found in Africa and Southeast Asia.

The course of infection is comparable to uncomplicated *vivax* malaria. The primary hosts of *P. knowlesi* are macaques; however, it can also cause severe malaria in humans mainly distributed in Southeast Asia, especially in Malaysia. Human infections with additional forms of simian malaria caused by *P. cynomolgi* and *P. simium* have low incidences (Ashley *et al.*, 2018). So far, a continuous, long-term *in vitro* cultivation of blood-stage *P. vivax* parasites is not possible (Thomson-Luque *et al.*, 2017). However, the simian infection with *P. cynomolgi* is considered a disease model for human *vivax* malaria (Markus, 2018).

All *Plasmodium* species have a complex life cycle in common that alters between the *Anopheles* mosquitoes and vertebrate hosts (Cowman *et al.*, 2016), which is depicted in Figure 1. The cycle begins with the transmission of sporozoites into the dermis of the host during the blood meal of a female *Anopheles* mosquito (White *et al.*, 2014). Other possible but less common transmission routes are mother-to-child transmission or via blood transfusion, especially in resource-poor (Ashley *et al.*, 2018). The sporozoites migrate towards the liver, invade hepatocytes, multiply and form schizonts. After 5.5-8 days, the schizonts burst and release merozoites into the blood stream, which enter red blood cells (RBC) and initiate the asexual cycle. For *P. falciparum*, *P. vivax*, and *P. ovale*, this cycle takes approximately 48 h, while it takes 72 h for *P. malariae* and *P. knowlesi*. The formation of dormant intrahepatic forms, the so-called hypnozoites, is characteristic for infections with *P. vivax* and *P. ovale* and enables relapses of the infection weeks or even years after primary infection (White *et al.*, 2014). Furthermore, there is evidence for non-hypnozoite-dependent recurrence of *P. vivax* malaria due to additional plasmodial sources, including parasites hiding in splenic dendritic cells, other cells in the spleen, the bone marrow, and the skin. This especially has to be taken into account with regard to treatment of *vivax* malaria (Markus, 2018). Different ligand-receptor interactions facilitate the attachment and infiltration of the parasites into RBCs via several pathways. The receptor predominantly responsible for the invasion of *P. vivax* parasites resembles the Duffy blood group antigen Fy^a or Fy^b. The Duffy-negative FyFy phenotype is widely distributed in the population of West Africa, leading to the carrier's resistance to *P. vivax* malaria. A subpopulation of the parasites leaves the asexual cycle and develops into the sexual stages, the so-called gametocytes, which are taken up by an *Anopheles* mosquito during the next blood meal (White *et al.*, 2014). The male gametocytes exflagellate in the midgut, where a zygote is formed by the fusion of male and female gametes. The zygote develops into a mobile ookinete capable of passing the mosquito gut wall. The emerging oocyst releases sporozoites which complete the life cycle by migrating into the mosquito's salivary glands (Ashley *et al.*, 2018).

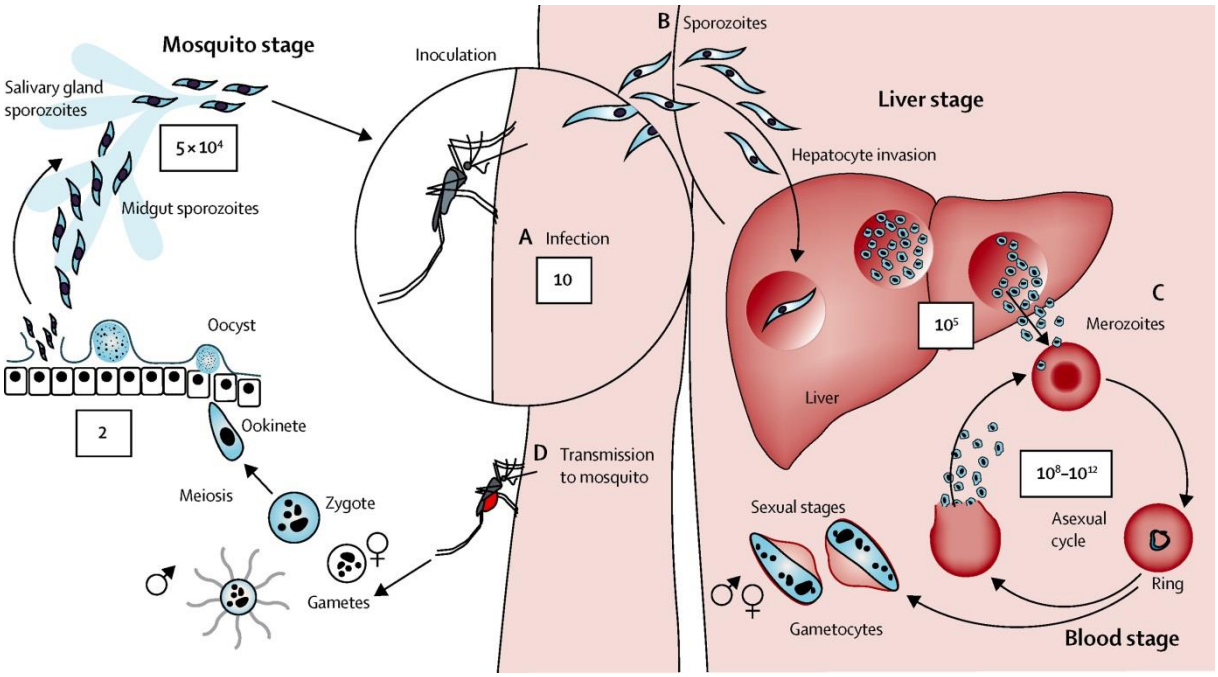

Figure 1. Life cycle of *Plasmodium falciparum*
Plasmodium parasites have a complex life cycle with a changing environment between the human host and *Anopheles* mosquitoes that consists of three stages: the mosquito stage, the liver stage, and the blood stage. The numbers of parasites during each stage are indicated in the boxes. (A) During the blood meal of an infected mosquito, it injects sporozoites into the dermis of a human being. (B) The sporozoites migrate towards the liver where they invade hepatocytes and form schizonts. (C) After approximately one week, the schizonts burst and release merozoites into the blood stream, which enter red blood cells and initiate the asexual cycle. Some parasites leave the cycle and develop into gametocytes, the sexual stages. (D) Gametocytes that are taken up by a mosquito develop into sporozoites and migrate into the salivary glands. The next bite of a mosquito completes the life cycle (White *et al.*, 2014).

1.1.2 Pathogenesis and clinical manifestation of malaria

Initial symptoms of malaria occur as soon as parasitemia is above a threshold of about 100 parasites per µL blood. Despite some variation for certain strains, typical durations of incubation are 10-14 days for *P. falciparum* and *P. knowlesi*, 2-3 weeks for *P. vivax* and *P. ovale*, and 18 days or longer for *P. malariae* (Ashley *et al.*, 2018). Major remodeling processes of the human RBCs by the parasites are the predominant cause of malaria symptoms. The aim is to convert terminally differentiated cells into an environment that enables the parasites to grow and hide from the host immune system. Therefore, numerous proteins are exported out of the parasites into the host RBCs. A vesicle-mediated trafficking network from the parasitic endoplasmic reticulum across the parasite membrane and the parasitophorous vacuole into the host cell facilitates translocation of the proteins. Their final destinations are the erythrocytic cytosol, the cytoskeleton, or the membrane. One prominent, extensively studied protein that is exported to the surface of *P. falciparum*-infected cells is the *P. falciparum* erythrocyte membrane protein 1 (*Pf*EMP1) family (Cowman *et al.*, 2016). This protein allows cytoadherence to endothelial surface receptors in veins and capillaries and sequestration in deep capillary beds, thereby enabling escape from the splenic clearance (Cowman *et al.*, 2016; White *et al.*, 2014). Reconstructing the cell membrane allows not only the export of parasite-derived proteins but also the import of nutrients. Intracellular parasites use the contents of human RBCs as their primary source of nutrients, releasing potentially

toxic free heme. This waste product has to be detoxified through lipid-mediated crystallization to the so-called malaria pigment, the biologically inert hemozoin (White *et al.*, 2014). Sequestration causes injuries to the host endothelial cells and microvascular obstruction. The clinical consequences depend on the affected organs. For example, they lead to a coma if the brain is involved, respiratory failures for the lungs, and placental malaria with maternal anemia, low birthweight, preterm labor, abortion, or stillbirth if the placenta is affected (Ashley *et al.*, 2018). Besides this morphological damage, the human host reacts with increased splenic immune function and filtrating clearance, resulting in an accelerated removal of parasitized, but also uninfected RBCs (White *et al.*, 2014). The loss of RBCs due to high spleen activity is one of the most important causes (another being intravascular hemolysis) of anemia during acute infection and is a very common feature of malaria (Ashley *et al.*, 2018). The release of merozoites into the blood activates the immune system, which increases the activity of monocytes and macrophages and releases proinflammatory cytokines that cause the typical malaria fever (White *et al.*, 2014).

Depending on the intensity of the symptoms, malaria is divided into uncomplicated and severe malaria. The symptoms of uncomplicated malaria are rather unspecific and include not only flu-like symptoms such as fever, chills, body-aches, headache, and cough, but also diarrhea and thrombocytopenia. Severe *P. falciparum* malaria is diagnosed via specific clinical (e.g. prostration, coma, convulsions, jaundice) and laboratory (hemoglobinuria, hypoglycemia, acidosis, acute kidney injury, asexual parasitemia in over 10% of infected RBCs) criteria. Typical manifestations of severe malaria are cerebral malaria, acute lung injury that can develop into an acute respiratory distress syndrome, acute kidney injury, and acidosis; severe anemia is commonly present amongst children (Ashley *et al.*, 2018). In contrast to *P. falciparum*, infections with *P. vivax* are usually not fatal, but they can also cause severe anemia and be followed by frequent relapses due to the formation of dormant hypnozoites in the liver (1.1.1). In children, these recurring infections can severely impair their development (Cowman *et al.*, 2016). Therefore, an early detection and appropriate treatment are essential to contain the consequences of *P. vivax* infection (Naing *et al.*, 2014).

1.1.3 Prevention and treatment of malaria

There are three different approaches to deal with malaria: vector control, chemoprevention, and case management. The first two try to prevent malaria from occurring, while case management means treating an actual infection using antimalarial drugs (WHO, 2017b). The approaches are described below.

Vector control

The goal of vector control is to stop the mosquito from biting humans and thereby block the transmission (WHO, 2017b). A commonly used method is sleeping under insecticide-treated mosquito nets (ITNs) (Tizifa *et al.*, 2018). In certain settings of sub-Saharan Africa, the use of ITNs was able to reduce the malaria incidence rate by 50% and the mortality rate in children under the age of 5 by 55%. However, the distribution of ITNs is still not sufficient; e.g., there were twelve countries in sub-Saharan Africa with less than 50% of the at-risk population having access to ITNs (WHO, 2017b). The second major strategy is indoor residual spraying (IRS). It has been proved to successfully eradicate malaria and control epidemics in several countries. However, IRS is costly, especially on a large scale, and it is not without risk to human health and the environment (Tizifa *et al.*, 2018). Moreover, *Anopheles* mosquitoes are

becoming increasingly resistant to all four classes of insecticides commonly used in both ITN and IRS (WHO, 2017b). One of the oldest strategies to fight malaria is larval source management, i.e. dealing with aquatic habitats that serve as potential breeding sites. Furthermore, there are numerous strategies under development such as house improvement, toxic sugar feeding, the release of genetically modified mosquitoes, and many more (Tizifa *et al.*, 2018). One novel, intensively studied system to manipulate natural *Anopheles* populations is the so-called gene drive system. It is based on site-specific selfish genes exploiting the host's gene repair system to introduce themselves into specific target sequences. Using this 'super-Mendelian' inheritance, the selfish genes can spread throughout entire populations. First used were homing endonuclease genes (HEG) encoding enzymes that recognize and cleave specific sequences located on chromosomes without a copy of the HEG. Cleaved chromosomes are repaired by the recombinational repair system of the cell using the intact HEG containing chromosome as a template. Using this approach, both chromosomes contain HEG after the repair, heterozygotes are transformed into homozygotes. HEGs can be engineered in a way that the recognition site is located in the middle of an essential gene that is destroyed after the recombinational repair (Burt, 2003). Newly developed RNA-guided gene drives based on the CRISPR-Cas9 endonuclease simplified this before rather complicated approach (Esvelt *et al.*, 2014). The use of this technique in the malaria vector *Anopheles* could significantly contribute to the control or even elimination of malaria (Gantz *et al.*, 2015; Hammond *et al.*, 2016). Targeting a gene that controls the differentiation of the two sexes in *Anopheles gambiae* in fact enabled the creation of 100% prevalence of sterile females within 7-11 generations, resulting in a total collapse of the population (Kyrou *et al.*, 2018). However, one potential issue is the occurrence of nuclease-resistant variants that block the gene drive through the population (Bull and Malik, 2017; Hammond *et al.*, 2016). In *Drosophila melanogaster*, evolution of resistance was mainly observed in the germline, but also after fertilization in the embryo. At the moment, this severely limits the applicability of the approach (Champer *et al.*, 2017). Moreover, the use of gene drive systems is heavily discussed with to respect to safety, but also ethical considerations. It has to be ensured that an accidental release of organisms carrying gene drive constructs into the environment is excluded (Akbari *et al.*, 2015).

Moreover, there are major efforts underway to study mosquito behavior. Detailed knowledge on flight, mating, feeding, and oviposition behavior of the vector can help researchers develop new control strategies, e.g., swarm spraying (Spitzen and Takken, 2018; Tizifa *et al.*, 2018).

Chemoprevention

The goal of chemoprevention is to suppress the outbreak of the disease after an infected mosquito's bite with drugs (WHO, 2017b). Chemoprophylaxis is especially recommended for pregnant women, young children, and travelers (Ashley *et al.*, 2018). In 2012, WHO recommended a seasonal malaria chemoprevention (SMC) for *P. falciparum* malaria control in the highly seasonal transmission areas across the Sahel sub-region. SMC comprises a monthly administration of sulfadoxine pyrimethamine and amodiaquine for up to four months to children between 3 and 59 months of age (WHO, 2012). Additionally, an intermittent preventive treatment of malaria in pregnancy is recommended (WHO, 2017b). So far, SMC has proved to be highly successful, significantly reducing the incidence of both uncomplicated and severe malaria by 82%; however, the delivery of the medicine to children remains a logistical challenge. Moreover, there is the threat of malaria parasites becoming resistant to sulfadoxine pyrimethamine and amodiaquine in the future (Greenwood *et al.*, 2017). For travelers, doctors

should choose a chemoprevention strategy based on the risks of infection, parasite drug resistance, and drug toxicity. Atovaquone-proguanil, doxycycline, mefloquine, and primaquine are commonly used (Kolifarhood *et al.*, 2017).

Developing a vaccine against malaria is challenging. RTS,S/AS01, also known as Mosquirix, is the first vaccine that has received a positive opinion from the European Medicines Agency to be used as vaccination in young children (EMA, 2015). It targets sporozoite stages via the *P. falciparum* circumsporozoite protein, a surface protein that is expressed at the pre-erythrocytic stage of the parasite (Cohen *et al.*, 2010). A large phase 3 clinical trial conducted in seven countries in sub-Saharan Africa demonstrated significant protection against *P. falciparum* malaria infection over a 3-4 years period. In older children (5-17 months), the vaccine efficacy was 36.3% with a booster dose at month 20 and 28.3% without a booster. The efficacy in infants (6-12 weeks) was lower: 25.9% with a booster and 18.3% without (RTS,S Clinical Trials Partnership, 2015). Efficacy varies between *Plasmodium* strains (Neafsey *et al.*, 2015), and the vaccination quickly loses its efficacy over time. A seven-year follow-up study revealed an efficacy of only 4.4% (Olotu *et al.*, 2016). However, the vaccine is still able to avert a substantial number of clinical malaria cases and can make an important contribution to fighting the disease, especially in combination with other strategies (RTS,S Clinical Trials Partnership, 2015). In addition to RTS,S/AS01, there are several other vaccines under development, e.g. a *P. falciparum* sporozoite vaccine that aims to induce sporozoite-based immunity through intravenous injection of irradiation-attenuated sporozoites (Richie *et al.*, 2015; Sissoko *et al.*, 2017). Another approach, targeting the merozoite stage proteins, aims to reduce the asexual replication rate of the parasites. *Pf*Rh5, which is critical for parasites trying to invade RBCs, is currently of particular interest (Ashley *et al.*, 2018; Crosnier *et al.*, 2011; Drew and Beeson, 2015). In contrast to targeting the asexual stages, transmission-blocking vaccines target sexual stage antigens in order to generate antibodies that are ingested during the mosquito blood meal, potentially providing immunity at population level (Sinden, 2017). In areas where malaria transmission is limited to a few months per year, mass vaccination campaigns shortly before the transmission season begins might be an effective way to take advantage of malaria vaccines with an initially high efficacy rate such as RTS,S/AS01 (Greenwood *et al.*, 2017).

Case management

After a prompt diagnosis, an effective treatment is essential to prevent a severe form of malaria from developing. WHO currently recommends an artemisinin-based combination therapy (ACT) for treating uncomplicated *P. falciparum* malaria (WHO, 2017b). Commonly used combinations are artesunate-amodiaquine, dihydroartemisinin-piperaquine, artesunate-mefloquine, artemether-lumefantrine, and artesunate plus sulfadoxine-pyrimethamine (Ashley *et al.*, 2018). The primary reason for applying combination therapies is to reduce the risk of resistance development (White, 1999). Artemisinin quickly reduces a large amount of parasites, while the partner drug clears the rest. Using chloroquine or an ACT is recommended for uncomplicated *P. vivax* malaria. Often, primaquine is used to remove latent liver stage infections and prevent a recurrence of the infection (WHO, 2017b).

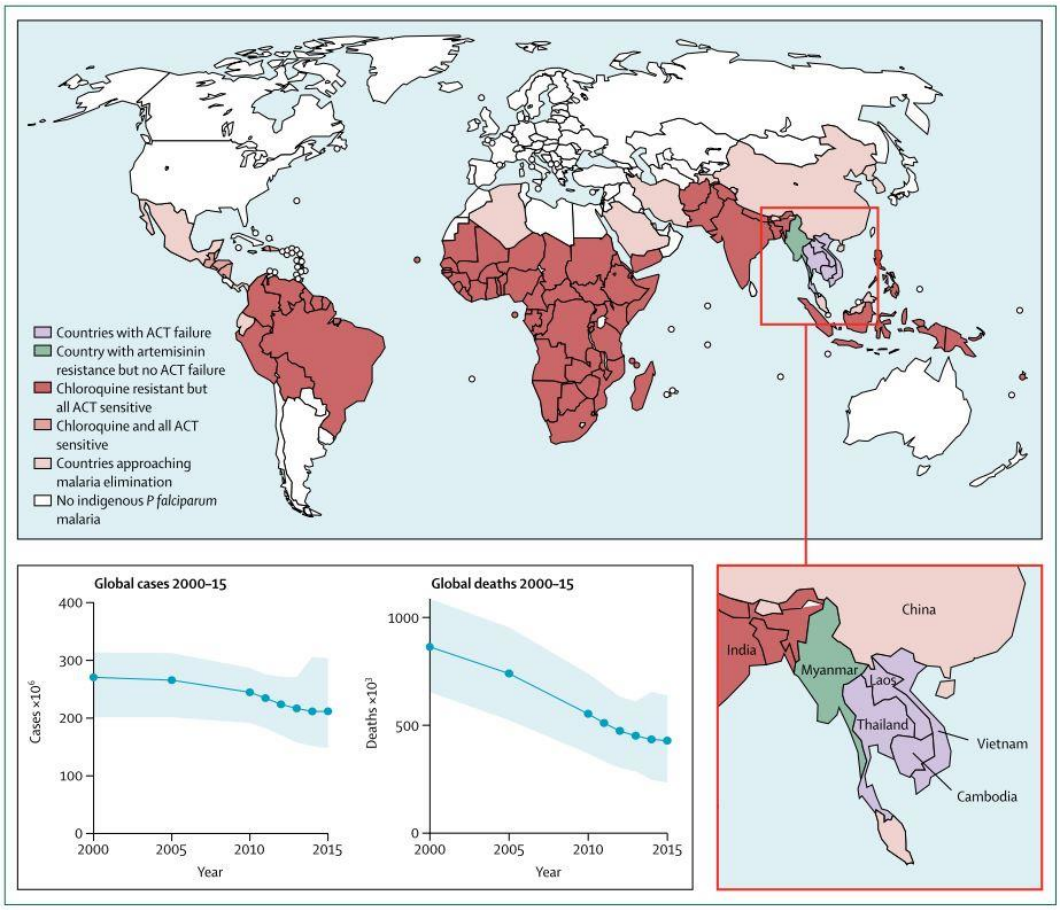

Figure 2. Global distribution of *Plasmodium falciparum* treatment failures
The local occurrence of drug resistant *P. falciparum* parasites is shown. Laos, Thailand, Vietnam, and Cambodia have had cases of ACT-resistant parasites. Fortunately, 13 countries are currently close to eliminating malaria as defined in the World Malaria Report 2016 (WHO, 2016). The global number of malaria cases and especially the number of malaria deaths (shown with 95% upper and lower uncertainty intervals) declined dramatically from 2000 to 2015. ACT: artemisinin-based combination therapy (Ashley *et al.*, 2018).

Partial resistance to artemisinin does not automatically result in complete treatment failure, but it does increase the challenge for the partner drug and thereby the risk of resistance developing against it. Artemisinin resistance has been observed in several countries of Southeast Asia (WHO, 2017b). High rates of ACT failures (over 10%) have been reported in Cambodia, Thailand, Laos, and Vietnam (Figure 2) (Ashley *et al.*, 2018; WHO, 2017b). In severe malaria, medical personnel must pay special attention to managing symptoms such as severe anemia, hypoglycemia, hypovolemia, acidosis, and others described above (Ashley *et al.*, 2018).

1.2 Pentose phosphate pathway

The pentose phosphate pathway (PPP) plays a central role in cellular biosynthetic metabolism. Along with the glycolysis and the tricarboxylic acid cycle, it was one of the first pathways discovered. Evolutionarily speaking, the biochemical reactions are presumably very old (Stincone *et al.*, 2015). There are indications that the reactions that enzymes nowadays catalyze have descended from enzyme-free, metal-catalyzed sugar phosphate interconversions in the reaction milieu of the prebiotic Archean ocean (Keller *et al.*, 2014).

In most tissues, the majority of glucose (80-90%) is oxidized via glycolysis. The PPP, also known as the hexose monophosphate shunt, represents an alternative cytosolic pathway for oxidizing the remaining 10-20% of glucose. It has two major functions (Wamelink *et al.*, 2008):

- Production of nicotinamide adenine dinucleotide phosphate (NADPH): this electron donor is essential in many biosynthetic pathways and for protecting against oxidative stress.
- Synthesis of ribose 5-phosphate: this is essential for nucleotide and nucleic acid synthesis (Wamelink *et al.*, 2008).

The PPP can be divided into two branches: oxidative and non-oxidative.

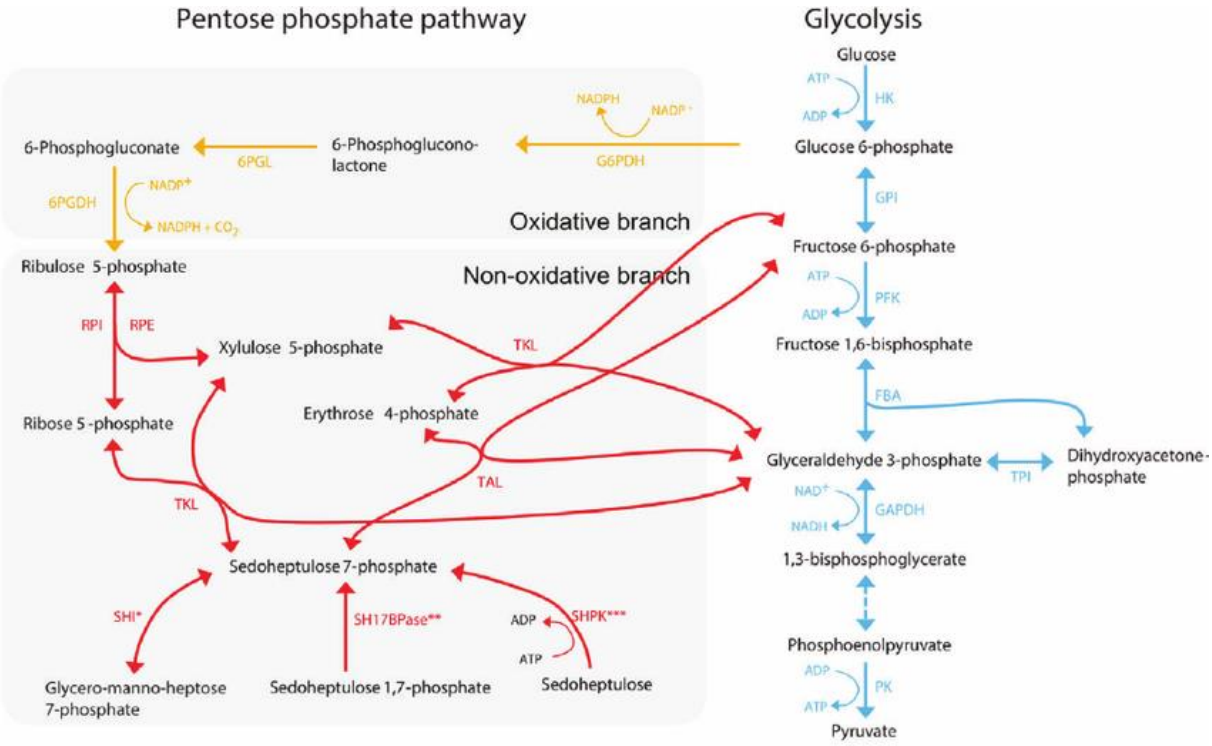

Figure 3. Schematic representation of the pentose phosphate pathway and glycolysis
The pentose phosphate pathway (PPP, left, gray background) is divided into an oxidative and non-oxidative branch. The reactions, potential reversibility of the reactions, and connections between the PPP and glycolysis (right) are indicated by arrows. Enzymes converting sedoheptulose 7-phosphate can be distinguished between * bacteria, ** fungi, and *** mammals. 6PGDH: 6-phosphogluconate dehydrogenase; 6PGL: 6-phosphogluconolactonase; ADP: adenosine diphosphate; ATP: adenosine triphosphate; FBA: fructose bisphosphate aldolase; G6PDH: glucose 6-phosphate dehydrogenase; GAPDH: glyceraldehyde 3-phosphate dehydrogenase; GPI: glucose phosphate isomerase; HK: hexokinase; NAD^+/NADH: oxidized/reduced nicotinamide adenine dinucleotide; $NADP^+$/NADPH: oxidized/reduced nicotinamide adenine dinucleotide phosphate; PFK: phosphofructokinase; PK: pyruvate kinase; RPE: ribulose 5-phosphate epimerase; RPI: ribose 5-phosphate isomerase; SH17BPase: sedoheptulose 1,7-bisphosphatase; SHI: sedoheptulose 7-phosphate isomerase; SHPK: sedoheptulokinase; TAL: transaldolase; TKL: transketolase; TPI: triosephosphate isomerase (Stincone *et al.*, 2015).

The oxidative branch

The oxidative branch consists of three irreversible reactions, indicated by the one-way arrows in Figure 3 (Stincone *et al.*, 2015). First, glucose 6-phosphate dehydrogenase (G6PD, EC 1.1.1.49) catalyzes the dehydrogenation of glucose 6-phosphate (G6P) to 6-phosphoglucono-δ-lactone and produces one molecule of NADPH. 6-Phosphogluconolactonase (6PGL, EC

3.1.1.31) rapidly hydrolyzes 6-phosphoglucono-δ-lactone, yielding one 6-phosphogluconate (6PG) (Wamelink *et al.*, 2008). This hydrolysis can also occur spontaneously; however, the activity of 6PGL is necessary for this reason: the δ form of 6-phosphogluconolactone is the only product of the G6PD reaction. Intermolecular rearrangements lead to the γ form. While only the δ form can undergo spontaneous hydrolysis and serve as a substrate for 6PGL, the γ form cannot be spontaneously hydrolyzed and also cannot be used as a substrate by 6PGL; it therefore represents a "dead end" on the pathway and accrues. Moreover, the accumulation of 6-phosphoglucono-δ-lactone may be toxic due to its reactivity with endogenous cellular nucleophiles. Therefore, 6PGL activity accelerates the spontaneously occurring hydrolysis of the δ form and prevents the formation and accumulation of the "dead end" γ form (Miclet *et al.*, 2001). 6-Phosphogluconate dehydrogenase (6PGD, EC 1.1.1.44) oxidatively decarboxylates the resulting 6PG, producing ribulose 5-phosphate, CO_2, and one additional molecule NADPH (Wamelink *et al.*, 2008). In summary, two NADPH molecules are generated for each molecule of G6P during the oxidative branch of the PPP (Stincone *et al.*, 2015).

The non-oxidative branch

The reactions of the non-oxidative branch are reversible, as indicated by the bidirectional arrows in Figure 3 (Stincone *et al.*, 2015). Ribulose 5-phosphate, the product of the oxidative branch, is either epimerized to xylulose 5-phosphate by ribulose 5-phosphate epimerase or isomerized to ribose 5-phosphate by ribose 5-phosphate isomerase. Ribose 5-phosphate can be used for the synthesis of nucleotides and nucleic acids. However, in many situations, more NADPH is needed for biosynthetic processes than ribose 5-phosphate for nucleotide synthesis. In these cases, transketolase converts ribose 5-phosphate and xylulose 5-phosphate into sedoheptulose 7-phosphate and glyceraldehyde 3-phosphate, respectively. Transaldolase further metabolizes these two products to erythrose 4-phosphate and fructose 6-phosphate, respectively. Transketolase also converts erythrose 4-phosphate and xylulose 5-phosphate to glyceraldehyde 3-phosphate and fructose 6-phosphate, respectively. Therefore, transketolase and transaldolase build a reversible connection between the PPP and glycolysis (Wamelink *et al.*, 2008), since glucose 6-phosphate isomerase can convert fructose 6-phosphate to G6P, the starting substrate for the oxidative PPP (Stincone *et al.*, 2015).

Localization of the PPP

As already indicated above, the PPP is located in the cytosol in most organisms; however, there are exceptions (Stincone *et al.*, 2015). The pathway can be distributed between the cytosol and other organelles (e.g. the plastid, peroxisomes, or glycosomes). This distribution can be observed in some plants and parasitic protozoa (Hannaert *et al.*, 2003; Kruger and von Schaewen, 2003). Part of the PPP can also occur in the endoplasmic reticulum. In vesicles formed in the endoplasmatic reticulum, five enzymes of the PPP were found, including a special enzyme was found called hexose 6-phosphate dehydrogenase (H6PD); it is similar to G6PD but has a broader range of substrates and is not selective regarding the choice of nucleotide cofactor (NAD^+ or $NADP^+$) (Bublitz and Steavenson, 1988; Senesi *et al.*, 2010; Stincone *et al.*, 2015).

1.2.1 Glucose 6-phosphate dehydrogenase

G6PD is a cytosolic housekeeping enzyme that is expressed in all cells of the body. As described above, it catalyzes the first, rate-limiting step of the oxidative PPP, the oxidation of G6P to 6-phosphoglucono-δ-lactone during the reduction of its cofactor $NADP^+$ to NADPH (Gomez-

Manzo *et al.*, 2016; Luzzatto *et al.*, 2016). G6PD is highly conserved in all living organisms except for *Archaebacteria* since they are not extensively exposed to oxygen in their environment; therefore, they do not have to defend against oxidative stress (Luzzatto *et al.*, 2016; Notaro *et al.*, 2000).

1.2.1.1 Human glucose 6-phosphate dehydrogenase and its deficiency

Structure and function of human G6PD

In human beings, the *g6pd* gene is located close to the telomeric region of the distal arm of the X chromosome (band Xq28). The complete sequence has a size of 18.5 kb, consisting of 13 exons and 12 introns. It encodes a product of 1,545 bp. Exon 1 and a part of exon 2 are not translated into protein; therefore, the gene results in a protein with 515 amino acids and 59 kDa per monomer (Cappellini and Fiorelli, 2008; Gomez-Manzo *et al.*, 2016). The enzyme is active as a homodimer or a homotetramer (Cohen and Rosemeyer, 1969). Each subunit has one tightly bound $NADP^+$ in addition to the binding sites of $NADP^+$ and G6P, thereby enhancing its structural stability (Au *et al.*, 2000). Under physiological conditions, hG6PD operates in RBCs at only approximately 1% of its maximal capacity. Therewith, oxidative stress leading to oxidation of NADPH (see 1.2.3) results in an activation of hG6PD (Preuss *et al.*, 2012b).

Genetics and molecular basis of G6PD deficiency

G6PD deficiency is the most common enzymopathy, affecting 400 million people worldwide. There are more than 400 different variants of G6PD caused by 217 mutations. Most of them (83.9%) are missense variants with substitutions of single nucleotides; 8.7% are multiple mutations with two or more substitutions; 5.1% of the mutants are caused by deletions; and 2.3% of the mutations affect introns (Gomez-Manzo *et al.*, 2016). There are many studies indicating that due to its X-linked heredity, G6PD deficiency is more common in males than in females (Cappellini and Fiorelli, 2008; Gomez-Manzo *et al.*, 2016). However, there are considerations indicating that this statement is not correct for the following reason: In males, there are two genotypes (hemizygous normal and hemizygous deficient), while there are three genotypes in females (homozygous normal, homozygous deficient, and heterozygous). In populations, homozygous females can be found less frequently than hemizygous males, while heterozygous females are much more common. With wide variations in heterozygous females, one half of the RBCs are normal, and the other half are G6PD deficient. Therefore, the phenotype of heterozygous women varies from normal to severely G6PD deficient with different clinical implications (Luzzatto *et al.*, 2016).

Clinical consequences of G6PD deficiency

Mutations in the *g6pd* gene are associated with more or less severe enzyme deficiency (Gomez-Manzo *et al.*, 2016); however, there is no complete loss of activity because this would presumably be lethal (Longo *et al.*, 2002; Pandolfi *et al.*, 1995). Depending on the mutation, there are different quantitative, but also qualitative changes in the properties of the enzyme. Based on the degree of deficiency and the clinical manifestations, the G6PD variants are divided into five classes (Table 1). A cluster of the most severe class I deficient variants is caused by different mutations in the dimerization domain of the enzyme, influencing the stability of the dimer. These variants are associated with chronic non-spherocytic hemolytic anemia (Luzzatto *et al.*, 2016).

Table 1. Classes of G6PD deficiency
The residual activity of classes IV and V slightly varies depending on the literature (Cappellini and Fiorelli, 2008; Luzzatto *et al.*, 2016).

	Residual activity	Symptoms
Class I	< 10%	Associated with chronic, non-spherocytic hemolytic anemia
Class II	< 10%	Associated with acute hemolytic anemia
Class III	10-60%	None in the steady state
Class IV	60-100%	None
Class V	> 100%	None

The central role of NADPH in metabolism is described below. In most cells, there are several sources of this electron donor (see 1.2.3); however, the situation in RBCs is different: they do not have a nucleus or mitochondria. For them, the only source of NADPH is the PPP (Gomez-Manzo *et al.*, 2016; Preuss *et al.*, 2012b). One of the major tasks of RBCs is to transport oxygen. Together with the iron contained in hemoglobin, endogenous formation of free radicals via the Fenton reaction is possible (Müller, 2004). Defense against this stress requires a significant amount of NADPH (see 1.2.3). Therefore, it is obvious that a G6PD deficiency has more severe consequences for erythrocytes than for other cells (Luzzatto *et al.*, 2016). Nevertheless, most G6PD deficient individuals stay asymptomatic throughout their life; often they are not even aware of their deficiency. Oxidative stress triggered by different events such as drug intake, infections, or the ingestion of fava beans can manifest as acute hemolysis (Cappellini and Fiorelli, 2008; Luzzatto *et al.*, 2016). Due to the connection to fava beans, this manifestation is also called favism (Luzzatto and Arese, 2018). Other symptoms besides acute hemolytic anemia include not only neonatal jaundice and chronic, non-spherocytic hemolytic anemia, but also more unspecific symptoms such as fatigue and back pain. Markers include increased lactate dehydrogenase, unconjugated bilirubin, and reticulocytosis (Cappellini and Fiorelli, 2008; Luzzatto *et al.*, 2016).

G6PD deficiency and malaria

The distribution areas of malaria and G6PD deficiency are strikingly similar. The highest frequencies of the deficiency were detected in Africa, Asia, the Mediterranean region, and in the Middle East. This led to the so-called malaria protection hypothesis (Cappellini and Fiorelli, 2008). It has been shown that the risk of severe *P. falciparum* malaria is reduced in G6PD deficient patients (Bienzle *et al.*, 1972; Clark *et al.*, 2009; Guindo *et al.*, 2007; Ruwende *et al.*, 1995). Moreover, there is evidence for partial resistance to not only *P. falciparum* but also *P. vivax* (Louicharoen *et al.*, 2009). Accordingly, the growth of parasites in cell culture is slower in G6PD deficient RBCs than in normal RBCs (Cappadoro *et al.*, 1998; Miller *et al.*, 1984; Roth *et al.*, 1983). Already in 1969 it was shown that parasitic growth is 2-80 times lower in G6PD deficient RBCs than in healthy cells (Luzzatto *et al.*, 1969). However, the mechanism of resistance is not yet fully understood. Most likely the immune response of the host differs between deficient and healthy cells. G6PD deficient erythrocytes containing ring stage parasites are more intensely phagocytosed than normal infected cells, most likely due to the deficiency causing impaired antioxidative defense (see also 1.2.3). The binding of autologous IgG and complement C3 fragments (Cappadoro *et al.*, 1998) – a factor that triggers phagocytosis (Turrini *et al.*, 1992) – is significantly higher in G6PD deficient, ring stage infected RBCs than in normal, ring stage infected cells (Cappadoro *et al.*, 1998). Band 3 cross-linking appears earlier in G6PD deficient, oxidatively damaged cells than in healthy cells, leading to

an earlier occurrence of band 3 auto-antibodies and earlier recognition by the immune system (Beppu *et al.*, 1990; Giribaldi *et al.*, 2001). This indicates that similar mechanisms remove G6PD deficient, infected RBCs as senescent and oxidatively stressed cells (Kay, 1984; Low *et al.*, 1985; Lutz *et al.*, 1988).

G6PD deficiency impacts not only a potential infection with malaria, but also the drug regime of infected, deficient patients. Primaquine is currently the only available drug that eliminates the hypnozoites of *P. vivax* and *P. ovale*. It is also able to rapidly sterilize mature gametocytes of *P. falciparum*. However, the main adverse effect is that it triggers dose-dependent hemolysis in G6PD deficient patients. The lack of sufficient testing for G6PD deficiency in malaria-endemic areas puts patients at risk of hemolysis if primaquine is applied, resulting in a current underuse of this drug (Recht *et al.*, 2018). Nevertheless in 2015, WHO recommended adding a single dose of primaquine (0.25 $mg \cdot kg^{-1}$) as a gametocytocide to the ACT for treating *P. falciparum* malaria. This dose effectively blocks transmission and is unlikely to cause severe adverse effects, regardless of the G6PD variants (Bancone *et al.*, 2016; WHO, 2015c).

1.2.1.2 Plasmodial glucose 6-phosphate dehydrogenase 6-phosphogluconolactonase

Structure and function of plasmodial GluPho

In 1994, O'Brien *et al.* isolated the gene for G6PD from *P. falciparum*. It is encoded on chromosome 14 and consists of one exon with 5.1 kb; the coding region has 2,730 bp with an AT content of 77.5% (O'Brien *et al.*, 1994). This is in accordance with the generally high AT composition (80.6%) of the plasmodial genome (Gardner *et al.*, 2002). The product consists of 910 amino acids with a molecular weight of 107 kDa per monomer (O'Brien *et al.*, 1994).

```
h      AASYQRLNS-------------------------------------------------     123
Pb     PESFENFDVYITQEERIALGCCGQKGNEKHKQVNVTSQFPNNHTSINII---NNIDNGCE     464
Pv     SESFERFNKYLTQLERENLIGTAPTS---WAAAAGNASFANDTDKVEHHPDEAILAKGTG     464
Pk     SESFEKFNKYLTQLEREDLVGVSNTI---WGEAAWKESFMNTAHSLELHSDEPNCEKGAS     464
Pf     SESFENFNKYLTTIEEEEAKKKYYAT---CYKMNGSD---------------YNISNNVA     472
Pm     SESFENFNKYLIEVEQEAHSNEYTCY----YNII----------------------GED     442
Po     PESFEKFNKYLNELEQEALASGFVDN----QKIFFQE---------------GNMKNGEE     449

h      ------------------------------------------------------------     123
Pb     SPMLTDSPKRYPCSSSYSSTSGTAVCPYSSQHDVKPSNNGCPYLSSQANTSDSSGCP-YI     524
Pv     A----ATPGEAPGGANGPA-----------THGEAHGGANGLST------PMQGKAVPTD     503
Pk     I----ATPVEVH-----------------------GDQGAPSI------PMQSNLSHTD     490
Pf     E-------------DNISI-----------DDEN--K-----TN------EYFQMCTPKN     495
Pm     K-------------SCSSD-----------LHKR--G-----TN------DEWSRCPPTD     465
Po     K-------------INGIP-----------NEDK--G-----EN------ELGKSAPTAN     472

h      -----HMNALHLGSQANRLFYLA    141
Pb     SYHTNKSGHLGCPYTITRMLYLA    547
Pv     DTSDEGHSGANHPFAINRILYLA    526
Pk     DTLDQVQSGTKCPFAINRVLYLA    513
Pf     CPDNVFSSNYNFPYVINRMLYLA    518
Pm     ATDV-AHSTANYTYVINRMLYLA    487
Po     SSED-NFSSYNHSYIANRMLYLA    494
```

Figure 4. Amino acid alignment of the insertion in the G6PD encoding region of different *Plasmodium* species
The insertion in the G6PD gene exists in all shown *Plasmodium* species; however, they differ in size and sequence (Clarke *et al.*, 2003). Conserved residues are indicated in gray. h: human (UniProtKB - P11413); *Pb*: *Plasmodium berghei* (PBANKA_1317500); *Pv*: *Plasmodium vivax* (PVX_117790); *Pk*: *Plasmodium knowlesi* (PKNH_1228300); *Pf*: *Plasmodium falciparum* (PF3D7_1453800); *Pm*: *Plasmodium malariae* (PmUG01_12063200); *Po*: *Plasmodium ovale* (PocGH01_12061100).

When discovered, this enzyme was noticeably much larger than G6PDs from other species known at that time. The C-terminal amino acids 310-910 have 39% homology to hG6PD. However, an insertion of 62 amino acids is not homologous (O'Brien *et al.*, 1994). This insertion is also found in other *Plasmodium* species; however, they differ in size and sequence (Figure 4) (Clarke *et al.*, 2003). Origin and function of the insertions are so far unknown. It has been shown for *P. berghei* that it is essential for the G6PD activity. Interestingly, after replacement of the *P. berghei* insertion with the insertion of *P. falciparum*, some of the *P. berghei* G6PD activity was preserved (Clarke *et al.*, 2003), although its original insertion is with 113 amino acids remarkably longer than the *P. falciparum* insertion with 62 amino acids (Figure 4). Further experiments need to be performed to fully understand the function of these insertions.

The function of the additional N-terminal amino acids was also unknown for a long time (O'Brien *et al.*, 1994; Shahabuddin *et al.*, 1994), but the enzyme was assumed to be bifunctional (O'Brien *et al.*, 1994; Scopes *et al.*, 1997). Clarke *et al.* could finally show in 2001 that the *P. berghei* enzyme, which has the same structure as the *P. falciparum* one, exerts both G6PD and 6PGL activity. It was thereby confirmed that a bifunctional enzyme combining glucose 6-phosphate dehydrogenase and 6-phosphogluconolactonase, called GluPho, catalyzes the first two steps of the PPP in *Plasmodium* (Clarke *et al.*, 2001; Jortzik *et al.*, 2011). Schematics of *Pf*GluPho and the human homologs are shown in Figure 5 (Preuss *et al.*, 2012b).

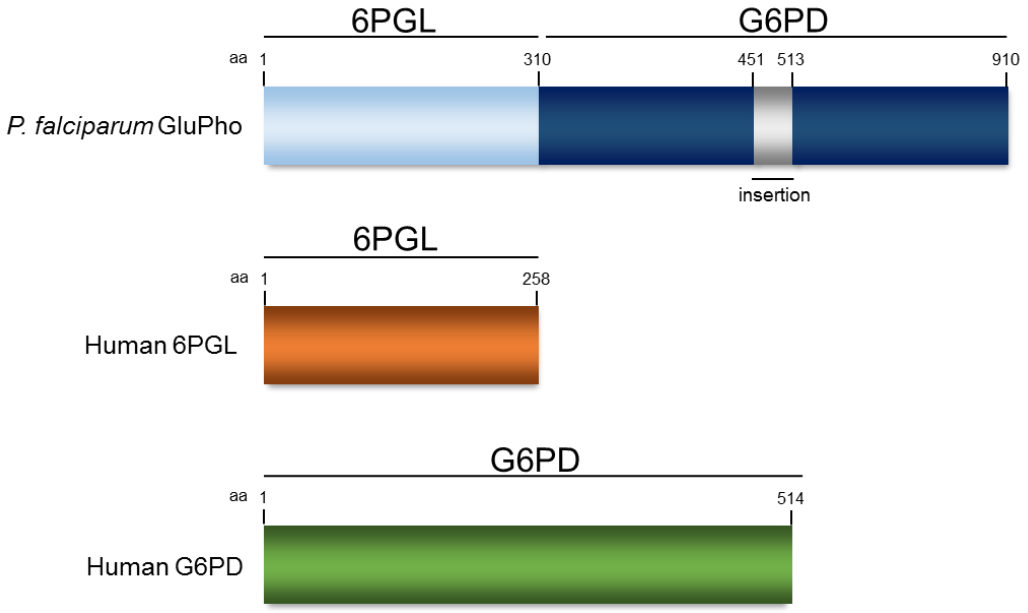

Figure 5. Schematics of *P. falciparum* glucose 6-phosphate dehydrogenase 6-phosphogluconolactonase and its human counterparts
In *P. falciparum*, the first two steps of the oxidative pentose phosphate pathway are catalyzed by the bifunctional enzyme GluPho that combines the G6PD and the 6PGL reaction; two distinct enzymes catalyze these reactions in human beings. The insertion in the G6PD part of *Pf*GluPho is specific for *Plasmodium*. The figure was modified after Preuss *et al.*, 2012b.

In accordance with *Pf*GluPho isolated from parasites (Ling and Wilson, 1988; O'Brien *et al.*, 1994), recombinant *Pf*GluPho is active in tetrameric form with a molecular mass of 443 kDa that is independent on the presence of substrates, product inhibitors, pH, or reducing agents. The G6PD activity of *Pf*GluPho most likely follows a rapid equilibrium random bi bi system,

meaning that both substrates have to bind before product formation occurs; however, there is no fixed order in which they have to bind (Jortzik *et al.*, 2011). In cocrystallization trials or inhibition studies, for example, this knowledge is of importance.

GluPho of *P. vivax* has not yet been characterized. The gene is located on chromosome 12, has only one exon with 2,784 bp, and encodes a protein with 927 amino acids (PlasmoDB PVX_117790). Regarding the primary sequences, *Pf*GluPho and *Pv*GluPho have 71.2% identical and 79.9% similar amino acids (Appendix 1), although there is a remarkable difference in AT content (80.6% in *P. falciparum*, 57.7% in *P. vivax* (Carlton *et al.*, 2008)).

Importance of GluPho for *Plasmodium* parasites

Prior to the validation of *Pf*GluPho as a drug target (see below), there had been several indications that this bifunctional enzyme was important for *Plasmodium* parasites. An initial indicator was that human G6PD deficiency leads to partial malaria resistance (see 1.2.1.1). Furthermore, the total activity of the oxidative PPP was noticeably 78-fold higher in infected RBCs than in healthy cells. The parasites were found to cause 82% of the PPP activity (Atamna *et al.*, 1994). Furthermore, RNA-mediated gene silencing of *Pf*GluPho resulted in an arrest of parasite growth at the trophozoite stage, increased gametocyte formation, and enhanced transcription of thioredoxin reductase (TrxR) (Crooke *et al.*, 2006). In 2015, attempted double crossover disruption of the gene for *Pf*GluPho finally proved this enzyme to be essential for the growth of asexual blood stage parasites, thereby validating it as a promising drug target (Allen *et al.*, 2015).

Naturally occurring *Pf*GluPho variants

Exposure to *Plasmodium* parasites for several hundred years has left marks on the human genome. One very prominent consequence — G6PD deficiency — has already been described above in detail (1.2.1.1). There are several other genetically encoded disorders that are associated with resistance to malaria such as sickle cell disease, thalassemia, hemoglobin C and E, pyruvate kinase deficiency, and the Duffy-negative phenotype (see 1.1.1) (Lopez *et al.*, 2010). However, not only does the human genome show signs of exposure to *Plasmodium* but also *vice versa*; during recent years, there have been extensive efforts to identify naturally occurring mutations in the plasmodial genome (Kirchner *et al.*, 2016; Neafsey *et al.*, 2008; Volkman *et al.*, 2007) that might increase the parasites' ability to deal with strong evolutionary selection pressure. Potentially, the mutations could lead to a failure of drug treatments (Haldar *et al.*, 2018) or resistance to the host's immune system. Analyzing these variations in detail will be a promising field for effective malaria surveillance and drug development (Kirchner *et al.*, 2016). Interestingly, several mutations in the gene that encodes GluPho have been identified while sequencing the plasmodial genome from the blood of malaria patients (PlasmoDB). Due to its central role in survival of the parasites (see above), these mutations might lead to improved parasitic resistance to oxidative stress and the host's immune system. We selected several of these naturally occurring *Pf*GluPho variants to investigate whether they lead to kinetic benefits compared to the wild type (wt) enzyme.

1.2.2 6-Phosphogluconate dehydrogenase

6PGD catalyzes the third step of the oxidative PPP. As described in 1.2, it decarboxylates its substrate 6PG to ribulose 5-phosphate while producing CO_2 and one molecule of NADPH (Stincone *et al.*, 2015). Consequently, it contributes as much NADPH as it does G6PD.

Human 6-phosphogluconate dehydrogenase

The gene for human 6PGD is located on chromosome 1 (band 1p36.22). The complete sequence has a size of 21.9 kb consisting of 18 exons and 18 introns and encodes a protein with 483 amino acids and 53.1 kDa per monomer (https://www.genecards.org/cgi-bin/carddisp.pl?gene=PGD). The enzyme is usually active in a dimeric form (Pearse and Rosemeyer, 1974b).

In contrast to the high prevalence of hG6PD deficiency (1.2.1.1), a deficiency of h6PGD is rather rare; only a few cases are known, the first having been described in 1964 (Brewer and Dern, 1964). However, if affected, the decreased enzyme activity can lead to clinical symptoms such as chronic non-spherocytic hemolytic anemia, jaundice, and decreased levels of reduced glutathione (Caprari *et al.*, 2001; Vives Corrons *et al.*, 1996).

Plasmodial 6-phosphogluconate dehydrogenase

The gene for *Pf*6PGD is located on chromosome 14. Similar to *Pf*GluPho and *Pv*GluPho, it has no introns. With a total length of 1,407 bp it encodes a protein of 468 amino acids (PlasmoDB PF3D7_1454700). Plasmodial 6PGD has not yet been characterized.

1.2.3 The role of NADPH for *Plasmodium* parasites

Maintaining cellular redox balance is essential for the malarial parasites to survive. This has already been indicated by the finding that G6PD deficiency — disturbing the redox balance — leads to partial resistance against malaria (see 1.2.1.1) (Becker *et al.*, 2004). The following section describes the sources of oxidative stress for the parasites and the role of NADPH in defending against this stress.

Sources of oxidative stress for *Plasmodium* parasites

During their complex life cycle with changing environments between *Anopheles* mosquitoes and the human host, *Plasmodium* parasites are continuously exposed to oxidative stress from different sources, including mosquitoes and human beings, but also from the parasites themselves (Becker *et al.*, 2004; Percario *et al.*, 2012). Reactive oxygen species (ROS) include, amongst many others, superoxide anions ($O_2\bullet^-$), hydroxyl radicals (•OH), hydrogen peroxide (H_2O_2), and singlet oxygen ($^1O_2$). At low concentrations, they serve as signaling molecules, while an excess can lead to severe oxidative damage to DNA, proteins, or lipids (Sharma *et al.*, 2012).

As described in 1.1.1, part of the plasmodial life cycle takes place in human erythrocytes, which contain large amounts of oxygen and iron; therefore, the conditions required for ROS formation via the Fenton reaction are endogenously given in these cells (Müller, 2004). The immune system of the human host reacts heavily to infection with the parasites, increasing phagocytosis of infected RBCs and parasites (Cappadoro *et al.*, 1998; Osier *et al.*, 2014) and producing larger amounts of reactive oxygen and nitrogen species. This plays a major role in the development of systemic complications in malaria patients (Becker *et al.*, 2004). Similarly, the immune system of *Anopheles* mosquitoes also reacts to the parasites. Ookinete invasion in the midgut leads to reduced detoxification of ROS through a lower expression of the mosquitoes' midgut catalase, resulting in increased exposure of the parasites to hydrogen peroxide (Molina-Cruz *et al.*, 2008). Furthermore, the parasites themselves produce large amounts of oxidative products due to their high metabolic rate. One central source of oxidative stress is the degradation of human hemoglobin by the parasites as their primary

source of nutrients (Becker *et al.*, 2004). Inside the food vacuole, hemoglobin is digested to amino acids, accompanied by the production of free heme. Most of the free heme is detoxified into crystalline hemozoin, also known as malaria pigment; however, small amounts escape neutralization, produce superoxide anions, hydroxyl radicals, and hydrogen peroxide, and are responsible for oxidative damage to DNA as well as lipid peroxidation (Atamna and Ginsburg, 1993; Egan *et al.*, 2002; Francis *et al.*, 1997).

Importance of NADPH for *Plasmodium* parasite survival

As a defense against oxidative stress, *Plasmodium* parasites have a complex antioxidative system located in several subcellular compartments (Kehr *et al.*, 2010). The major antioxidative systems — the glutathione and thioredoxin systems — dependent on the supply of NADPH as an electron donor (Gomez-Manzo *et al.*, 2016; Jortzik and Becker, 2012; Preuss *et al.*, 2012b). Therefore, the amount of NADPH (usually below 100 µM) exceeds the amount of $NADP^+$ under physiological conditions (Becker *et al.*, 2003; Wamelink *et al.*, 2008).

Tripeptide glutathione, consisting of glutamic acid, cysteine, and glycine, is the most abundant and important low molecular weight thiol in most living organisms (Dalle-Donne *et al.*, 2009). The reduced form (GSH) reaches a concentration of approximately 2 mM in the cytosol of the parasites, while the oxidized form (GSSG) generally has less than 10 µM (Becker *et al.*, 2003). Amongst other functions, GSH plays an essential role in detoxifying free, protein-bound, and membrane-associated heme by destroying the tetrapyrrole ring (Atamna and Ginsburg, 1995). Moreover, it scavenges radicals that can cause damages in human RBCs (Becker *et al.*, 2003; Dalle-Donne *et al.*, 2009). NADPH-dependent glutathione reductase (GR) is mainly responsible for reducing GSSG to GSH (Becker *et al.*, 2003; Jortzik and Becker, 2012). The finding that glutathione synthesis is essential for parasitic development in *P. berghei* underscores the glutathione system's importance to the parasites (Vega-Rodriguez *et al.*, 2009); a lack of GR leads to an arrest of parasitic development in the mosquito (Buchholz *et al.*, 2010; Pastrana-Mena *et al.*, 2010); in *P. falciparum*, a disruption of enzymes in the glutathione synthesis pathway has so far been unsuccessful, indicating an essential role in parasite development (Patzewitz *et al.*, 2012).

Thioredoxin (Trx) is a small, redox-active protein that functions as a cellular redox messenger. Using its CXXC active site motif, reduced *Pf*Trx is able to transfer reducing equivalents to target proteins such as thioredoxin-dependent peroxidases or GSSG. TrxR reduces thioredoxin using its CXXXXC motif in an NADPH-dependent manner (Jortzik and Becker, 2012; Kanzok *et al.*, 2000). In *P. falciparum*, there are three different isoforms of classic Trx, including cytosolic *Pf*Trx1 (Jortzik and Becker, 2012; Kehr *et al.*, 2010). Among its numerous functions, *Pf*Trx1 can directly fight against oxidative stress by detoxifying hydrogen peroxide (Rahlfs *et al.*, 2003) and reduce both GSSG and *S*-nitrosoglutathione (GSNO, see 1.3.2) (Kanzok *et al.*, 2000). *P. falciparum* parasites express one cytosolic and one mitochondrial isoform of TrxR, which also catalyze the reduction of a range of low molecular weight compounds in addition to Trx (Jortzik and Becker, 2012; Kehr *et al.*, 2010). TrxR of *P. falciparum* has been shown to be essential for the survival of intraerythrocytic parasites (Krnajski *et al.*, 2002).

The fact that two of the major antioxidative systems – both essential for *Plasmodium* parasites – depend on NADPH underscores the importance of the PPP as the primary source of this reducing equivalent (Preuss *et al.*, 2012b).

Alternative NADPH sources besides the pentose phosphate pathway

In addition to the PPP, there are also other enzymes in the metabolism that can produce NADPH. Some examples of cytosolic enzymes are the cytosolic isoforms of isocitrate dehydrogenase, glutamate dehydrogenase, methylenetetrahydrofolate dehydrogenase, and aldehyde dehydrogenase (Fan *et al.*, 2014; Lee *et al.*, 2002; Stincone *et al.*, 2015; Storm *et al.*, 2011; Wermuth *et al.*, 1977). Furthermore, *de novo* biosynthesis of NADPH through the phosphorylation of NAD^+/NADH, catalyzed by NAD kinases, has to be taken into account (Bieganowski *et al.*, 2006; Pollak *et al.*, 2007). NADPH is assumed to be unable to diffuse across membranes, highlighting the importance of compartment-specific NADPH recycling and *de novo* biosynthesis (Pollak *et al.*, 2007). Due to its cytosolic localization (in most organisms, see 1.2), the PPP contributes significantly to this NADPH pool. Human RBCs have neither a nucleus nor mitochondria, underscoring the importance of the PPP for these cells as their major source of NADPH (Beutler, 1994; Stincone *et al.*, 2015). *Plasmodium* parasites possess isocitrate dehydrogenase and glutamate dehydrogenase. In theory, these enzymes could significantly contribute to the NADPH supply (Werner *et al.*, 2005; Wrenger and Muller, 2003). However, the contribution from isocitrate dehydrogenase is still unclear. Glutamate dehydrogenase has been shown not to contribute much to the NADPH supply required for oxidative defense and to be dispensable for the parasite's asexual stage growth (Storm *et al.*, 2011). This supports the central role of *Pf*GluPho for the parasites (Allen *et al.*, 2015).

1.2.4 Pentose phosphate pathway as a drug target

The enzymes of the PPP are considered promising targets for treating different diseases. Well known and commonly used antimalarial drugs such as artemisinin exert their effects by disturbing the cellular redox balance (Cumming *et al.*, 1997; Kavishe *et al.*, 2017). The following chapter describes the potential of G6PD and 6PGD as promising antiparasitic and anticancer drug targets.

1.2.4.1 The pentose phosphate pathway as a target for antiparasitic drugs

The essential need for a sufficient supply of the electron donor NADPH to maintain the cellular redox balance of *Plasmodium* parasites has been described in 1.2.3. The oxidative PPP is the main source of NADPH for the parasites (Preuss *et al.*, 2012b; Stincone *et al.*, 2015); therefore, this pathway is considered a promising target for the development of new antimalarial drugs (Allen *et al.*, 2015).

*Pf*GluPho as a drug target

After several indications of the importance of *Pf*GluPho to the parasites (1.2.1), its essentiality for the survival of asexual blood stage parasites was finally proved in 2015 (Allen *et al.*, 2015). Moreover, there are major differences between the plasmodial enzyme and the human homologs, underscoring the applicability of *Pf*GluPho as a target for new antimalarial drugs (Allen *et al.*, 2015; Jortzik *et al.*, 2011). The most obvious structural difference is that in *Plasmodium*, the two enzymes that catalyze the G6PD and 6PGL reactions in the oxidative PPP are fused to the bifunctional GluPho, while two distinct enzymes in human beings catalyze these two steps (Figure 5) (Preuss *et al.*, 2012b). The structure of hG6PD is – in contrast to *Pf*GluPho and *Pv*GluPho – well known (Au *et al.*, 2000). *Pf*GluPho is active in a tetrameric form (Jortzik *et al.*, 2011), while hG6PD exists as a monomer, dimer, or tetramer depending on the ionic strength, pH, and presence of substrates (Wrigley *et al.*, 1972). One additional structural difference is the *Plasmodium*-specific insertion (Figure 4) that was shown to be essential for

the G6PD activity of *Pb*GluPho (Clarke *et al.*, 2003). Besides the structural differences, there are also some functional ones. *Pf*GluPho follows a rapid equilibrium, random bi bi mechanism, meaning both substrates have to bind before the product can begin to form. The binding order of the substrates is not fixed; however, they cannot bind simultaneously (Jortzik *et al.*, 2011). Human G6PD follows a rapid equilibrium, random order mechanism in which both substrate binding sites can act independently from each other (Wang *et al.*, 2002). Furthermore, the affinity of *Pf*GluPho to its substrates is higher than the affinity of the human counterparts (Jortzik *et al.*, 2011). Taken together, these differences enable the development of compounds that specifically inhibit the plasmodial enzyme.

*Pf*6PGD as a drug target

*Pf*6PGD contributes to the plasmodial supply of NADPH in the same amounts as *Pf*GluPho (Stincone *et al.*, 2015). By using RNA interference, 6PGD could be shown to be essential for the parasitic protozoan *Trypanosoma* (*T.*) *brucei*, which causes human African trypanosomiasis. One possible explanation is that the inhibition of 6PGD leads to the accumulation of the substrate 6PG, which inhibits the phosphoglucose isomerase, the key enzyme of glycolysis (Hanau *et al.*, 2004; Marchand *et al.*, 1989). Due to the connection of glycolysis to the PPP, inhibiting the isomerase will force more glucose into the PPP, resulting in a feedback loop with increasing 6PG concentrations and greater inhibition of glycolysis. Since the blood stages of the trypanosomes depend on energy production through glycolysis, this loop is expected to be lethal for the parasites (Hanau *et al.*, 2004). In *Saccharomyces* and *Drosophila*, simultaneous inhibition of G6PD could be shown to relieve the fatal effect of 6PGD inhibition, most likely because during G6PD inhibition, there is no accumulation of 6PG (Gvozdev *et al.*, 1976; Lobo and Maitra, 1982). Therefore, 6PGD is considered a promising target for drugs against African trypanosomes (Hanau *et al.*, 2004). However, it has so far not been possible to confirm *Pf*6PGD as a suitable target for the development of new antimalarial drugs.

1.2.4.2 The human pentose phosphate pathway as a target for anticancer drugs

Compared to healthy cells, cancer cells have altered requirements in their metabolism. The rapidly dividing cells have a great need for nucleic acid biosynthesis and the production of NADPH, which are essential for fatty acid synthesis, defense against oxidative stress, etc. Due to their accelerated metabolism, cancer cells are usually exposed to significantly higher concentrations of ROS than normal cells (Cho *et al.*, 2018; De Santis *et al.*, 2018; Patra and Hay, 2014). The PPP is responsible for generating the precursors to nucleic acid formation and is a major contributor to the supply of NADPH (Stincone *et al.*, 2015). Accordingly, both G6PD and 6PGD activity have been shown to increase in many cancer cells (Dutu *et al.*, 1980; Hong *et al.*, 2018; Jonas *et al.*, 1992). Thus, G6PD deficiency (1.2.1.1) is inversely correlated to cancer incidence and mortality (Cocco *et al.*, 1987; Dore *et al.*, 2016; Dore *et al.*, 2018). Cancer cells have developed various mechanisms to regulate the PPP in order to meet their needs; one example is modulating the tumor suppressor p53 (Patra and Hay, 2014). One of the physiological roles of p53 is to inhibit the expression of the glucose transporter genes for GLUT1 and GLUT4 (Schwartzenberg-Bar-Yoseph *et al.*, 2004). A loss of p53 enhances glucose uptake in cancer cells, thereby increasing the flux through glycolysis and the PPP and helping the cancer cells to survive. For this reason, modulation of p53 is common in many human cancer cell lines (De Santis *et al.*, 2018; Patra and Hay, 2014). Besides the inactivation of oncosuppressors, the activation of oncogenes can also lead to enhanced G6PD activity

(Tarrado-Castellarnau *et al.*, 2016). In addition to the role of the PPP during tumor development and growth, it also plays a role in tumor cells' resistance to cancer therapies. In response to ionizing radiation or chemotherapies, the levels of ROS increase, leading to an increase in PPP activity. This augmented activity reduces oxidative stress and can thereby lead to the cancer cells resisting the treatment (Patra and Hay, 2014). Accordingly, it has been shown that inhibition of either G6PD or 6PGD can reverse resistance to anticancer drugs (Hong *et al.*, 2018; Ma and Cheng, 2018; Zheng *et al.*, 2017).

These observations strongly indicate that a specific inhibition of both the G6PD and the 6PGD reaction could be promising strategies for anticancer therapy (Cho *et al.*, 2018; Elf *et al.*, 2017; Lin *et al.*, 2015). So far, only a few inhibitors for these enzymes are known (Jang *et al.*, 1997; Mele *et al.*, 2018; Preuss *et al.*, 2013). One example of a well-known hG6PD inhibitor is dehydroepiandrosterone (DHEA) (Gordon *et al.*, 1995; Schwartz *et al.*, 1986).

1.3 Post-translational protein modifications

Post-translational modifications (PTM) are important regulators of protein functions. They have fundamental control over various aspects such as gene expression, cell signaling and interactions between cells, protein trafficking, cell proliferation and differentiation, or enzyme localization, activity, and stability. Therefore, they play major roles in both physiological and pathophysiological events (Doerig *et al.*, 2015; Jortzik *et al.*, 2012). Although cysteine only accounts for 2% or less of the total amino acids in eukaryotic, eubacterial, and archaeal proteins (Pe'er *et al.*, 2004), it contributes significantly to biochemical reactions based on thiol-dependent catalysis due to its special chemical characteristics. It is able to form disulfide bonds that influence the structure of a protein, bind metal ions, and, importantly, it is able to mediate redox regulation and signaling reacting to the redox potential of the cells. Amongst many possible cysteine modifications, *S*-glutathionylation and *S*-nitrosation are two of the most prominent ones (Jortzik *et al.*, 2012).

1.3.1 Protein *S*-glutathionylation

As indicated in 1.2.3, glutathione has important antioxidative properties and is involved in the detoxification of various reactive oxygen species. The glutathione redox couple, i.e. GSH and GSSG, is one important regulator of redox-dependent cellular functions. Glutathione can mediate signaling processes to proteins by modifying the oxidation status of cysteines, the so-called *S*-glutathionylation. In this process, glutathione is reversibly bound to the thiol groups of cysteine residues, generating *S*-glutathionylated proteins (Becker *et al.*, 2003; Dalle-Donne *et al.*, 2009). The modification is favored to cysteine residues with a basic three-dimensional environment – caused, e.g., by positively charged arginine, histidine, or lysine residues in the proximity – and a therefore low pK_a value. The pK_a of cysteine thiols is typically around 8.5; however, it may vary between 3.5 and over 12, depending on the environment. A low pK_a value is often associated with a stable thiolate anion, thereby enabling the formation of *S*-glutathionylation (Zhang *et al.*, 2018).

There are several possible mechanisms for how the modification can be generated (Figure 6). Non-enzymatic possibilities include the thiol-disulfide exchange between reduced protein thiols and GSSG or GSNO, or direct interaction of GSH with oxidized protein intermediates such as *S*-nitrosyl, sulfenic acid, or a thiyl radical. Sulfenic acids are highly unstable and can be further oxidized to sulfinic acid, followed by the irreversible overoxidation to sulfonic acid

(Belcastro *et al.*, 2017; Jortzik *et al.*, 2012). Therefore, *S*-glutathionylation of sulfenic acids can protect the protein from irreversible deactivation (Zhang *et al.*, 2018). Moreover, the enzymes glutaredoxin and glutathione *S*-transferase (GST) can promote the modification. Glutaredoxin, sulfiredoxin, thioredoxin, GST, or free GSH can remove it (Jortzik *et al.*, 2012; Zhang *et al.*, 2018). As described above, during periods of oxidative stress, the modification protects thiols from irreversible oxidation and serves in addition as a storage form of GSH (Becker *et al.*, 2003; Dalle-Donne *et al.*, 2009).

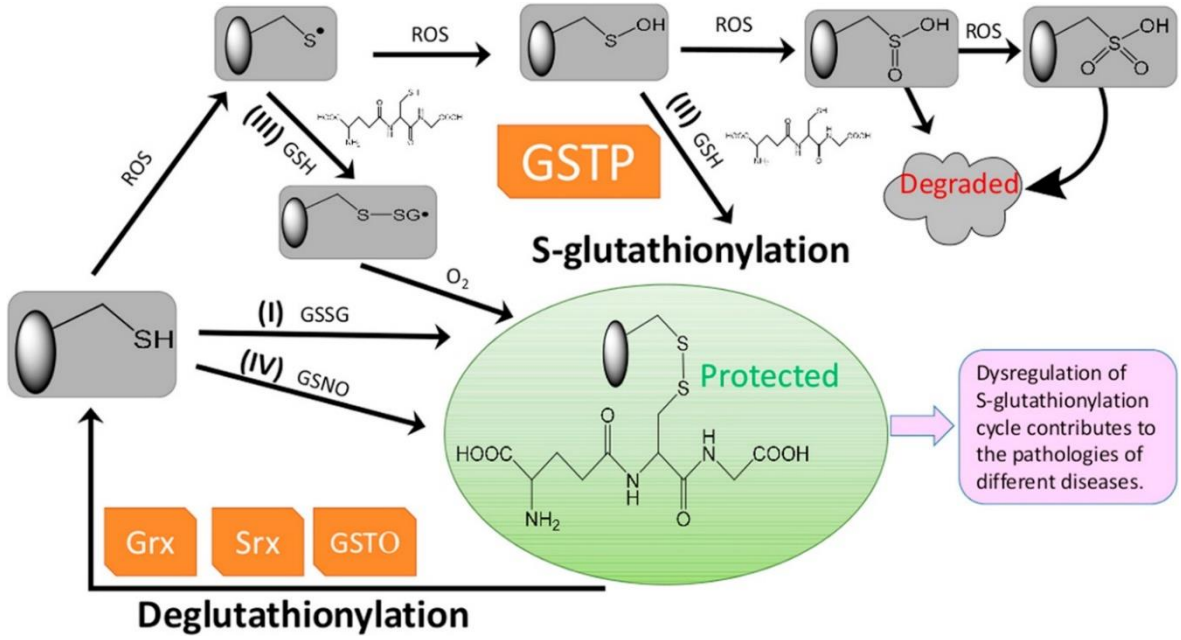

Figure 6. *S*-glutathionylation and deglutathionylation of proteins
S-glutathionylation can be mediated both non-enzymatically and enzymatically. For non-enzymatic reactions, there are the following possibilities: (I) Thiol-disulfide exchange can directly occur between a protein thiol (PSH) and glutathione disulfide (GSSG). (II) Reactive oxygen species (ROS) can oxidize PSH to sulfenic acid (PSOH) which can interact with reduced glutathione (GSH). This prevents the protein from irreversible overoxidation over sulfinic acid (SO_2H) to sulfonic acid (SO_3H) what would indicate an irreversible deactivation. (III) PSH can be oxidized to a thiyl radical (PS•) that is able to react with GSH to a thiyl radical glutathionyl intermediate (PSSG•). PSSG• can further react with O_2 to PSSG. (IV) In addition to GSSG, PSH can also react with *S*-nitrosoglutathione (GSNO) to PSSG. In addition, *S*-glutathionylation can also be mediated by enzymes such as the glutathione *S*-transferase P (GSTP). Deglutathionylation can conducted by glutaredoxin (Grx), sulfiredoxin (Srx), or the glutathione *S*-transferase omega (GSTO) (Zhang *et al.*, 2018).

In 2011, a large-scale proteomic approach was performed, identifying 493 targets of *S*-glutathionylation in *P. falciparum* (Kehr *et al.*, 2011). This means, even under physiological conditions, approximately 10% of the proteome from *P. falciparum* was found to be *S*-glutathionylated, underscoring the importance of this modification for the redox-regulatory mechanism (Jortzik *et al.*, 2012).

1.3.2 Protein *S*-nitrosation

Nitric oxide (NO) is a gaseous radical known to have important signaling functions in cellular metabolism. It is continuously synthesized from L-arginine by three isoforms of the nitric oxide synthase (NOS), the so-called endothelial NOS, the neuronal NOS, and the inducible NOS. NO is involved in numerous physiological processes such as platelet adhesion, vasorelaxation, endothelial regeneration, and inhibition of leukocyte chemotaxis. Furthermore, it plays a role

in pathophysiological events such as cardiovascular diseases (Belcastro *et al.*, 2017), cancer (Yarlagadda *et al.*, 2017), and degenerative diseases (Zhang *et al.*, 2017). During their life cycle, *Plasmodium* parasites encounter nitrosative stress derived from the human host and *Anopheles* mosquitoes since the production of NO is part of the immune system (Ferrari *et al.*, 2011; Jeney *et al.*, 2014; Peterson *et al.*, 2007b). The expression of NOS due to, e.g., hemozoin formation (Akman-Anderson *et al.*, 2007; Jaramillo *et al.*, 2003) can lead to inflammatory levels of NO deteriorating the development of the parasites (Luckhart *et al.*, 1998; Peterson *et al.*, 2007b). In the human host, *Plasmodium* infection leads to the expression of the inducible NOS in macrophages, contributing to the clearance of the parasites from RBCs (Ranjan *et al.*, 2016). Under physiological conditions, NO concentrations are low (around 10 nM). However, activation of the inducible NOS in response to pathophysiological processes can result in concentrations over 1 µM (Belcastro *et al.*, 2017).

Protein *S*-nitrosation is defined as the reversible addition of a nitrosyl group to a reactive cysteine thiol of a protein, resulting in a protein *S*-nitrosothiol (Jortzik *et al.*, 2012). In many publications, this process is described as *S*-nitrosylation; however, technically speaking, *S*-nitrosylation means the coordination of NO to transition metal ions in enzymes (Belcastro *et al.*, 2017). Therefore, the covalent bond between NO and cysteines is called *S*-nitrosation in this thesis. As described above (1.3), the modification can have various impacts on the properties of the affected protein. The NO moiety can be removed both enzymatically (e.g. via GSNO reductase and superoxide dismutase) and nonenzymatically (via thioredoxin and glutathione). In addition to the direct reaction of the nitrosyl group with cysteine thiols, *S*-nitrosation can occur via the transfer of NO from one *S*-nitrosated protein to another protein thiol, called transnitrosation (Jortzik *et al.*, 2012). A naturally occurring low molecular weight *S*-nitrosothiol is GSNO (Broniowska *et al.*, 2013). There are several possibilities for how GSNO can be generated, e.g., through the degradation of protein *S*-nitrosothiols by glutathione (Benhar *et al.*, 2009; Broniowska *et al.*, 2013). In addition to its reactivity with cysteine thiols, GSNO is able to transnitrosate proteins (Broniowska *et al.*, 2013).

1.3.3 Protein phosphorylation

Protein phosphorylation is one of the most important regulators of cellular functions. It is defined as the covalent attachment of a phosphate group to a target molecule (Doerig *et al.*, 2015). However, since this modification was not a major subject of this study, this section should only give a short overview.

Protein kinases and phosphatases are mediators of reversible protein phosphorylation, mediating changes to central cellular functions such as proliferation and differentiation of cells, as well as cell migration and homeostasis, e.g., by modifying enzyme activities. In eukaryotes, the targets of protein kinases are usually serine, threonine, or tyrosine – residues that have an alcohol group; however, histidine and aspartic acid can also be phosphorylated, especially in prokaryotes (Doerig *et al.*, 2015).

To study phosphorylation it is possible to mimic this modification by mutation of the respective residue to glutamic acid (Kim *et al.*, 2015).

1.4 Objectives of the study

Malaria is still one of the world's most deadly infectious diseases, causing almost half a million deaths per year (WHO, 2017b). Effective treatment of the disease is threatened by increasing resistance of *Plasmodium* strains to commonly used drugs; therefore, there is an urgent need to characterize new drug targets and develop new antimalarial drugs (Ashley *et al.*, 2018; WHO, 2017b).

Plasmodium parasites are continuously exposed to oxidative stress from different sources; maintaining the cellular redox balance is crucial for their survival. Some antimalarial drugs that act by increasing oxidative stress are already being used (Becker *et al.*, 2004). The most important antioxidative systems of *Plasmodium* parasites depend on NADPH as an electron donor (Jortzik and Becker, 2012; Mohring *et al.*, 2014). Since the oxidative PPP is the major source of NADPH for the parasites, it seems reasonable that inhibiting this pathway might be an effective strategy for new antimalarial drugs (Allen *et al.*, 2015; Haeussler *et al.*, 2018). There are two NADPH-producing steps in the oxidative PPP which are considered potential targets for new antimalarial drugs: the G6PD reaction, catalyzed in *Plasmodium* by the bifunctional GluPho (Jortzik *et al.*, 2011), and the 6PGD reaction (Haeussler *et al*., 2018).

The two most detrimental *Plasmodium* species are *P. falciparum* and *P. vivax* (Ashley *et al.*, 2018). However, due to its usually mild course of infection, *P. vivax* has been underestimated for many years (Cowman *et al.*, 2016). Moreover, long-term *in vitro* cultivation of blood stage *P. vivax* parasites is still not possible (Thomson-Luque *et al.*, 2017). Therefore, limited information on *P. vivax* is available. The redox system of *P. vivax* shows high homologies to *P. falciparum*, including the presence of a bifunctional GluPho in the PPP (Mohring *et al.*, 2014). *Pf*GluPho has already been characterized, and a first set of inhibitors has been identified (Jortzik *et al.*, 2011; Preuss *et al.*, 2012a). In contrast, there was no information on *Pf*6PGD and *Pv*GluPho/*Pv*G6PD in the literature. Attempts to transfer our knowledge of the *P. falciparum* redox system and its inhibitors to *P. vivax* can therefore be very valuable in facilitating drug discovery against *vivax* malaria. The aim of this thesis was to address the following topics:

- Recombinant production, purification, and characterization of naturally occurring *Pf*GluPho variants, *Pf*6PGD wt and mutants, h6PGD, and *Pv*GluPho/*Pv*G6PD
- Crystallization of *Pf*GluPho and *Pf*6PGD to solve their three-dimensional structures and to enable structure-based drug design and optimization
- Investigation of the impact of two post-translational modifications – *S*-glutathionylation and *S*-nitrosation – on *Pf*GluPho, *Pf*6PGD, and *Pv*G6PD
- Characterization of compounds optimized for *Pf*GluPho and identification of inhibitors for *Pf*6PGD and *Pv*G6PD

2 Materials

2.1 Instruments

Instrument	Company
Äkta FPLC system (pump P-920, monitor UPC-900, injection valve INV-907, mixer M-925, fraction collector Frac-900, column material Superdex 200 prep grade)	GE Healthcare, Freiburg
Autoclave	Webeco, Bad Schwartau
Autoclave VX-95	Systec, Wettenberg
BioRAPTR Microfluidic Workstation	Beckman Coulter, Brea, CA, USA
BioSpectrometer basic	Eppendorf, Hamburg
Centrifuge 5415R	Eppendorf, Hamburg
Centrifuge Megafuge 1.0 R	Heraeus Instruments, Hanau
Centrifuge MiniSpin	Eppendorf, Hamburg
Centrifuge Sorvall RC 6+ (rotor SS-34 and F9S-4x1000y)	Thermo Scientific, Dreieich
CLARIOstar plate reader	BMG Labtech, Ortenberg
Crystallization robot Honeybee 961 (peristaltic pump Masterflex® US®, vacuum pump 6035A080-02)	Digilab, Marlborough, MA, USA
Dry block heater 2	IKA®-Werke, Staufen im Breisgau
Echo 555 Liquid Handler	Labcyte, San Jose, CA, USA
Electrophoresis Chamber B1, B1A, B2	Owl Separation System Inc., Portsmouth, NH, USA
Electrophoresis Chamber Mini-PROTEAN 3 cell	Bio-Rad, Munich
Electrophoresis Power Supply-EPS 200	Pharmacia Biotec, Dübendorf Switzerland
Electroporator Gene Pulser Xcell	Bio-Rad, Munich
Evolution™ 300 UV-Vis-Spectrophotometer	Thermo Scientific, Dreieich
FAS Digi Gel Imaging System	Nippon Genetics, Düren
Heating block neoBlock II	neoLab, Heidelberg
Heating block Thermomixer comfort	Eppendorf, Hamburg
High-purity water system OPTILAB-Plus	MembraPure, Henningsdorf
Icemaker F80C	Icematic Deutschland, Meerbusch
Incubation shaker KS 500	Junke & Kunkel, IKA®-Werke, Staufen im Breisgau
Incubation shaker SM25	Edmund Bühler GmbH, Tübingen
Incubation system (incubator: CERTOMAT® H, shaker: CERTOMAT® R)	B. Braun, Melsungen
Incubation system (incubator: mytron, shaker: Orbital)	Thermo Scientific, Dreieich
Incubator shaker Innova® 44	Eppendorf, Hamburg
Intas ECL ChemoStar	Intas Science Imaging Instruments GmbH, Göttingen
Magnetic stirrer CAT M15	MAGV Laborbedarf, Rabenau-Londorf
Magnetic stirrer color squid	IKA®-Werke, Staufen im Breisgau

Magnetic stirrer HI 300N	Hanna Instruments, Kehl am Rhein
Magnetic stirrer RCTbasic	IKA®-Werke, Staufen im Breisgau
Microprocessor pH Meter	Knick, Berlin
Multichannel pipette Discovery 1-10 µL	HTL Lab Solutions, Warsaw, Poland
Multichannel pipette Discovery 20-200 µL	HTL Lab Solutions, Warsaw, Poland
Multichannel pipette Transferpette S-12	Brand GmbH, Wertheim
Multidrop™ Combi Reagent Dispenser	Thermo Fisher Scientific, Waltham, MA, USA
OptiMax X-ray Processor	M&S Laborgeräte, Wiesloch
PCR cycler Mastercycler	Eppendorf, Hamburg
PCR cycler Mastercycler gradient	Eppendorf, Hamburg
Peltier Cryobath System TPS 1500 W	Thermo Scientific, Dreieich
PHERAstar FS microplate reader	BMG Labtech, Cary, NC, USA
Pipette Eppendorf Research plus	Eppendorf, Hamburg
Pipette Gilson Pipetman P10, P20, P100, P200, P1000	Gilson, Middleton
Pipetting robot Lissy	Zinsser Analytic, Frankfurt
Power Pac 300 and 1000	Bio-Rad, Munich
Precision scale ABT 120-5 DM	Kern & Sohn, Balingen
Rotilabo®-X-ray-cassette	Roth, Karlsruhe
Scale 440-47N	Kern & Sohn, Balingen
Scale 474-32	Kern & Sohn, Balingen
Shaker KS 500	IKA®-Werke, Staufen im Breisgau
Shaker Unimax 2010	Heidolph Instruments, Schwabach
Spectrophotometer Beckman DU 650	Thermo Scientific, Dreieich
Spectrophotometer BioPhotometer	Eppendorf, Hamburg
Stereomicroscope SMZ1000	Nikon GmbH, Düsseldorf
Stereomicroscope system (M165 C, KL 1500 LED, camera EC 3	Leica Microsystems, Wetzlar
Tecan Infinite M200 multiplate reader	Tecan, Männedorf, Switzerland
TPS 1500W Peltier Cryobath System Recirculator	Thermo Scientific, Dreieich
Trans-Blot® Turbo™ Transfer System	Bio-Rad, Munich
Ultrasound homogenizer Sonoplus HD 2070	Bandelin electronic, Berlin
Ultrasound waterbath Sonorex RK100	Bandelin electronic, Berlin
Vacuum pump Vacubrand CVC 3000	VWR, Darmstadt
Viewlux plate reader	Perkin Elmer, Waltham, MA, USA
Vortex mixer MS2 Minishaker	IKA®-Werke, Staufen im Breisgau
Western blot Trans-Blot® SD semi-dry transfer cell	Bio-Rad, Munich

2.2 Chemicals

All chemicals used were of the highest purity available.

Chemical	Company
1,2-Propanediol	Sigma-Aldrich, Steinheim
1,4-Dithiothreitol (DTT)	Roth, Karlsruhe
2-Methyl-2,4-pentanediol (MPD)	Roth, Karlsruhe
6-Aminohexanoic acid	Merck, Darmstadt
6PG	Sigma, Steinheim
Acetic acid	Roth, Karlsruhe
Acrylamide/Bisacrylamide (Rotiphorese Gel 30 (37.5:1))	Roth, Karlsruhe
Agar-agar	Roth, Karlsruhe
Agarose (peqGold Universal Agarose)	Roth, Karlsruhe
Ammonium acetate	Roth, Karlsruhe
Ammonium dihydrogen phosphate	Sigma, Steinheim
Ammonium persulfate (APS)	Roth, Karlsruhe
Ammonium phosphate	Sigma, Steinheim
Ammonium sulfate	Roth, Karlsruhe
Betaine	Sigma, Steinheim
Bicine	Roth, Karlsruhe
Bis-Tris	Roth, Karlsruhe
Bovine serum albumin (BSA)	Roth, Karlsruhe
Calcium chloride	Applichem, Darmstadt
Carbenicillin	Roth, Karlsruhe
Chloramphenicol	Roth, Karlsruhe
Coomassie Brilliant Blue R250	Sigma, Steinheim
Coumaric acid	Sigma, Steinheim
Cystatin	Sigma, Steinheim
Dimethyl sulfoxide (DMSO)	Roth, Karlsruhe
Dipotassium phosphate	Roth, Karlsruhe
DNA-Dye NonTox	Applichem, Darmstadt
Ethanol	Roth, Karlsruhe
Ethylenediaminetetraacetic acid (EDTA)	Roth, Karlsruhe
Ethylene glycol	Roth, Karlsruhe
FOScholine®12	Cube Biotech GmbH, Monheim am Rhein
G6P	Sigma, Steinheim
Glutathione (GSH)	Sigma, Steinheim
Glutathione disulfide (GSSG)	Sigma, Steinheim
Glycerol	Roth, Karlsruhe
Glycyl-glycyl-glycine (Gly-Gly-Gly)	Sigma, Steinheim
Hepes	Roth, Karlsruhe
Hydrochloric acid (fuming, 37%)	Roth, Karlsruhe
Hydrogen peroxide	Roth, Karlsruhe
Imidazole	Roth, Karlsruhe
Iodoacetyl-PEG2-biotin	Thermo Scientific, Dreieich
Iodoacteamide (IAA)	Sigma, Steinheim

Isopropanol	Roth, Karlsruhe
Isopropyl-β-D-1-thiogalactopyranoside (IPTG)	Roth, Karlsruhe
Kanamycin sulfate	Roth, Karlsruhe
Lithium chloride	Roth, Karlsruhe
Lithium nitrate	Roth, Karlsruhe
Luminol	Sigma, Steinheim
Magnesium chloride	Sigma, Steinheim
MES	Roth, Karlsruhe
Methanol	Roth, Karlsruhe
Milk powder	Roth, Karlsruhe
MME 550	Fluka
Monopotassium phosphate	Roth, Karlsruhe
MOPS	Roth, Karlsruhe
N,N,N',N'-Tetramethylethylenediamine (TEMED)	Sigma, Steinheim
N,N-Dimethyldodecylamine N-oxide	Cube Biotech GmbH, Monheim am Rhein
$NADP^+$	Biomol, Hamburg
NADPH	Biomol, Hamburg
n-Decyl-β-D-maltopyranoside	Cube Biotech GmbH, Monheim am Rhein
n-Dodecyl-β-D-maltoside	SERVA Electrophoresis GmbH, Heidelberg
Neocuproine	Aldrich, Steinheim
N-Ethylmaleimide (NEM)	Sigma, Steinheim
Nicotinamide adenine dinucleotide (NAD^+)	Biomol, Hamburg
Ni-NTA agarose	Invitrogen, Karlsruhe
n-Octyl-β-D-glucopyranoside	Cube Biotech GmbH, Monheim am Rhein
PEG (polyethylene glycol) 1,500	Roth, Karlsruhe
PEG 3,350	Sigma-Aldrich, Steinheim
PEG 4,000	Roth, Karlsruhe
PEG 400	Roth, Karlsruhe
PEG 6,000	Roth, Karlsruhe
PEG 600	Aldrich, Steinheim
PEG 8,000	Roth, Karlsruhe
Pepstatin A	Sigma, Steinheim
Phenylmethanesulfonyl fluoride (PMSF)	Roth, Karlsruhe
Polyethylene glycol sorbitan monolaurate (TWEEN 20)	Sigma, Steinheim
Ponceau S	Sigma, Steinheim
Potassium chloride	Roth, Karlsruhe
Potassium citrate	Roth, Karlsruhe
Resazurin	Sigma, St. Louis, MO, USA
S-Nitrosoglutathione (GSNO)	Sigma-Aldrich, Steinheim
Sodium acetate	Roth, Karlsruhe
Sodium ascorbate (NaAsc)	Sigma, Steinheim
Sodium bromide	Sigma, Steinheim
Sodium chloride	Roth, Karlsruhe
Sodium citrate	Roth, Karlsruhe
Sodium dodecyl sulfate (SDS)	Sigma, Steinheim

Sodium hydroxide	Roth, Karlsruhe
Talon Metal Affinity Resin	Clontech, Takara Bio Europe SAS, Saint-Germain-en-Laye, France
Trichloroacetic acid (TCA)	Sigma, Steinheim
Tris-(hydroxymethyl)-aminomethan (Tris)	Roth, Karlsruhe
Tris-HCl	Roth, Karlsruhe
Triton X-100	Roth, Karlsruhe
Tryptone/Peptone	Roth, Karlsruhe
Xylitol	Sigma, Steinheim
Yeast extract	Oxoid, Basingstroke, England

Inhibitor	**Source**
Coruleoellagic acid (CEA)	Kindly provided by Herbert Zimmermann, Heidelberg
Ellagic acid (EA)	Sigma-Aldrich, Steinheim
Flavellagic acid (FEA)	Kindly provided by Herbert Zimmermann, Heidelberg
ML304	Kindly provided by Anthony Pinkerton, La Jolla, CA, USA
MMV Malaria Box	Medicines for Malaria Venture (MMV), Geneva, Switzerland
Novel G6PD inhibitors	Kindly provided by Dieter E. Kaufmann, Clausthal-Zellerfeld
SBI-0797750 and derivatives	Kindly provided by Anthony Pinkerton, La Jolla, CA, USA

2.3 Consumables

Consumable	**Company**
Cannula 0.7 x 50 mm	Unimed, Lausanne, Switzerland
Chemiluminescence film Amersham hyperfilm™ ECL	GE Healthcare, Freiburg
Clear tape HDClear	ShurTec Brands, Avon, OH, USA
Cover slips, round 21 mm Ø	Menzel, Brunswick
Crystallization plate 24 well, Cryschem™ M plate	Hampton Research, Aliso Viejo, CA, USA
Crystallization plate 24 well, VDX plate	Hampton Research, Aliso Viejo, CA, USA
Crystallization plate 96 well, MRC 2 well	Jena Bioscience, Jena
DNA ladder GeneRuler 1 kb	Thermo Scientific, Dreieich
Echo qualified 384 low dead volume microplate	Labcyte, San Jose, CA, USA
Falcon™ tube 15 mL, 50 mL	Greiner Bio-One, Frickenhausen
Filter holders 0.2 µM	Whatman GmbH, Dassel
Masterblock 96 well, PP, V-bottom	Greiner Bio-One, Frickenhausen
Membrane filter ME 25, 0.45 µM	Whatman GmbH, Dassel
Micropipettes 5 µL, 10 µL	Brand GmbH, Wertheim
Microplate 1,536-well, PS, solid bottom, black	Corning, Corning, NY, USA
Microplate 384-well, PP, flat bottom, natural	Greiner Bio-One, Frickenhausen
Microplate 384-well, PP, V-bottom, natural	Greiner Bio-One, Frickenhausen

Microplate 96-well, PP, half area, flat bottom, transparent	Greiner Bio-One, Frickenhausen
Microplate 96-well, PP, V-bottom, transparent	Greiner Bio-One, Frickenhausen
Microscope lens paper	Glaswarenfabrik Karl Hecht, Sondheim
Multiply PCR tube 0.2 mL	Sarstedt, Numbrecht
Nitrocellulose blotting membrane, 0.45 µm	GE Healthcare, Freiburg
Parafilm 'M' laboratory film	Bemis, Neenah, WI, USA
Pasteur pipette 150 mm	Hirschmann Laborgeräte, Eberstadt
Petri dish, 15 cm Ø	Sarstedt, Numbrecht
Pipette tips and tubes, disposable	Eppendorf, Hamburg
Pipette tips Omnitip™ FastRack 10 µL, 200 µL	Ulplast, Warsaw, Poland
Plate sealer EASYseal™, clear	Greiner Bio-One, Frickenhausen
Plate sealer SILVERseal	Greiner Bio-One, Frickenhausen
Precision wipes tissue	Kimberly-Clark GmbH, Koblenz
Protein ladder Unstained Protein Molecular Weight Marker	Thermo Scientific, Dreieich
Restore Plus Western Blot Stripping Buffer	Thermo Scientific, Dreieich
Roti®-PVDF membrane	Roth, Karlsruhe
Semi-micro cuvettes, polystyrol	Sarstedt, Numbrecht
Serological pipette 5 mL, 10 mL, 25 mL	Greiner Bio-One, Frickenhausen
Silicone oil 550	Merck, Darmstadt
Syringe 1 mL Plastipak™	Becton Dickinson, Madrid, Spain
Syringe 10 mL	B. Braun, Melsungen
UV-Cuvettes micro	Brand GmbH, Wertheim
Vivaspin 20,000 MWCO, 30,000 MWCO	Sartorium Stedim Biotech, Göttingen
Zeba™ Spin Desalting Columns, 7 K MWCO, 0.5 mL, 2 mL	Thermo Scientific, Dreieich

2.4 Biological materials

2.4.1 Vectors

Vector	Antibiotic resistance	Company
pET28a(+)	Kanamycin	Novagen, Darmstadt
pQE30	Carbenicillin	Qiagen, Hilden
pRAREII	Chloramphenicol	Novagen, Darmstadt
pBluescript SK (+)	Carbenicillin	Stratagene, San Diego, CA, USA

2.4.2 *E. coli* strains

E. coli strain	Genotype	Source
BL21 (DE3)	F'-*omp*T *hsd*S_B (r_B-m_B-) *gal dcm* (DE3)	Invitrogen, Karlsruhe
C41 (DE3)	F^{-} ompT gal hsdS_B ($r_B^-m_B^-$) dcm lon (DE3)	Avidis SA, St. Beauzire, France

C43 (DE3)	F^{-} ompT gal $hsdS_B$ ($r_B^- m_B^-$) dcm lon (DE3)	Avidis SA, St. Beauzire, France
KRX	[F', *tra*D36, Δ*omp*P, *pro*A^+B^+, *lac*Iq, Δ(*lac*Z)M15] Δ*omp*T, *end*A1, *rec*A1, *gyr*A96 (Nal^r), *thi*-1, *hsd*R17 (r_k^-, m_k^+), $e14^-$ ($McrA^-$), *rel*A1, *sup*E44, Δ(*lac-pro*AB), Δ(*rha*BAD)::T7 RNA polymerase	Promega, Mannheim
Lemo21 (DE3)	*fhuA2 [lon] ompT gal (λ DE3) [dcm] ΔhsdS/ pLemo*(Cam^R) *λ DE3 = λ sBamHIo ΔEcoRI-B int::(lacI::PlacUV5::T7 gene1) i21 Δnin5* pLemo = pACYC184-*PrhaBAD-lysY*	New England Biolabs, Frankfurt am Main
M15	F-, Φ80ΔlacM15, thi, lac^-, mtl^-, $recA^+$, KmR	Qiagen, Hilden
SHuffle T7	F' *lac*, *pro*, *lacI*^{q} / *Δ(ara-leu)7697 araD139 fhuA2 lacZ::T7 gene1 Δ(phoA)PvuII phoR ahpC* galE (or U) galK λatt*::pNEB3-r1-*cDsbC* ($Spec^R$, *lacI*^{q}) *ΔtrxB rpsL150*(Str^R) *Δgor Δ(malF)3*	New England Biolabs, Frankfurt am Main
SHuffle T7 Express	*fhuA2 lacZ::T7 gene1* [lon] *ompT ahpC gal λatt*::pNEB3-r1-*cDsbC* ($Spec^R$, *lacI*^{q}) Δ*trxB sulA11 R(mcr-73::miniTn10*--Tet^S)2 [dcm] *R(zgb-210::Tn10* --Tet^S) *endA1 Δgor Δ(mcrC-mrr)114::IS10*	New England Biolabs, Frankfurt am Main
XL1-Blue	*rec*A1 *en*dA1 *gyr*A96 *thi*-1 *hsd*R17 *sup*E44 *rel*A1 *lac* [F' *pro*AB *lac*I^q *ZΔM*15 Tn*10* (Tet^r)]	Stratagene, Amsterdam, The Netherlands

2.4.3 Antibodies

Antibody	Company
Anti-glutathione monoclonal antibody	Virogen, Watertown, MA, USA
Anti-6xHis-tag monoclonal antibody	Dianova, Hamburg
Horseradish peroxidase (HRP) anti-mouse antibody	Thermo Scientific, Dreieich
Monoclonal biotin antibody (33): sc-101339	Santa Cruz Biotechnology, Dallas, TX, USA

2.4.4 Enzymes

Restriction enzyme	Restriction site	Company
*BamH*I	5'...G^GATCC...3'	Thermo Scientific, Dreieich
*Dpn*I	5'...GA^{CH3}^ATTC...3'	Thermo Scientific, Dreieich
*Hind*III	5'...A^AGCTT...3'	Thermo Scientific, Dreieich
*Sal*I	5'...G^TCGAC...3'	Thermo Scientific, Dreieich

Enzymes for molecular biology	Function	Company
T4-DNA ligase	Nucleotide fragment ligation	Thermo Scientific, Dreieich
Pfu DNA polymerase	DNA amplification	Promega, Mannheim
RedTaq® polymerase	DNA amplification	Sigma, Steinheim

Other enzymes	Function	Company
Diaphorase from *Clostridium klyveri*	Enzyme assay, reduction of resazurin	Sigma, St. Louis, MO, USA
DNaseI	DNA digestion	Roche, Mannheim
Lysozyme	Cell lysis	Sigma, Steinheim

2.4.5 Oligonucleotides

Primers for cloning of *Pv*GluPho and *Pv*G6PD	
OPvGPN	5'-atatGGATCCGATTGCCAGGCGCTGGCGAA-3'
OPvGPC	5'-atatGTCGACTCAGTTGATGTCCAACAAGTCGT-3'
*Pv*G6PDs	5'-CGGGATCCCTGAATAGGAGGGAATGCCTA-3'
*Pv*G6PDas	5'-atatGTCGACTCAGTTGATGTCCAACAAGTCGT-3'

Primers for site-directed mutagenesis	
*Pf*GluPho^{S899E}s	5'-CTGAGTTTGTTAGAAAAGAGTCTTTTTATGAAGACGATT-3'
*Pf*GluPho^{S899E}as	5'-AATCGTCTTCATAAAAAGACTCTTTTCTAACAAACTCAG-3'
*Pf*GluPho^{S900E}s	5'-CTGAGTTTGTTAGAAAATCCGAATTTTATGAAGACGATT-3'
*Pf*GluPho^{S900E}as	5'-AATCGTCTTCATAAAATTCGGATTTTCTAACAAACTCAG-3'
*Pf*GluPho^{S315Y}s	5'-AAAATTATACAAAATATATTGAAGAAATTTATG-3'
*Pf*GluPho^{S315Y}as	5'-CATAAATTTCTTCAATATATTTTGTATAATTTT-3'
*Pf*GluPho^{L395F}s	5'-ATAGTTATATATTTCAAACGATGTTTATTATG-3'
*Pf*GluPho^{L395F}as	5'-CATAATAAACATCGTTTGAAATATATAACTAT-3'
*Pf*GluPho^{F507L}s	5'-TCATCAAATTATAATTTGCCATATGTTATAAA-3'
*Pf*GluPho^{F507L}as	5'-TTTATAACATATGGCAAATTATAATTTGATGA-3'
*Pf*6PGD^{W104L}s	5'-GCGGCAACGAATTGTATATCAACTCT-3'
*Pf*6PGD^{W104L}as	5'-AGAGTTGATATACAATTCGTTGCCGC-3'
*Pf*6PGD^{C281S}s	5'-TGCCCGACGATGTCTGCTGCGTTAGAT-3'
*Pf*6PGD^{C281S}as	5'-ATCTAACGCAGCAGACATCGTCGGGCT-3'

2.5 Buffers and Solutions

2.5.1 Stock solutions

Solution	Concentration	Solved in	Storage
APS	10% (w/v)	$_{dd}H_2O$	-20 °C
Carbenicillin	50 mg·mL^{-1}	50% (v/v) Ethanol	-20 °C
Chloramphenicol	35 mg·mL^{-1}	100% Ethanol	-20 °C
Cystatin	40 µM	$_{dd}H_2O$	-20 °C
IPTG	1 M	$_{dd}H_2O$, sterile filtrated	-20 °C
Kanamycin	25 mg·mL^{-1}	$_{dd}H_2O$, sterile filtrated	-20 °C
Pepstatin A	300 µM	DMSO	-20 °C
PMSF	100 mM	DMSO	-20 °C
SDS	10% (w/v)	$_{dd}H_2O$	-20 °C

2.5.2 Buffers for chemocompetent *E. coli* cells

Buffer	Composition	
TFB1 buffer for chemocompetence	100 mM	Rubidium chloride
	50 mM	Manganese chloride
	30 mM	Potassium acetate
	10 mM	Calcium chloride
	15%	Glycerol
	pH 5.8	
TFB2 buffer for chemocompetence	10 mM	MOPS
	10 mM	Rubidium chloride
	75 mM	Calcium chloride
	pH 8.0	

2.5.3 Medium for bacterial cell culture

Medium	Composition	
Lysogeny broth (LB)	10 g	Tryptone
	5 g	Yeast extract
	10 g	Sodium chloride
	Adjusted to 1 L with $_dH_2O$ and autoclaved before use	
Terrific Broth (TB)	12 g	Tryptone
	24 g	Yeast extract
	9.4 g	Dipotassium phosphate
	2.2 g	Monopotassium phosphate
	4 mL	Glycerol
	Adjusted to 1 L with $_dH_2O$ and autoclaved before use	
2xYT	16 g	Tryptone
	10 g	Yeast extract
	5 g	Sodium chloride
	Adjusted to 1 L with $_dH_2O$ and autoclaved before use	
Agar plates	10 g	Tryptone
	5 g	Yeast extract
	10 g	Sodium chloride
	15 g	Agar
	Adjusted to 1 L with $_dH_2O$ and autoclaved before use	
	Respective antibiotics are added after autoclaving at 50-60 °C	

2.5.4 Buffers for protein purification

Buffer	Composition	
Lysis buffer for:	500 mM	Sodium chloride
– *Pf*GluPho wt and mutants	50 mM	Tris
– *Pf*G6PD	pH 7.8	
– *Pf*6PGD wt and mutants		
– h6PGD		

Elution buffer (Ni-NTA) for: – *Pf*GluPho wt and mutants – *Pf*G6PD – *Pf*6PGD wt and mutants – h6PGD	500 mM 50 mM 10-500 mM pH 7.8	Sodium chloride Tris Imidazole
Elution buffer (Talon) for: – *Pf*G6PD	500 mM 50 mM 10-200 mM pH 7.8	Sodium chloride Tris Imidazole

2.5.5 Buffers for electrophoresis

Buffer	**Composition**	
DNA sample buffer (6x)	0.1% 60% 1 mM pH 8.3	Bromophenol blue Saccharose Tris adjusted with HCl
Tris-Borat-EDTA (TBE) buffer (5x)	89 mM 89 mM 2 mM pH 8.3	Tris Boric acid EDTA adjusted with HCl
Electrophoresis buffer	192 mM 25 mM 0.1% (w/v) pH 8.3	Glycine Tris SDS adjusted with HCl
SDS sample buffer (4x)	250 mM 8% (w/v) 40% (v/v) 0.03% (w/v) (200 mM	Tris-HCl, pH 6.8 SDS Glycerol Bromophenol blue DTT)
SDS sample buffer (1x)	62.5 mM 2% (w/v) 25% (v/v) 0.01% (w/v) (50 mM	Tris-HCl, pH 6.8 SDS Glycerol Bromophenol blue DTT)
Coomassie staining solution	160 mg *ad* 1 L 3 mL	Coomassie Brilliant Blue R 250 $_{dd}H_2O$, 2 h stirring HCl, fuming, 37%
Separating gel buffer	1.5 M pH 8.8	Tris
Sample gel buffer	0.5 M pH 6.8	Tris

2.5.6 Gels

Gel	Composition	
Agarose gel	0.7%	Agarose in TBE buffer
SDS-PAGE separating gel (12%)	5.1 mL	$_{dd}H_2O$
	3.75 mL	Separating gel buffer
	6 mL	Acrylamide/bisacrylamide (30%)
	0.15 mL	SDS (10%)
	75 µL	APS (10%)
	7.5 µL	TEMED
SDS-PAGE sample gel (4%)	3.05 mL	$_{dd}H_2O$
	1.25 mL	Sample gel buffer
	0.65 mL	Acrylamide/bisacrylamide (30%)
	0.05 mL	SDS (10%)
	25 µL	APS (10%)
	5 µL	TEMED

2.5.7 Buffers for semi-dry Western blotting

Buffer	Composition	
Anode buffer I	300 mM	Tris
Anode buffer II	25 mM	Tris
Cathode buffer	40 mM	6-Aminohexanoic acid
Western blot transfer buffer	25 mM	Tris
	192 mM	Glycine
	10% (v/v)	Ethanol
	pH 8.3	
Tris-buffered saline (TBS)	10 mM	Tris
	0.9%	Sodium chloride
	pH 7.4	adjusted with HCl
TBS with Tween 20 (TBST)	0.05% (v/v)	Tween 20 in TBS buffer
Ponceau S solution	2%	Ponceau S
	3%	TCA
Ponceau S destaining solution	1%	Acetic acid
Blocking buffer	5% (w/v)	Milk powder in TBST buffer
Luminol mixture	1.25 mM	Luminol
	0.0093% (v/v)	Hydrogen peroxide
	100 mM	Tris-HCl
	pH 8.6	
Coumaric acid	0.11%	Coumaric acid in DMSO
Chemiluminescence mixture	1 mL	Luminol mixture
	10 µL	Coumaric acid

2.5.8 Assay buffers

Buffer	Composition	
Enzyme activity buffer	100 mM	Tris-HCl
	10 mM	Magnesium chloride
	0.5 mM	EDTA
	pH 8.0	
GSNO buffer	50 mM	Tris
	1 mM	EDTA
	0.2 mM	Neocuproine
	pH 7.4	
Blocking buffer	8 M	Urea
	50 mM	Tris
	1 mM	EDTA
	0.1 mM	Neocuproine
	pH 8.0	
Labeling buffer	4 M	Urea
	50 mM	Tris
	1 mM	EDTA
	0.01 mM	Neocuproine
	pH 8.0	

2.6 Protein crystallization

To crystallize the proteins, the purification buffers were exchange via size exclusion chromatography to the buffers stated below.

Buffer	Composition	
Crystallization buffer for:	300 mM	Sodium chloride
– *Pf*6PGD wt and mutants	50 mM	Tris
	pH 7.8	
Crystallization buffer for:	150 mM	Lithium citrate
– *Pf*GluPho	50 mM	Tris
– *Pf*G6PD	pH 7.8	

To find conditions of protein crystallization, commercially available crystallization screens were used.

Screen	Company
Additive Screen HT HR2-138	Hampton Research, Aliso Viejo, CA, USA
JBScreen Classic HTS I	Jena Bioscience, Jena
JBScreen Classic HTS II	Jena Bioscience, Jena
JBScreen Wizard 1 HTS	Jena Bioscience, Jena
JBScreen Wizard 2 HTS	Jena Bioscience, Jena
JCSG Core I Suite (NeXtal Tubes)	Qiagen, Hilden
JCSG Core II Suite (NeXtal Tubes)	Qiagen, Hilden
JCSG Core III Suite (NeXtal Tubes)	Qiagen, Hilden

JCSG Core IV Suite (NeXtal Tubes)	Qiagen, Hilden
MemStart + MemSys HT-96	Molecular Dimensions Limited, Sufflok, UK
MPD Suite (PrNeXtal DWBlock)	Qiagen, Hilden
XP Screen	Jena Bioscience, Jena

3 Methods

The work was performed using the following recombinantly produced enzymes:

- From *Plasmodium falciparum*: *Pf*GluPho wt (PlasmoDB accession number PF3D7_1453800; Jortzik *et al*., 2011), *Pf*GluPho^{S315Y}, *Pf*GluPho^{L395F}, *Pf*GluPho^{F507L} (plasmids kindly provided by the working group of Prof. Becker), *Pf*GluPho^{S899E}, and *Pf*GluPho^{S900E} (plasmids generated within this thesis), *Pf*G6PD (Jortzik *et al.*, 2011), and *Pf*6PGD wt (PF3D7_1454700, plasmid generated within my master thesis, Haeussler, 2015), *Pf*6PGD^{C281S} and *Pf*6PGD^{W104L} (plasmids generated within this thesis)
- From *Plasmodium vivax*: *Pv*GluPho and *Pv*G6PD as the C-terminal part *Pv*GluPho (PVX_117790; plasmids kindly provided by the working group of Prof. Becker)
- From *Homo sapiens*: the homologs hG6PD (Jortzik *et al.*, 2011) and h6PGD (plasmid generated within this thesis)

3.1 Molecular biological methods

3.1.1 Plasmid preparation

Plasmid DNA from *E. coli* cells was purified using the QIAprep Spin Miniprep Kit (Qiagen, Hilden) or the PureYield Plasmid Miniprep System (Promega, Mannheim) following the instructions of the manufacturer. In brief, the pellet of up to 3 mL overnight culture of *E. coli* cells containing the plasmid of interest was lysed, neutralized, and transferred to the kit's column. After washing, the plasmid DNA was eluted from the silica membrane column.

3.1.2 Determining DNA concentration

The DNA concentration of a sample was determined spectrophotometrically at a wavelength of 260 nm using the BioPhotometer with UV cuvettes or the BioSpectrometer basic (both Eppendorf, Hamburg). To evaluate the purity of the sample, the ratio of absorbance at 260 nm and at 280 nm was calculated. A ratio of approximately 1.8 was defined as pure.

3.1.3 Agarose gel electrophoresis

To analyze DNA mixtures, agarose gel electrophoresis was performed. This technique separates DNA fragments, e. g. polymerase chain reaction (PCR) products or restricted plasmid DNA, by their size. The DNA sample was mixed 5:1 with DNA-Dye NonTox and loaded on a 0.7% agarose gel. The DNA fragments were separated electrophoretically in 1x TBE running buffer by applying 100 V for approximately 45 min. The 1 kb DNA ladder GeneRuler was used to estimate the size of the DNA bands. The DNA bands were afterwards visualized with LED light in the gel documentation chamber FAS Digi Gel Imaging System (Nippon Genetics, Düren).

3.1.4 Molecular cloning

The DNA plasmids used for heterologous overexpression of *Pf*GluPho, *Pf*G6PD, and hG6PD were produced previously as described in Jortzik *et al*., 2011. The coding sequences for the N-terminally 6xHis-tagged proteins *Pf*6PGD and h6PGD were ordered as codon-optimized synthetic genes from Eurofins/MWG (Ebersberg). They were subcloned into the expression vector pQE30 using the restriction sites *BamH*I and *Hind*III and verified via sequencing. The

gene of *Pv*GluPho containing no introns was amplified via PCR using a *vivax* EcoR DNA-library – obtained from the Malaria Research and Reference Reagent Resource Center (MR4) – as a template using the primers listed in 2.4.5, introducing the restriction sites for *BamH*I and *Sal*I. This construct was cloned into the cloning vector pBluescript SK (+) and verified via sequencing. For heterologous overexpression, the *Pv*GluPho gene was subcloned into the expression vectors pQE30 and pET28a using the same restriction sites. The G6PD part of *Pv*GluPho (aa 310-927) was amplified via PCR (bp 930-2,784) using primers listed in 2.4.5 and cloned into the expression vector pQE30 for heterologous overexpression as described below.

Restriction digestion

The vector containing the gene of interest and the desired target vector (pQE30 or pET28a) were cleaved with the respective restriction enzymes for 1 h at 37 °C. The DNA fragments were purified using the QIAquick PCR Purification Kit (Qiagen, Hilden) following the instructions of the manufacturer. The size of the obtained DNA fragments was analyzed by agarose gel electrophoresis (3.1.3).

Ligation

The DNA fragments were ligated with T4-DNA ligase for 5-10 min at 37 °C. Afterwards, 5 µL of the ligation mixture was transformed into competent *E. coli* cells (KRX). The transformed *E. coli* cells were plated onto an agar plate containing the respective antibiotics (carbenicillin in case of pQE30, kanamycin in case of pET28a). The remaining ligation mixture was stored overnight at 4 °C. In case the transformation was not successful, it was repeated using the overnight ligation.

Verifying the insert

To check the correct insertion of the gene of interest into the desired vector, the plasmids from several bacterial colonies after transformation were prepared as described in 3.1.1. Afterwards, the plasmids were digested using the same restriction enzymes as used for cloning for 5 min at 37 °C and the size of the fragments were analyzed using agarose gel electrophoresis (3.1.3). Plasmids containing the inserts of the correct sizes were used for further procedures.

3.1.5 Site-directed mutagenesis

Prior to this thesis, the following *Pf*GluPho mutants were generated by the working group of Prof. Becker: *Pf*GluPho^{S315Y}, *Pf*GluPho^{L395F}, and *Pf*GluPho^{F507L}. The *Pf*GluPho mutants *Pf*GluPho^{S899E} and *Pf*GluPho^{S900E}, as well as the *Pf*6PGD mutants *Pf*6PGD^{W104L} and *Pf*6PGD^{C281S} were generated within this thesis via site-directed mutagenesis using PCR.

Briefly, *Pf*GluPho wt and *Pf*6PGD wt, both in pQE30, were used as templates, the oligonucleotide primers (2.4.5) containing the desired mutated codons were added in order to insert the mutations with the *Pfu* DNA polymerase (Table 2). The PCR reaction products were purified using the QIAquick PCR Purification Kit (Qiagen, Hilden) following the manufacturer's instructions. *Dpn*I digested methylated, non-mutated template plasmids for 1 h at 37 °C before they were transformed into *E. coli* KRX cells. Insertion of the correct mutation was confirmed by sequencing in an in-house facility.

Table 2. Site-directed mutagenesis of *Pf*GluPho and *Pf*6PGD using PCR

Reaction mixture	
Template DNA	*ad* 100 ng
Forward primer	*ad* 400 nM
Reverse primer	*ad* 400 nM
dNTP mixture	*ad* 200 µM
10x *Pfu* buffer	5 µL
Pfu DNA polymerase	1 µL
Sterile H_2O	*ad* 50 µL

	*Pf*6PGD^{C281S}	*Pf*6PGD^{W104L}	*Pf*GluPho^{S899E}	*Pf*GluPho^{S900E}
Denaturation	95 °C for 90 sec	95 °C for 90 sec	94 °C for 90 sec	94 °C for 90 sec
Cycles	18	18	24	24
Denaturation	95 °C for 30 sec	95 °C for 30 sec	94 °C for 30 sec	94 °C for 30 sec
Annealing	75 °C for 30 sec	69 °C for 30 sec	55 °C for 60 sec	65 °C for 60 sec
Elongation	68 °C for 90 sec	68 °C for 90 sec	68 °C for 9 min	68 °C for 9 min
Final elongation	68 °C for 90 sec	68 °C for 90 sec	68 °C for 9 min	68 °C for 9 min

3.2 Microbiological methods

For the work with *E. coli*, autoclaved medium containing the appropriate antibiotics was used exclusively. The work was performed in a sterile environment close to a flame, and only autoclaved or sterilized instruments were used. After the experiments, any medium and instruments that were in contact with *E. coli* cells were autoclaved or incubated with 70% ethanol.

3.2.1 Preparation of competent *E. coli* cells

Competent *E. coli* cells have the ability to take up plasmid DNA from the environment. This competence is used for molecular cloning or recombinant protein production. The glycerol stocks of the respective cell lines were stored at -80 °C. A sample of the stock was streaked onto an agar plate containing the appropriate antibiotics and incubated overnight at 37 °C. A single colony was transferred to 10 mL LB medium containing the appropriate antibiotics, and the cells were allowed to grow overnight at 37 °C under constant shaking at 180 rpm. 1 mL of this culture was transferred to 100 mL LB medium with antibiotics, and the optical density measured at a 600 nm wavelength (OD_{600}) was monitored until 0.7 was reached. The culture was cooled on ice for 5 min, followed by a centrifugation step at 3,000 rpm and 4 °C for 5 min. The supernatant was completely discarded, and the cells were resuspended in a total volume of 30 mL cold TFB1 buffer. The cells were incubated on ice for 90 min, followed by a second centrifugation step at 2,000 rpm and 4 °C for 5 min. The supernatant was discarded and the cells were resuspended in 2 mL cold TFB2 buffer. Aliquots of 125 µL were frozen in liquid nitrogen for 1 min and stored at -80 °C until transformation.

3.2.2 Transformation of competent *E. coli* cells

Chemically competent *E. coli* cells were transformed in order to insert the desired plasmid DNA into the cells. An overview of the vectors and *E. coli* cell lines used for the different proteins is given in Table 3. First, a 100-125 µL *E. coli* cell suspension was thawed on ice and then incubated with plasmid DNA for 30 min. A heat shock for 90 sec at 42 °C was performed,

forcing the cells to internalize the plasmid. Afterwards, the cells were allowed to rest for 2 min on ice prior to adding 400 µL LB medium, followed by incubation for 1 h at 37 °C under constant shaking (180 rpm). After incubation, the cells were plated onto LB agar plates containing the appropriate antibiotics and incubated overnight at 37 °C. If no colony was visible, the transformation was repeated and *E. coli* cell density was increased before the cells were streaked onto the plate. For this, the cell suspension was centrifuged for 2 min at 13,400 rpm, 300 µL of the supernatant was discarded, and the pellet was resuspended and transferred completely to the plate. Plates containing colonies were stored at 4 °C for up to four weeks.

Table 3. Vectors, *E. coli* cell lines and antibiotics used for transformation
C: carbenicillin, K: kanamycin, Cam: chloramphenicol.

	Vector	*E. coli* cell line	Antibiotics
h6PGD	pQE30	M15	C, K
*Pf*6PGD	pQE30	M15	C, K
*Pf*G6PD	pQE30	M15	C, K
*Pf*GluPho	pQE30	M15, pRAREII	C, K, Cam
*Pv*G6PD	pQE30	M15, pRAREII	C, K, Cam
*Pv*GluPho	pQE30	Various	Various
*Pv*GluPho	pET28a	Various	Various

3.2.3 Heterologous overexpression in *E. coli* cells

The exact conditions of heterologous overexpression for each protein used in this thesis are given in Table 4. In order to recombinantly produce the protein of interest, a single colony of *E. coli* cells containing the corresponding plasmid DNA was inoculated into 3 mL LB medium and grown at 37 °C. To ensure consistent cell growth behavior, all incubation steps were performed under constant shaking at 180 rpm. After 8 h, 3 mL were transferred to 50-100 mL of LB or TB medium, and the cells were allowed to grow overnight at 37 °C. Using this culture, 1 L of LB or TB medium was inoculated to an OD_{600} of 0.1, and the cells were grown at 37 °C. As soon as an OD_{600} of 0.6-0.8 was reached, cells were induced with 1 mM IPTG. Heterologous overexpression was allowed for 4 h at 37 °C or for 20 h at room temperature (RT, 22 °C). Cells were harvested via centrifugation (15 min, 8,000 rpm, 4 °C), resuspended in 500 mM NaCl, 50 mM Tris, pH 7.8 with the addition of protease inhibitors (100 µM PMFS, 150 nM pepstatin A, 40 nM cystatin), and stored at -20 °C until lysis.

Table 4. Conditions of heterologous overexpression for recombinant proteins
Different conditions of heterologous overexpression were tested for each protein. Shown here are the conditions that resulted in the highest yield of active protein. C: carbenicillin, K: kanamycin, Cam: chloramphenicol. hG6PD was heterologously overexpressed as described in Jortzik *et al*., 2011.

	E. coli cells	Antibiotics	Medium	Temperature [°C]	Duration [h]
h6PGD	M15	C, K	LB	37	4
*Pf*6PGD	M15	C, K	LB	22	20
*Pf*G6PD	M15	C, K	TB	22	20
*Pf*GluPho	M15, pRAREII	C, K, Cam	TB	22	20
*Pv*G6PD	M15, pRAREII	C, K, Cam	LB, TB	37	4
*Pv*GluPho	Various	Various	LB, TB, 2xYT	16-37	4-20

3.3 Protein biochemical methods

To preserve the integrity of the proteins, all steps were performed at 4 °C if not stated otherwise.

3.3.1 Purification of recombinant protein by affinity chromatography

In this thesis, affinity chromatography using the hexahistidly-tag (6xHis-tag) of the proteins was the first step of purification. *E. coli* cell pellets were thawed, DNaseI and 16 mg lysozyme were added to each liter of *E. coli* culture, and the suspension was stirred for 2-16 h, depending on the solubility of the protein. If this prolonged lysis was not enough to overcome limited solubility, the cell suspension was adjusted to a higher volume. The exact conditions of purification for each protein used in this thesis are given in Table 5. To further increase the efficiency of lysis, the cells were manually sonicated three times for 30 sec each at 70% maximum power. The cell debris was centrifuged for 30 min at 18,000 rpm, and the supernatant containing the recombinant protein was applied to Ni-NTA or Talon column that had been equilibrated with 500 mM NaCl, 50 mM Tris, pH 7.8. The supernatant was allowed to run slowly through the column, while the recombinant protein bound to the column via its 6xHis-tag. To remove nonspecifically bound proteins, the column was washed with the buffer stated above before the protein was eluted with increasing concentrations of imidazole (up to 500 mM for Ni-NTA, up to 200 mM for Talon). The different fractions were analyzed using SDS-PAGE (3.3.2).

Table 5. Conditions of purification for recombinant proteins
Different conditions of purification were tested for each protein. Shown here are the conditions that resulted in the highest yield of active protein. The human homolog hG6PD was purified as described in Jortzik *et al*., 2011.

	Duration of lysis [h]	Volume of lysis [mL per L *E. coli* culture]	Column material	Imidazole concentration for elution [mM]
h6PGD	16	20-40	Ni-NTA	75
*Pf*6PGD	2	20-30	Ni-NTA	75
*Pf*G6PD	16	50-70	Talon	25
*Pf*GluPho	16	50	Ni-NTA	50
*Pv*G6PD	16	50-70	Ni-NTA	40
*Pv*GluPho	Various	Various	Ni-NTA	Various

3.3.2 Gel electrophoresis

Denaturing sodium dodecyl sulfate polyacrylamide gel electrophoresis (SDS-PAGE) separates proteins depending on their molecular weight and was used in this thesis to control the purity of protein samples and before protein immunoblotting. SDS denatures and coats the proteins, giving them a negative charge proportional to their molecular weight. The reduction of disulfide bonds via DTT fully unfolds the three-dimensional structure of the proteins. Within an electric field, the proteins migrate through the gel towards the positively charged anode, thereby separating them by size (Laemmli, 1970).

SDS sample buffer was added to each protein sample; for the exact compositions, see Table 6. The samples were boiled for 5 min at 95 °C and applied to a 12% polyacrylamide gel (5 µL of pellet, flow-through, and washing fraction; 18 µL of elution fractions, entire sample of final purity and analysis of *S*-glutathionylation, 2 µL of the 1:10 diluted sample for analysis for

S-nitrosation). Upon applying 200 V for approximately 40 min, the proteins migrated through the gel. As soon as the smallest proteins reached the lower end of the gel, the gel was washed with water three times and followed by staining with Coomassie Brilliant Blue. The efficiency of washing and staining was enhanced by briefly heating the gel in a microwave (40 sec, 700 W). After staining, excessive Coomassie was removed by washing the gel with water. For Western blot analysis, the gel was not washed and stained but directly used to blot the proteins to the membrane.

Table 6. Sample preparation for SDS-PAGE
SB: sample buffer. All SB included DTT, except for the SB used for the identification of *S*-glutathionylation.

	Protein sample	Protein amount	SB	Volume of SB
Protein purification	Pellet	Small amount pellet	4x	5 µL
	Flow-through	3 µL	4x	5 µL
	Washing	3 µL	4x	5 µl
	Elution	20 µL	4x	5 µL
	Final purity	*Ad* 7.5 µg protein	1x	Equal to volume of protein sample
S-glutathionylation	Identification	*Ad* 2.5 µg protein	1x	Equal to volume of protein sample
	Reversibility	*Ad* 2.5 µg protein	1x	Equal to volume of protein sample
S-nitrosation	Initial sample	60-200 µg protein	4x	¼ of the blocking buffer volume used for resuspension
	1:10 dilution	2 µL of the initial sample	1x	18 µL

3.3.3 Size exclusion chromatography

In this thesis, size exclusion chromatography was performed for three different reasons: to improve the purity of a protein, to study the oligomerization behavior, and to simultaneously change the buffer in case a different buffer was used for crystallization than for purification. Size exclusion chromatography separates the proteins according to their molecular weight in their native form by using a separation column. The smaller the proteins, the better they can infiltrate the porous matrix of the separation column; therefore, larger proteins elute from the column first.

The experiments were performed with a HiLoad 16/600 Superdex 200 prep grade column connected to an ÄKTA/Unicorn FPLC system (GE Healthcare, Freiburg). Prior to the experiments, the column was calibrated with a size exclusion calibration kit (GE Healthcare, Freiburg) and equilibrated with the appropriate buffer. If applicable, the sample was incubated with 5 mM DTT, 1-5 mM H_2O_2, or 100 µM NADPH and centrifuged for 15 min at 13,400 rpm in order to remove potential solid particles. Afterwards, the sample was applied to the column and eluted at a flow rate of 1 mL·min^{-1}. Eluting proteins were detected spectrophotometrically at 280 nm, fractions of 2 mL were collected, peak areas and kAV values were evaluated using the Unicorn 4.11 and 7.1 software. The final purity of the protein was controlled by SDS-PAGE (3.3.2).

3.3.4 Determination of protein concentration

Protein concentration was determined in two different ways. The first was the Bradford assay. A standard curve was created containing 0-20 µg·mL^{-1} BSA in 500 µL water, before 125 µL of Bradford reagent (Bio-Rad, Munich) was added. After exactly 15 min, absorption was measured spectrophotometrically at 595 nm. The samples were treated in the same way, and concentration was calculated based on the standard curve.

The second way was by measuring the absorbance of the protein solution at 260 and 280 nm using the Eppendorf BioSpectrometer basic. The concentration was calculated using the molecular weight and the extinction coefficient of the proteins.

Table 7. Molecular weights and extinction coefficients of proteins
Molecular weights including the 6xHis-tag and extinction coefficients were calculated using the online tool of JustBio (www.justbio.com). Concentration of hG6PD was only determined using the Bradford assay.

	Molecular weight [kDa]	Extinction coefficient [M^{-1}cm^{-1}]
h6PGD	54.4	62,700
*Pf*6PGD wt	54.0	65,520
*Pf*6PGD^{C281S}	54.0	65,460
*Pf*6PGD^{W104L}	53.9	59,830
*Pf*G6PD	67.9	60,200
*Pf*GluPho wt, *Pf*GluPho^{L395F}, *Pf*GluPho^{S899E}, *Pf*GluPho^{S900E}	108.3	111,630
*Pf*GluPho^{F507L}	108.2	111,630
*Pf*GluPho^{S315Y}	108.3	112,910
*Pv*G6PD	71.8	57,590
*Pv*GluPho	109.5	91,740

3.3.5 Protein immunoblotting

Western blot analysis was used to identify either 6xHis-tagged proteins or post-translationally modified proteins using specific antibodies (see Table 8).

First, an SDS-PAGE gel was run (chapter 3.3.2), and the proteins were transferred to a polyvinylidene difluoride (PVDF) or nitrocellulose membrane. Before use, the PVDF membrane was activated by soaking in 100% methanol. For the transfer, filter papers, gel, and membrane were soaked in buffer (three papers in anode buffer I, two papers and the membrane in anode buffer II, five papers and the gel in the cathode buffer). The five filter papers (cathode buffer) were placed quickly and without air bubbles onto the graphite cathode plate, followed by the gel, membrane, two filter papers (anode buffer II) and three filter papers (anode buffer I). The proteins were transferred from the gel to the membrane by applying 13 V for 30 min. Alternatively, twelve filter papers, the gel, and the membrane were soaked in Western blot transfer buffer. Six papers were placed at the anodic bottom of the transfer cassette, followed by the membrane, the gel, and the remaining six filter papers. The proteins were transferred by applying 25 V and 1 A for 30 min. To control blotting efficiency, the membrane was stained in Ponceau S for 30 sec and destained with 1% acetic acid until the bands were visible. Afterwards, the membrane was completely destained by washing it several times in TBST. To prevent non-specific binding of the antibodies to unoccupied protein binding sites, the

membrane was blocked with 5% (w/v) non-fat milk in TBST for 1 h at 22 °C or overnight at 4 °C. The membrane was washed three times for 5 min in TBST before the primary antibody was applied (for the antibody dilutions, see Table 8). After incubation with the primary antibody for 1 h at 22 °C, the membrane was washed again in TBST as described above, and the secondary antibody was applied for 1 h at 22 °C, followed by a final washing step in TBST. The secondary antibody coupled to a horseradish peroxidase enabled visualization of the proteins labeled by antibodies. Therefore, the membrane was incubated for 1 min with the chemiluminescence mixture, and chemiluminescence was detected with either an X-ray film or the Intas ECL ChemoStar Imager connected to ChemoStar TS software. If applicable, the antibodies were removed afterwards by incubating the membrane in Restore Plus Western Blot Stripping Buffer for 7 min.

Table 8. Antibodies used for Western blot analysis

Identification of…	Primary antibody	Secondary antibody
… 6xHis-tag	1:1,000	Anti-mouse, 1:20,000
… *S*-glutathionylation	1:250	Anti-mouse, 1:10,000
… *S*-nitrosation	1:1,000	Anti-mouse, 1:10,000

3.3.6 Enzyme assays

In this thesis, the G6PD activities of full-length *Pf*GluPho, *Pf*G6PD and *Pv*G6PD, the activity of *Pf*6PGD, and the activities of the human homologs hG6PD and h6PGD were examined. The enzymes catalyze the following reactions:

$$\text{Glucose 6-phosphate} + NADP^+ \xrightarrow{\text{G6PD}} \text{6-phosphoglucono-δ-lactone} + NADPH + H^+$$

$$\text{6-Phosphogluconate} + NADP^+ \xrightarrow{\text{6PGD}} \text{ribulose 5-phosphate} + CO_2 + NADPH + H^+$$

The activity of the enzymes was determined spectrophotometrically by measuring the absorption of the initial reduction of the cofactor $NADP^+$ to NADPH at 340 nm according to Beutler, 1984. All enzymatic measurements were carried out at 25 °C. Briefly, the reaction mixture contained the cofactor $NADP^+$ and varying concentrations of enzyme (around 5-50 nM) in the assay buffer described in 2.5.8. The exact cofactor and substrate concentrations used for each enzyme are described in Table 9.

Table 9. Cofactor/substrate concentrations used for G6PD/6PGD enzyme activity assays
The concentrations given are considered saturated. * According to Jortzik *et al*., 2011; N/A: not applicable.

	Cofactor $NADP^+$ [µM]	Substrate G6P [µM]	Substrate 6PG [µM]
h6PGD	200	N/A	400
hG6PD*	200	200	N/A
*Pf*6PGD mutants	50	N/A	200
*Pf*6PGD wt	100	N/A	200
*Pf*GluPho mutants	200	200	N/A
*Pf*GluPho wt*	200	200	N/A
*Pv*G6PD	200	800	N/A

The reaction was started by adding the appropriate substrate. The K_M for $NADP^+$ was determined by titrating $NADP^+$ at the saturating concentrations of the corresponding substrate, the K_M for the substrate was determined *vice versa* by titrating the substrate at the saturating concentration of $NADP^+$. All measurements were performed using the Evolution 300 spectrophotometer (Thermo Scientific, Dreieich) at a final assay volume of 500 µL. For evaluations, only linear signal increase was considered. Specific activities were calculated using Microsoft Excel; K_M and V_{max} were analyzed using GraphPad Prism 5.

3.3.7 Protein *S*-glutathionylation

Potential protein *S*-glutathionylation of the plasmodial enzymes was studied via Western blot analysis and enzyme activity measurements.

Western blot analysis

Purified enzymes were reduced with 5 mM DTT for 30 min. Afterwards, DTT was removed using Zeba™ Spin Desalting Columns according to the instructions of the manufacturer. Each protein was adjusted to a final concentration of 2 $mg \cdot mL^{-1}$ and incubated with 0, 2, 6, or 10 mM GSSG for 10 min at 37 °C, followed by desalting as described above. To identify *S*-glutathionylated proteins, samples were prepared for SDS-PAGE with 1x sample buffer without DTT (see Table 6). Sample buffer with DTT was used to study the reversibility of the modification. Western blot analysis was performed as described in 3.3.5 using a monoclonal anti-glutathione antibody (Virogen, Watertown, MA, USA; diluted 1:250 in 5% (w/v) non-fat milk in TBST) and a horseradish peroxidase-conjugated goat anti-mouse antibody (Dianova, Hamburg; diluted 1:10,000 in 5% (w/v) non-fat milk in TBST).

Enzyme activity

To investigate the time and concentration-dependent impact of *S*-glutathionylation on enzyme activity, prereduced enzyme was incubated with 0-10 mM GSSG at 37 °C for 15 min. The activity was determined as described in 3.3.6. To study the reversibility of the modification, *S*-glutathionylated protein was incubated with 5 mM DTT for up to 1 h at 4 °C before the activity was determined.

3.3.8 Protein *S*-nitrosation

Potential protein *S*-nitrosation on *Pf*GluPho/*Pf*G6PD, *Pv*G6PD, and *Pf*6PGD was studied via Western blot analysis, MALDI-TOF MS, and enzyme activity measurements. The physiologically relevant small molecular weight *S*-nitrosothiol GSNO served as an NO donor, which is able to release NO and transnitrosate proteins (Broniowska *et al.*, 2013; Hess *et al.*, 2005).

Biotin-switch assay and Western blot analysis

Since no antibody for directly detecting *S*-nitrosation is available, the biotin-switch assay was performed for *S*-nitrosated proteins as described in Wang *et al*., 2014, enabling the detection of *S*-nitrosated thiol groups via Western blot analysis using an anti-biotin antibody. 0.6-0.8 $mg \cdot mL^{-1}$ prereduced enzyme was incubated with 0 or 1 mM GSNO in GSNO buffer (chapter 2.5.8) for 1 h at 22 °C in the dark. The reaction was stopped by adding 100% ice-cold acetone, followed by protein precipitation for 30 min at -20 °C. After centrifugation of the samples at 8,000 g and 4 °C for 5 min, the supernatant was discarded and the pellets were washed three times with 70% ice-cold acetone, each time followed by centrifugation (first 8,000 g, followed

by 5,000 g, 4 °C, 5 min). Residual free cysteine thiols were blocked by resuspending the pellets in blocking buffer (chapter 2.5.8) containing 200 mM IAA, followed by incubation in the dark for 45 min at 50 °C. The reaction was stopped by adding 100% ice-cold acetone, followed by protein precipitation and washing of the pellets with 70% ice-cold acetone as described above. To switch *S*-nitrosated thiols to biotinylated thiols, the pellets were dissolved in labeling buffer (chapter 2.5.8) containing 20 mM sodium ascorbate and 0.2 mM iodoacetyl-PEG2-biotin and incubated for 1 h in the dark at 25 °C. Samples without sodium ascorbate served as a negative control. The reaction was again stopped by adding 100% ice-cold acetone, followed by protein precipitation and washing of the pellets with 70% ice-cold acetone as described above. The final pellets were resuspended in blocking buffer and applied to SDS-PAGE. Western blot analysis was performed as described in 3.3.5, using the monoclonal anti-biotin antibody (33): sc-101339 (Santa Cruz, Dallas, TX, USA; diluted 1:1,000 in 5% (w/v) non-fat milk in TBST) and a horseradish peroxidase-conjugated goat anti-mouse antibody (Dianova, Hamburg; diluted 1:10,000 in 5% (w/v) non-fat milk in TBST).

MALDI-TOF MS

To identify the cysteine residues of *Pf*6PGD that had been affected by *S*-nitrosation, matrix-assisted laser desorption/ionization time-of-flight-mass spectrometry (MALDI-TOF MS) was used. After incubating the reduced protein with varying concentrations GSNO, excess GSNO was removed via desalting as described above, and residual free thiols were blocked with 20 mM NEM. The MALDI-TOF MS analyses were performed in two different facilities (Core Facility of Mass Spectrometry and Elemental Analysis, Philipps University Marburg; Protein Analytics, Justus Liebig University Giessen).

Enzyme activity

The enzymes were reduced and desalted as described in 3.3.7. Afterwards, the proteins were incubated with 0-1,000 µM GSNO in GSNO buffer for up to 180 min at RT in the dark. The effect of *S*-nitrosation on enzyme activity and the potential reversibility of the effect were determined as described in 3.3.6 and 3.3.7.

3.3.9 Stability tests of *Pf*GluPho and *Pf*G6PD

Despite numerous trials, it was not yet been possible to crystallize *Pf*GluPho or the C-terminal part *Pf*G6PD. This might be due to weak protein stability at RT in the buffer used so far (500 mM NaCl, 50 mM Tris, pH 7.8). Therefore, differential scanning fluorimetry (DSF) was performed in order to find additives or alternative buffer ingredients that would increase the stability of the enzyme and therefore improve the possibility of protein crystallization. Within this thesis, the effects of promising additives/buffer ingredients on protein stability during storage at RT were tested on both *Pf*GluPho and *Pf*G6PD.

*Pf*GluPho and *Pf*G6PD were heterologously overexpressed and purified as described above (3.2-3.3). The purified enzymes were highly concentrated using Vivaspin 30,000 tubes in order to ensure that the remaining buffer was kept to a minimum. Afterwards, the proteins were diluted into stock solutions of promising chemicals found via DSF (100-300 mM sodium chloride, 50 mM bicine, pH 9.0, 50 mM Hepes, pH 6.0, 1 mM GSH/GSSG, 2 mM Gly-Gly-Gly, 2 mM $NADP^+$, 2 mM G6P, 100 mM calcium chloride, 100 mM sodium bromide, 100 mM ammonium sulfate, 50-500 mM lithium citrate, 50-500 mM sodium citrate, 1 mM betaine, 1 mM xylitol, and different combinations). Protein concentration was determined immediately as described in 3.3.4. The proteins were then stored in the dark at RT, and

concentration was determined on a regular basis as described in 3.3.4. Before each measurement, the samples were centrifuged for 5 min at 13,400 rpm to remove potentially degraded protein.

3.4 Structural biology methods

Detailed characterization of a protein is largely facilitated by the knowledge of its three-dimensional structure (Chayen and Saridakis, 2008). This may enable statements about the enzyme mechanism or – especially in the case of cocrystallization with a substrate or cofactor – give insights into the binding sites of the enzyme. Moreover, knowing the structure of an enzyme makes rational drug design possible. Improving a compound based on the structure of the target protein largely enhances the chance of a significant and specific effect on the target (Chen *et al.*, 2012).

3.4.1 Protein crystallization using the vapor diffusion technique

The first step in elucidating the three-dimensional structure of a protein is to crystallize it. This step can be very challenging since proteins are highly colloidal with respect to their physiochemical properties, size, and conformational stability, making them sensitive to any change in the environmental conditions (Gavira, 2016). It is therefore necessary to find chemical, biochemical, and physical conditions that allow transition of the protein in solution to crystalline material (McPherson and Gavira, 2014). This first-order phase transition is called nucleation, which is followed by growth of the crystal. An essential premise of nucleation is the generation of protein in a supersaturated phase, meaning that the protein concentration in solution is higher than its actual solubility limit. The saturation state depends on the concentration of both the protein and precipitant, as illustrated in the phase diagram of Figure 7. If both concentrations are low, the protein is in a stable, undersaturated phase where no nucleation is possible. Increasing one or even both concentrations shifts the protein to supersaturation, a non-equilibrium condition. In the labile phase, both nucleation and crystal growth can occur, whereas in the metastable phase only the growth of already existing crystals is possible. The highest level of supersaturation is reached in the precipitation phase. Under this condition, nucleation and crystal growth are unlikely. There are several ways to generate a supersaturated state, e.g., adding or removing salt, altering the temperature, adding ligands or polymers, etc. (Chayen and Saridakis, 2008; Holcomb *et al.*, 2017; McPherson and Gavira, 2014).

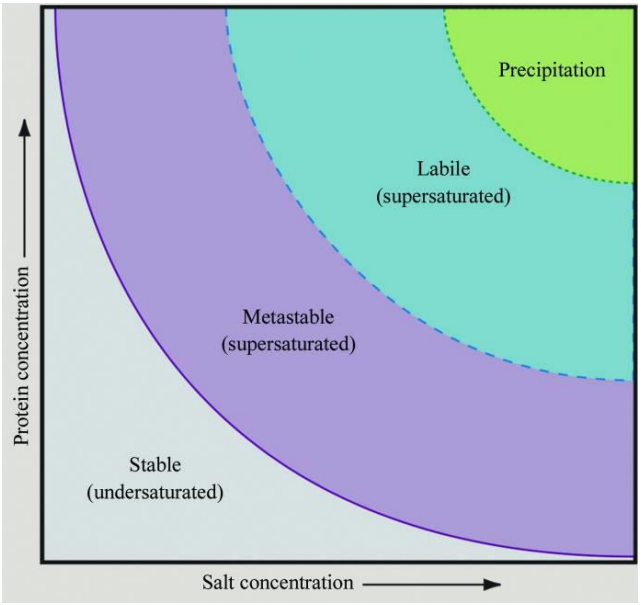

Figure 7. Phase diagram for protein crystallization
The phase diagram shows the influence of protein concentration and precipitant concentration on the saturation state of a protein. The precipitant may be a salt or a polymer. The premise of crystallization is supersaturation of the protein. If both protein and precipitant concentrations are low, the protein is in a stable, undersaturated state. Increasing protein or precipitant concentration transitions it to the metastable, labile, or precipitation phase (Chayen and Saridakis, 2008; Holcomb *et al.*, 2017; McPherson and Gavira, 2014). The figure was taken from McPherson and Gavira, 2014.

There are several techniques to reach the supersaturation state such as microbatch crystallization and dialysis. In this thesis, the vapor diffusion technique was used, which is based on vapor diffusion between a drop containing precipitant and protein in a concentration below the solubility limit and the reservoir containing the precipitant solution. Diffusion slowly increases the concentration of the protein, promotes supersaturation, and may thereby enable nucleation. There are two variants to the vapor diffusion technique: the sitting drop and the hanging drop approach. The difference between these is the position of the protein/precipitant mixture as shown in Figure 8. In the sitting drop approach, it sits in a well in the middle of or next to the reservoir solution, while in the hanging drop approach it hangs over the reservoir solution from an inverted cover slide (Chayen and Saridakis, 2008; Holcomb *et al.*, 2017; McPherson and Gavira, 2014).

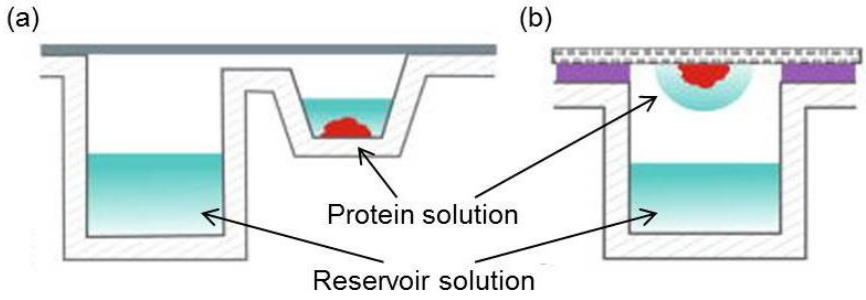

Figure 8. Protein crystallization using the vapor diffusion technique
Vapor diffusion can be performed in two different approaches: the sitting drop (a) and the hanging drop (a) technique. Diffusion between the protein solution and the reservoir solution results in an adjustment of the concentrations and may allow protein crystal formation. This figure was modified from Caffrey and Cherezov, 2009.

3.4.2 Screening the crystallization condition

Finding a condition that allows protein crystal formation is mainly empirical (McPherson and Gavira, 2014). Commercially available crystallization screens (see 2.6) can be used as a starting point. They are based on conditions that previously resulted in successful protein crystallization (Chayen and Saridakis, 2008). Additionally, screens designed in the laboratory of Prof. Becker consisting of common precipitants were used in this thesis. The screenings were performed using the Honeybee crystallization robot 961 in 96-well two-drop trays. The robot pipetted drops comprising 200 nL reservoir solution and 200 nL protein solution into the trays next to the reservoir with 100 µL reservoir solution. A drop comprising 200 nL reservoir solution and 200 nL buffer was placed into the second tray to enable differentiation between salt and protein crystals. In some screenings, this control drop was replaced by the screening of a second condition, e. g., another protein concentration or a cocrystallization trial. This enabled the screening of 192 different conditions in one plate. The plates were afterwards sealed with clear adhesive tape, stored at RT if not stated otherwise, and controlled for crystals or crystal-like precipitation on a regular basis using a stereomicroscope.

3.4.3 Additives

An additive is defined as any chemical substance or small molecular weight compound that is added to the crystallization trial described above (3.4.2). A rational approach is the use of additives that bind to the protein for physiological reasons, e. g. substrates, cofactors, or inhibitors. However, other classes of substances may also be used (Holcomb *et al.*, 2017; McPherson and Gavira, 2014). The use of additives may facilitate or promote nucleation and crystal growth by enhancing protein solubility or structural rigidity (Holcomb *et al.*, 2017).

In this thesis, substrates, cofactors, products, and inhibitors were used as additives (Table 10). The molar concentration of the additive in the drop was at least 2.5-fold higher than the protein concentration in order to enable binding of one additive molecule to each protein molecule. Furthermore, we used the Additive Screen HT HR2-138 from Hampton Research (Aliso Viejo, CA, USA). The procedure for using this Additive Screen was almost the same as the one described in 3.4.2, except that 90 µL of a promising reservoir solution was mixed with 10 µL of the additive solution. This mixture was used to prepare the 200 nL drops.

Table 10. Physiological additives used for crystallization trials

	Additive
*Pf*6PGD	6PG $NADP^+$

	Additive
*Pf*G6PD	G6P $NADP^+$

	Additive
*Pf*GluPho	G6P $NADP^+$ NADPH SBI-0797750

3.4.4 Optimization of initial crystallization conditions

Crystalline material yielded during an initial screen is often not suitable for X-ray diffraction analysis. The quality of these crystals (e.g. suitable size for X-ray diffraction analysis) may be improved by slightly varying the initial conditions (McPherson and Gavira, 2014). In this thesis, crystal quality was optimized via the vapor diffusion technique in 24-well crystallization plates with hanging and sitting drops. For hanging drops, 2 µL of protein solution was mixed with 2 µL of reservoir solution in the center of a microscope cover slip. The slip was put face-down

onto the well containing 800 µL of reservoir solution. To seal the wells hermetically, the clefts around the wells were covered with silicone oil before the slips were emplaced. For the sitting drops, 2 µL of protein solution and 2 µL of reservoir solution were put into the middle of a sitting drop crystallization plate, surrounded by 800 µL of reservoir solution. The plates were sealed with a clear adhesive tape. These plates were then stored at 4-22 °C and controlled for crystals on a regular basis.

3.4.5 Data collection and processing

Crystals of appropriate size and quality were used for X-ray diffraction analysis. The resulting diffraction pattern was then used to calculate the three-dimensional protein structure.

Dr. Karin Fritz-Wolf processed the data on crystals obtained within this thesis at the Max Planck Institute for Medical Research (MPI), Heidelberg. Prior to data collection, the crystals were transferred to a cryoprotection buffer containing glycerol or ethylene glycol in addition to the actual crystallization buffer and were stored in liquid nitrogen. Diffraction data was collected at X10SA (detector: Pilatus) of the Swiss Light Source, Villigen, Switzerland. Diffraction data were collected at 100 K and processed with XDS (Kabsch, 2010).

3.5 Methods for characterization of "small molecule" inhibitors

3.5.1 IC_{50} determination

One important characteristic parameter of a compound is its median inhibitory concentration (IC_{50}). It indicates the compound concentration at which, e.g., the activity of an enzyme is reduced to 50% of its initial value (Cheng and Prusoff, 1973).

If not stated otherwise, the IC_{50} determinations in this thesis were based on the enzyme assay described in 3.3.6 in the presence of different compound concentrations. For the assessment of the compounds, following enzyme concentrations were used: 5-10 nM *Pf*GluPho, 1-6 nM *Pv*G6PD, 2 nM *Pf*6PGD, 1-2 nM hG6PD, and 1 nM h6PGD. All measurements were performed in 96-well plates, half area (Greiner Bio-One, Frickenhausen), using the Tecan Infinite M200 plate reader (Tecan, Maennedorf, Switzerland) at a minimum assay volume of 75 µL. First, the compounds were dissolved *ad* 10 mM in 100% DMSO and afterwards diluted in enzyme activity buffer to different concentrations around the expected IC_{50}. The final concentration of DMSO was not allowed to exceed 1%. The compound dilution series was added to a mixture of enzyme and $NADP^+$ in enzyme activity buffer. In case of substrate saturation, the concentrations given in Table 9 were used. However, to enable the identification of competitive inhibitors, the cofactor and substrate were usually added in concentrations close to the K_M of the enzyme, given in Table 11. The reaction was started by adding the appropriate substrate. A negative control containing no compound was defined as 0% inhibition, a positive control containing no substrate as 100% inhibition. The increase in NADPH was monitored by measuring either absorption at 340 nm or fluorescence at an excitation wavelength of 340 nm and an emission wavelength of 460 nm (ex340/em460). For evaluations, only the initial linear increase of absorption/fluorescence was considered. The IC_{50} values were calculated using GraphPad Prism 5.

Table 11. Cofactor/substrate concentrations close to K_M used for IC_{50} determinations
* Determined in Jortzik *et al.*, 2011. ǂ Depending on the individual K_M of the enzyme batch used. N/A: not applicable.

	Cofactor $NADP^+$ [µM]	Substrate G6P [µM]	Substrate 6PG [µM]
h6PGD	4.5	N/A	26
hG6PD*	19	125	N/A
*Pf*6PGD	9	N/A	11
*Pf*GluPho*	10	15	N/A
*Pv*G6PD	15	70-85ǂ	N/A

3.5.2 Determination of the mechanism of inhibition

To further characterize a compound, its most likely mechanism of inhibition (MOI) was determined by using the assay described above (3.5.1) with one modification. To determine the MOI against $NADP^+$, the cofactor was titrated at different compound concentrations around IC_{50}, while the substrate was kept in saturation (Table 9). *Vice versa*, to determine the MOI against the substrate, it was titrated at fixed concentrations of $NADP^+$ in saturation. The initial linear slope was used to plot the Michealis-Menten curves and the Lineweaver-Burk plots and to calculate K_M and V_{max} using GraphPad Prism 5. The most likely MOI was evaluated using the decision criteria listed in Table 12.

Table 12. Decision criteria for determining the mechanism of inhibition
(Cornish-Bowden, 2004)

Mechanism of inhibition	Increase of inhibitor concentration		
	K_M	V_{max}	Lineweaver-Burk plots
Competitive	↑	↔	Intersection at the ordinate
Non-competitive	↔	↓	Intersection at the abscissa
Uncompetitive	↓	↓	Parallel lines
Mixed type	Mixed characteristics		

3.5.3 Reversibility of inhibition

Besides the MOI, a second important characteristic of a compound is the potential reversibility of its inhibition. To test this, the enzymes were incubated with high inhibitor concentrations. The activity of this incubation mixture was determined in order to ensure that the compound concentration was high enough to completely inhibit the enzyme. Afterwards, the enzyme/inhibitor mixture was diluted to a compound concentration below IC_{50} and incubated for 10 min on ice to allow potential dissociation of the inhibitor from the protein. For comparison, controls containing either no inhibitor or inhibitor in the concentration remaining after dilution were prepared in parallel. To start the reaction, substrate and cofactor were added either in saturation (Table 9) or at concentrations close to K_M (Table 11). The activity measurements were performed based on the assay described in 3.3.6 using the Tecan Infinite M200 plate reader (Tecan, Maennedorf, Switzerland) in 96-well plates, half area (Greiner Bio-One, Frickenhausen), with a final assay volume of 50-80 µL. The activity of the control without any inhibitor was defined as 100%. If the activity of the sample after dilution was significantly below the activity of the controls, inhibition was considered irreversible; however, if the activity of the sample was equal to the controls, inhibition was considered reversible.

3.5.4 Testing compounds in high-throughput screening assay format

Within this thesis, many compounds were tested in a high-throughput screening assay format at the Sanford Burnham Prebys Medical Discovery Institute in La Jolla, CA, USA using the assays described below.

3.5.4.1 Diaphorase-coupled assay

For the first test of new compounds, the assay described in 3.3.6 was coupled to the enzyme diaphorase, which uses NADPH to reduce resazurin to the highly fluorescent resorufin. For each molecule of converted G6P, one molecule of resorufin is generated, which allows the determination of G6PD activity by measuring fluorescence of resorufin (Figure 9). The actual fluorescence wavelengths of resorufin are ex530/em590; however, due to available filter combinations for the plate reader, ex530/em580 were used. This shift to higher wavelengths (the fluorescence of NADPH itself is ex340/em460) increases the sensitivity of the assay. Moreover, it avoids interference with the fluorescence of the compounds themselves, which is very common in the UV range (Preuss *et al.*, 2012a).

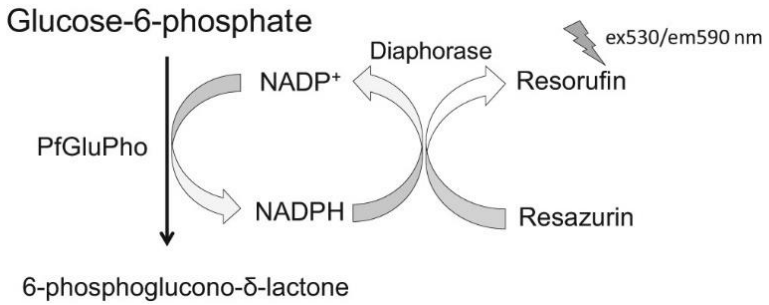

Figure 9. Diaphorase-coupled screening assay
*Pf*GluPho converts glucose 6-phosphate to 6-phosphoglucono-δ-lactone. The thereby generated NADPH is used by diaphorase to reduce resazurin to resorufin. The fluorescence of resorufin can be measured at ex530/em590 (Preuss *et al.*, 2012a).

The assays for *Pf*GluPho and hG6PD described in Preuss *et al*., 2012a and Preuss *et al*., 2013 were used with slight modifications. The same assay was used for *Pv*G6PD, appropriate concentrations were determined by titration of each component. Exact assay concentrations are given in Table 13. Varying volumes of compound dissolved in 100% DMSO were transferred to columns 5-34 of a 1,536-well plate using the Echo Liquid Handler (Labcyte, San Jose, CA, USA). Columns 1-4 served as positive controls without substrate; columns 35-38 served as negative controls without compound. Additional DMSO was added to all wells in order to equilibrate the DMSO concentration across the plate. A volume of 2.5 µL of enzyme mix (Table 13) was added to all wells using the Multidrop Combi Reagent Dispenser (Thermo Fisher Scientific, Waltham, MA, USA). To start the reaction, 2.5 µL of substrate mix (Table 13) was added to columns 5-34 using the Combi. Substrate mix without G6P was added to columns 1-4 for positive control. The plate was centrifuged at 1,500 rpm for 1 min and incubated in the dark for 2 hours. Fluorescence of resorufin was then detected at ex530/em580 using a Viewlux plate reader (PerkinElmer, Waltham, MA, USA). IC_{50} values were calculated using CBIS (Chemical and Biological Information Systems, www.cheminnovation.com).

Table 13. Concentrations used for the diaphorase-coupled assay
The final assay concentrations are given.

		*Pf*GluPho	*Pv*G6PD	hG6PD
Highest compound concentration [µM]		4	4	79
Enzyme mix	Tris, pH 7.5 [mM]	50	50	50
	Tween 20 [%]	0.005	0.005	0.005
	BSA [mg·mL^{-1}]	1	1	1
	Enzyme [µg·mL^{-1}]	0.075	0.15	0.15
Substrate mix	Tris, pH 7.5 [mM]	50	50	50
	Tween 20 [%]	0.005	0.005	0.005
	BSA [mg·mL^{-1}]	1	1	1
	$MgCl_2$ [mM]	3.3	3.3	3.3
	Diaphorase [U·mL^{-1}]	1	1	1
	Resazurin [µM]	25	60	140
	G6P [µM]	20	30	125
	$NADP^+$ [µM]	4	12	6

3.5.4.2 Orthogonal assay

Determination of IC_{50} values

In order to exclude an interaction with the diaphorase-coupled assay, IC_{50} values were determined using the orthogonal assay directly detecting the fluorescence of NADPH. Plates were prepared as described in 3.5.4.1. For hG6PD, 99 µM were used as the highest compound concentration. The enzyme mix contained 0.05 µg·mL^{-1} *Pf*GluPho, 0.025 µg·mL^{-1} *Pv*G6PD, and 0.045 µg·mL^{-1} hG6PD, respectively. The reaction was started by adding the substrate mix described above (Table 13) without diaphorase and resazurin. The plates were centrifuged, and the reaction was read kinetically using the PHERAstar multiwell plate reader (BMG LABTECH, Cary, NC, USA) at ex350/em460 (due to filter availability) over 45 min. The reaction rate was calculated by dividing the relative fluorescence units (RFU) by time. For analysis, only the linear signal increase was considered. CBIS was used to calculate IC_{50} values.

Determination of the mechanism of inhibition

The most potent inhibitors were mechanistically characterized as described in 3.5.2 with slight modifications. Varying inhibitor concentrations around IC_{50} were transferred to a 1,536-well plate using the Echo Liquid Handler. The enzyme mix containing 0.04-0.05 µg·mL^{-1} *Pf*GluPho was added to the plate. Enzyme and substrate mixes (without diaphorase and resazurin, Table 13) were dispensed using the BioRAPTR Microfluidic Workstation (Beckman Coulter, Brea, CA, USA). After centrifuging the plate, the NADPH fluorescence increase was monitored at ex350/em460 (due to filter availability) with the PHERAstar multiwell plate reader. For the analysis, only the linear slope was considered. Based on the data, Lineweaver-Burk plots were created, and K_M and V_{max} values were calculated with GraphPad Prism 5 software. The mechanism of inhibition was evaluated using the criteria given in Table 12.

3.5.5 Screening the MMV Malaria Box

DMSO tolerance test

The MMV Malaria Box comprises 200 drug-like and 200 probe-like compounds with known antimalarial activity. Until December 2015, it could be ordered free of charge from MMV

(Spangenberg *et al.*, 2013). Like many others, compounds of the MMV Malaria Box are dissolved in 100% DMSO. High concentrations of DMSO can change the conformation of some proteins and thereby influence their activity (Rammler, 1967). Therefore, a DMSO tolerance test was performed before screening MMV Malaria Box by measuring *Pf*6PGD activity under varying DMSO concentrations (0-5%). The assay was performed as described in 3.3.6 using the Tecan Infinite M200 plate reader (Tecan, Maennedorf, Switzerland) with a final assay volume of 75 µL. The initial linear slope was used to calculate the activity in comparison to the control without DMSO.

Screening of the MMV Malaria Box

The MMV Malaria Box was screened based on the assay described in 3.3.6 containing $NADP^+$ and 6PG at concentrations close to the K_M to allow identification of competitive inhibitors (Table 11). The compounds were added in a final concentration of 10 µM before the reaction was started. The final DMSO concentration was 1%; therefore, a negative control containing 1% DMSO but no compound was defined as 0% inhibited. The positive control contained no 6PG and was defined as 100% inhibited. All measurements were performed in 384-well plates with a final assay volume of 100 µL using the Tecan Infinite M200 plate reader (Tecan, Maennedorf, Switzerland). Microsoft Excel was used to calculate the activity of the enzyme compared to the controls. This determination was repeated four times. For all compounds that showed an inhibition of ≥ 50% in at least three of the four determinations, IC_{50} values were determined as described in 3.5.1 applying substrate and cofactor at K_M concentrations (Table 11).

3.5.6 Characterization of compounds in *P. falciparum* cell culture

Cultivation of *Plasmodium falciparum* parasites

P. falciparum 3D7 and NF54-*attB* parasites were grown in continuous culture as described by Trager and Jensen, 1976 with slight modifications (Akoachere *et al.*, 2005). Parasites were maintained at 1-10% parasitemia and 3.3% hematocrit in an RPMI 1640 culture medium supplemented with A+ erythrocytes (purchased from the blood bank of the University Hospital Giessen and Marburg, UKGM), 0.5% (w/v) lipid-rich-bovine serum albumin (Albumax), 9 mM (0.16%) glucose, 0.2 mM hypoxanthine, 2.1 mM L-glutamine, 25 mM Hepes, and 22 $\mu g \cdot mL^{-1}$ gentamicin. All incubations were carried out at 37 °C in 3% O_2, 3% CO_2, and 94% N_2. Parasites were synchronized in culture to ring stages as a starting population by treating them with 5% (w/v) sorbitol (Lambros and Vanderberg, 1979). *P. falciparum* trophozoites were enriched via magnetic separation (Paul *et al.*, 1981). Cell lysates were obtained via saponin lysis (Sturm *et al.*, 2009). Parasitemia was counted using Giemsa-stained blood smears (Rahbari *et al.*, 2017).

In vitro activity of compounds against *Plasmodium falciparum* parasites

To investigate the effect of the compound SBI-0797750 on asexual blood stage parasites, its activity against the *P. falciparum* 3D7 strain was determined using the [^{3}H]-hypoxanthine incorporation assay (Desjardins *et al.*, 1979; Kasozi *et al.*, 2013) and against *P. falciparum* 3D7 and NF-54-*attB* parasites using the SYBR Green I-based fluorescence assay (Ekland *et al.*, 2011; Rahbari *et al.*, 2017). Stock solutions of the inhibitors were dissolved in DMSO. For the [^{3}H]-hypoxanthine incorporation assay, serial double dilutions of the inhibitor (100 µL) were prepared in hypoxanthine-free medium in 96-well microtiter plates. Synchronized ring-stage parasites in hypoxanthine-free complete medium (100 µL) were added to each well (0.15-0.20% parasitemia and 1.25% final hematocrit). After 44 h incubation at 37 °C in a gaseous

mixture (3% O_2, 3% CO_2, and 94% N_2), 50 µL of [^{3}H]-hypoxanthine (final concentration of 0.5 µCi/well) were added per well, and the plate was further incubated for 24 h. After a total incubation of 68 h, the plates were frozen at -80 °C for at least 24 h. To measure the effect of the compound, the plates were then thawed, and each well was harvested on a glass fiber filter (Perkin-Elmer, Rodgau-Jügesheim) and dried. Radioactivity from each well was measured in counts per minute (Desjardins *et al.*, 1979; Kasozi *et al.*, 2013). For the SYBR Green-I assay, serial double dilutions of the inhibitor (50 µL) in complete medium were performed in 96-well microtiter plates, half area (µClear bottom). Synchronized ring-stage parasites in complete medium (50 µL) were added to each well (0.15% parasitemia and 1.25% final hematocrit) and incubated for 44 h (3D7) or 48 h (NF-54-*attB*) at 37 °C. Afterwards, 20 µL of 5x SYBR Green in lysis buffer (20 mM Tris-HCl, 5 mM EDTA, 0.16% (w/v) saponin, and 1.6% (v/v) Triton X-100) were added to each well and incubated for 24 h at RT in the dark. Fluorescence was measured using the CLARIOstar plate reader at ex494/em530. The IC_{50} values were determined by curve-fitting the percentage of growth inhibition (in relation to controls) against the log of drug concentration with a variable slope sigmoidal function (Microsoft Excel) (Ekland *et al.*, 2011; Rahbari *et al.*, 2017). Infected RBCs were used as a positive control, uninfected RBCs as a negative control (Rahbari, 2017).

A potential impact of combinations of SBI-0797750 with chloroquine, methylene blue, or artemisinin on asexual blood stage *P. falciparum* 3D7 parasites was investigated using the [^{3}H]-hypoxanthine incorporation assay as described above (Desjardins *et al.*, 1979; Fivelman *et al.*, 2004). The resulting IC_{50} values allowed the detection of potential combination effects.

4 Results

4.1 GluPho and G6PD from *Plasmodium falciparum*

Bifunctional *Pf*GluPho catalyzes the first two steps of the oxidative PPP in *Plasmodium*; the C-terminal part – *Pf*G6PD – comprises amino acid residues 339-911 (Jortzik *et al.*, 2011).

4.1.1 Heterologous overexpression and purification of *Pf*GluPho and *Pf*G6PD

Recombinant *Pf*GluPho wt and *Pf*G6PD were produced as described in Jortzik *et al*., 2011 using a pQE30 expression vector and *E. coli* M15 cells, for *Pf*GluPho containing pRAREII. Representative gels of the *Pf*GluPho purification are shown in Figure 10a, b. For the affinity chromatography of *Pf*G6PD, Talon was used as an alternative column material within this thesis, resulting in high purity of the protein (Figure 10c, d). The yield of pure and active proteins varied from 0.3 to 3 mg per liter *E. coli* cell culture. The proteins were stored at 4 °C for up to five days, long-term storage conditions were -80 °C and 50% glycerol.

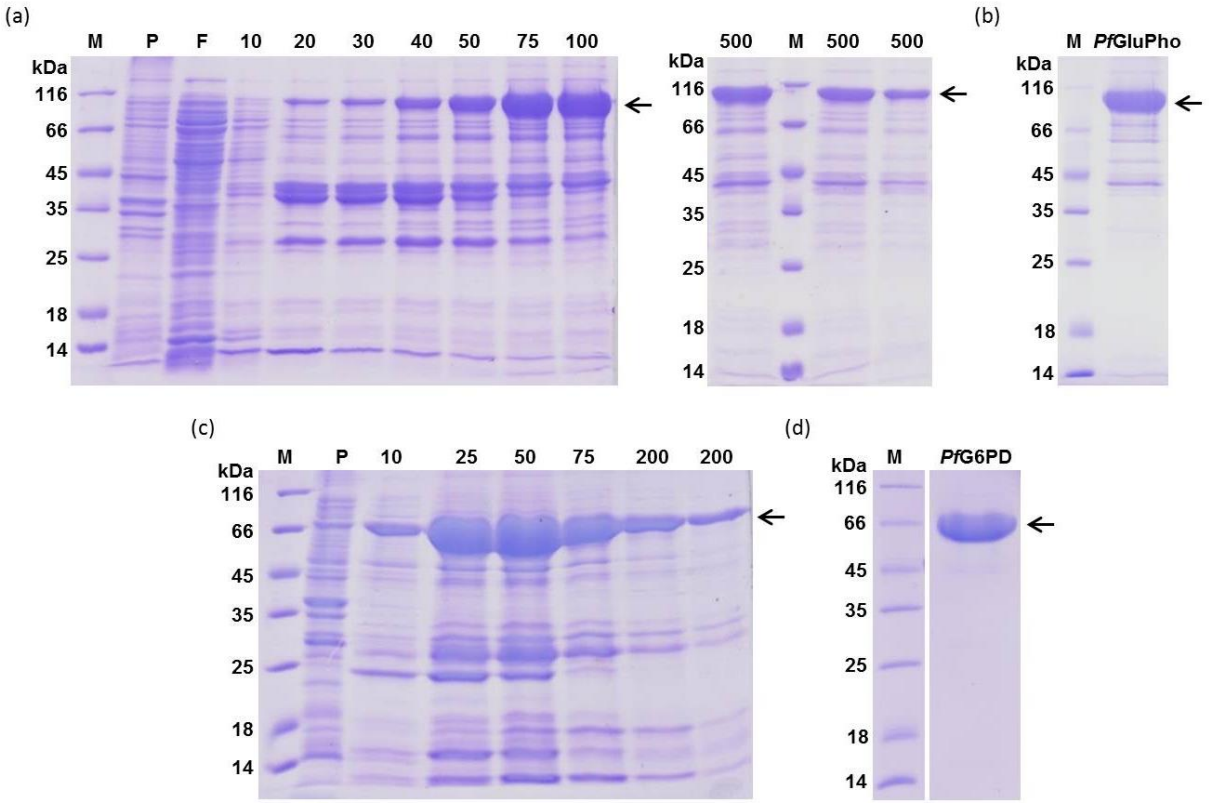

Figure 10. Purification of *Pf*GluPho wt and *Pf*G6PD
(a) *Pf*GluPho was purified via affinity chromatography using Ni-NTA as column material. Purest fractions (75-500 mM imidazole) were pooled and applied to size exclusion chromatography. (b) To control the final purity of *Pf*GluPho, 7.5 µg of protein were applied to a 12% SDS-PAGE gel. (c) *Pf*G6PD was purified via affinity chromatography using Talon as column material. Purest fractions (25-200 mM imidazole) were pooled and applied to size exclusion chromatography. (d) To control the final purity of *Pf*G6PD, 7.5 µg of protein were applied to a 12% SDS-PAGE gel. The numbers above the lanes indicate the imidazole concentration used for elution. M: Unstained Protein Molecular Weight Marker; P: pellet; F: flow-through.

4.1.2 Characterization of naturally occurring *Pf*GluPho variants

The naturally occurring *Pf*GluPho variants investigated in this thesis were identified via an *in silico* analysis of the protein with the former ID: PF14_0511 (now PF3D7_1453800) in the malaria database PlasmoDB. Prominent single nucleotide polymorphisms resulting in an amino acid exchange were S315Y, L395F, and F507L. So far, it is unknown whether these mutations have an impact on the kinetic parameters of the enzyme. Furthermore, proteomic approaches identified several amino acid residues of *Pf*GluPho to be phosphorylated *in vivo*, the phosphorylation of the C-terminally located Ser-Ser pair (S899 and S900) was reported by several groups (Lasonder *et al.*, 2012; Pease *et al.*, 2013; Treeck *et al.*, 2011). To study the potential impact of the mentioned mutations and phosphorylations on the properties of *Pf*GluPho, site-directed mutagenesis was performed. The naturally occurring phosphorylations were mimicked by replacement of the two serines on position 899 and 900 by glutamic acids (Kim *et al.*, 2015). The mutants were heterologously overexpressed and purified using the same protocol as for the wt enzyme (chapter 4.1.1), resulting in comparable yield and purity. The mutants were stored at -80 °C and 50% glycerol until kinetic determinations.

Oligomerization behavior of naturally occurring *Pf*GluPho variants

Simultaneous to the improvement in purity, size exclusion chromatography was used to study the oligomerization behavior of *Pf*GluPho variants. The reduced mutants eluted as tetramers with molecular masses of approximately 480 kDa from the size exclusion chromatography column (Figure 11b-f), indicating that the oligomerization is not primarily based on disulfide bonds between the subunits. Since this behavior was also observed for the wt enzyme (Figure 11a), none of the mutations changed the oligomerization behavior of *Pf*GluPho. Similar to full-length *Pf*GluPho, reduced *Pf*G6PD eluted from size exclusion chromatography after 65 min (= 65 mL) in a tetrameric form with approximately 260 kDa (not shown).

Kinetic characterization of naturally occurring *Pf*GluPho variants

To investigate a potential impact of the mutations on *Pf*GluPho, the kinetic parameters were determined in comparison to the wt enzyme. An overview of the kinetic data is shown in Table 14. Parts of the measurements were performed by members of Prof. Becker's group (Stegmayer, 2013) and by Max Reichmann, a master student supervised by myself in the laboratory (Reichmann, 2018). The values for the wt enzyme determined within this thesis are in good accordance with values from the literature (Jortzik *et al.*, 2011). The V_{max} values of the mutants ranged between 4.0 and 6.0 $U \cdot mg^{-1}$ and therefore did not majorly differ from the wt enzyme (5.9 ± 1.0 $U \cdot mg^{-1}$ for G6P, 5.9 ± 0.6 $U \cdot mg^{-1}$ for $NADP^+$). Likewise, the K_M values were with a range of 18.4 and 29.2 µM for G6P and of 3.7 and 6.2 µM for $NADP^+$ comparable to the values of the wt (G6P: 20.3 ± 5.6 µM; $NADP^+$: 6.1 ± 1.3 µM).

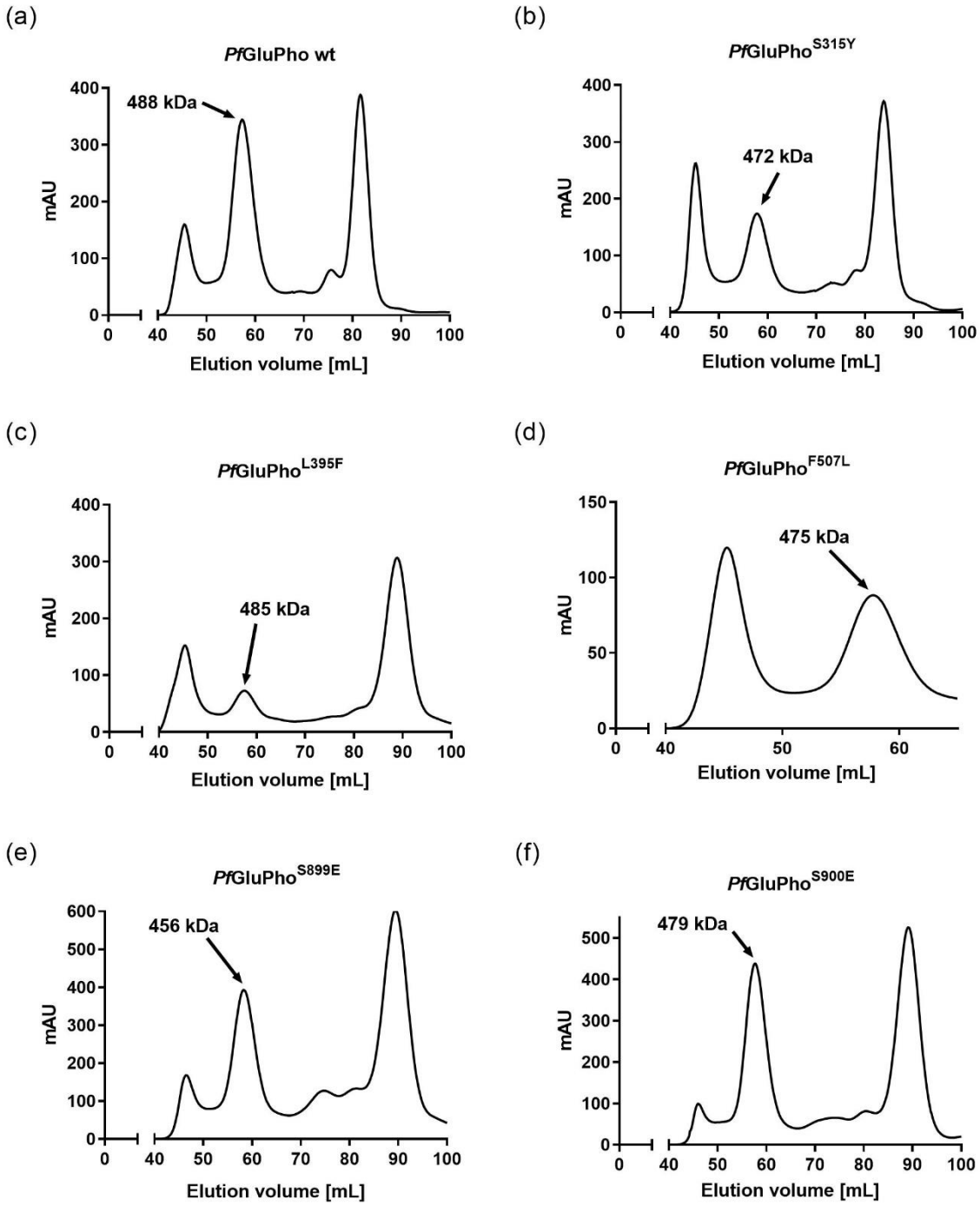

Figure 11. Size exclusion chromatography of *Pf*GluPho wt and mutants
Reduced *Pf*GluPho wt and mutants eluted after approximately 58 mL in a tetrameric form from the size exclusion chromatography column. The experiment for *Pf*GluPho^{F507L} (d) was stopped after 65 mL due to technical reasons. The *Pf*GluPho peaks are indicated by arrows; the other peaks resulted from proteins that could not be removed using affinity chromatography.

Table 14. Kinetic characteristics of *Pf*GluPho variants

Values are represented as mean values ± standard deviations (SD) of at least two independent determinations, each including at least two independent measurements. * Values from Jortzik *et al*., 2011 are given for comparison. ǂ Catalytic efficiency (k_{cat}/K_M) from Jortzik *et al*., 2011 was calculated from mean values to allow for comparison.

		*Pf*GluPho wt*	*Pf*GluPho wt	*Pf*GluPho^{S315Y}	*Pf*GluPho^{L395F}	*Pf*GluPho^{F507L}	*Pf*GluPho^{S899E}	*Pf*GluPho^{S900E}
V_{max} [U·mg^{-1}]	G6P	5.2 ± 1.6	5.9 ± 1.0	4.4 ± 1.1	4.5 ± 0.9	6.0 ± 1.4	5.6 ± 0.1	6.0 ± 1.1
	$NADP^+$	4.6 ± 0.8	5.9 ± 0.6	4.6 ± 1.5	4.0 ± 1.1	5.0 ± 0.3	5.2 ± 0.2	6.0 ± 0.6
K_M [µM]	G6P	19.2 ± 3.9	20.3 ± 5.6	23.4 ± 7.1	29.2 ± 4.1	24.1 ± 4.4	24.1 ± 2.8	18.4 ± 5.1
	$NADP^+$	6.5 ± 2.2	6.1 ± 1.3	5.1 ± 1.0	4.0 ± 0.2	3.7 ± 0.1	6.2 ± 0.5	5.8 ± 1.5
k_{cat} [sec^{-1}]	G6P	8.6 ± 1.5	10.7 ± 1.8	7.9 ± 2.0	8.1 ± 1.6	10.9 ± 2.5	10.1 ± 0.2	10.8 ± 1.9
	$NADP^+$	8.2 ± 1.2	10.1 ± 0.9	8.3 ± 2.7	7.2 ± 2.0	9.1 ± 0.5	9.3 ± 0.4	10.8 ± 1.2
Catalytic efficiency [M^{-1}·sec^{-1}]	G6P	$4.4 \cdot 10^{5}$ ǂ	$5.8 \cdot 10^{5}$ ± $1.5 \cdot 10^{5}$	$3.7 \cdot 10^{5}$ ± $2.0 \cdot 10^{5}$	$2.9 \cdot 10^{5}$ ± $9.4 \cdot 10^{4}$	$4.5 \cdot 10^{5}$ ± $2.2 \cdot 10^{4}$	$5.2 \cdot 10^{5}$ ± $2.3 \cdot 10^{5}$	$6.2 \cdot 10^{5}$ ± $2.2 \cdot 10^{5}$

4.1.3 Crystallization of *Pf*GluPho and *Pf*G6PD

Parts of the crystallization trials were performed in collaboration with the master student Max Reichmann (Reichmann, 2018).

Stability tests on *Pf*GluPho and *Pf*G6PD

To enable protein crystallization, stability of the protein at the temperature used for crystallization trials over several days or weeks is essential (McPherson and Gavira, 2014). So far, the stability of *Pf*GluPho and *Pf*G6PD at RT – the most commonly used condition – was not sufficient; the protein often degraded within minutes after preparation of the drops. To enhance the stability, a fluorescence-based thermal shift assay screening for new buffer conditions or additives that enhance the stability of *Pf*GluPho was carried out in the group of Prof. Becker. Within this thesis, the effects of promising buffers and chemicals (listed in 3.3.9) on the stability of *Pf*GluPho and *Pf*G6PD were tested.

Both *Pf*GluPho and *Pf*G6PD were most stable in a lithium citrate/Tris buffer, pH 7.8. Down to 75 mM lithium citrate, *Pf*GluPho was stable for two weeks at RT (Figure 12). During this time, most crystals are able to grow. Higher lithium citrate concentrations enhanced the stability even more. However, crystallization trials showed that lithium citrate tends to build salt crystals; therefore, the salt concentration was kept to a minimum of 75 mM lithium citrate as the lowest concentration that could stabilize the enzyme for two weeks. Since the buffer concentration is halved after preparing the drops, the protein was prepared in the following buffer: 150 mM lithium citrate, 50 mM Tris, pH 7.8. Buffer exchange prior to crystallization was performed via size exclusion chromatography as described in chapter 3.3.3.

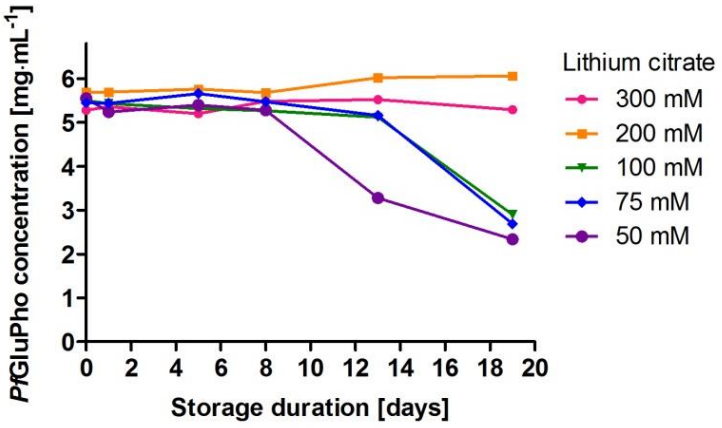

Figure 12. Stability of *Pf*GluPho in lithium citrate buffer
The stability of *Pf*GluPho at room temperature was tested under various concentrations of lithium citrate with 50 mM Tris, pH 7.8. One representative of two independent determinations is shown.

Crystallization of *Pf*G6PD

Using the newly identified buffer (150 mM lithium citrate, 50 mM Tris, pH 7.8), the crystallization conditions of *Pf*G6PD were screened in sitting drops by using the screens listed in 2.6 as well as screens designed in-house. The most promising crystals were found using 10 mg·mL^{-1} *Pf*G6PD in 0.1 M MES, pH 5.0, 10% (w/v) PEG 6,000, final pH 6.0 (JCSG Core I Suite, F1, Figure 13); therefore, this condition was used for further optimization.

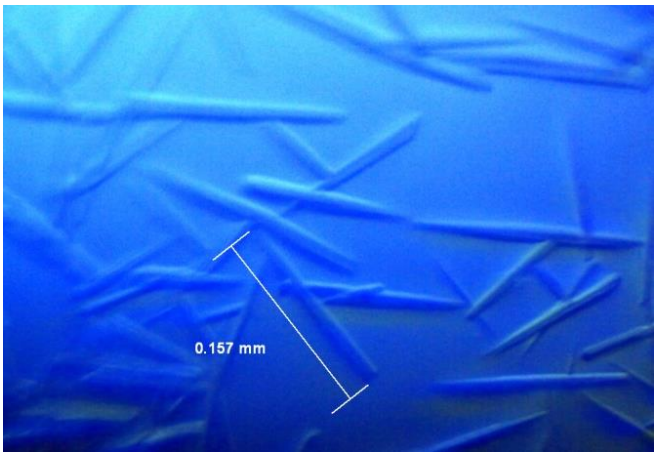

Figure 13. Initially obtained *Pf*G6PD crystals
During a screening for crystallization conditions, the most promising *Pf*G6PD crystals grew in sitting drops using 10 mg·mL^{-1} *Pf*G6PD in 0.1 M MES, pH 5.0, 10% (w/v) PEG 6,000, final pH 6.0 (JCSG Core I Suite, F1).

Variations in pH and PEG concentrations, as well as the addition of ethylene glycol and G6P improved the crystal quality; the best crystals (14.4 mg·mL^{-1} *Pf*G6PD, 0.1 M MES, pH 6.0, 9% (v/v) PEG 6,000, 40% ethylene glycol, 2.9 mM G6P) had a resolution of 7 Å. Although this is a slight improvement over the crystals obtained previously (8.5 Å), it is still too low to solve the three-dimensional structure of the protein. Using the hanging drop approach instead of sitting drops improved the size of the crystals (Figure 14); however, they were unstable and therefore not suitable for X-ray diffraction analysis.

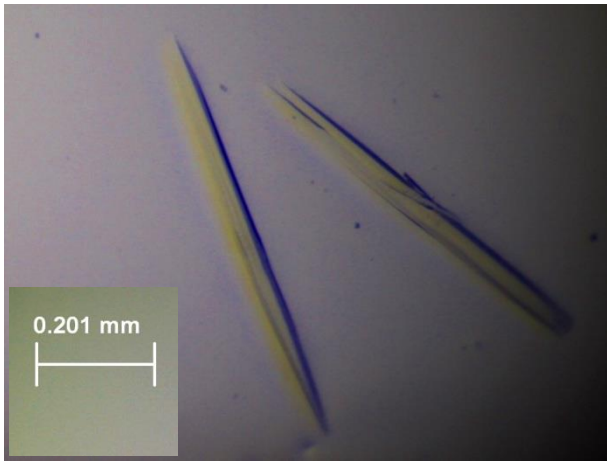

Figure 14. Crystals obtained during optimization trials of *Pf*G6PD crystallization
Crystals were obtained in hanging drops at 10 mg·mL^{-1} *Pf*G6PD, 0.2 M MES, pH 6.0, 8% PEG 6,000.

Crystallization of *Pf*GluPho

Screening for crystallization conditions of *Pf*GluPho showed that most crystals were found when adding at least 40% MPD. The major problem during optimization trials using this precipitant was phase separation within the reservoir solution (Figure 15a, b). The microcrystals obtained were not suitable for X-ray diffraction analysis due to their limited size (Figure 15c).

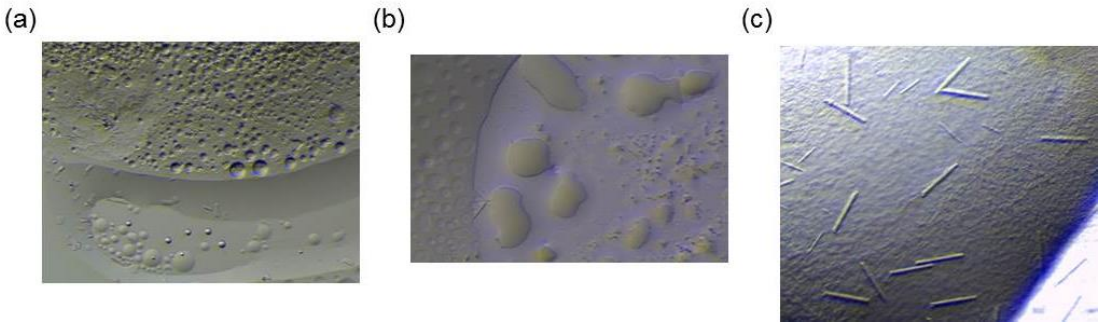

Figure 15. Crystallization of *Pf*GluPho wt using MPD
Phase separation was observable using 11.5 mg·mL^{-1} *Pf*GluPho wt, 48% MPD, 0.1 (a) or 0.2 (b) M potassium citrate. (c) 11.5 mg·mL^{-1} *Pf*GluPho wt, 48% MPD, 0.15 M sodium citrate, 0.1 M Hepes, pH 7.5.

The affinity for MPD was also observed during crystallization trials of the mutant *Pf*GluPho^{S899E} (Figure 16). X-ray diffraction analysis revealed a disordered plate type, meaning that the crystal structure was disturbed and therefore not suitable for structure determination.

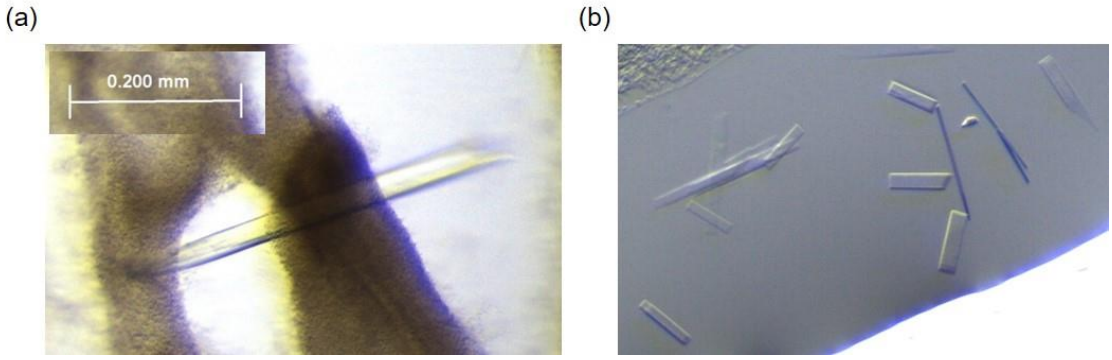

Figure 16. Crystals of *Pf*GluPho^{S899E}
(a) 13.1 mg·mL^{-1}*Pf*GluPho^{S899E}, 47% MPD, 0.25 M Hepes, pH 7.5, 5 mM G6P. (b) 13.1 mg·mL^{-1}*Pf*GluPho^{S899E}, 50% MPD, 0.1 M ammonium dihydrogen phosphate, 0.1 M Hepes, pH 7.5.

In summary, it was so far not possible to crystallize *Pf*GluPho or *Pf*G6PD in a sufficient quality. Further possible approaches to solve the three-dimensional structure of these enzymes will be discussed in 5.5.1.1.

4.2 GluPho and G6PD from *Plasmodium vivax*

4.2.1 Heterologous overexpression and purification of *Pv*GluPho and *Pv*G6PD

*Pv*GluPho
Similar to *P. falciparum*, the first two steps of the oxidative PPP in *P. vivax* are catalyzed by the bifunctional enzyme *Pv*GluPho (Mohring *et al.*, 2014). Angeles Stegmayer first attempted to recombinantly produce the enzyme. However, since this turned out to be extremely challenging, this important enzyme was characterized in the meantime by using the C-terminal *Pv*G6PD, comprising amino acids 310-927 (Stegmayer, 2013). A new attempt to produce full-length *Pv*GluPho was performed by a master student supervised by myself in the laboratory, Isabell Berneburg (data not shown here, for details see Berneburg, 2017). Different vectors (pQE30, pET28a) and *E. coli* strains (M15, BL21, KRX, XL1-Blue, SHuffle T7, SHuffle T7 Express, C41, C43, Lemo21) cultivated in different media (LB, TB, 2xYT) under various temperatures

(16-37 °C) for different durations (4-20 h) as well as co-expression with chaperones (pGRO7, pKEJ7, pGroRARE) and additional plasmid (pRAREII) were employed to overexpress recombinant *Pv*GluPho. The expression of the enzyme as well as the result of subsequent purification steps were checked via Western blot analyses using an anti-6xHis-tag antibody as described in chapter 3.3.5. The major problem was degradation of the protein during overexpression. The most promising condition was overexpression of *Pv*GluPho in *E. coli* Lemo21 cells using LB medium, 100 µM rhamnose and 400 µM IPTG at 18 °C for 4 h. Since the solubility of the protein tended to be low, *E. coli* cells were lysed under the addition of various detergents (Triton X-100, glycerol, n-octyl-β-D-glucopyranoside, FOScholine®12, n-decyl-β-D-maltopyranoside, n-dodecyl-β-D-maltoside, and N,N-dimethyldodecylamine N-oxide); simultaneously, different buffer systems were tested (500 mM NaCl, 50 mM Tris or Hepes, pH 7.8). Cell lysis using N,N-dimethyldodecylamine N-oxide or glycerol as detergents and Hepes buffer were the most promising conditions. The protein was purified via affinity chromatography using Ni-NTA as column material. Western blot analysis of samples after purification resulted in a clear band at the expected height of 110 kDa. Reduced *Pv*GluPho eluted from size exclusion chromatography as a tetramer of approximately 383 kDa. The G6PD activity was tested using the assay described in chapter 3.3.6 for *Pf*GluPho. Unfortunately, however, the protein did not show any activity (Berneburg, 2017). In summary, it has so far not been possible to produce active full-length *Pv*GluPho; the following experiments were conducted using its C-terminal part, *Pv*G6PD. Further conditions need to be tested to produce *Pv*GluPho.

*Pv*G6PD

The gene for *Pv*G6PD in the pQE30 expression vector was transformed into competent *E. coli* M15 cells containing pRAREII, and heterologously overexpressed. The N-terminal 6xHis-tag was used for purification via affinity chromatography with Ni-NTA as column material (Figure 17a). In order to improve purity, size exclusion chromatography was performed (see chapter 3.3.3). The final purity was controlled using SDS-PAGE, loading 7.5 µg of protein onto the gel (Figure 17b). The yield of pure, soluble, and active protein per liter *E. coli* cell culture was 0.1-0.4 mg.

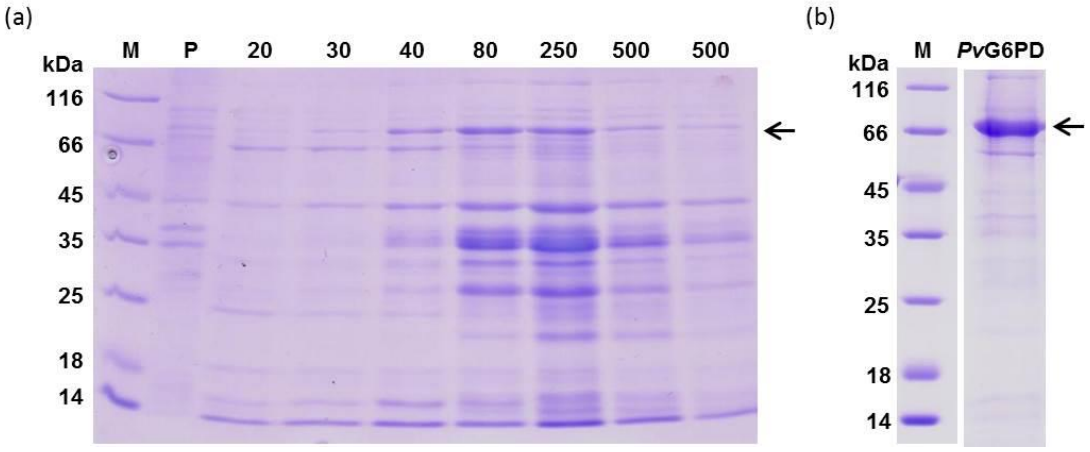

Figure 17. Purification of *Pv*G6PD

(a) *Pv*G6PD was purified via affinity chromatography using Ni-NTA as column material. Purest fractions (40-500 mM imidazole) were pooled and applied to size exclusion chromatography. (b) To control the final purity of *Pv*G6PD, 7.5 µg of protein was applied to a 12% SDS-PAGE gel. The numbers above the lanes indicate the imidazole concentration used for elution. M: Unstained Protein Molecular Weight Marker; P: pellet.

Attempts to increase the yield were performed using a similar approach as described above for *Pv*GluPho (various *E. coli* cells, media, temperatures, and durations for expression, different buffers and detergents). However, none of the tested conditions resulted in an increased yield (not shown; Berneburg, 2017). The protein was stored at 4 °C for up to five days, long-term storage conditions were -80 °C and 50% glycerol.

Oligomerization behavior of *Pv*G6PD

Simultaneous to the improvement in purity, size exclusion chromatography was used to study the oligomerization behavior of *Pv*G6PD. Prior to each run, the enzyme was reduced by 5 mM DTT. Under this condition, *Pv*G6PD eluted as a peak of approximately 390 kDa indicating that the protein is presumably present as a hexamer (Figure 18). This hexameric conformation of the reduced enzyme indicates that oligomerization is not primarily based on intermolecular disulfide bonds.

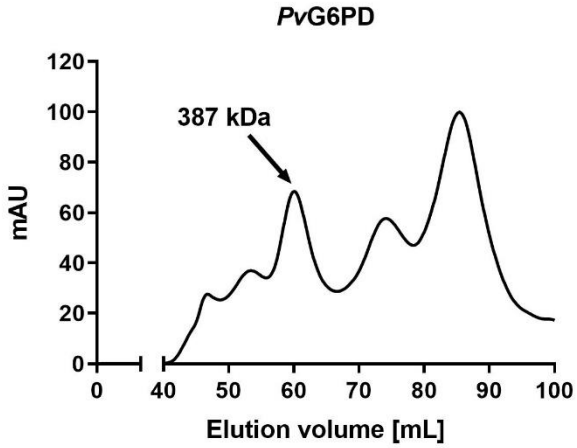

Figure 18. Size exclusion chromatography of *Pv*G6PD

Reduced *Pv*G6PD eluted from the size exclusion chromatography column after 60 mL with a molecular mass of approximately 390 kDa. The *Pv*G6PD peak is indicated by arrows; the other peaks result from proteins that could not be removed using affinity chromatography.

4.2.2 Kinetic characterization of *Pv*G6PD

The kinetic parameters of *Pv*G6PD were determined within my own master thesis (Haeussler, 2015) and confirmed later (Berneburg, 2017) using the assay established for *Pf*GluPho measuring the NADPH production. The specific activity of *Pv*G6PD was determined to be 4.6 ± 0.3 $U \cdot mg^{-1}$, with K_M values of 80.2 ± 19.8 µM and 14.8 ± 2.9 µM for G6P and $NADP^+$, respectively (Figure 19). Due to the high K_M for G6P, standard assay conditions were slightly changed; 800 µM of G6P was defined as saturation for *Pv*G6PD. An overview of the kinetic parameters is given in Table 15.

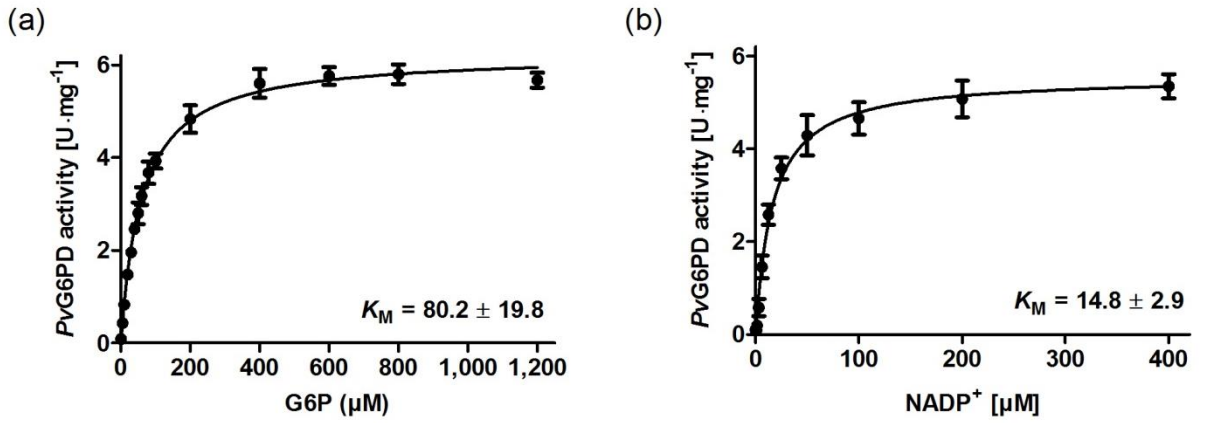

Figure 19. K_M determinations for *Pv*G6PD
Representative Michaelis-Menten curves (mean values ± SD of three measurements) for the K_M determinations of *Pv*G6PD. The K_M values for G6P (a) and $NADP^+$ (b) are shown as mean values ± SD of four independent determinations (see also Table 15).

Table 15. Kinetic characteristics of *Pv*G6PD
Values are represented as mean values ± SD of four independent determinations, each including at least three independent measurements.

V_{max} [U·mg^{-1}]		K_M [µM]		k_{cat} [sec^{-1}]		Cat. efficiency [M^{-1}·sec^{-1}]
G6P	$NADP^+$	G6P	$NADP^+$	G6P	$NADP^+$	G6P
5.6 ± 0.7	5.5 ± 0.4	80.2 ± 19.8	14.8 ± 2.9	6.7 ± 0.8	6.5 ± 0.4	$8.2 \cdot 10^4$

4.3 6PGD from *Plasmodium falciparum*

4.3.1 Heterologous overexpression and purification of *Pf*6PGD and h6PGD

The coding sequences for *Pf*6PGD wt and h6PGD were ordered as codon-optimized synthetic genes, cloned into the pQE30 expression vector using the restriction sites *BamH*I and *Hind*III, and transformed into competent *E. coli* M15 cells used for heterologous overexpression. *Pf*6PGD wt was for the first time heterologously overexpressed and purified within my master thesis (Haeussler, 2015) and optimized within this thesis. The proteins were purified via affinity chromatography using the N-terminal 6xHis-tag and Ni-NTA as a column material (Figure 20a, c). In order to improve the purity, size exclusion chromatography was performed as described in chapter 3.3.3; all enzymes eluted with a comparable pattern under all tested conditions (see also 4.3.4, Figure 27). The final purity was controlled using SDS-PAGE, loading 7.5 µg of protein onto the gel (Figure 20b, d). The yield of pure, soluble, and active protein was up to 1 mg *Pf*6PGD wt and 11 mg h6PGD per liter *E. coli* cell culture. For short-term storage up to five days, *Pf*6PGD wt was stored at 4 °C. This condition was only used to investigate post-translational modifications. Long-term storage conditions of *Pf*6PGD and h6PGD were -80 °C and 50% glycerol.

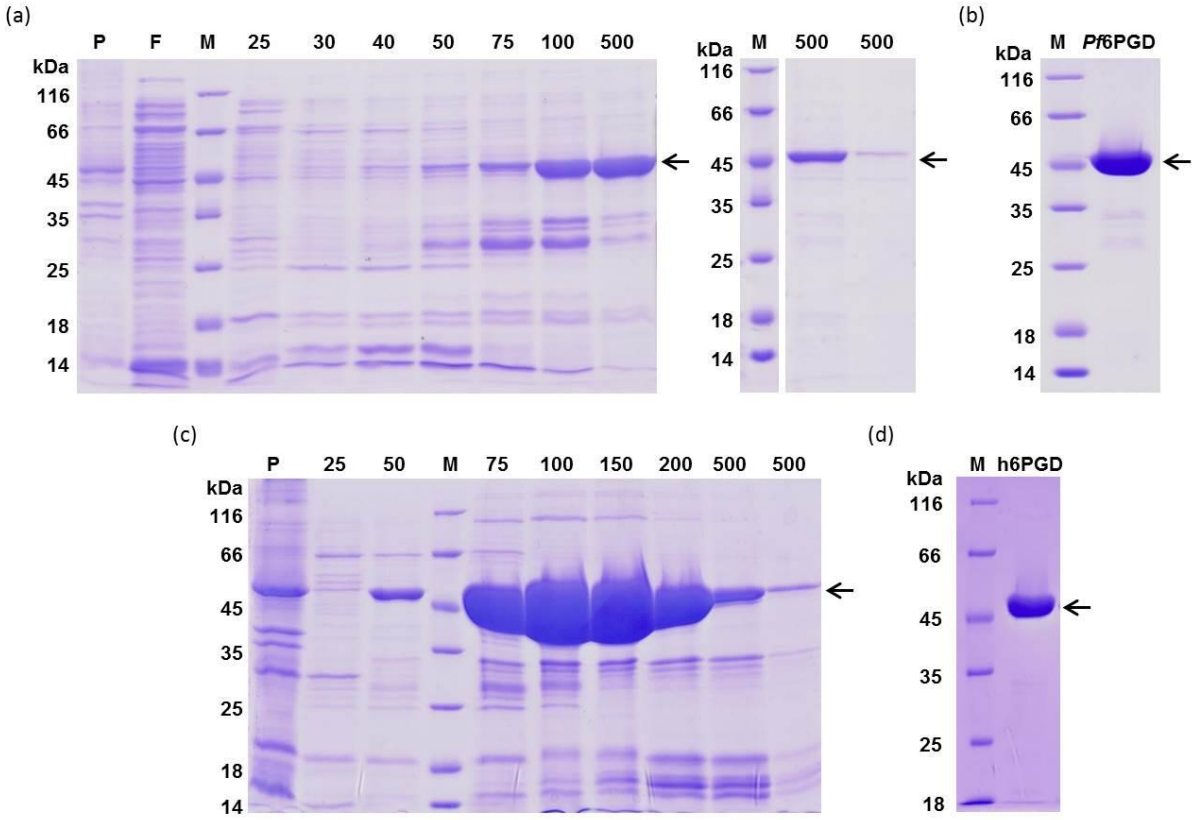

Figure 20. Purification of *Pf*6PGD wt and h6PGD
(a) *Pf*6PGD wt was purified via affinity chromatography using Ni-NTA as column material. Purest fractions (100-500 mM imidazole) were pooled and applied to size exclusion chromatography. (b) To control the final purity of *Pf*6PGD wt, 7.5 µg protein were applied to a 12% SDS-PAGE gel. (c) h6PGD was purified via affinity chromatography using Ni-NTA as column material. Purest fractions (75-500 mM imidazole) were pooled and applied to size exclusion chromatography. (d) To control the final purity of h6PGD, 7.5 µg protein were applied to a 12% SDS-PAGE gel. The numbers above the lanes indicate the imidazole concentrations used for elution. M: Unstained Protein Molecular Weight Marker; P: pellet; F: flow-through.

4.3.2 Crystallization of *Pf*6PGD

Crystallization of native *Pf*6PGD wt

To find an initial condition that enables crystallization of native *Pf*6PGD wt, a screening was performed within my master thesis with a protein concentration of 6 mg·mL^{-1}, using screens listed in 2.6 and screens designed in-house for PEG, MPD, and ammonium sulfate (Haeussler, 2015). Crystals grew under two main conditions containing either (I) lithium nitrate and PEG 3,350 or (II) sodium citrate, pH 5.6, PEG 4,000, glycerol, and ammonium acetate or ammonium sulfate. The initial conditions were optimized by varying the precipitant concentrations and using a higher protein concentration (10 mg·mL^{-1}) in 24-well plates using the hanging drop approach. Crystals suitable for X-ray diffraction analysis grew under 25% (v/v) PEG 4,000, 15% glycerol, 0.085 M sodium citrate, pH 5.6, and 0.17 M ammonium acetate (Figure 21) (Haeussler *et al.*, 2018).

Figure 21. Crystals of native *Pf*6PGD wt
Crystals of native *Pf*6PGD wt, grown in hanging drops. 10 mg·mL^{-1} *Pf*6PGD wt, 25% (v/v) PEG 4,000, 15% glycerol, 0.085 M sodium citrate, pH 5.6, and 0.17 M ammonium acetate.

Crystallization of *Pf*6PGD wt in complex with 6PG and NADP$^+$

First, cocrystallization with substrate and cofactor was attempted under the conditions that were successful for native *Pf*6PGD wt; however, the obtained crystals did not show sufficient X-ray diffraction patterns. Therefore, new screenings were performed yielding crystals that were immediately suitable for X-ray diffraction analysis, or after a small variation of the conditions. The crystals in complex with 6PG were grown in sitting drops at 7.6 mg·mL^{-1} *Pf*6PGD wt, 24% (w/v) PEG 1,500, 20% glycerol (JCSG Core II Suite, E11, Figure 22a), and 5 mM 6PG, the crystals in complex with NADP$^+$ at 15.4 mg·mL^{-1} protein, 25% MME550, 0.1 M Hepes, pH 4.6, and 5 mM NADP$^+$ (Figure 22b) (Haeussler *et al.*, 2018).

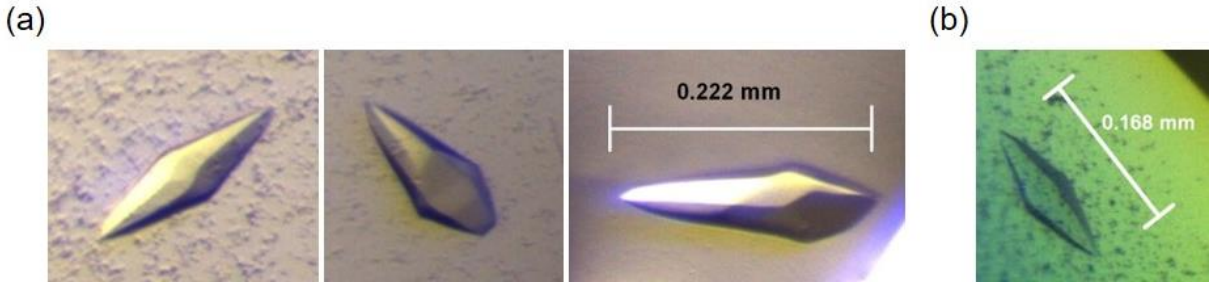

Figure 22. Crystals of *Pf*6PGD wt in complex with 6PG and NADP$^+$
(a) 7.6 mg·mL^{-1} *Pf*6PGD wt, 24% (w/v) PEG 1,500, 20% glycerol (JCSG Core II Suite, E11), and 5 mM 6PG. (b) 15.4 mg·mL^{-1} protein, 25% MME550, 0.1 M Hepes, pH 4.6, and 5 mM NADP$^+$.

4.3.3 Structure of *Pf*6PGD

Dr. Anton Meinhart, Dr. Ilme Schlichting, and Dr. Miroslaw Tarnawski collected diffraction data of the crystals at X10SA (detector: Pilatus) of the Swiss Light Source at the Paul Scherrer Institute in Villigen, Switzerland. Data processing using the XDS program package (Kabsch, 2010) was performed by Dr. Karin Fritz-Wolf at MPI Heidelberg. The structures were solved with the molecular replacement method. Coordinates and measured reflection amplitudes are accessible in the RCSB PDB Protein Data Bank under the PDB codes 6FQX (apo-*Pf*6PGD), 6FQY (in complex with NADP$^+$), and 6FQZ (in complex with 6PG). The enzyme complexed with 6PG diffracted to the highest resolution of 1.9 Å, while native *Pf*6PGD wt and complexed with

$NADP^+$ had a resolution of 2.8 and 2.9 Å, respectively. In one monomer of the $NADP^+$ complexed structure, residues 1-67, 85-92, and 129-133 were only weakly defined; however, the corresponding region of the other monomer was well defined. Moreover, a short surface loop comprising residues 306-314 showed weak electron density. Apart from that, all structures were well defined. The enzyme complexed with 6PG showed significant density for 6PG in each subunit in the difference electron density map. For the bound $NADP^+$, however, only the adenine moiety and the three phosphate groups were well defined; the rest of $NADP^+$ was not visible (see 4.3.3.3) (Haeussler *et al.*, 2018).

4.3.3.1 Overall structure of *Pf*6PGD

The structure revealed that *Pf*6PGD is a functional homodimer that contains 468 amino acids per subunit. Subunits A and B of the homodimer each contain two domains, one with the 6PG and the other one with the $NADP^+$ binding site, and a C-terminal tail of domain 2. Domain 1 is the smaller domain; it comprises residues 1-176 and is a βαβ domain, composed of a mixed parallel and anti-parallel 6-stranded β sheet. The larger domain 2 (residues 177-468) is in contrast mainly α-helical. The C-terminal tail comprises residues 434-468 of one subunit, and penetrates domain 2 of the adjacent subunit. This interaction very tightly links the two monomers of the dimer (Figure 23) (Haeussler *et al.*, 2018).

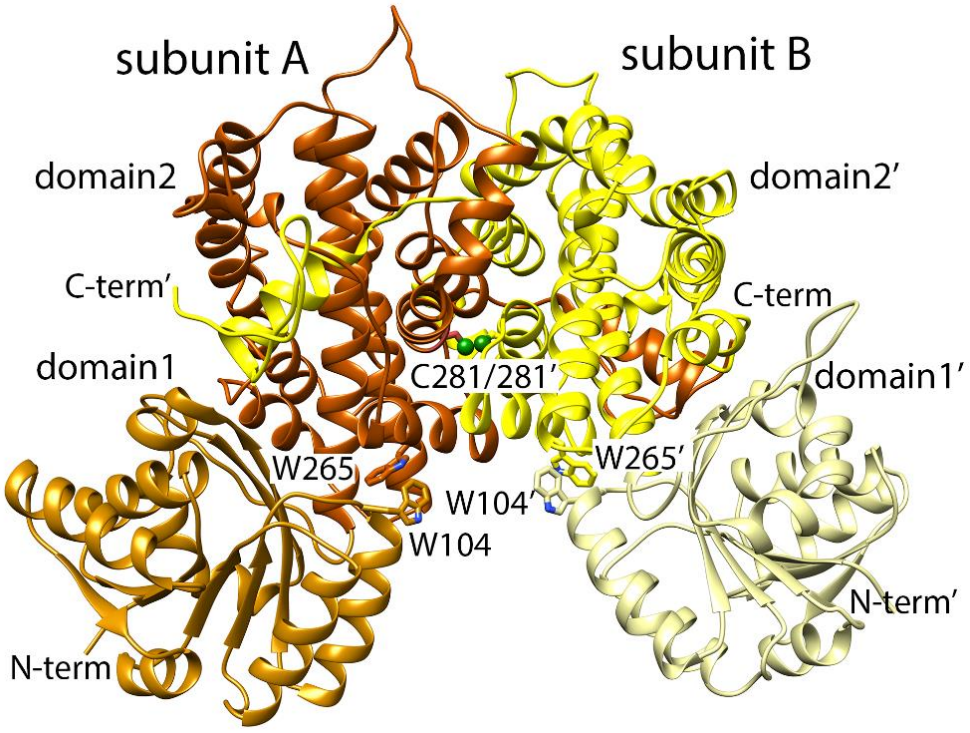

Figure 23. Overall structure of the *Pf*6PGD dimer
The structure of the apoenzyme is shown. In subunit A, domain 1 and domain 2 are colored amber and brown, respectively, in subunit B light-yellow and yellow. All parts of subunit B are marked with ‘. The important residues C281, W104, and W265 are shown as ball and stick models (Haeussler *et al.*, 2018).

With this overall structure, *Pf*6PGD shares major similarities with other members of the highly conserved 6PGD family, e.g. from humans (2JKV (to be published)), *Lactococcus lactis* (Sundaramoorthy *et al.*, 2007), or *Geobacillus stearothermophilus* (Cameron *et al.*, 2009). Apart from the similarities to the 6PGD family, there are also interactions between

Plasmodium-specific residues; in two of our three structures (apo and $NADP^+$ complex), the *Plasmodium*-specific cysteine residues C281 and C281' link the subunits, forming a disulfide bridge between them. Cysteine C281 is not only present in *P. falciparum* 6PGD, but in all five human pathogenic species (shown in the amino acids alignment in Appendix 2). Furthermore, the *Plasmodium*-specific W104 in domain 1 interacts with the strictly conserved residue W265 in domain 2. An alignment of 6PGDs from different species highlighting important residues is given in Figure 24 (also see chapters below). To investigate whether these interactions play a role in the mechanism of *Pf*6PGD, the mutants *Pf*6PGD^{C281S} and *Pf*6PGD^{W104L} were created by using site-directed mutagenesis as described in chapter 3.1.5. For heterologous overexpression and purification of *Pf*6PGD mutants, the same protocol was used as for the wt enzyme, resulting in comparable yield and purity (chapter 4.3.1). For oligomerization behavior and kinetic characterization of the mutant enzymes, see chapters 4.3.4 and 4.3.5, respectively (Haeussler *et al.*, 2018).

```
Pf   ---MCDIGLIGLAVMGQNLSLNISSKGFKIGVYNRTYERTEETMKRAKEE--NLVVYGYK   55
Tb   --MSMDVGVVGLGVMGANLALNIAEKGFKVAVFNRTYSKSEEFMKANASAPFAGNLKAFE   58
Gs   HMAKHQIGVIGLAVMGKNLALNIESKGYSVAVYNRLREKTDEFLQ-EA-K--GKNIVGTY   56
Sc   --MSADFGLIGLAVMGQNLILNAADHGFTVCAYNRTQSKVDHFLANEA-K--GKSIIGAT   55
Oa   -MAQADIALIGLAVMGQNLILNMNDHGFVVCAFNRTVSKVDDFLANEA-K--GTKVLGAH   56
Hs   -MAQADIALIGLAVMGQNLILNMNDHGFVVCAFNRTVSKVDDFLANEA-K--GTKVVGAQ   56
          :..:::*.*** ** **  .:*: : .:**  .: :. :          : .

Pf   TVEELINNLKKPRKVILLIKAGPAVDENISNILKHFEKGDIIIDGGNEWYINSERRIKLC   115
Tb   TMEAFAASLKKPRKALILVQAGAATDSTTEQLKKVFEKGDILVDTGNAHFKDQGRRAQQL   118
Gs   SIEEFVNALEKPRKILLMVKAGAPTDATIEQLKPHLEKGDIVIDGGNTYFKDTQRRNKEL   116
Sc   SIEDFISKLKRPRKVMLLVKAGAPVDALINQIVPLLEKGDIIIDGGNSHFPDSNRRYEEL   115
Oa   SLEEMVSKLKKPRRIILLVKAGQAVDNFIEKLVPLLDIGDIIIDGGNSEYRDTMRRCRDL   116
Hs   SLKEMVSKLKKPRRIILLVKAGQAVDDFIEKLVPLLDTGDIIIDGGNSEYRDTTRRCRDL   116
     ::: :   *::**: ::::** .*   .::   :: ***::* **  : :  ** .

Pf   KEKDVEYLAMGVSGGEAGARYGCSFMPGGSKYAYDCVKEILEKCSAQ-VGNSPCVTYIGP   174
Tb   EAAGLRFLGMGISGGEEGARKGPAFFPGGTLSVWEEIRPIVEAAAAKADDGRPCVTMNGS   178
Gs   AELGIHFIGTGVSGGEEGALKGPSIMPGGQKEAHELVRPIFEAIAAK-VDGEPCTTYIGP   175
Sc   KKKGILFVGSGVSGGEEGARYGPSLMPGGSEEAWPHIKNIFQSISAK-SDGEPCCEWVGP   174
Oa   KDKGILFVGSGVSGGEDGARYGPSLMPGGNKEAWPHIKAIFQGIAAKVGTGEPCCDWVGD   176
Hs   KAKGILFVGSGVSGGEEGARYGPSLMPGGNKEAWPHIKTIFQGIAAKVGTGEPCCDWVGD   176
        .: ::. *:**** **  * :::***   .   :: *.:  :*:   . **    *

Pf   GSSGNYVKMVHNGIEYGDMQLISESYVIMKHILKYDNQKLSEVFNKWNE-GILNSYLIEI   233
Tb   GGAGSCVKMYHNSGEYAILQIWGEVFDILR-AMGLNNDEVAAVLEDWKSKNFLKSYMLDI   237
Gs   DGAGHYVKMVHNGIEYGDMQLIAEAYFLLKHVLGMDAAELHEVFADWNK-GELNSYLIEI   234
Sc   AGAGHYVKMVHNGIEYGDMQLICEAYDIMKRLGGFTDKEISDVFAKWNN-GVLDSFLVEI   233
Oa   DGAGHFVKMVHNGIEYGDMQLICEAYHLMKDVLGLGHKEMAKAFEEWNK-TELDSFLIEI   235
Hs   EGAGHFVKMVHNGIEYGDMQLICEAYHLMKDVLGMAQDEMAQAFEDWNK-TELDSFLIEI   235
      .:*  *** **. **. :*:  * : :::        ::  .: .*:.   *.*::::*

Pf   TANILAKKDDLTNNYLVDMILDIAGAKGTGKWTMLEATERGIPCPTMCAALDARNISVFK   293
Tb   SIAAA-RAKDKDGSYLTEHVMDRIGSKGTGLWSAQEALEIGVPAPSLNMAVVSRQFTMYK   296
Gs   TADIFTKIDEETGKPLVDVILDKAGQKGTGKWTSQNALDLGVPLPIITESVFARFLSAMK   294
Sc   TRDIL-KFDDVDGKPLVEKIMDTAGQKGTGKWTAINALDLGMPVTLIGEAVFARCLSALK   292
Oa   TASIL-KFQDADGKHLLPKIRDSAGQKGTGKWTAISALEYGVPVTLIGEAVFARCLSSLK   294
Hs   TANIL-KFQDTDGKHLLPKIRDSAGQKGTGKWTAISALEYGVPVTLIGEAVFARCLSSLK   294
     :     : .:  .. *   : * * ***** *:  .* : *:*   :  :: :* ::  *

Pf   ELRTKAESNFNKDNILIDPNEDLNDF----ENDLLNALYCCKIISYTQGLFLLKQVSEEM   349
Tb   TERQANASNAPGITQSPGYTLKNKSPSGPEIKQLYDSVCIAIISCYAQMFQCLREMDKVH   356
Gs   DERVKASKVLAGPAVKP-FEGDRAHF----IEAVRRALYMSKICSYAQGFAQMKAASEEY   349
Sc   NERIRASKVLPGPEVPKDAVKDREQF----VDDLEQALYASKIISYAQGFMLIREAAATY   348
Oa   DERIQASKKLKGPQNIP-FEGDKKSF----LEDIRKALYASKIISYAQGFMLLRQAATEF   349
Hs   DERIQASKKLKGPQKFQ-FDGDKKSF----LEDIRKALYASKIISYAQGFMLLRQAATEF   349
       *    .            .         . :  ::  . * .*:* :  ::
```

```
Pf   NWKLNLGEIARIWRGGCIIRAVFLDRIANAYKNNEKLELLFLDNEFSDDIKNKLPSLRKI   409
Tb   NFGLNLPATIATFRAGCILQGYLLKPMTEAFEKNPNISNLMCA--FQTEIRAGLQNYRDM   414
Gs   NWNLRYGDIAMIFRGGCIIRAQFLQKIKEAYDRDPALSNLLLDSYFKDIVERYQDALREI   409
Sc   GWKLNNPAIALMWRGGCIIRSVFLGQITKAYREEPDLENLLFNKFFADAVTKAQSGWRKS   408
Oa   GWTLNYGGIALMWRGGCIIRSVFLGKIKDAFDRNPGLQNLLLDDFFKSAVENCQDSWRRA   409
Hs   GWTLNYGGIALMWRGGCIIRSVFLGKIKDAFDRNPELQNLLLDDFFKSAVENCQDSWRRA   409
     .: *.       :*.***::. :*  : .*: .:  :. *:    *   :       *

Pf   VLM-ATKYSIPIPAFSASLAYFQMVTSQ-NLPLNLVQAQRDYFGSHTYRRTDRE------   461
Tb   VALITSKLEVSIPVLSASLNYVTAMFTPTLKYGQLVSLQRDVFGRHGYERVDKDGR----   470
Gs   VAT-AAMRGIPVPGSASALAYYDSYRTA-VLPANLIQAQRDYFGAHTYERVDKE------   461
Sc   IAL-ATTYGIPTPAFSTALSFYDGYRSE-RLPANLLQAQRDYFGAHTFRVLPECASDNLP   466
Oa   IST-GVQAGIPMPCFTTALSFYDGYRHA-MLPANLIQAQRDYFGAHTYELLAKP------   461
Hs   VST-GVQAGIPMPCFTTALSFYDGYRHE-MLPASLIQAQRDYFGAHTYELLAKP------   461
     :        :  *  :::* :            .*:. ** ** ** * :.   .

Pf   --GNYHTLW--------------      468
Tb   ----ESFQWPELQ----------      479
Gs   --GIFHTEWLK------------      470
Sc   VDKDIHINWTGHGGNVSSSTYQA      489
Oa   -GQFIHTNWTGHGGSVSSSSYNA      483
Hs   -GQFIHTNWTGHGGTVSSSSYNA      483
             *
```

Figure 24. Amino acid alignment of 6PGDs from different species
Residue C281 (green) forming a disulfide bridge with C281 of the second subunit, W104 interacting with W265 (magenta), and R36 (yellow) involved in $NADP^+$ binding are specific for *Plasmodium*. In contrast, all residues involved in 6PG binding are conserved (cyan), other residues involved in $NADP^+$ binding (gray) and the flexible loop (boxes) are similar in most species. *Pf*: *Plasmodium falciparum* (UniProtKB - Q8IKT2); *Tb*: *Trypanosoma brucei* (UniProtKB - P31072); *Gs*: *Geobacillus stearothermophilus* (UniProtKB - I3NI58); *Sc*: *Saccharomyces cerevisiae* (UniProtKB - P38720); *Oa*: *Ovis aries* (UniProtKB - P00349); *Hs*: *Homo sapiens* (UniProtKB - P52209). * Identical residues, : very similar residues, . similar residues.

4.3.3.2 Substrate binding site of *Pf*6PGD

The binding site for 6PG is located in a pocket of domain 2, but residues from domain 1 and the C-terminal tail are also involved in binding the substrate (Figure 25a). The carboxyl-group of 6PG is hydrogen bonded by S128 and G129 (both from domain 1), the gluconate moiety interacts with N102 (domain 1), K182, H185, N186, E189, (domain 2) and H453' of the adjacent subunit (C-terminal tail). The oxygens of the phosphate group are hydrogen bonded with R287, Y190 (domain 2), and R447' (C-term), respectively. A flexible loop comprising residues 255-262 borders one site of the substrate binding pocket; the sidechain of K260 stacks against the substrate. This lysine is conserved in many species (Figure 24) (Haeussler *et al.*, 2018).

In the native structure, one molecule of PEG is located in the binding pocket in a position similar to the binding of 6PG; however, the binding is mainly hydrophobic. Interestingly, superimposition of the apo-*Pf*6PGD structure and in complex with 6PG shows that the flexible loop (residues 255-262) bordering the 6PG binding site has a more open conformation in the apoenzyme structure (Figure 25b); therefore, the substrate binding pocket seems to be more easily accessible in the apo and $NADP^+$ structures and less accessible in the 6PG complex. Also K260, which interacts with 6PG once it is bound, adopts a different conformation with an open active site loop (Haeussler *et al.*, 2018).

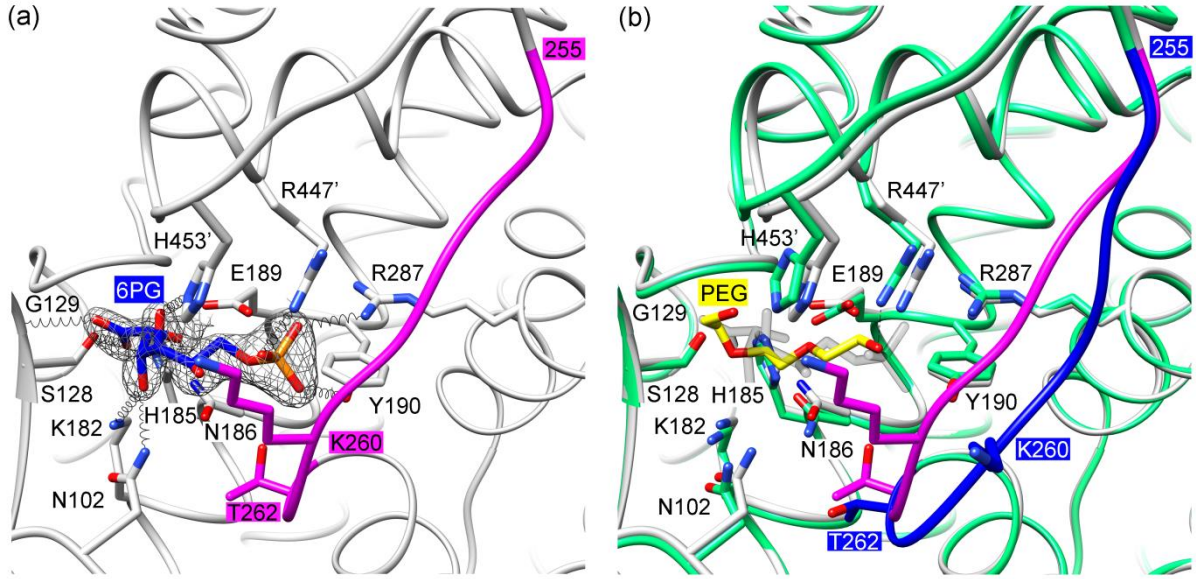

Figure 25. Substrate binding site of *Pf*6PGD
(a) 6PG as seen in the *Pf*6PGD structure complexed with substrate. The flexible active site loop comprises amino acids 255-262 (magenta). Hydrogen bonds between 6PG and the enzyme are shown by tiny black spirals. (b) In apo-*Pf*6PGD, the substrate binding site is occupied by a PEG molecule. Superimposition of apo-*Pf*6PGD (green) and the structure in complex with 6PG (gray) shows that the active site loop adopts an open conformation without 6PG bound, and a closed conformation with 6PG bound (colored blue and magenta, respectively) (Haeussler *et al.*, 2018).

4.3.3.3 Cofactor binding site of *Pf*6PGD

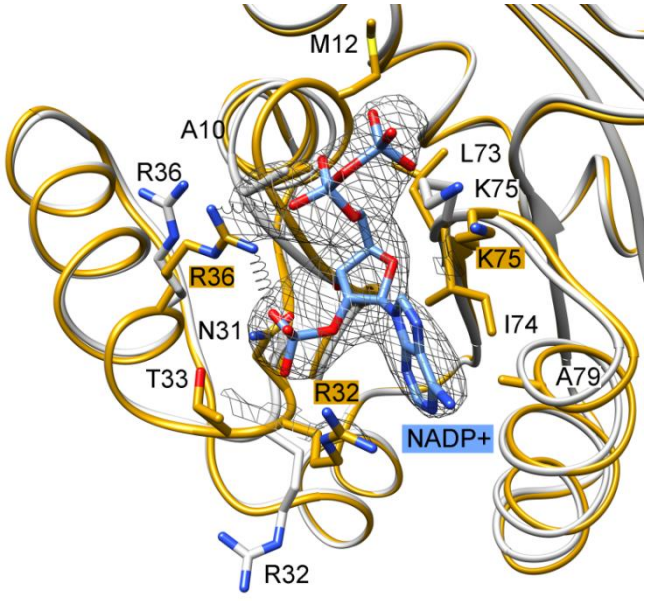

Figure 26. Cofactor binding site of *Pf*6PGD
$NADP^+$ is covered by a composite omit map at 2.9 Å resolution. Structures in complex with $NADP^+$ (amber) and 6PG (gray) are superimposed; residues with different conformations in the two structures are labeled twice. Hydrogen bonds are indicated by tiny black spirals (Haeussler *et al.*, 2018).

The binding site for $NADP^+$ is located in a cleft of domain 1 and is highly conserved within the 6PGD family (Figure 26). As mentioned above (4.3.3), $NADP^+$ is only partially defined by

electron density; only the adenine moiety and the three phosphate groups were visible, but not the ribose and the nicotinamide moiety, implying flexibility of the molecule. The phosphate groups showed a different conformation in the two subunits. Amino acids A10-M12, N31, R32, T33, and R36 form the binding pocket on one side, and residues A79, L73, I74, and K75 on the other side. One phosphate of $NADP^+$ interacts with R32, whose guanidinium group stacks against the adenine (see also 4.3.5). Superimposition of *Pf*6PGD in complex with 6PG and in complex with $NADP^+$ shows that R32 and R36 adopt a different conformation upon ligand binding (Figure 26). While most of the pocket residues are strictly conserved, R36 is replaced by a lysine in mammals and bacteria (Figure 24) (Haeussler *et al.*, 2018).

4.3.4 Oligomerization behavior of *Pf*6PGD, mutants and h6PGD

The oligomerization behavior of native, reduced, and oxidized *Pf*6PGD wt, as well as in the presence of the product NADPH, was studied using size exclusion chromatography. Under all conditions tested, *Pf*6PGD wt eluted after 79 mL, corresponding to a molecular mass of approximately 78 kDa (Figure 27a-d). The theoretical mass of the *Pf*6PGD dimer is with 108 kDa larger than 78 kDa; however, it is clearly larger than a monomeric enzyme with 54 kDa. Proteins tend to elute from size exclusion chromatography with a smaller than theoretical mass; therefore, the presence of a *Pf*6PGD dimer is most likely. Recombinant h6PGD eluted after 78 mL as a dimer with a molecular mass of 84 kDa (Figure 27g) (Haeussler *et al.*, 2018).

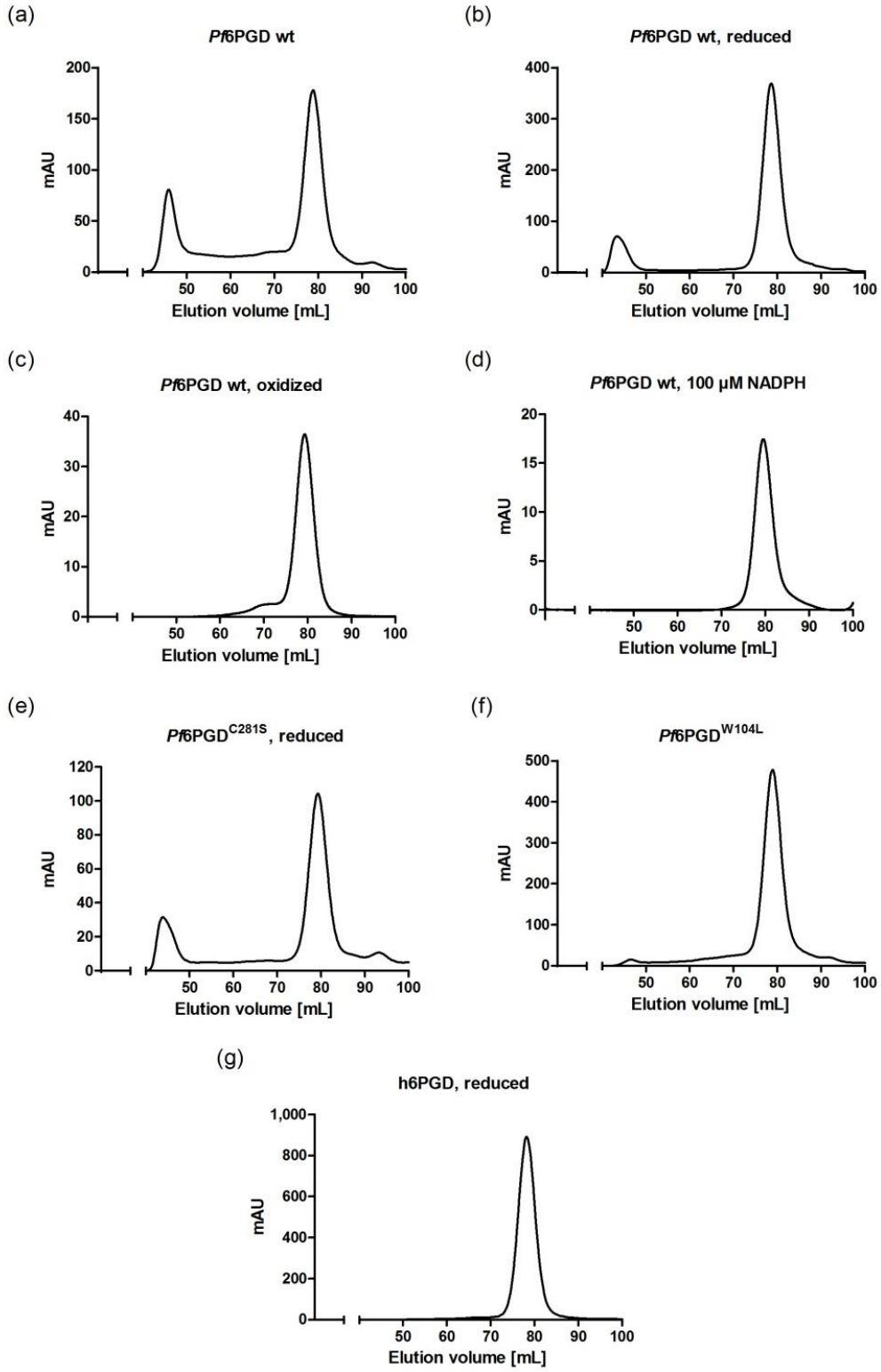

Figure 27. Size exclusion chromatography of *Pf*6PGD and h6PGD

*Pf*6PGD wt eluted from the size exclusion chromatography column after approximately 79 mL as a dimer of 78 kDa under all conditions tested (native (a), reduced (b), oxidized (c), and in the presence of NADPH (d)). Similarly, mutants *Pf*6PGD^{C281S} (e) and *Pf*6PGD^{W104L} (f) eluted after 79 mL as 78 kDa dimers, and h6PGD after 78 mL as an 84 kDa dimer (g). The additional peaks resulted from proteins that could not be removed using affinity chromatography.

4.3.5 Kinetic characterization of *Pf*6PGD wt, mutants, and h6PGD

The reduction of $NADP^+$ to NADPH was measured to determine the kinetic parameters of the enzymes. *Pf*6PGD wt showed a specific activity of 8.0 ± 1.8 $U \cdot mg^{-1}$ and K_M values of 11.3 ± 2.7 µM for 6PG and 9.0 ± 4.2 µM for $NADP^+$. The k_{cat} values were determined to be 7.1 ± 2.5 sec^{-1} for 6PG and 7.6 ± 2.2 sec^{-1} for $NADP^+$ (Table 16). Representative Michaelis-Menten curves are shown in Figure 28. The crystal structure of *Pf*6PGD wt revealed two interactions that can only be found in *Plasmodium*: a disulfide bridge between the *Plasmodium*-specific cysteines C281 of the two monomers and an interaction between the *Plasmodium*-specific W104 and the highly conserved W265 (4.3.3.1). In order to investigate a potential impact upon catalysis, site-directed mutagenesis was performed, creating the mutants *Pf*6PGD^{C281S} and *Pf*6PGD^{W104L}. All kinetic parameters of the mutants – especially the K_M for 6PG of *Pf*6PGD^{W104L} – were slightly lower than those of the wt enzyme (Table 16). The interaction of W104 and W265 most likely supports the rearrangement of the initially only partially bound $NADP^+$ by linking the cofactor domain with the substrate binding pocket domain. This interaction is disturbed in *Pf*6PGD^{W104L}, resulting in decreased kinetic parameters (Haeussler *et al.*, 2018). The mechanistic reason for the slightly decreased kinetic parameters of *Pf*6PGD^{C281S} is so far unclear.

Table 16. Kinetic characteristics of *Pf*6PGD wt, *Pf*6PGD^{C281S}, *Pf*6PGD^{W104L}, and h6PGD
Each value is a mean value ± SD from at least three independent determinations.

	*Pf*6PGD wt	*Pf*6PGD^{C281S}	*Pf*6PGD^{W104L}	h6PGD
Specific activity [$U \cdot mg^{-1}$]	8.0 ± 1.8	5.0 ± 0.4	5.8 ± 0.9	22.1 ± 1.2
K_M 6PG [µM]	11.3 ± 2.7	8.4 ± 1.8	5.8 ± 0.8	33.7 ± 7.1
K_M $NADP^+$ [µM]	9.0 ± 4.2	4.7 ± 1.0	4.8 ± 0.8	6.9 ± 2.0
k_{cat} 6PG [sec^{-1}]	7.1 ± 2.5	5.0 ± 0.6	5.2 ± 0.3	22.2 ± 0.3
k_{cat} $NADP^+$ [sec^{-1}]	7.6 ± 2.2	4.8 ± 0.6	5.7 ± 0.6	21.4 ± 0.8

One aim of this thesis was to find inhibitors for *Pf*6PGD. The human homolog h6PGD was used to test the identified inhibitors for selectivity. Prior to inhibitor testing, the recombinant h6PGD was shown to have a higher specific activity than the plasmodial enzyme (22.1 ± 1.2 $U \cdot mg^{-1}$) and K_M values of 33.7 ± 7.1 µM for 6PG and 6.9 ± 2.0 µM for $NADP^+$. Notably, the k_{cat} values 21.4 ± 0.8 sec^{-1} for $NADP^+$ and 22.2 ± 0.3 sec^{-1} for 6PG were substantially higher than the corresponding values for *Plasmodium* (Table 16) (Haeussler *et al.*, 2018).

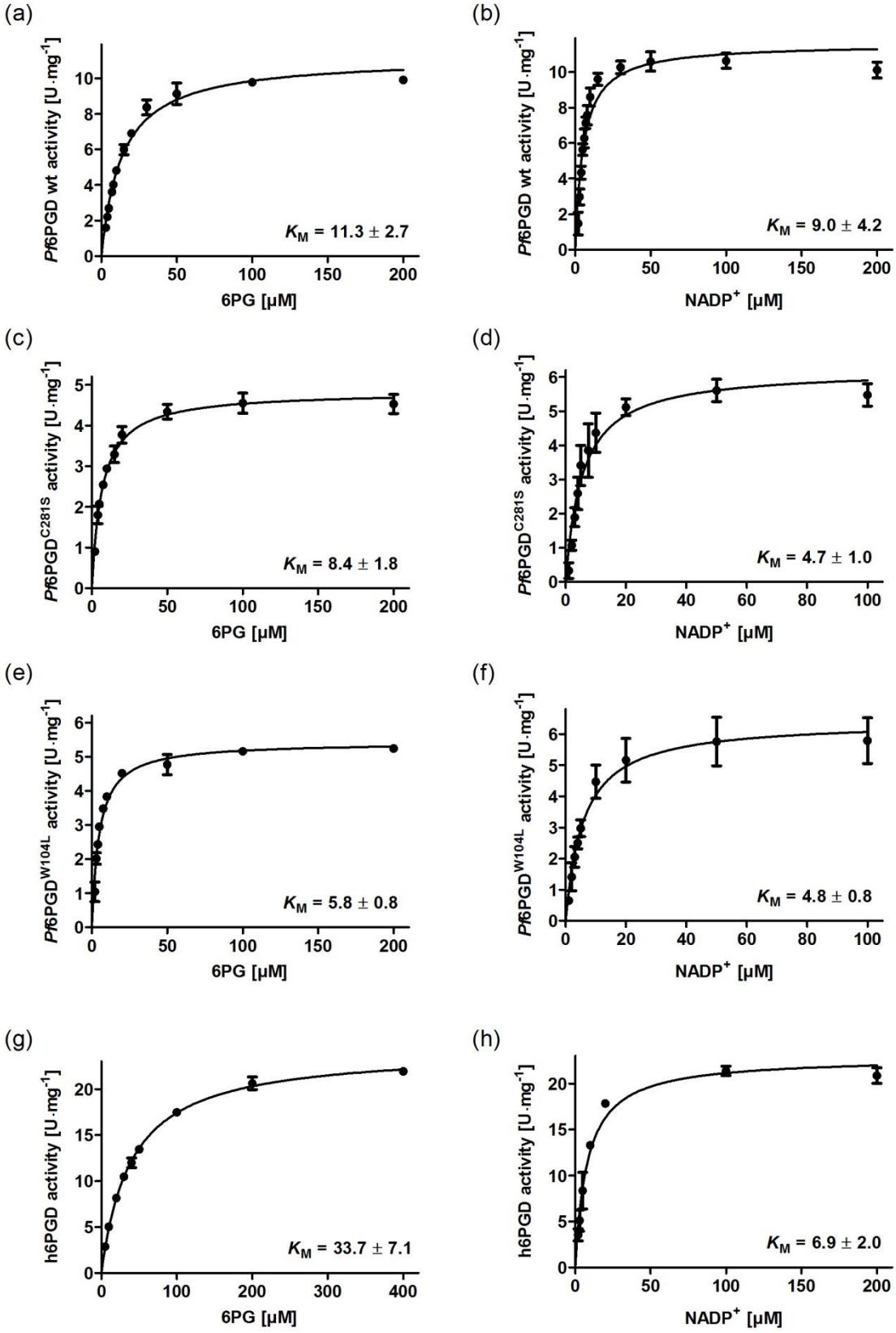

Figure 28. K_M determinations for 6PG and $NADP^+$ of 6PGD
Representative Michaelis-Menten curves (mean values ± SD of three measurements) for the K_M determinations for 6PG and $NADP^+$ of *Pf*6PGD wt (a, b), *Pf*6PGD^{C281S} (c, d), *Pf*6PGD^{W104L} (e, f), and h6PGD (g, h). The K_M values are shown as mean values ± SD of three independent determinations (see also Table 16).

Test of NAD^+ as an alternative cofactor

NAD^+ was tested as an alternative cofactor for *Pf*6PGD wt and h6PGD. For *Plasmodium*, the measurements revealed an activity of 8.0 $U \cdot mg^{-1}$ using 100 µM $NADP^+$ (Table 16), but was below the detection limit of the spectrophotometer of 0.001 $\Delta A \cdot min^{-1}$ using 100 µM NAD^+. The highest NAD^+ concentration tested was 2.5 mM, resulting in a *Pf*6PGD activity between 0.0 and 1.1 $U \cdot mg^{-1}$, depending on the batch of enzyme. Therefore, it was concluded that *Pf*6PGD is specific for $NADP^+$. Similarly, h6PGD did not show any activity at the tested NAD^+ concentrations (0.05-2.5 mM). Structural analysis revealed for *Plasmodium* that the specificity is most likely due to the interaction of the negatively charged phosphates from $NADP^+$ with the positively charged arginine residues R32 and R36 (Figure 26). In NAD^+, this negative charge is missing and prevents NAD^+ from binding to *Pf*6PGD (Haeussler *et al.*, 2018).

Mechanistic considerations

Because it was possible to crystallize *Pf*6PGD in complex with 6PG and with $NADP^+$, it can be assumed that substrate and cofactor can bind independently from each other. This observation was confirmed enzymatically using the assay described in chapter 3.3.6. Thereby, $NADP^+$ and 6PG were titrated at different fixed concentrations of the substrate/cofactor, and the relationship between initial enzyme velocity and substrate concentrations was analyzed in Lineweaver-Burk plots. The intersections left of the ordinates point towards a sequential mechanism (Figure 29), meaning that both substrate and cofactor have to bind before the product formation can be initiated (Haeussler *et al.*, 2018).

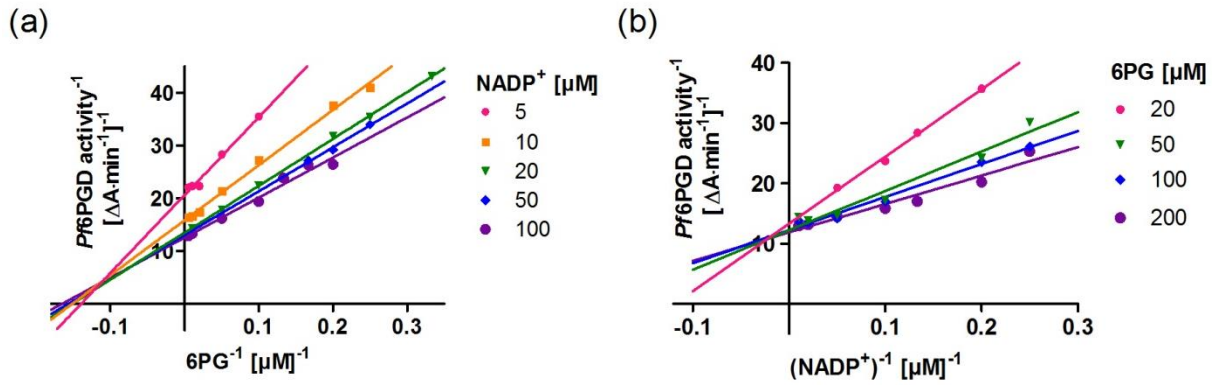

Figure 29. Sequential enzyme mechanism of *Pf*6PGD
The substrate 6PG (a) and the cofactor $NADP^+$ (b) were titrated at different fixed concentrations of the cofactor/substrate. The Lineweaver-Burk plots intersect left of the ordinate, pointing towards a sequential enzyme mechanism (Haeussler *et al.*, 2018).

4.3.6 Crystallization trials of *Pf*6PGD mutants

To investigate potential impacts of the mutations on *Pf*6PGD structure, the mutants were crystallized under similar conditions as found for native wt enzyme (Figure 30). However, the stability of the crystals was very low, therefore it was not possible to assemble them for X-ray diffraction analysis. Further crystallization trials need to be performed to elucidate potential impacts of the mutations on the overall structure of *Pf*6PGD.

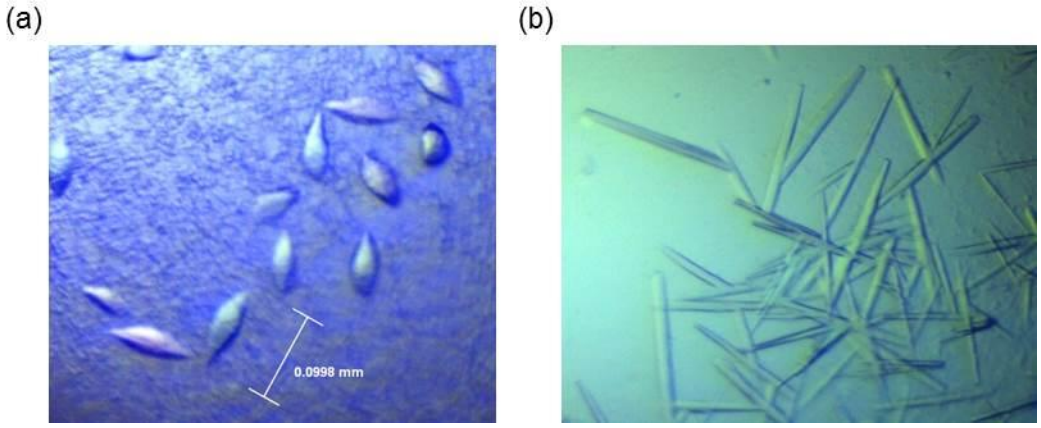

Figure 30. Crystals of *Pf*6PGD^{W104L} and *Pf*6PGD^{C281S}
*Pf*6PGD mutants were crystallized at 4 °C using the sitting drop approach. (a) 15 mg·mL^{-1} *Pf*6PGD^{W104L}, 24% (v/v) PEG 3,350, 0.2 M ammonium sulfate, 4 mM 6PG. (b) 8.3 mg·mL^{-1} *Pf*6PGD^{C281S}, 30% (v/v) PEG 4,000, 0.1 M sodium citrate, pH 5.6, 0.05 M ammonium sulfate, 4 mM 6PG.

4.4 Post-translational modification of cysteines

The two PTMs, protein *S*-glutathionylation and *S*-nitrosation, are – amongst other functions – important regulators of enzyme activity (Belcastro *et al.*, 2017; Jortzik *et al.*, 2012). Therefore, the effects of these two modifications on enzymes of the oxidative PPP from *P. falciparum* and *P. vivax* were studied within this thesis.

4.4.1 *S*-glutathionylation

4.4.1.1 *S*-glutathionylation studies on *Pf*GluPho, *Pf*G6PD, and *Pv*G6PD

*Pf*GluPho and the G6PD parts of *P. falciparum* and *P. vivax* GluPho were reduced and afterwards incubated with 0-10 mM GSSG, followed by removal of unbound glutathione via desalting. Potential *S*-glutathionylation of the enzymes was visualized with Western blot analysis using an anti-glutathione antibody. As shown in Figure 31, neither *Pf*GluPho nor the two G6PDs showed a signal at concentrations up to 6 mM GSSG. At 10 mM GSSG, the proteins precipitated visibly during sample preparation; therefore, it was not possible to apply sufficient amounts of the protein to Western blot analysis, resulting in a lack of protein bands in the Ponceau stains (right side of Figure 31). The result indicates that none of the three enzymes are prone to regulation via *S*-glutathionylation under the tested conditions.

In contrast to this finding, it has been stated previously that the G6PD activity of *Pf*GluPho is redox-regulated via *S*-glutathionylation (Jortzik *et al.*, 2011). Therefore, it was tested whether such a feigned redox-regulation can be observed for *Pv*G6PD as well. Prereduced *Pv*G6PD was incubated with 0-10 mM GSSG for 15 min at 37 °C before the activity was measured using the assay described in chapter 3.3.6. Indeed, *Pv*G6PD activity decreased dramatically at very high GSSG concentrations (Figure 32a), as shown before for *Pf*GluPho (Figure 32b). However, since Western blot analysis clearly showed that none of the three tested enzymes were *S*-glutathionylated, and Ponceau staining showed a lack of protein bands at 10 mM GSSG (Figure 31), the loss of activity is likely based on a loss of conformation rather than redox-regulation. This is further supported by the fact that adding DTT could not restore the activity of the samples (data not shown).

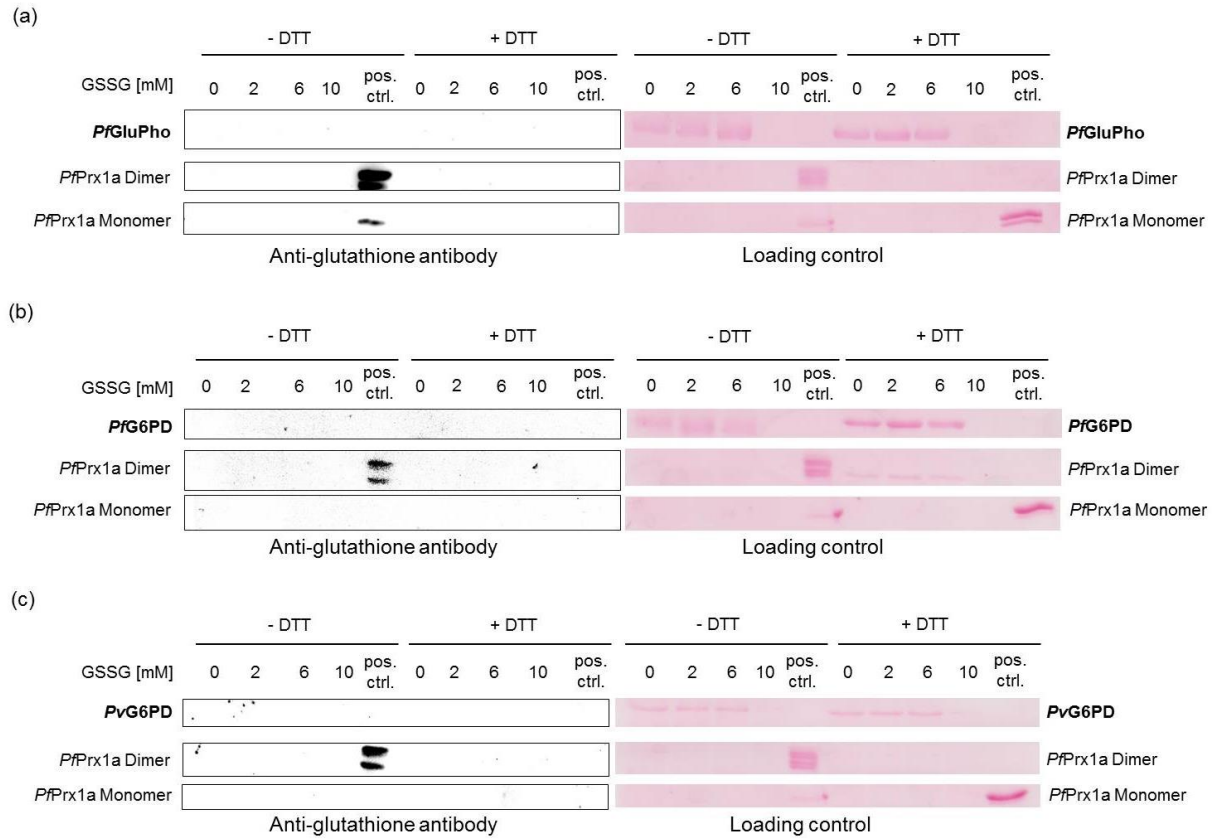

Figure 31. Western blot analysis of *S*-glutathionylation of *Pf*GluPho, *Pf*G6PD, and *Pv*G6PD
Prereduced enzymes were incubated with 0-10 mM GSSG for 10 min at 37 °C; potential *S*-glutathionylation was detected via Western blot analysis using an anti-glutathione antibody. The reversibility of potential *S*-glutathionylation was studied by reducing SDS-PAGE with DTT. Samples of *S*-glutathionylated *Pf*Prx1a were prepared in parallel as a positive control. *Pf*Prx1a exists in a dimeric form without DTT, while adding DTT shifts the conformation to a monomeric form. Ponceau staining of the membrane used for Western blotting served as a loading control. Representative blots from at least two independent experiments are shown. Pos. ctrl.: positive control.

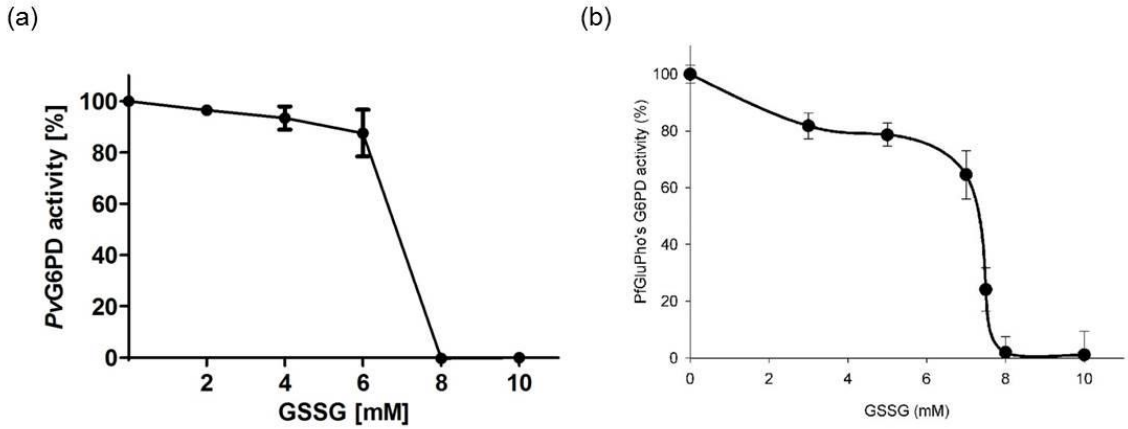

Figure 32. Activity of *S*-glutathionylated *Pv*G6PD and *Pf*GluPho
(a) Reduced *Pv*G6PD was incubated with different concentrations of GSSG (0-10 mM) for 15 min, activity of the sample incubated with 0 mM GSSG was defined as 100%. Values shown are mean values ± SD from three determinations. (b) Activity of *Pf*GluPho after incubation with different GSSG concentrations. Panel (b) was taken from Jortzik *et al*., 2011 for comparison.

4.4.1.2 *S*-glutathionylation studies of *Pf*6PGD

Western blot analysis

*Pf*6PGD wt was reduced, *S*-glutathionylated, and afterwards subjected to Western blot analysis as described above (4.4.1.1). Figure 33a indicates that GSSG does not *S*-glutathionylate *Pf*6PGD under the tested conditions. To ensure application of comparable protein quantities to each lane, the anti-glutathione antibody was removed from the membrane, and 6xHis-tagged proteins were detected using an anti-6xHis-tag antibody. As shown in Figure 33b, all lanes contained the same amounts of *Pf*6PGD except for the sample treated with 10 mM GSSG, most likely caused by precipitation of the protein in the presence of high GSSG concentration (see kinetic analysis below) (Haeussler *et al.*, 2018).

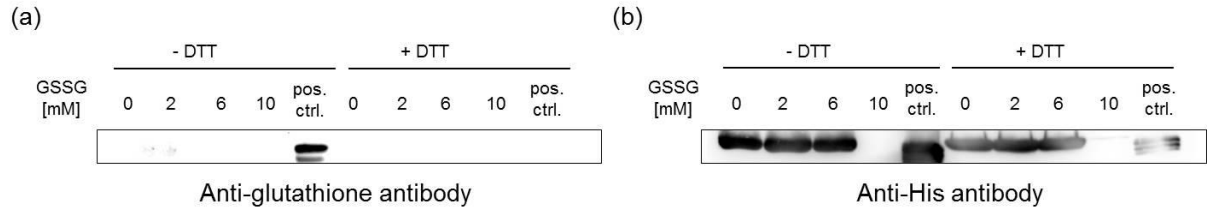

Figure 33. Western blot analysis of *S*-glutathionylation of *Pf*6PGD
(a) *S*-glutathionylated protein was detected using an anti-glutathione antibody. Reducing SDS-PAGE was used to study the reversibility of the modification. *S*-glutathionylated *Pf*Prx1a served as a positive control. (b) After chemiluminescence detection, the anti-glutathione antibody was removed from the membrane used in panel (a), and the His-tagged proteins were detected using an anti-6xHis-tag antibody. Pos. ctrl.: positive control (Haeussler *et al.*, 2018).

Impacts of *S*-glutathionylation on *Pf*6PGD activity

To fully exclude a regulation of *Pf*6PGD by *S*-glutathionylation, the reduced enzyme was incubated with different GSSG concentrations, followed by activity determination. Incubation of reduced *Pf*6PGD wt with up to 8 mM GSSG had no impact on enzyme activity (Figure 34); in contrast, 10 mM GSSG resulted in an immediate and complete loss of *Pf*6PGD activity. This observation is in accordance with the likely precipitation of the protein observed in the anti-6xHis-tag Western blot (Figure 33b). Recovery of the activity by adding 5 mM DTT was not successful, indicating that high GSSG levels led to an irreversible change in *Pf*6PGD conformation (Haeussler *et al.*, 2018).

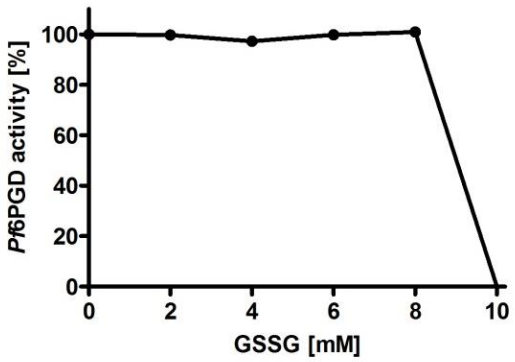

Figure 34. Activity of *S*-glutathionylated *Pf*6PGD
Reduced *Pf*6PGD wt was incubated with different concentrations of GSSG (0-10 mM) for 15 min; activity of the sample incubated with 0 mM GSSG was defined as 100%. Values shown are mean values ± SD from two independent determinations, each including three measurements.

4.4.2 *S*-nitrosation

S-nitrosation is considered an important mediator of redox regulation (Jortzik *et al.*, 2012). In 2014, our group performed a large-scale proteomic analysis to identify targets of protein *S*-nitrosation in *P. falciparum* parasite lysate after treatment with *S*-nitrosoglutathione (GSNO). Interestingly, *Pf*GluPho and *Pf*6PGD were found to be likely targets of *S*-nitrosation (Wang *et al.*, 2014); therefore, one aim of this thesis was to confirm the accessibility of these enzymes, including the *P. vivax* homolog to *S*-nitrosation, and to study the potential functional effects of this important post-translational modification. As an NO donor, we used the physiologically relevant nitrosating agent GSNO. This small-molecular-weight *S*-nitrosothiol is able to release NO and transnitrosate proteins (Broniowska *et al.*, 2013; Hess *et al.*, 2005).

4.4.2.1 *S*-nitrosation studies on *Pf*GluPho, *Pf*G6PD, and *Pv*G6PD

To study the susceptibility of *Pf*GluPho, *Pf*G6PD, and *Pv*G6PD to *S*-nitrosation, reduced enzymes were incubated with 1 mM GSNO and subjected to the biotin-switch assay followed by Western blot analysis using an anti-biotin antibody. Samples without GSNO and/or without sodium ascorbate were prepared in parallel as controls. As shown in Figure 35a, samples treated with 1 mM GSNO and sodium ascorbate resulted in a prominent signal for all three enzymes, indicating that they are targets of *S*-nitrosation.

To elucidate whether the modification has an impact on the activity of *Pf*GluPho, *Pf*G6PD, and *Pv*G6PD, the enzymes were incubated with different GSNO concentrations, and the activity was measured at various time points. As shown in Figure 35b, the impact was with a maximal inhibition of only 20-25% marginal. Since there is no major difference in Western blot and kinetic analyses between *Pf*GluPho and *Pf*G6PD, it can be assumed that at least some of the *S*-nitrosation sites of *Pf*GluPho are located in the G6PD part. After 3 h, 5 mM DTT was added to the samples incubated with 1,000 µM GSNO to study the reversibility of the modification; the enzymes did not regain full activity (*Pf*GluPho: 91.3 ± 9.5%, *Pf*G6PD: 81.7 ± 9.6%, *Pv*G6PD: 79.2 ± 6.5%), indicating that they are not extensively regulated via *S*-nitrosation.

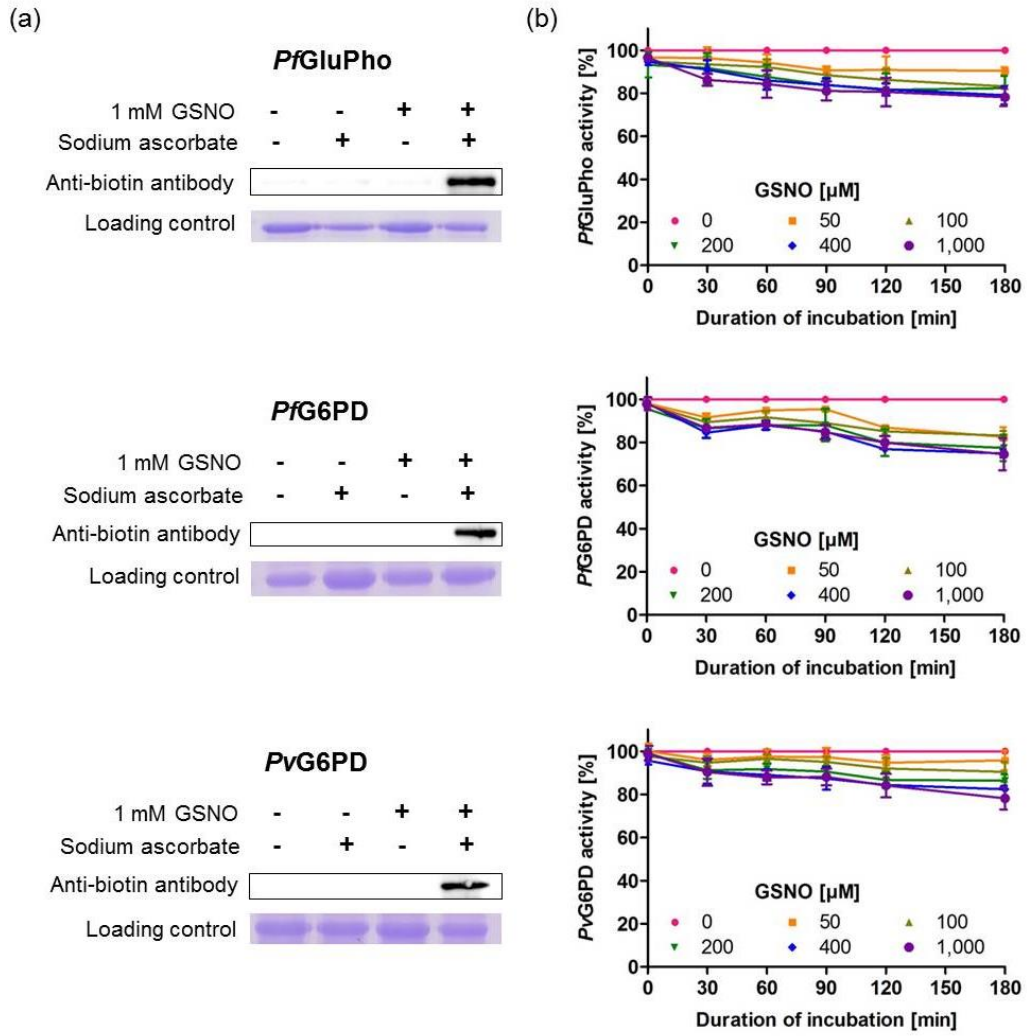

Figure 35. Analysis of *S*-nitrosation of *Pf*GluPho, *Pf*G6PD, and *Pv*G6PD
(a) Reduced enzymes were incubated with 1 mM GSNO for 1 h at 22 °C in the dark and subjected to the biotin-switch assay. Controls without sodium ascorbate and/or GSNO were prepared in parallel. *S*-nitrosated proteins were detected indirectly with Western blot analysis using an anti-biotin antibody. Coomassie staining of the samples served as a loading control. Representative blots from at least two independent experiments are shown. (b) To study the impact of *S*-nitrosation on enzyme activity, reduced enzymes were incubated with different concentrations of GSNO for 180 min at 22 °C in the dark. Activity of the samples was measured at different time points. Activity of the sample with 0 µM GSNO was defined as 100%. Values shown are mean values ± SD from at least three independent determinations.

4.4.2.2 *S*-nitrosation studies on *Pf*6PGD

Western blot analysis

To test the susceptibility of *Pf*6PGD to *S*-nitrosation, samples were prepared as described above (chapter 4.4.2.1). The sample treated with 1 mM GSNO and sodium ascorbate resulted in a prominent signal (Figure 36a). As a loading control, the anti-biotin antibody was removed and an anti-6xHis-tag Western blot was performed, showing that – especially for the controls treated without GSNO – *Pf*6PGD was indeed applied to each lane (Figure 36b) (Haeussler *et al.*, 2018).

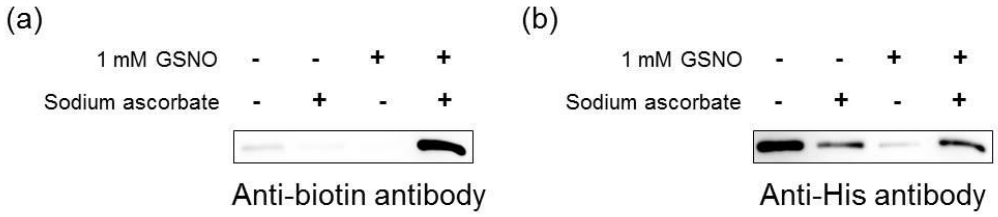

Figure 36. Western blot analysis of *S*-nitrosation on *Pf*6PGD
(a) *S*-nitrosated protein was indirectly detected after a biotin-switch assay by using an anti-biotin antibody. Samples without sodium ascorbate were prepared in parallel as a control. (b) As a loading control after chemiluminescence detection, the anti-biotin antibody was removed from the membrane used in panel (a); afterwards, 6xHis-tagged proteins were detected using an anti-6xHis-tag antibody (Haeussler *et al.*, 2018).

Impacts of *S*-nitrosation on *Pf*6PGD activity

To investigate the impact of *S*-nitrosation on *Pf*6PGD activity, enzyme activity was determined after incubation with different GSNO concentrations. The downregulation of *Pf*6PGD activity increased with increasing GSNO concentrations and longer incubation periods. The maximal inhibition of approximately 65% was reached after incubation with 1,000 µM GSNO for 90 min (Figure 37). Upon removal of the *S*-nitrosation caused by the highest GSNO concentration via reduction with 5 mM DTT, *Pf*6PGD wt regained 100% activity (99.4 ± 3.3%), showing the full reversibility and potential redox-regulatory function of the modification (Haeussler *et al.*, 2018).

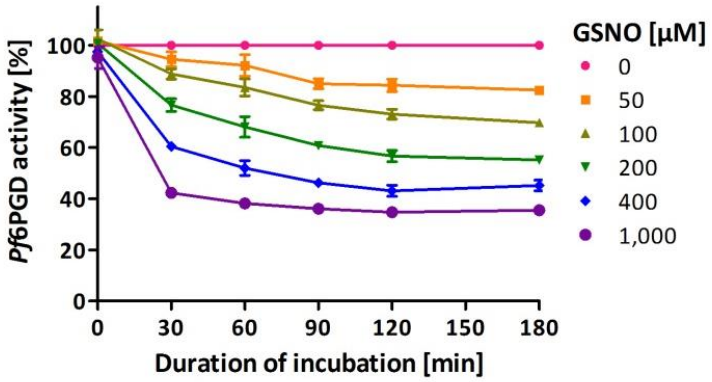

Figure 37. Time and concentration-dependent inhibition of *Pf*6PGD via *S*-nitrosation
Reduced *Pf*6PGD wt was incubated with different concentrations of GSNO (0-1,000 µM) for up to 180 min. Activity of each sample was measured directly after adding GSNO and at different time points. Activity of the sample with 0 µM GSNO was defined as 100%. Values shown are mean values ± SD from three independent determinations (Haeussler *et al.*, 2018).

MALDI-TOF MS analysis of *S*-nitrosated *Pf*6PGD

Since *S*-nitrosation results in a time and concentration-dependent inhibition of *Pf*6PGD, there was the hypothesis that the modification of specific cysteine residues close to the binding sites might be involved in the regulation of this enzyme. Numerous samples treated with different GSNO concentrations were prepared, and modified cysteine residues were identified via MALDI-TOF MS. Surprisingly, all eleven cysteines of *Pf*6PGD seemed to be accessible to *S*-nitrosation; no specific modification pattern could be determined (Haeussler *et al.*, 2018).

Crystallization trials of *S*-nitrosated *Pf*6PGD

Since MALDI-TOF MS did not reveal a specific pattern of *S*-nitrosation sites, *Pf*6PGD was crystallized after *S*-nitrosation with 1 mM GSNO to structurally identify the binding sites. Before crystallization it was ensured that the activity of the enzyme was indeed downregulated. Crystals were obtained under the same conditions as in complex with 6PG (JCSG Core II Suite, E11: 24% (w/v) PEG 1,500, 20% glycerol, Figure 38). However, the resolution of 3.2 Å was not sufficient, a resolution of at least 2.5 Å would be necessary to identify NO-modified cysteine residues; therefore, further experiments need to be conducted to identify residues that are responsible for regulation.

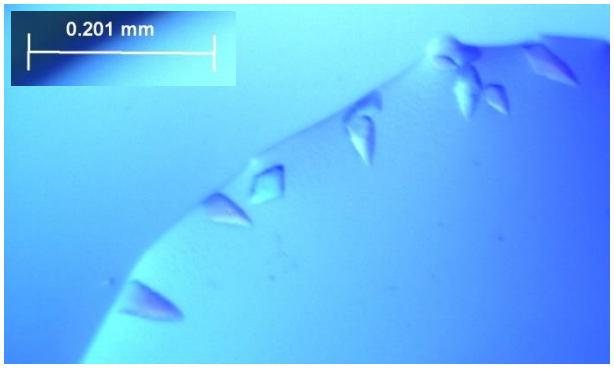

Figure 38. Crystals of *S*-nitrosated *Pf*6PGD wt
S-nitrosated *Pf*6PGD wt crystallized in sitting drops at 8.4 mg·mL^{-1} protein, 24% (w/v) PEG 1,500, and 20% glycerol (JCSG Core II Suite, E11).

4.5 Assessment of enzyme inhibitors

The electron donor NADPH is of essential importance to maintain the cellular redox balance of *Plasmodium* parasites (summarized in chapter 1.2.3). Enzymes of the oxidative PPP as the main source of NADPH are therefore considered promising targets for the development of antimalarial drugs, as already proven for *Pf*GluPho (Allen *et al.*, 2015). One aim of this thesis was to characterize the effect of different compounds on *Pf*GluPho, *Pf*6PGD, and *Pv*G6PD.

4.5.1 Ellagic acid

Ellagic acid (EA) is a phenolic lactone that was identified to be an active component of traditional West African medicine to treat malaria (Soh *et al.*, 2009). The structures of EA and its two derivatives flavellagic acid (FEA) and coruleoellagic acid (CEA) are shown in Figure 39 (Sturm *et al.*, 2009).

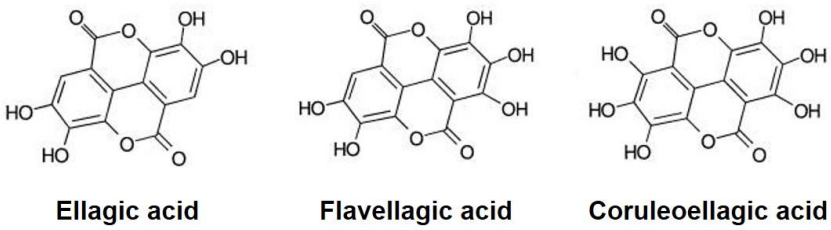

Figure 39. Structures of ellagic acid and its derivatives flavellagic acid and coruleoellagic acid
The figure was modified from Sturm *et al.*, 2009.

Similar to *Pf*GluPho with an IC_{50} of 77 ± 22 nM (Allen *et al.*, 2015), EA inhibits *Pv*G6PD with an IC_{50} of 32.5 ± 13.4 nM (Figure 40a) as determined within my master thesis. Moreover, FEA and CEA inhibit *Pv*G6PD in the same range, with IC_{50} values of 37.2 ± 5.8 nM and 44.4 ± 1.9 nM, respectively (Figure 40b, c; Haeussler, 2015).

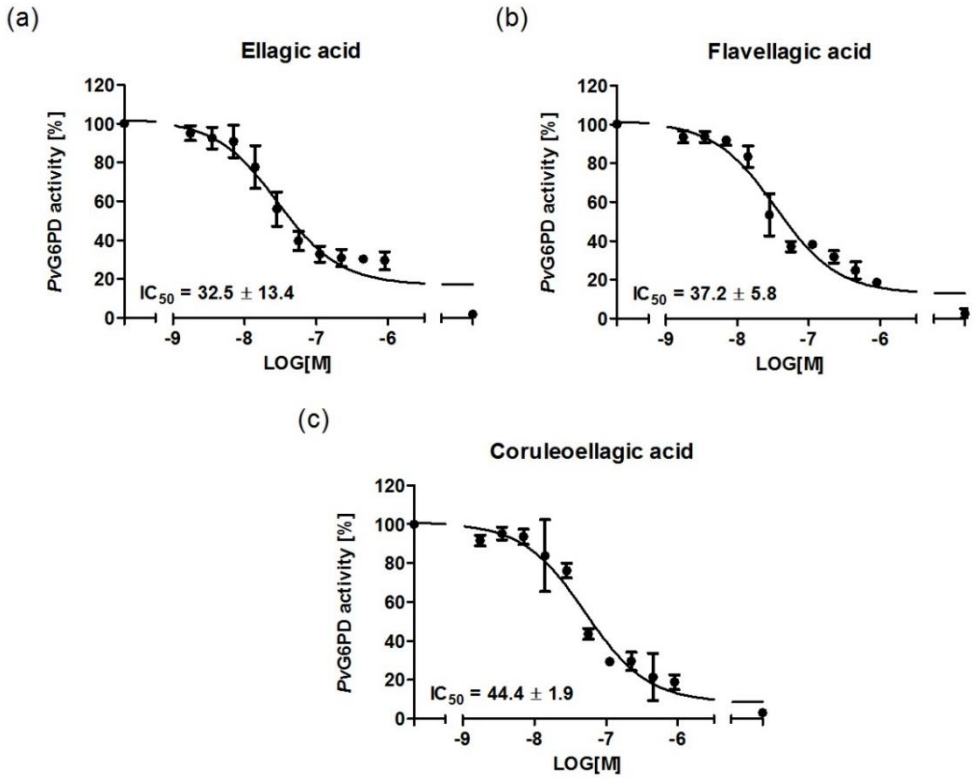

Figure 40. IC_{50} values of ellagic acid, flavellagic acid, and coruleoellagic acid for *Pv*G6PD
The IC_{50} values of ellagic acid (a), flavellagic acid (b), and coruleoellagic acid (c) for *Pv*G6PD were determined under substrate saturation. Given are mean values ± SD of at least four measurements.

The mode of inhibition of *Pv*G6PD by EA was determined to be a mixed type inhibition against both G6P and $NADP^+$ (Figure 41). This is identical with the type of inhibition determined for *Pf*GluPho (Allen *et al.*, 2015).

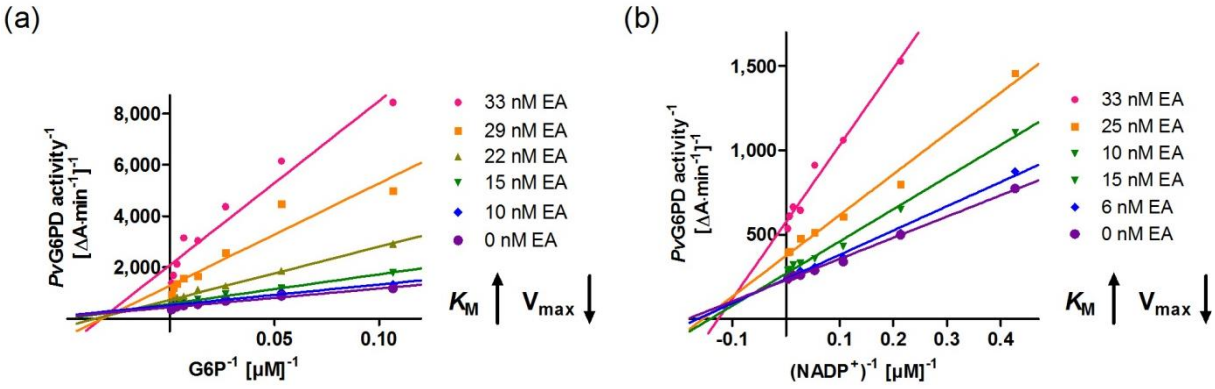

Figure 41. Mode of inhibition of *Pv*G6PD by ellagic acid
The Lineweaver-Burk plots for titration of G6P (a) or $NADP^+$ (b) show that high ellagic acid concentrations result in low V_{max} values and increased K_M values. This indicates that ellagic acid acts as a mixed-type inhibitor of *Pv*G6PD with respect to both G6P and $NADP^+$. Representative graphs from four independent determinations are shown.

Reversibility of the *Pf*GluPho inhibition by EA

Within this thesis, the reversibility of the inhibition of *Pf*GluPho by EA was tested. The enzyme was incubated with a high EA concentration (10 µM), and afterwards diluted to a concentration of 10 nM, which is below IC_{50}. The activity of the undiluted sample was 0.0 $U \cdot mg^{-1}$, showing that 10 µM EA completely inhibited *Pf*GluPho. The activity of the diluted sample was 1.3 ± 0.2 $U \cdot mg^{-1}$. Control samples containing either no EA or 10 nM EA (the concentration remaining after dilution) were prepared in parallel. The control without EA had an activity of 1.4 ± 0.1 $U \cdot mg^{-1}$, the control containing EA had 1.3 ± 0.2 $U \cdot mg^{-1}$, the identical activity as the sample incubated with a high EA concentration. This clearly shows that the inhibition of *Pf*GluPho by EA is fully reversible (Allen *et al.*, 2015). The generally low *Pf*GluPho activity might be caused by an activity loss during the incubation period.

4.5.2 ML304

ML304 was identified as a selective inhibitor for *Pf*GluPho via a high-throughput screening of the MLSMR chemical library, the structure is shown in Figure 42. With an IC_{50} of 190 nM for *Pf*GluPho and 80 µM for hG6PD, its effect is highly selective for *Plasmodium* (Maloney *et al.*, 2012).

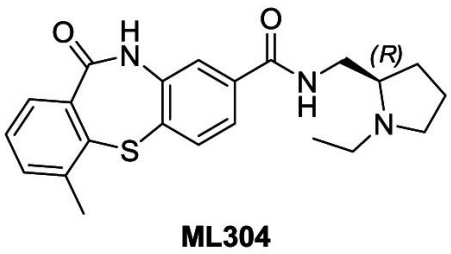

Figure 42. Structure of ML304
(Maloney *et al.*, 2012)

This promising compound was therefore tested on *Pv*G6PD. Under conditions of substrate saturation, ML304 inhibited *Pv*G6PD with an IC_{50} of 15.3 ± 0.9 µM. Application of substrate and cofactor in concentrations close to the K_M values of *Pv*G6PD resulted in a lower IC_{50} of 2.6 ± 0.8 µM (Figure 43).

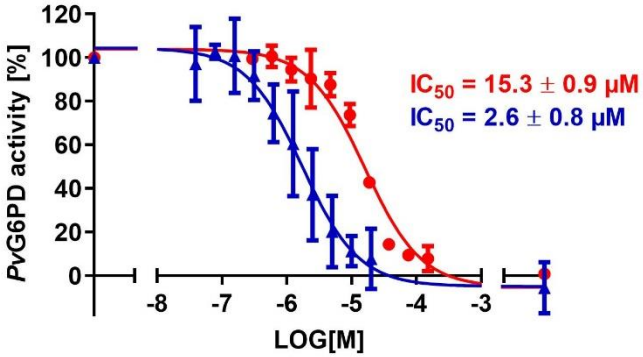

Figure 43. IC_{50} determination of ML304 for *Pv*G6PD
The IC_{50} of ML304 for *Pv*G6PD was determined under substrate saturation (red) and under substrate concentrations close to K_M values (blue). The IC_{50} is clearly shifted to a lower compound concentration when the substrates are added at K_M concentrations. Representative determinations (mean values ± SD) including four (red) and eight (blue) measurements are shown.

This change in IC_{50} depending on the substrate concentration was confirmed by mode of inhibition studies, which showed that ML304 acts as a competitive inhibitor towards G6P for both *Pv*G6PD and *Pf*GluPho (K_i = 0.7 ± 0.3 µM for *Pv*G6PD) and as a mixed type inhibitor towards $NADP^+$ for *Pv*G6PD (K_i = 16.3 ± 8.8 µM), while it acts as a non-competitive inhibitor for *Pf*GluPho (Figure 44).

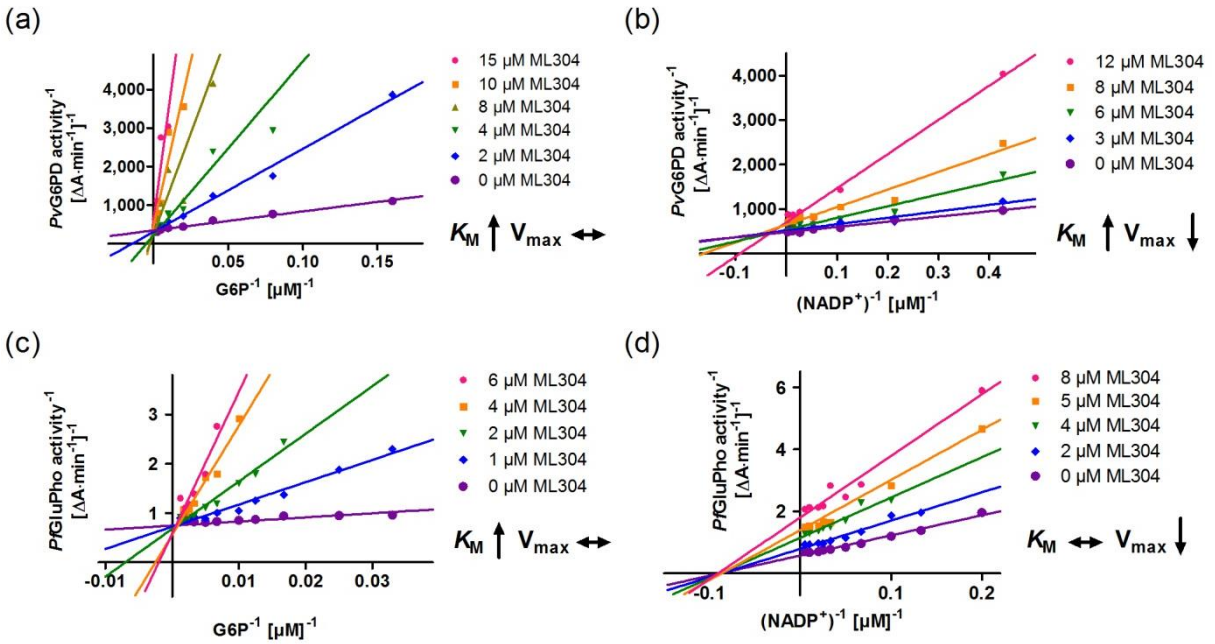

Figure 44. Mode of inhibition of *Pv*G6PD and *Pf*GluPho by ML304
(a, c) Most likely, ML304 acts as a competitive inhibitor with respect to G6P for both enzymes. The higher the concentration of ML304, the higher the K_M values of both enzymes for G6P were, while V_{max} stayed constant. (b) With respect to $NADP^+$, ML304 acts as a mixed type inhibitor on *Pv*G6PD (d) and as a non-competitive inhibitor on *Pf*GluPho.

4.5.3 The novel ML304 derivative SBI-0797750

To further improve the efficiency of compound ML304 (4.5.2), the structure-activity-relationship was analyzed at the Sanford Burnham Prebys Medical Discovery Institute (SBP), La Jolla, CA, USA. Within this thesis, 85 novel compound formulations derived from these analyses were tested against *Pf*GluPho, *Pv*G6PD, and hG6PD in high-throughput screening assay format. The structures of the compounds are not shown due to ongoing patenting processes.

4.5.3.1 Adjustment of the diaphorase-coupled assay to *Pv*G6PD

For *Pf*GluPho and hG6PD, the diaphorase-coupled assay was used as described in Preuss *et al.*, 2012a and Preuss *et al.*, 2013 with minor modifications. Within this thesis, the same assay was used for *Pv*G6PD for the first time; therefore, the assay concentrations had to be adjusted to the *P. vivax* enzyme.

Determination of appropriate G6P and $NADP^+$ concentrations for *Pv*G6PD

For the assessment of the compounds, substrate and cofactor were added in concentrations close to K_M to allow the identification of competitive inhibitors. Prior to compound characterization, the K_M values were redetermined in high-throughput screening assay format

(final assay volume of up to 8 µL; the minimum final assay volume used elsewhere in this thesis was 75 µL). The K_M for $NADP^+$ was in good accordance with the previously determined value, while the K_M for G6P, 30 µM, was notably lower (Table 15, Figure 45); therefore, 30 µM G6P and 12 µM $NADP^+$ were used for compound characterization on *Pv*G6PD at SBP.

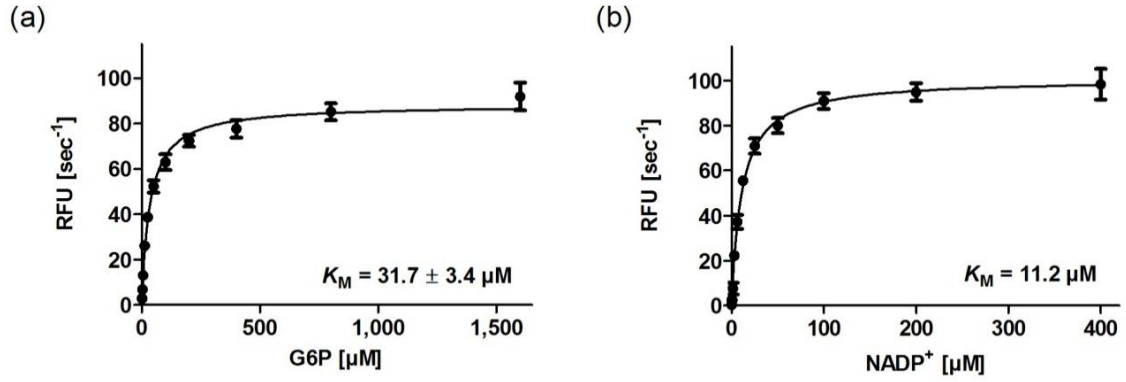

Figure 45. K_M determination for *Pv*G6PD in high-throughput screening assay format
The K_M values for G6P (a) and $NADP^+$ (b) of *Pv*G6PD were determined in high-throughput screening assay format by using the orthogonal assay, measuring the fluorescence of NADPH. Michealis-Menten curves (mean values ± SD) of one determination each including eight measurements, are shown. RFU: relative fluorescence units.

Determination of appropriate resazurin and diaphorase concentrations for *Pv*G6PD

To find the optimal resazurin concentration, *Pv*G6PD activity was determined using the diaphorase-coupled assay with different resazurin concentrations. As observed in Preuss *et al*., 2012a, very high resazurin concentrations led to a decrease in fluorescence signal. The highest activity was reached by adding 60 µM resazurin (Figure 46a). Since this concentration is higher than the substrate concentrations used in the assay (30 µM G6P, 12 µM $NADP^+$), it was ensured that resazurin was not limiting the reaction; therefore, 60 µM were used for the assessment of compounds on *Pv*G6PD. Similarly, the activity was determined by adding varying diaphorase concentrations. Since there were no major differences in activity between the diaphorase concentrations (Figure 46b), 1 $U \cdot mL^{-1}$ was used as in the assays for *Pf*GluPho and hG6PD.

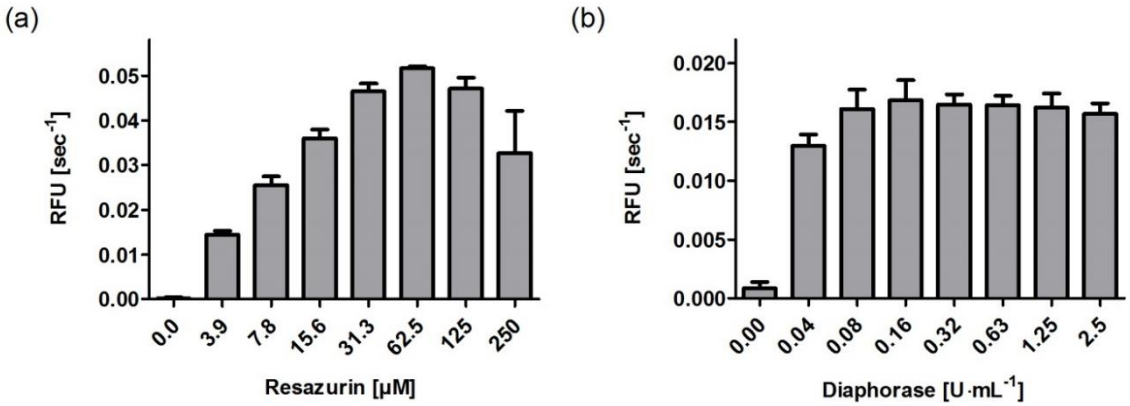

Figure 46. Determination of resazurin and diaphorase concentrations used in high-throughput assay format for *Pv*G6PD
*Pv*G6PD activity was determined using the diaphorase-coupled assay with varying resazurin (a) and diaphorase (b) concentrations. Mean values ± SD of one representative determination, each including eight measurements, are shown. RFU: relative fluorescence units.

Determination of an appropriate *Pv*G6PD concentration

To find a *Pv*G6PD concentration resulting in a linear signal increase for 2 h, activity was determined using different *Pv*G6PD concentrations. At the same time, the signal increase should be as high as possible in order to ensure a good range for later enzyme inhibition. Therefore, a *Pv*G6PD concentration of 0.15 µg·mL^{-1} was chosen (Figure 47).

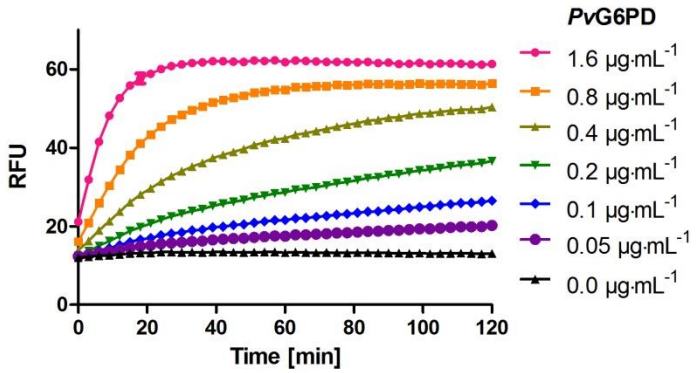

Figure 47. Determination of *Pv*G6PD concentration used in high-throughput assay format
*Pv*G6PD activity was measured using the diaphorase-coupled assay. Mean values ± SD of one representative determination including eight measurements are shown. RFU: relative fluorescence units.

4.5.3.2 IC_{50} determination on *Pf*GluPho, *Pv*G6PD, and hG6PD

First, the IC_{50} values were determined by using the diaphorase-coupled assay, measuring the fluorescence of the product resorufin at ex530/em590. SBI-0797750 turned out to be the most promising compound, with an IC_{50} of 5.2 ± 1.4 nM for *Pf*GluPho and 26.5 ± 7.3 nM for *Pv*G6PD; the human homolog hG6PD was not inhibited at 79 µM SBI-0797750 as the highest concentration tested. For the seven most promising compounds, false positive results due to interactions with the diaphorase-coupled assay were excluded by measuring the IC_{50} values using the orthogonal assay directly detecting the fluorescence of NADPH. The orthogonal assay resulted in comparable IC_{50} values (Table 17), for SBI-0797750 of 6.7 ± 1.8 nM and 31.0 ± 3.1 for *Pf*GluPho and *Pv*G6PD, respectively (Figure 48a, b). The inhibition of hG6PD at 99 µM as the highest concentration tested was below 50% (Figure 48c). This difference clearly shows that the inhibition of SBI-0797750 is highly selective for the plasmodial enzymes.

Table 17. IC_{50} values of the most promising novel compound formulations
IC_{50} values were determined using the orthogonal assay. Values given are mean values ± SD from two determinations, each including two measurements.

	*Pf*GluPho [nM]	*Pv*G6PD [nM]	hG6PD [nM]
SBI-0786225	102.6 ± 18.5	195.6 ± 23.9	> 99,000
SBI-0796683	10.1 ± 1.4	41.4 ± 3.6	> 99,000
SBI-0797749	18.4 ± 2.2	100.7 ± 10.5	> 99,000
SBI-0797750	6.7 ± 1.8	31.0 ± 3.1	> 99,000
SBI-0797751	24.1 ± 2.1	142.6 ± 12.2	> 99,000
SBI-0798044	16.0 ± 2.7	66.3 ± 6.0	> 99,000
SBI-0799057	16.2 ± 1.7	72.2 ± 8.1	> 99,000

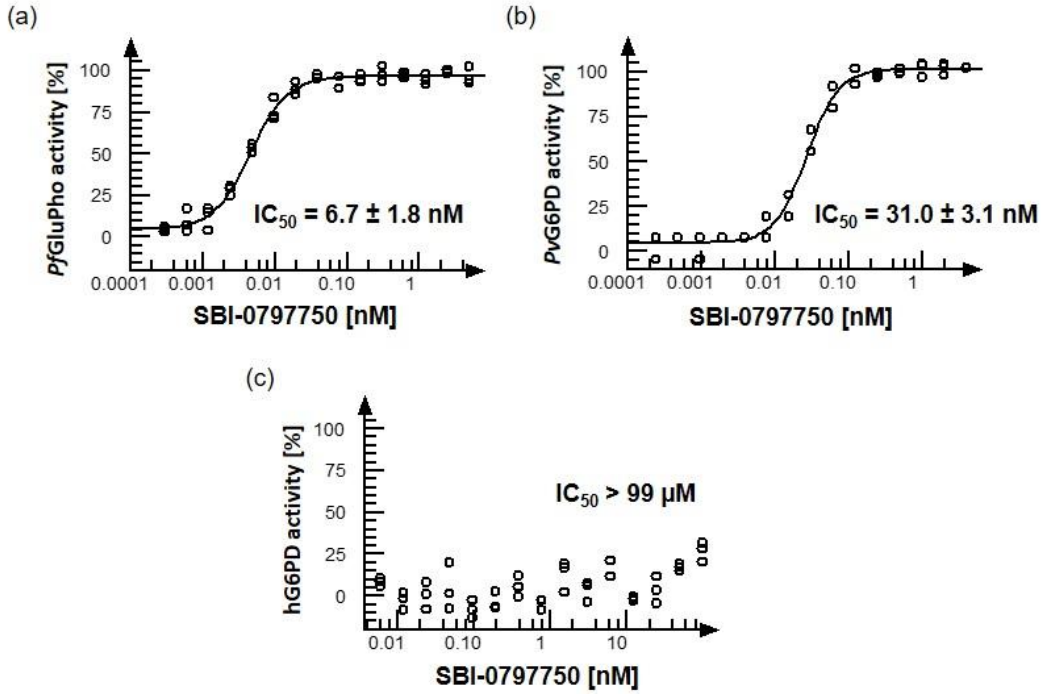

Figure 48. IC_{50} determination for SBI-0797750 on *Pf*GluPho, *Pv*G6PD, and hG6PD
The IC_{50} values of SBI-0797750 for *Pf*GluPho (a), *Pv*G6PD (b), and hG6PD (c) were determined by using the orthogonal assay measuring the fluorescence of NADPH. Representative measurements are shown. IC_{50} values given are mean values ± SD from two determinations, each including two measurements.

Although SBI-0797750 was optimized to inhibit *Pf*GluPho, its effect was tested on *Pf*6PGD. As expected, no inhibition could be detected at the highest tested concentration of 100 µM (data not shown).

4.5.3.3 Mechanism of inhibition of SBI-0797750

The most likely mechanism of inhibition was determined by titrating G6P or $NADP^+$ at different concentrations of SBI-0797750. The higher the concentration of the compound, the more increased the K_M value for G6P, while V_{max} stayed nearly constant (Figure 49a). This indicates that SBI-0797750 competes with G6P for the substrate binding site. Similarly, increasing compound concentrations led to increasing K_M values for $NADP^+$; however, V_{max} decreased (Figure 49b), suggesting a mixed type inhibition of SBI-0797750 against $NADP^+$. The most likely mechanism of inhibition was also determined for the other six compounds listed in Table 17, all resulting in a competitive inhibition with respect to G6P and a mixed type inhibition with respect to $NADP^+$.

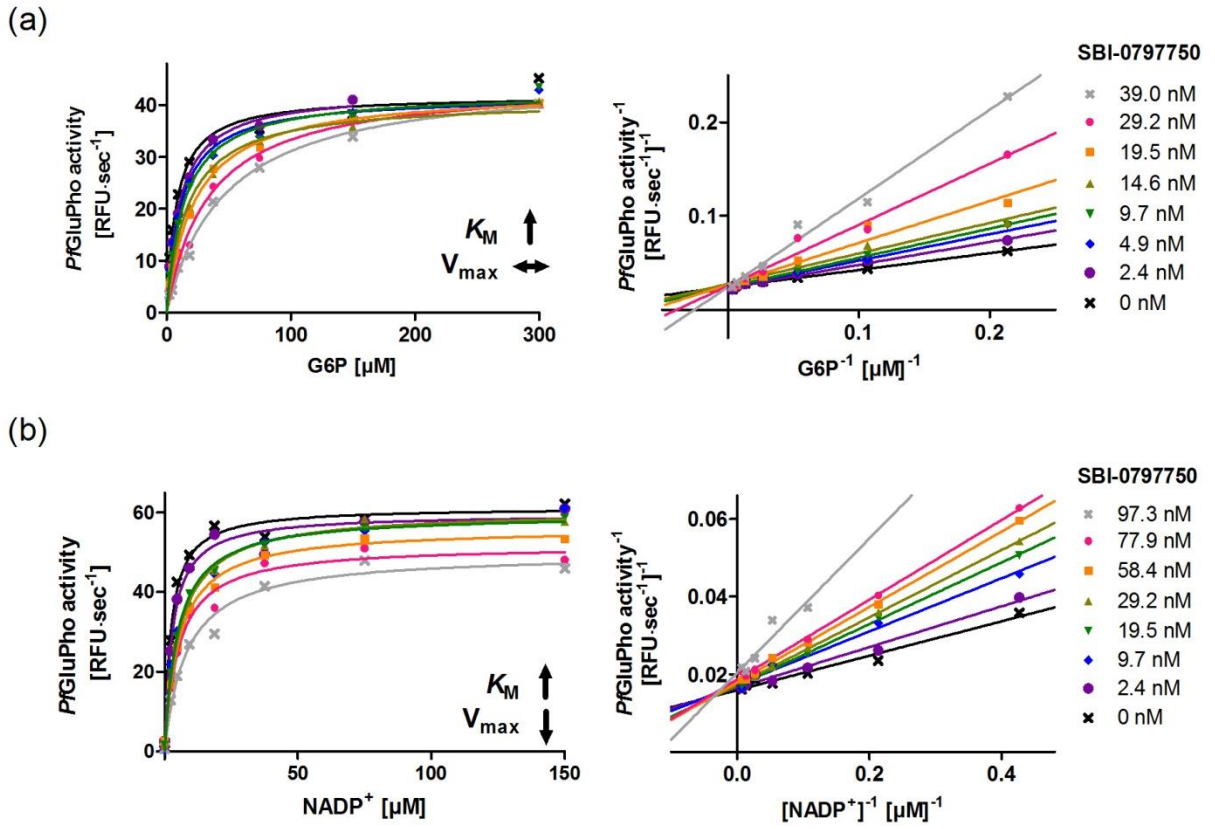

Figure 49. Mechanism of inhibition of SBI-0797750 against *Pf*GluPho
(a) Varying compound concentrations were titrated against G6P. SBI-0797750 acts as a competitive inhibitor against *Pf*GluPho since the K_M value for G6P increased with increasing compound concentrations while V_{max} stayed constant. (b) Titration of $NADP^+$ against different compound concentrations. The K_M value for $NADP^+$ was increasing while V_{max} was decreasing, indicating a mixed-type inhibition. RFU: relative fluorescence units.

4.5.3.4 Reversibility of the *Pf*GluPho inhibition by SBI-0797750

To test whether the inhibition of *Pf*GluPho by SBI-0797750 is reversible, the enzyme was incubated with a high compound concentration (1.65 µM). Afterwards, the sample was diluted to a final SBI-0797750 concentration below IC_{50} (3.3 nM) and incubated again to allow the compound to dissociate before the activity was measured. Controls containing either 3.3 nM SBI-0797750 or none were prepared in parallel. The control containing 3.3 nM SBI-0797750 was included for comparison since this concentration is expected to still cause inhibition (IC_{50}: 6.7 ± 1.8 nM). The activity of the control without SBI-0797750 was defined as 100%, the control containing 3.3 nM SBI-0797750 had an activity of 77.2 ± 1.6%, and the diluted sample had an almost identical activity with 79.2 ± 1.5%. Measuring the undiluted sample containing 1.65 µM SBI-0797750 had 2.4 ± 0.3% activity (Figure 50), indicating that the enzyme was inhibited before dilution. The small remaining activity might be due to the competition of the compound with G6P, which was added in saturation (see above, Figure 49a). Adding substrate and cofactor at K_M concentrations indeed resulted in an activity of only 0.3 ± 0.2%. This data clearly indicates that inhibition of *Pf*GluPho by SBI-0797750 is fully reversible.

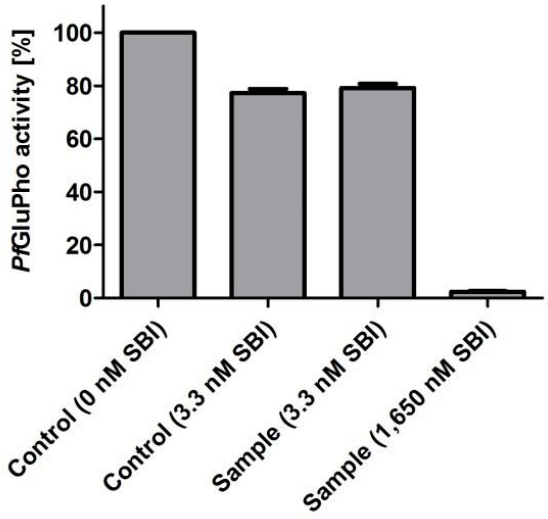

Figure 50. Reversibility of the *Pf*GluPho inhibition by SBI-0797750
The reversibility of the *Pf*GluPho inhibition by SBI-0797750 was determined by incubating the enzyme with a high compound concentration (1,650 nM), followed by dilution. The diluted sample had the same activity as a control containing the same final compound concentration (3.3 nM), while the undiluted sample was completely inhibited. Mean values ± SD from three independent determinations, each including two measurements, are shown.

4.5.3.5 *In vitro* activity of SBI-0797750 against *P. falciparum*

The effect of SBI-0797750 on the growth of blood stage *P. falciparum* 3D7 parasites was tested using the [^{3}H]-incorporation assay, resulting in a growth inhibition of the parasites with an IC_{50} of 64.6 ± 9.6 nM. Measurements using the SYBR Green assay resulted in an even lower IC_{50} of 22.5 ± 2.2 nM, while the growth of *P. falciparum* NF54-*attB* parasites was inhibited with an IC_{50} of 83.8 ± 17.3 nM. To test for synergistic effects with known antimalarial drugs, SBI-0797750 was simultaneously applied to *P. falciparum* 3D7 with either chloroquine, methylene blue, or artemisinin. However, these drug combinations did not result in synergistic improvement of the compound efficiency, but rather in antagonism (data not shown).

4.5.4 Discovery of a novel series of G6PD inhibitors

In order to identify potential novel inhibitors of plasmodial G6PD, several libraries of the Helmholtz Center for Infection Research in Brunswick, Germany, were screened prior to this thesis against *Pf*GluPho. Based on this screening, Prof. Dr. Dieter E. Kaufmann and Dr. Viktor Zapol'skii developed a compound library (Figure 51). The compounds were tested on *Pf*GluPho, *Pv*G6PD, and – to test for selectivity – on hG6PD. Parts of the IC_{50} values were determined by Dr. Esther Jortzik and Isabell Berneburg (Berneburg, 2017). An overview of the IC_{50} values is given in Table 18.

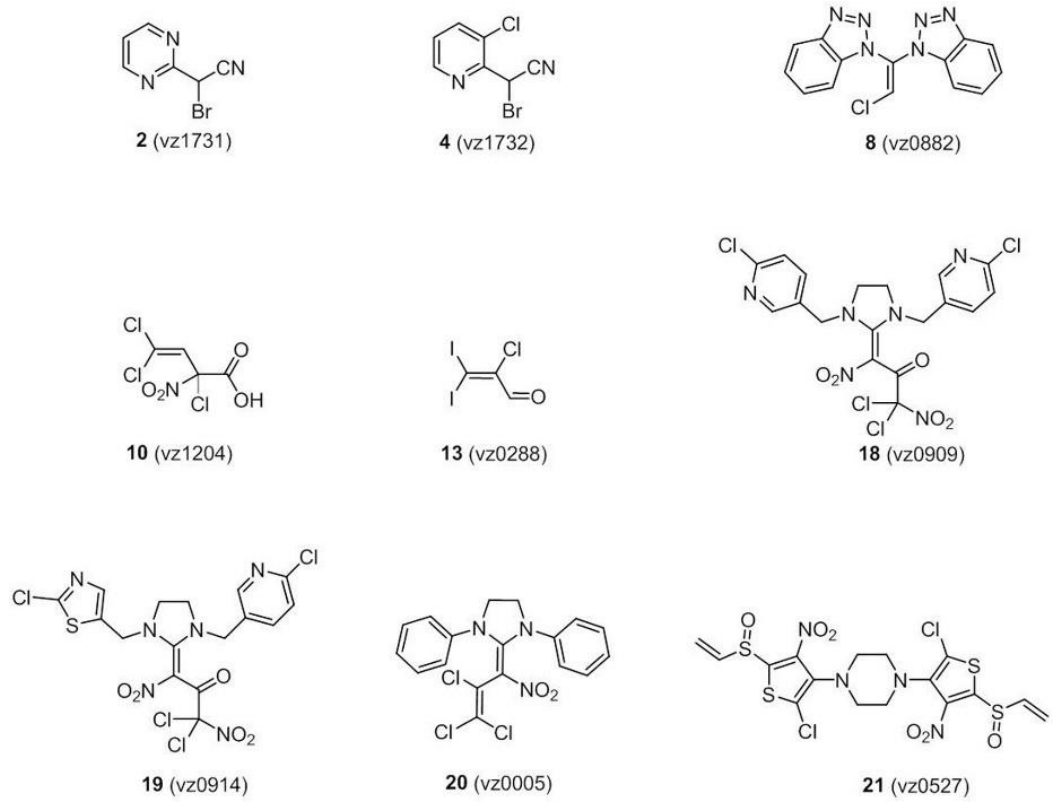

Figure 51. Compound library developed by Prof. Dr. Kaufmann and Dr. Zapol'skii

Table 18. IC_{50} values of novel compounds on *Pf*GluPho, *Pv*G6PD, and hG6PD
Values are presented as mean values ± SD of at least two independent determinations, each including at least two independent measurements. For hG6PD, only one enzyme batch was used. N. d.: not determined due to low solubility/reproducibility.

	*Pf*GluPho [µM]	*Pv*G6PD [µM]	hG6PD [µM]
2 (vz1731)	11.7 ± 9.9	2.1 ± 0.1	91.7 ± 35.0
4 (vz1732)	0.9 ± 0.2	0.2 ± 0.0	34.7 ± 21.0
8 (vz0882)	18.1 ± 10.4	12.8 ± 7.8	n. d.
10 (vz1204)	n. d.	23.5 ± 3.7	> 100
13 (vz0288)	29.6 ± 23.2	23.3 ± 7.8	> 100
18 (vz0909)	23.6 ± 14.3	9.1 ± 2.8	26.0 ± 1.8
19 (vz0914)	8.4 ± 8.4	5.6 ± 0.6	29.6 ± 5.0
20 (vz0005)	> 100	> 100	> 100
21 (vz0527)	1.7 ± 0.3	0.2 ± 0.1	8.3 ± 2.7

The two most potent compounds were **21** (vz0527) and **4** (vz1732), with IC_{50} values of 1.7 ± 0.3 µM for *Pf*GluPho and 0.2 ± 0.1 µM for *Pv*G6PD, and 0.9 ± 0.2 µM for *Pf*GluPho and 0.2 ± 0.0 µM for *Pv*G6PD, respectively. The corresponding IC_{50} values for hG6PD were at least five times higher, indicating a small selectivity for the plasmodial enzyme. Limited solubility or stability of the compounds caused the partially high standard deviations (e.g. **19** (vz0914): 8.4 ± 8.4 µM for *Pf*GluPho).

The most potent compound for *Pf*GluPho – compound **4** (vz1732) – was further characterized by determining its mode of inhibition. In contrast to the other compounds described in this thesis, it was found to act non-competitively against both the substrate G6P and the coenzyme $NADP^+$ (Figure 52). This indicates that compound **4** (vz1732) does not compete with substrate or cofactor for the binding sites.

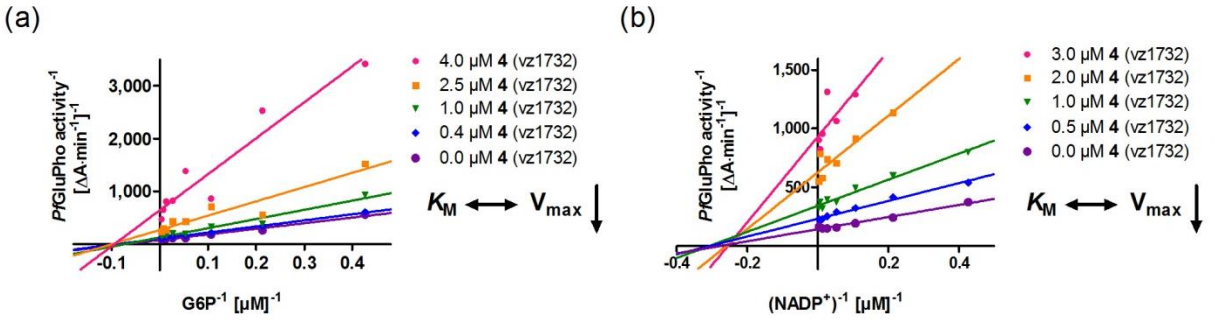

Figure 52. Mechanism of inhibition of compound 4 (vz1732) against *Pf*GluPho
The compound shows non-competitive inhibition against both G6P (a) and $NADP^+$ (b). The higher the concentration of compound **4** (vz1732), the lower the V_{max} was, while the K_M values for G6P and $NADP^+$ stayed constant. The graphs represent two independent determinations each.

4.5.5 Screening the MMV Malaria Box with *Pf*6PGD

DMSO tolerance test of *Pf*6PGD

Like many others, compounds of the MMV Malaria Box are dissolved in DMSO (Spangenberg *et al.*, 2013). Since these compounds were the first to be tested on *Pf*6PGD, DMSO tolerance of the enzyme was assessed first. To do so, the activity was measured by adding 0-5% DMSO; activity of the samples with 0% DMSO was defined as 100% (Figure 53). Adding 1% DMSO resulted in an activity of 101.0 ± 2.5%; higher concentrations resulted in a higher activity of *Pf*6PGD (up to 110.0 ± 5.4% by adding 5% DMSO). Therefore, it was ensured that no more than 1% DMSO was added to the assay characterizing the effect of compounds on *Pf*6PGD (Haeussler *et al.*, 2018).

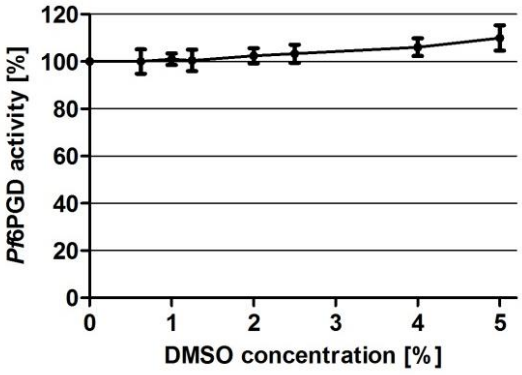

Figure 53. DMSO tolerance test of *Pf*6PGD
The activity of *Pf*6PGD was measured by adding 0-5% DMSO. Activity of the sample with 0% DMSO was defined as 100%. Values shown are mean values ± SD of three determinations, each including two measurements.

Primary screening of the MMV Malaria Box

For screening the MMV Malaria Box, substrate and cofactor were added in concentrations close to K_M in order to minimize the risk of false negative results due to competition of the compounds with 6PG and $NADP^+$ for the binding sites. The effect of 10 µM compound on *Pf*6PGD activity in comparison to a DMSO control was determined in quadruplicate. Out of the 400 compounds, 55 inhibited *Pf*6PGD at the tested concentration by ≥ 50% in at least three of the four determinations. These compounds were cherry-picked for further characterization (Haeussler *et al.*, 2018).

IC_{50} determination

To confirm and further quantify the effect of the 55 hits from the MMV Malaria Box compounds, the IC_{50} values against *Pf*6PGD were determined. 26 compounds could indeed be confirmed to inhibit the plasmodial enzyme with an IC_{50} below 10 µM: 10 compounds were even below 5 µM. Structures and IC_{50} values of the nine best compounds are shown in Table 19. To test for selectivity, the effect on h6PGD was tested in parallel. MMV666125 showed a slightly higher preference for the plasmodial enzyme (2.6 µM on *Pf*6PGD vs. 4.9 µM on h6PGD); however, the overall effect on h6PGD was comparable to the effect on *Pf*6PGD. The two most promising compounds were MMV011895 and MMV007228, with IC_{50} values of 1.6 ± 0.6 µM and 1.8 ± 0.1 µM, respectively (Figure 54). These compounds can be used as starting points for further improvement (Haeussler *et al.*, 2018).

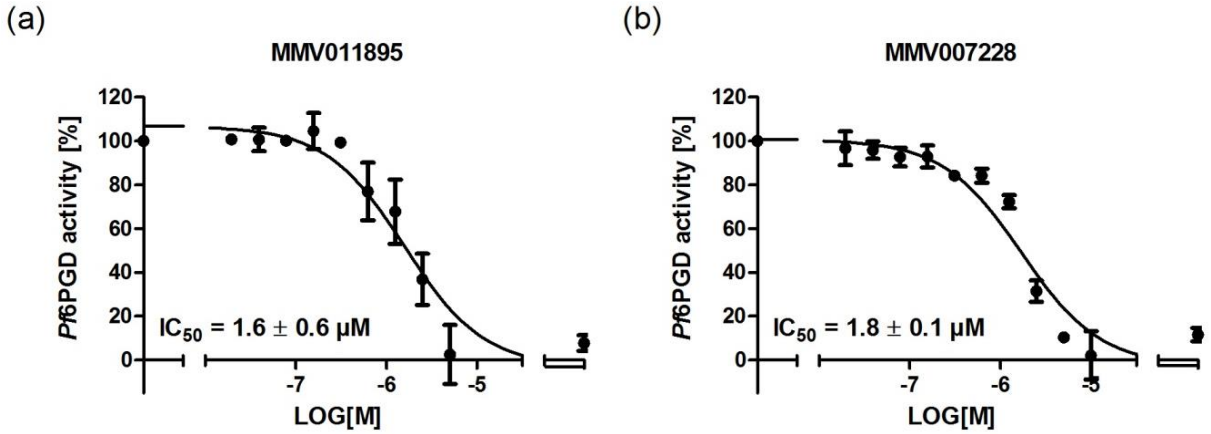

Figure 54. IC_{50} determinations for MMV011895 and MMV007228 on *Pf*6PGD

The best two compounds of the MMV Malaria Box were MMV011895 (a) and MMV007228 (b). Mean values ± SD from three measurements are shown.

Table 19. Structures and IC_{50} values of the MMV Malaria Box compounds on *Pf*6PGD and h6PGD
IC_{50} values of the nine most efficient MMV Malaria Box compounds against *Pf*6PGD and h6PGD. Structures of the compounds were generated using the online tool Pubchem Sketcher V2.4 (https://pubchem.ncbi.nlm.nih.gov/edit2/index.html). *Pf*6PGD: mean values ± SD from three determinations, h6PGD: mean values from two determinations (Haeussler *et al.*, 2018).

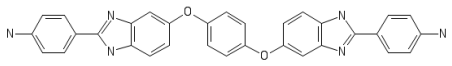	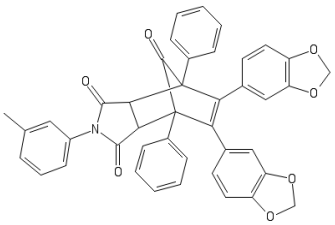	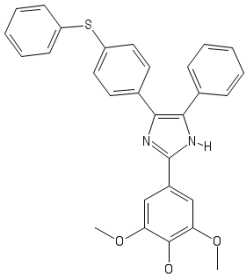
MMV011895: *Pf*6PGD: 1.6 ± 0.6 µM h6PGD: 2.1 µM	MMV007228: *Pf*6PGD: 1.8 ± 0.1 µM h6PGD: 2.7 µM	MMV007273: *Pf*6PGD: 2.1 ± 0.6 µM h6PGD: 1.8 µM
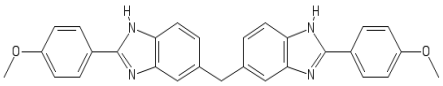	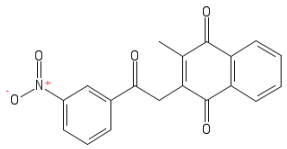	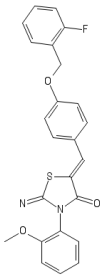
MMV007384: *Pf*6PGD: 2.5 ± 0.1 µM h6PGD: 2.4 µM	MMV666125: *Pf*6PGD: 2.7 ± 0.2 µM h6PGD: 4.9 µM	MMV007199: *Pf*6PGD: 2.9 ± 0.5 µM h6PGD: 1.3 µM
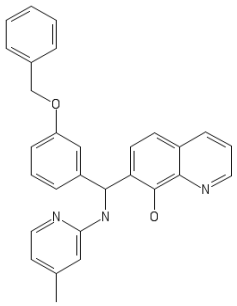	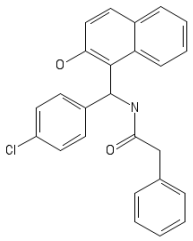	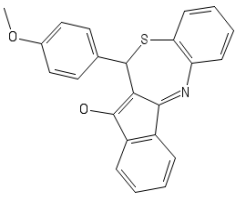
MMV000720: *Pf*6PGD: 3.1 ± 2.1 µM h6PGD: 2.2 µM	MMV665972: *Pf*6PGD: 4.0 ± 0.2 µM h6PGD: 4.3 µM	MMV000563: *Pf*6PGD: 4.2 ± 1.0 µM h6PGD: 3.5 µM

5 Discussion

5.1 Naturally occurring GluPho variants from *Plasmodium falciparum*

Exposure to *Plasmodium* parasites has left marks in the human genome; one prominent example is hG6PD deficiency, whose worldwide distribution shows remarkable similarity to the distribution of malaria and leads to partial resistance against the disease (see 1.2.1.1) (Cappellini and Fiorelli, 2008). However, during recent years, extensive research on the plasmodial genome also elucidated genome-wide diversity of *Plasmodium* species (Kirchner *et al.*, 2016; Neafsey *et al.*, 2008; Volkman *et al.*, 2007). One hypothesis is that these variants grant the parasites evolutionary benefits to deal with strong selection pressure (Haldar *et al.*, 2018). Interestingly, there are also naturally occurring mutations within the *Pf*GluPho gene, listed in the malaria database PlasmoDB. This enzyme plays a central role in the maintenance of cellular redox balance and the survival of the parasites (Allen *et al.*, 2015; Preuss *et al.*, 2012b); it can therefore be hypothesized that these mutations might lead to altered enzymatic activity and advantages in the defense against oxidative stress or altered redox regulation. To test this hypothesis, the naturally occurring mutants *Pf*GluPho^{L395F} and *Pf*GluPho^{F507L}, located in the G6PD domain of the *Pf*GluPho gene, as well as *Pf*GluPho^{S315Y}, located in the linker domain between 6PGL and G6PD, were created. Interestingly, F507 is located in an insertion sequence that is specific for G6PD genes of *Plasmodium*, differs in size and sequence between the species (Figure 4), and – most importantly – has been shown to be essential for G6PD activity in *P. berghei* (Clarke *et al.*, 2003). However, none of the tested mutants showed major differences when compared to the wt enzyme; *Pf*GluPho wt and all mutants eluted as tetramers from size exclusion chromatography, as already shown for the recombinant wt enzyme (Jortzik *et al.*, 2011), and for *Pf*GluPho isolated from parasites (Ling and Wilson, 1988; O'Brien *et al.*, 1994). The kinetic parameters of the wt enzyme determined within this thesis were in good accordance with values from literature (Jortzik *et al.*, 2011), and none of the kinetic parameters (substrate affinities, k_{cat} values, or catalytic efficiency) of the tested mutants *Pf*GluPho^{L395F}, *Pf*GluPho^{F507L}, and *Pf*GluPho^{S315Y} showed major differences to the wt enzyme (Table 14).

In proteomic approaches, several amino acid residues of *Pf*GluPho were found to be naturally phosphorylated. Interestingly, several groups identified S899 and S900, located at the C-terminal end of the *Pf*GluPho gene, to be phosphorylated (Lasonder *et al.*, 2012; Pease *et al.*, 2013; Treeck *et al.*, 2011). These two serines are highly conserved in and specific for *Plasmodium* (Appendix 3). Phosphorylation is known to be a central mediator of various cellular functions such as cell proliferation and differentiation, migration, and homeostasis; most importantly for this thesis, it is also a common regulator of enzyme activity (Doerig *et al.*, 2015). Detecting phosphorylation via Western blot analyses or kinetic determinations, as used within this thesis to investigate the other two PTMs *S*-glutathionylation and *S*-nitrosation, has two disadvantages: (I) phosphorylation is mainly mediated via protein kinases (Doerig *et al.*, 2015), making the investigation more difficult and laborious; (II) even if one were able to insert phosphorylation into the protein, it is unclear which amino acid residue would be affected. *Pf*GluPho has several naturally occurring phosphorylation sites (including S327, Y329, S330, S332, S477, T492, S701, S899, and S900, PlasmoDB); within this thesis, the focus was on S899 and S900. Identification of modified residues, e.g., via MALDI-TOF MS, would have been necessary. One easy possibility to directly investigate the impact of phosphorylation on specific residues is the insertion of phosphomimetic mutations by

exchanging the – in this case serines with glutamic acids (Kim *et al.*, 2015). Similar to the other tested *Pf*GluPho mutants, the phosphorylation-mimicking mutants *Pf*GluPho^{S899E} and *Pf*GluPho^{S900E} did not show any significant differences to the wt. Thus, most likely, the phosphorylation of serines 899 and 900 does not strongly regulate the *in vivo* activity of *Pf*GluPho.

This indicates that neither the studied naturally occurring mutants of *Pf*GluPho nor the phosphorylation of the two C-terminally located serine residues seem to provide major kinetic advantages. However, the variants might influence other characteristics of the enzyme such as protein-protein interaction, giving them benefits over the wt enzyme.

5.2 GluPho and G6PD from *Plasmodium vivax*

*Pf*GluPho, the key enzyme of the oxidative PPP of *P. falciparum*, has already been shown to be a promising target for the development of new antimalarial drugs (Allen *et al.*, 2015). The corresponding enzyme of *P. vivax* – *Pv*GluPho – also exists as a bifunctional enzyme and shows at the amino acid level a remarkable 71.2% identity and 79.9% similarity to *Pf*GluPho (Appendix 1) (Mohring *et al.*, 2014), indicating that it might be a drug target in *P. vivax*. Therefore, this central enzyme and its inhibition by selected small molecules were characterized within this thesis.

5.2.1 Recombinant production of *Pv*GluPho and *Pv*G6PD

Heterologous overexpression and purification of full-length *Pv*GluPho is extremely challenging. Two master students in Prof. Becker's group, Angeles Stegmayer and Isabell Berneburg, tested various conditions (I) for expression, including a variation of vectors, *E. coli* strains, media, temperatures, durations of overexpression, additional plasmids, and (II) for purification, including different buffers, detergents, etc.; however, none of the tested conditions resulted in pure, active *Pv*GluPho. Western blot analyses using anti-6xHis-tag antibodies showed the presence of *Pv*GluPho fragments of different sizes at all stages of protein production (Berneburg, 2017; Stegmayer, 2013). These fragments could be either caused by degradation of the protein or by incomplete translation of the gene. One common problem of protein translation of plasmodial genes in *E. coli* is the difference in codon usage. *E. coli* uses the codons AGG/AGA, CGA (arginine), CUA (leucine), AUA (isoleucine), and CCC (proline) at a total frequency of 1.8% (Kane, 1995), but in the mRNAs of *Pv*GluPho and *Pv*G6PD they have a frequency of 8.1% and 6.5%, respectively, potentially causing the poor quality of the synthesized protein (Kane, 1995). This can partially be overcome by using the additional plasmid pRAREII, which is supplying tRNAs for rare codons (Novagen, 2004); however, tRNA for CGA, which *E. coli* uses at a frequency of 0.3% and is present in the mRNAs of *Pv*GluPho and *Pv*G6PD at frequencies of 1.0% and 1.2%, respectively, is not encoded by pRAREII (Kane, 1995; Novagen, 2004). This might explain the high number of *Pv*GluPho fragments even when using pRAREII. Isabell Berneburg suggested in her master thesis that a slow, highly controlled expression of *Pv*GluPho can improve that quality of the produced protein, indicated by a lower number of protein fragments. The best results were achieved using a low temperature and short expression duration in LB medium, and *E. coli* Lemo21 cells (Berneburg, 2017). Lemo21 is a BL21 strain containing an additional plasmid with a gene that encodes T7 lysozyme under the control of a rhamnose promotor. Since T7 lysozyme is an inhibitor of the T7 RNA polymerase, the amount of expressed protein correlates negatively with the amount of added

rhamnose, thereby enabling a high control of expression (Schlegel *et al.*, 2012). One additional issue was the low solubility of *Pv*GluPho, which we attempted to overcome with detergents (Berneburg, 2017). However, not only detergents but also other additives such as metals, (charged or uncharged) amino acids, sugars, or reducing agents are in many cases able to increase the solubility of a protein (Leibly *et al.*, 2012). Alternatively, larger fusion tags could be used that are known to increase protein solubility such as GST or maltose-binding protein tags. However, these large tags might also affect other protein characteristics such as oligomerization behavior (Gräslund *et al.*, 2008).

In order to still characterize this enzyme that is presumably important for the survival of *P. vivax* parasites, experiments were performed using the C-terminal part, *Pv*G6PD. Similar to the full-length enzyme, heterologous overexpression was rather challenging, resulting in a relatively low yield of 0.1-0.4 mg of enzyme per liter *E. coli* cell culture by using pRAREII as an additional plasmid to overcome the codon bias (Novagen, 2004). Improvement of yield and quality of expression might be possible using genes optimized for the production within *E. coli* as host. One commonly used approach is the improvement of codon usage by encoding amino acids with a synonymous codon that is more frequently used in *E. coli* (Raab *et al.*, 2010). If expression in the bacterial system remains challenging, the use of other production hosts such as yeast (*Pichia pastoris* or *Saccharomyces cerevisiae*), insect cells, or even mammalian cells might be considered (Gräslund *et al.*, 2008).

5.2.2 Kinetic characterization of *Pv*G6PD

So far, the key enzyme of the oxidative PPP from *P. vivax* has not been characterized. Comparison of the kinetic parameters of *Pf*GluPho and *Pv*G6PD shows that K_M values are notably higher in *P. vivax*, while k_{cat} values are lower (Table 20). While the K_M for G6P of *Pf*GluPho is 20.3 ± 5.6 µM, it is four-times higher in *Pv*G6PD with 80.2 ± 19.8 µM; the K_M for $NADP^+$ is 2.5-times higher in *Pv*G6PD (14.8 ± 2.9 µM *vs*. 6.1 ± 1.3 µM). Less obvious, but the k_{cat} values are still over 1.5-times higher in *P. falciparum* (G6P: 10.7 ± 1.8 sec^{-1} for *Pf*GluPho, 6.7 ± 0.8 sec^{-1} for *Pv*G6PD). The difference becomes even more evident in the catalytic efficiency for *Pf*GluPho, $5.3 \cdot 10^5$ $M^{-1} \cdot sec^{-1}$, which is more than six-times higher than in *P. vivax* ($8.2 \cdot 10^4$ $M^{-1} \cdot sec^{-1}$, see Table 20). The PPP is the major source of the electron donor NADPH for *Plasmodium* parasites and is crucial to maintain their cellular redox balance (see 1.2). Therefore, the *P. falciparum* enzyme is likely to have advantages over *P. vivax* when competing with the human G6PD for substrates. However, whether this contributes to the higher pathogenicity of *P. falciparum* over *P. vivax* can only be speculated and deserves to be studied in more detail. Notably, when comparing the K_M for G6P of *Pf*GluPho and *Pf*G6PD (Table 20), it becomes evident that *Pf*G6PD has a higher K_M for G6P and a lower catalytic efficiency than the full-length enzyme (K_M: 33.2 ± 1.2 µM for *Pf*G6PD, 19.2 ± 3.9 µM for *Pf*GluPho; catalytic efficiency: $1.9 \cdot 10^5$ $M^{-1} \cdot sec^{-1}$ for *Pf*G6PD, $4.5 \cdot 10^5$ $M^{-1} \cdot sec^{-1}$ for *Pf*GluPho, see Jortzik *et al*., 2011). This might be due to structural advantages of the fusion of the protein. The same is likely true for *P. vivax*, so the full-length *Pv*GluPho might have lower K_M values than *Pv*G6PD. Interestingly, in hG6PD, V_{max} and corresponding k_{cat} values are notably higher than in the plasmodial enzymes (Table 20); however, since the K_M values of hG6PD are also higher, this results in a comparable catalytic efficiency. This indicates that the fusion of G6PD with the second enzyme of the PPP, allowing for direct substrate transfer within the pathway, might give the *Plasmodium* parasites some kinetic advantage over the human homolog. Kinetic characterization of full-length *Pv*GluPho remains to be conducted in future studies.

Table 20. Comparison of kinetic parameters from *P. vivax* and *P. falciparum*
* Values from Jortzik *et al*., 2011 are shown for comparison. Catalytic efficiency (k_{cat}/K_M) was calculated from mean values to enable comparison to the values published in Jortzik *et al*., 2011.

		*Pv*G6PD	*Pf*G6PD*	*Pf*GluPho wt	*Pf*GluPho wt*	hG6PD*
V_{max} [U·mg^{-1}]	G6P	5.6 ± 0.7	5.5 ± 0.2	5.9 ± 1.0	5.2 ± 1.6	64.4 ± 11
	$NADP^+$	5.5 ± 0.4	5.5 ± 0.1	5.9 ± 0.6	4.6 ± 0.8	57.7 ± 15
K_M [µM]	G6P	80.2 ± 19.8	33.2 ± 1.2	20.3 ± 5.6	19.2 ± 3.9	116 ± 8.5
	$NADP^+$	14.8 ± 2.9	6.1 ± 0.7	6.1 ± 1.3	6.5 ± 2.2	17.5 ± 2.8
k_{cat} [sec^{-1}]	G6P	6.7 ± 0.8	6.3 ± 0.3	10.7 ± 1.8	8.6 ± 1.5	64.6 ± 8.9
	$NADP^+$	6.5 ± 0.4	6.3 ± 0.1	10.1 ± 0.9	8.2 ± 1.2	56.9 ± 15
Catalytic efficiency [M^{-1}·sec^{-1}]	G6P	$8.2\cdot10^4$	$1.9\cdot10^5$	$5.3\cdot10^5$	$4.5\cdot10^5$	$5.6\cdot10^5$

5.2.3 Oligomerization behavior of *Pv*G6PD

G6PDs from most organisms exist in three different oligomerizations; as monomers such as *Bos taurus* (Ibrahim *et al.*, 2015), dimers as in *Trypanosoma brucei* (Heise and Opperdoes, 1999), or tetramers such as *Sus scrofa* (Cho and Joshi, 1990). The oligomerization of the human enzyme highly depends on the ionic strength, pH, and presence of substrates in its environment and exists in all three forms (Wrigley *et al.*, 1972). Recombinant full-length *Pf*GluPho has previously been shown to be present in a tetrameric form (Jortzik *et al.*, 2011) which was confirmed in this thesis; furthermore, the same oligomerization was found for *Pf*G6PD. Interestingly, *Pv*G6PD showed a different behavior; it eluted in a presumably hexameric form from size exclusion chromatography. Such a hexameric oligomerization has not been previously described for G6PDs (Brenda, EC 1.1.1.49) and might actually represent an artificial state since *Pv*G6PD occurs as a fusion protein with 6PGL under physiological conditions (Mohring *et al.*, 2014). The oligomerization state of full-length *Pv*GluPho is presumably different – based on the high sequence identity with *Pf*GluPho (Appendix 1) likely tetrameric. This likely artificial oligomerization status might be one explanation for the lower affinity of *P. vivax* G6PD to its substrates compared to *P. falciparum* GluPho (Table 20). Due to the hexameric oligomerization, substrate binding sites might be less accessible than in the – presumably tetrameric – physiological conformation. First experiments using full-length *Pv*GluPho performed by Isabell Berneburg indicated that it exists in a tetrameric form; however, the enzyme used for size exclusion chromatography was not active, therefore this oligomerization status might not be reliable (Berneburg, 2017). Further experiments with active full-length *Pv*GluPho are essentially important for verifying the characteristics of this central enzyme of *P. vivax*.

5.3 6PGD from *Plasmodium falciparum*

*Pf*6PGD catalyzes the third step of the oxidative PPP and has not been characterized before. Since it contributes to the NADPH supply of the parasites in the same amounts as *Pf*GluPho, it might also be important for the survival of the parasites (Haeussler *et al.*, 2018). Therefore, one aim of the thesis was the structural and kinetic characterization of *Pf*6PGD.

5.3.1 Structure of *Pf*6PGD

The overall structure of *Pf*6PGD is remarkably similar to the structure of other members of the 6PGD family; it is active as a homodimer, each monomer consisting of one substrate and one cofactor binding domain and a C-terminal tail threading through the adjacent subunit as observed, e.g., in *Homo sapiens* (Hitosugi *et al.*, 2012), *Lactococcus lactis* (Sundaramoorthy *et al.*, 2007), and *Geobacillus stearothermophilus* (Cameron *et al.*, 2009). The high similarity of *Pf*6PGD to other members of the 6PGD family is already noticeable at the primary sequence level (Table 21) (Haeussler *et al.*, 2018). Further characteristics of the structure will be discussed in the chapters below.

Table 21. Comparison of the amino acid sequences of 6PGDs from different species to *Pf*6PGD
The table contains species from which the three-dimensional structure of 6PGD is known. UniProtKB for *Pf*6PGD: Q8IKT2; for the other species it is given in parentheses.

	Identity to *Pf*6PGD	Similarity to *Pf*6PGD
Geobacillus stearothermophilus (I3NI58)	49.2%	65.0%
Alicyclobacillus acidocaldarius (C8WVH6)	46.9%	65.2%
Escherichia coli (P00350)	45.9%	63.6%
Klebsiella pneumoniae (P41576)	45.7%	63.4%
Lactococcus lactis (P96789)	45.6%	64.7%
Saccharomyces cerevisiae (P38720)	44.4%	61.3%
Homo sapiens (P52209)	43.4%	61.3%
Ovis aries (P00349)	43.4%	61.3%
Dyadobacter fermentans (C6VSE5)	42.7%	62.3%
Corynebacterium glutamicum (Q8NQI2)	40.1%	60.9%
Trypanosoma brucei (P31072)	34.6%	54.4%
Geobacter metallireducens (Q39SD5)	21.5%	32.9%
Pseudomonas syringae (S3MGN3)	21.1%	34.6%

5.3.2 Oligomerization behavior of *Pf*6PGD

As determined within this thesis, native, reduced, and oxidized *Pf*6PGD wt, as well h6PGD were present in a dimeric form. Reduced dimeric *Pf*6PGD indicates that dimerization is not primarily based on intermolecular disulfide bonds. This was further confirmed by the oligomerization of *Pf*6PGD^{C281S}; although the *Plasmodium*-specific disulfide bridge between the cysteine residues 281 of the two subunits A and B (Figure 23) was missing, there was no change in the dimeric conformation of the enzyme. Therefore, this disulfide bridge is not essential for dimerization. This oligomerization state is in accordance with previous studies on the 6PGDs of various species such as those isolated from human RBCs (Pearse and Rosemeyer, 1974b), *Lactococcus lactis* (Sundaramoorthy *et al.*, 2007), *Saccharomyces cerevisiae* (He *et al.*, 2007), and *Trypanosoma brucei* (Phillips *et al.*, 1998). All these structures have the C-terminal tail in common. As seen in our structure, the C-term of one subunit threads through the adjacent subunit, thereby linking the two monomers very tightly (Haeussler *et al.*, 2018). However, despite this close interaction, there are additional interactions between the α-helices located in the dimer interface. He *et al*., 2007 created mutants lacking the C-terminal tail; although less stable than the full-length enzyme, the truncated mutants were still present in a dimeric form yet did not show any enzymatic activity. In the structure of *Saccharomyces cerevisiae* 6PGD, they found the highly conserved residues R446 and H452

(Figure 24) to be involved in binding citrate molecules that were located in the 6PG binding site (He *et al.*, 2007). It has been shown before that in *Lactococcus lactis*, the corresponding R447 most likely plays an important role in anchoring 6PG during its oxidative decarboxylation since none of the mutants R447K, R447A, R447D, or R447W showed enzyme activity (Tetaud *et al.*, 1999). Similar in our *Pf*6PGD structure in complex with 6PG, R447 and H453 located on the C-terminal tail have been shown to be involved in substrate binding (Figure 25a; Haeussler *et al*., 2018). Therefore, it can be concluded that the primary function of the C-term is not an involvement in dimerization but in the enzyme mechanism. To test this hypothesis, a truncated version of *Pf*6PGD could be generated, missing the C-terminal amino acids 434-468.

The oligomerization behavior of *Pf*6PGD wt has also been tested in the presence of its product NADPH. For *T. brucei*, a dimer-tetramer equilibrium has been described, with NADPH shifting it more towards the tetrameric form (Hanau *et al.*, 2013). However, in *Plasmodium* there was no difference compared to other conditions tested (Figure 27), indicating that there is no dimer-tetramer equilibrium (Haeussler *et al.*, 2018).

5.3.3 Kinetic parameters of *Pf*6PGD

Within this thesis, *Pf*6PGD was kinetically characterized. All kinetic parameters of *Pf*6PGD were in a similar range as the corresponding parameters of the enzyme preceding the pathway – *Pf*GluPho (Table 14, Table 16, see also Jortzik *et al*., 2011). The kinetic parameters of the enzyme from various organisms with known three-dimensional 6PGD structures are in a very broad range of 1-118 µM for the K_M for $NADP^+$ and of 3.5-153 µM for 6PG (Table 22).

Table 22. Comparison of kinetic parameters of 6PGDs from different species
All values are given from species with known three-dimensional structures. N. d.: not defined.

Organism	Specific activity [U·mg^{-1}]	K_M $NADP^+$ [µM]	K_M 6PG [µM]	Reference
Plasmodium falciparum	8.0 ± 1.9	9.0 ± 4.2	11.3 ± 2.7	This thesis
Trypanosoma brucei	3.2	1	3.5	Hanau et al., 1996
Trypanosoma cruzi	32	5.9 ± 0.2	22.2 ± 0.4	Esteve and Cazzulo, 2004
Homo sapiens	10	30	20	Pearse and Rosemeyer, 1974a
	22.1 ± 1.2	6.9 ± 2.0	33.7 ± 7.1	This thesis
Ovis aries	18.8 ± 0.9	6.76 ± 1.6	16.1 ± 1.3	Dyson *et al.*, 1973
	n. d.	2.9	22.7	Topham *et al.*, 1986
Corynebacterium glutamicum	143	17 ± 3	34 ± 13	Moritz *et al.*, 2000
Geobacillus stearothermophilus	87	25	20	Veronese *et al.*, 1974
Saccharomyces cerevisiae	34.9 ± 0.6	25 ± 1	153 ± 4	Rendina *et al.*, 1984
	n. d.	35 ± 6	50 ± 9	He *et al.*, 2007
Escherichia coli	24.35 ± 0.30	49 ± 7	93 ± 1	Chen *et al.*, 2010
Klebsiella pneumoniae	12.92 ± 0.34	118 ± 23	107 ± 4	Chen *et al.*, 2010

Various methodologies (see references in Table 22) such as different enzyme sources (e.g. recombinant enzyme, isolated from cell culture or tissue), assay buffers (e.g. Tris buffer, triethanolamine buffer, different pH values), or temperatures (20-43 °C) might partially explain this variation. However, the K_M values of the parasites *P. falciparum* and trypanosomes are noticeably lower than the values of most other organisms (*P. falciparum*: 9.0 µM for $NADP^+$, 11.3 µM for 6PG; trypanosomes: 1-5.9 µM for $NADP^+$, 3.5-22.2 µM for 6PG; Hanau *et al*., 1996; Esteve and Cazzulo, 2004). The glucose metabolism plays an essential role in malaria infections (Preuss *et al.*, 2012b). In malaria-infected red blood cells, glucose metabolism in total and the PPP in particular have been shown to be increased (Atamna *et al.*, 1994). The comparably low K_M values in *Plasmodium* and *T. brucei* and *cruzi* show the high affinity of the enzymes for their substrates, underscoring the central role of the PPP and therefore of 6PGD during parasitic infection. In trypanosomes, 6PGD has already been validated as a promising target for the development of new drugs against the parasitic disease African trypanosomiasis (Hanau *et al.*, 2004). This – together with the fact that *Pf*GluPho as the other NADPH-producing enzyme of the PPP is essential for the parasites (Allen *et al.*, 2015) – suggests that *Pf*6PGD is a promising target for new antimalarial drugs (Haeussler *et al.*, 2018).

One aim of this thesis was to find an initial set of inhibitors for *Pf*6PGD. To enable selectivity testing of identified compounds, the corresponding human enzyme – h6PGD – was recombinantly produced and kinetically characterized in parallel. Notably, the specific activity determined in this thesis was 22.1 ± 1.2 $U \cdot mg^{-1}$, significantly higher than the value published for h6PGD isolated from RBCs (10 $U \cdot mg^{-1}$, Pearse and Rosemeyer, 1974a). While the K_M value of recombinant h6PGD for 6PG was close to the value in the literature (33.7 ± 7.1, 20 µM in Pearse and Rosemeyer, 1974a), the K_M for $NADP^+$ was notably lower in this thesis (6.9 ± 2.0 µM, 30 µM in Pearse and Rosemeyer, 1974a). The different protein sources and consequently different purification procedures might explain these discrepancies; purification of recombinant h6PGD performed within this thesis took a maximum of two days, while purification of h6PGD from RBCs takes about three weeks (Pearse and Rosemeyer, 1974a). During this time, the enzyme is likely to lose activity. Moreover, the assay buffer conditions for determining the kinetic parameters were slightly different; in Pearse and Rosemeyer, 1974a, the assay buffer had a pH of 9.0, while the buffer used in this thesis had a pH of 8.0. The activity of an enzyme depends on the pH in its environment. With increasing pH, the activity increases until it reaches a maximum (pH optimum); as soon as this pH is surpassed, the activity decreases again (Bisswanger, 2017). The cytosolic pH in human cells is around 7.0-7.4 (Bright *et al.*, 1987; Dechant *et al.*, 2010; Llopis *et al.*, 1998; Poburko *et al.*, 2011). Therefore, it can be assumed that the pH optimum of h6PGD – located in the cytosol – is around 7, and the pH used in this thesis, 8.0, is closer to the optimum as 9.0 used in the literature. However, further enzymatic studies need to be conducted in order to determine the exact pH optimum.

<u>NAD^+ as an alternative cofactor</u>

The 6PGD activity of *T. brucei* has been shown to be specific for $NADP^+$, and NAD^+ does not act as a cofactor (Hanau *et al.*, 1996). Since the kinetic behavior of *Pf*6PGD seems to be similar to the behavior of *Tb*6PGD (both low K_M values, similar mechanism, see 5.3.4), NAD^+ was tested within this thesis as an alternative cofactor. The activity of both *Pf*6PGD and h6PGD was indeed found to be specific for $NADP^+$. The interaction of the negatively charged phosphate groups of $NADP^+$ with the positively charged arginine residues R32 and R36 can structurally explain the specificity in *P. falciparum* (Figure 26) (Haeussler *et al.*, 2018). A negatively charged

residue, e.g. aspartate, was previously shown to prefer NAD^+ as a cofactor, while positively charged residues such as arginine prefer $NADP^+$ binding (Chen *et al.*, 2010; Zhang *et al.*, 2014). R32 is conserved amongst different species, while R36 is specific for *Plasmodium* and is replaced in *H. sapiens* and *T. brucei* by a lysine. However, lysine is also positively charged and able to interact with the phosphate groups of $NADP^+$. In two NAD^+-specific 6PGDs from *Haloferax volcanii* (Pickl and Schönheit, 2015) and *Bacillus subtilis* (Zamboni *et al.*, 2004), the positively charged residues are replaced with uncharged amino acids leucine and alanine, or the negatively charged tyrosine and leucine, respectively (Figure 55).

```
Pf   --MCDIGLIGLAVMGQNLSLNISSKGFKIGVYNRTYERTEETMKRAKEE--NLVVYGYKT   56
Tb   -MSMDVGVVGLGVMGANLALNIAEKGFKVAVFNRTYSKSEEFMKANASAPFAGNLKAFET   59
Hs   MAQADIALIGLAVMGQNLILNMNDHGFVVCAFNRTVSKVDDFLANE-AK--GTKVVGAQS   57
Hv   ---MQLGVIGLGRMGRIVVDRVLDAGHEVVAFDLSAEAVAAAA--------DAGAEPADS   49
Bs   -MFNSIGVIGLGVMGSNIALNMANKGENVAVYNYTRDLTDQ-LIQK-LD--GQSLSPYYE   55
         .:.::**. **  :  .: . *  : .::: : .
```

Figure 55. Amino acid alignment of $NADP^+$- and NAD^+- specific 6PGDs
Relevant residues involved in the specific cofactor binding are marked in yellow. *Pf*, *Tb*, and *Hs* are specific for $NADP^+$, while *Hv* and *Bs* are specific for NAD^+. *Pf*: *Plasmodium falciparum* (UniProtKB - Q8IKT2); *Tb*: *Trypanosoma brucei* (UniProtKB - P31072); *Hs*: *Homo sapiens* (UniProtKB - P52209); *Hv*: *Haloferax volcanii* (UniProtKB – D4GST8); *Bs*: *Bacillus subtilis* (UniProtKB - P12013). * Identical residues, : very similar residues, . similar residues.

5.3.4 Mechanistic considerations of *Pf*6PGD

Flexible loop rearranges upon substrate binding

Attempts to cocrystallize *Pf*6PGD with $NADP^+$ but without the substrate resulted in only partially bound $NADP^+$; the adenine moiety and the three phosphate groups were visible, while the catalytically important nicotinamide moiety was not defined by electron density, most likely due to flexibility. The active site loop (amino acids 255-262, bordering the 6PG binding site, Figure 25a) adopted an open conformation as seen in our apo structure. As soon as 6PG binds, the active site loop adopts a closed conformation (Figure 56a). This movement of the active site loop is also visible in structures of other species. As long as the substrate binding pocket is empty or filled solely with solvent molecules such as PEG (seen in our apo-*Pf*6PGD, Figure 25b) or H_2O, the active site loop is in an open conformation, also seen, e.g., in *Klebsiella pneumoniae* (2ZYG (Chen *et al.*, 2010)). In h6PGD, the inhibitor 3-phosphoglycerate forces the active site loop into the open conformation (4GWG (Hitosugi *et al.*, 2012)). The 12 additional C-terminal amino acids of h6PGD are disordered with an open active site loop but cover the active site of h6PGD as soon as the loop adopts its closed conformation (Figure 56b). The closed conformation is adopted as soon as the substrate pocket is occupied by a ligand or at least an anion such as sulfate (1PGO (Adams *et al.*, 1994), 1PGJ (Phillips *et al.*, 1998), 2JKV (to be published), 2PGD (Adams *et al.*, 1991), 2W90 (Cameron *et al.*, 2009)), phosphate (1PGN (Adams *et al.*, 1994)), or citrate (2P4Q (He *et al.*, 2007)) interacting with the positively charged R447’ and with loop residues (Haeussler *et al.*, 2018).

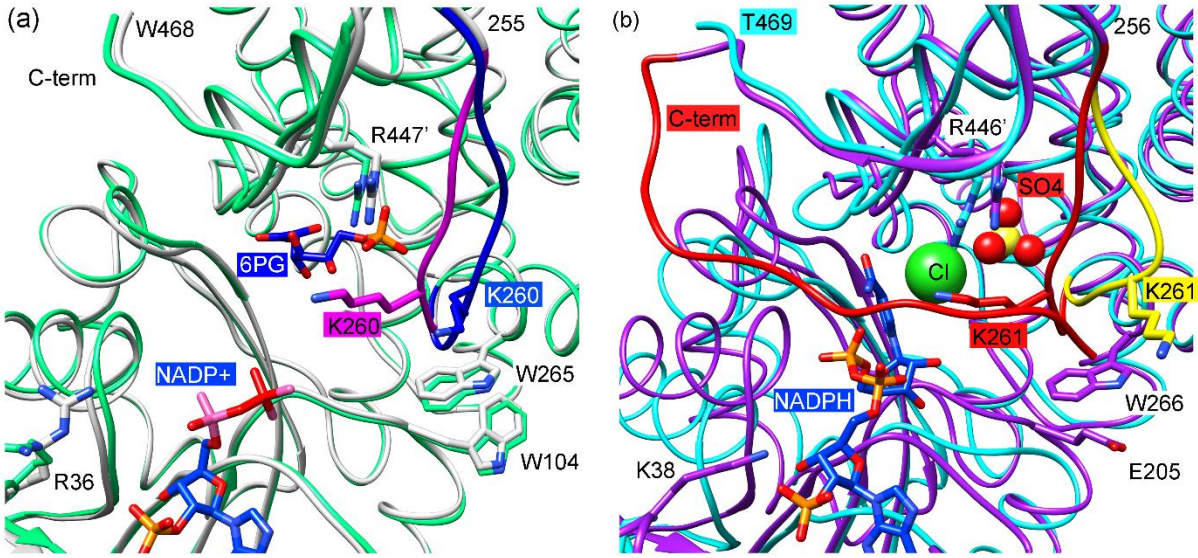

Figure 56. Active site loop in plasmodial and human 6PGD
(a) Superimposition of apo-*Pf*6PGD structure (green), and in complex with 6PG (gray); the active site loop (255-262) is colored blue and magenta, respectively, and changes its conformation upon substrate binding. (b) Superimposition of the human apo-structure (light blue, 4GWG (Hitosugi *et al.*, 2012)) and in complex with NADPH (magenta, 2JKV (to be published)). The active site loop is colored yellow and red, respectively. Sulfate and a Cl ion occupy the substrate binding site of the NADPH complex structure, resulting in a closed conformation of the active site loop (red) and a ordered long C-terminus (red) (Haeussler *et al.*, 2018).

6PG and $NADP^+$ can bind independently from each other

The substrate 6PG alone binds in the catalytically relevant position. Without 6PG and therefore with an open active site loop (Figure 56a), $NADP^+$ is bound in a flexible waiting position; adenosine is fixed, while nicotinamide and the second ribose are flexible and therefore not in the conformation required for catalysis. However, this indicates that 6PG and $NADP^+$ can bind independently from each other. Enzymatic analysis supported this consideration since Lineweaver-Burk plots of substrate/cofactor titrations intersected left of the ordinates. This points towards a sequential enzyme mechanism, meaning both substrate and cofactor have to bind before product formation can be initiated (Figure 29) (Haeussler *et al.*, 2018). This is in accordance with mechanistic characterizations of the 6PGDs of other species such as sheep (Price and Cook, 1996), *Trypanosoma brucei* (Hanau *et al.*, 1996), *Saccharomyces cerevisiae* (He *et al.*, 2007), and *Corynebacterium glutamicum* (Moritz *et al.*, 2000). In the case of a ping-pong mechanism, meaning that the product is released before all substrates are bound, parallel lines would have been expected in the Lineweaver-Burk plots (Bisswanger, 2017). The crystal structures in complex with either $NADP^+$ or 6PG suggest that *Pf*6PGD follows a random-order sequential mechanism which would be in accordance with the mechanism found for *T. brucei* (Hanau *et al.*, 1996).

Interestingly, amongst the numerous 6PGD crystal structures from different species, there is no structure with solely bound $NADP^+$, but there are structures in complex with the products NADPH and ribulose 5-phosphate (2IYP from *Lactococcus lactis* (Sundaramoorthy *et al.*, 2007)), with the product NADPH, chloride, and sulfate (2JKV from *Homo sapiens* (to be published)), or with NADPH and sulfate (1PGO from *Ovis aries* (Adams *et al.*, 1994)). Although the binding pocket is highly conserved, the conformation of the NADPH varies amongst the structures. Additionally, the cofactor binding domain adopts slightly different orientations in

all compared structures, while there are almost no differences seen for the substrate binding domain and the C-terminal tail, including the substrate binding site. The substrate 6PG is bound very similarly in all structures, independent of the presence of the cofactor (Haeussler *et al.*, 2018). These findings support our binding considerations.

Interaction between W265 and W104 is catalytically important

The strictly conserved W265 is in direct proximity to the active site loop and interacts with the non-conserved W104. This interaction links the cofactor binding domain with the substrate binding domain (Figure 23). It is therefore likely important for the communication between the two domains and for helping force $NADP^+$ into the catalytically relevant binding position. Site-directed mutagenesis of the *Plasmodium*-specific W104 was performed in order to investigate a potential impact on the mechanism; all kinetic parameters of *Pf*6PGD^{W104L}, especially the K_M value for 6PG, were decreased compared to the wt enzyme (Table 16), supporting the hypothesis that replacing the tryptophan side chain with leucine disturbs their linkage between domain 1 and domain 2 and therewith the catalysis (Haeussler *et al.*, 2018).

A second interaction specific for *Plasmodium* is a disulfide bridge between the cysteine residues 281 of the two subunits (Figure 23). This disulfide formation was prevented by creating the mutant *Pf*6PGD^{C281S}. Similar to *Pf*6PGD^{W104L}, the kinetic parameters of *Pf*6PGD^{C281S} were decreased compared to the wt (Table 16). Size exclusion chromatography showed that the disulfide bridge was not necessary for maintaining the dimeric conformation of the enzyme (Figure 27e); moreover, it is not in close proximity to the binding sites; therefore, the mechanistic reasons for the decreased kinetic parameters are so far unclear. The disulfide bridge was only visible in the apo-structure and the structure in complex with $NADP^+$, but not in complex with 6PG. Whether the interaction was missing due to mechanistic reasons or radiation damage was unclear (Haeussler *et al.*, 2018). Further experiments, e.g. further crystallization trials to detect potential changes in the overall structure need to be performed to elucidate the cause of the changed kinetic parameters in *Pf*6PGD^{C281S}.

5.4 Post-translational cysteine modifications

The importance of post-translational modifications of reactive cysteine residues in the regulation of different protein properties has gained more and more attention (Belcastro *et al.*, 2017; Jortzik *et al.*, 2012). Therefore, the effect of two important PTMs – *S*-glutathionylation and *S*-nitrosation – was studied on enzymes of the PPP of *P. falciparum* and *P. vivax*.

5.4.1 *S*-glutathionylation

S-glutathionylation has multiple functions in various metabolic pathways. It can regulate not only protein folding and stability but also the activity of enzymes; moreover, it serves as a storage form of reduced glutathione during episodes of oxidative stress, and prevents irreversible oxidation of proteins (Becker *et al.*, 2003; Dalle-Donne *et al.*, 2009). Currently, there is no information on *S*-glutathionylation of G6PDs or 6PGDs in the dbGSH database of cysteine *S*-glutathionylation (http://csb.cse.yzu.edu.tw/dbGSH/). In 2011, Jortzik *et al*. showed that *S*-glutathionylation does not regulate hG6PD activity, while it does inhibit *Pf*GluPho's G6PD activity. A large proteomic approach was performed to reveal targets of protein *S*-glutathionylation in *Plasmodium* parasites. However, neither *Pf*GluPho nor *Pf*6PGD could be detected to be part of the plasmodial glutathionylome (Kehr *et al.*, 2011). Together

with *Pv*G6PD, this could be confirmed within this thesis; neither *Pf*GluPho, *Pf*G6PD and *Pv*G6PD, nor *Pf*6PGD were prone to *S*-glutathionylation under the tested conditions. Incubation with very high GSSG concentrations led to precipitation of all four tested enzymes (Figure 31, Figure 33). Therefore, the previous hypothesis that the G6PD activity of *Pf*GluPho decreases after incubation with high GSSG concentrations (Jortzik *et al.*, 2011) is rather an artefact due to protein precipitation than specific redox-regulation. In this thesis, *S*-glutathionylated proteins were detected via Western blot analyses using an anti-glutathione antibody. In Jortzik *et al*., 2011, several cysteine residues of *Pf*GluPho were detected to be *S*-glutathionylated via MALDI-TOF-MS of samples incubated with 10 mM GSSG; however, this might be an artefact since this very high GSSG concentration leads to protein precipitation (Figure 31, Figure 33), potentially giving access to cysteine residues that are not accessible in native protein conformation.

The cytosol where the oxidative PPP of *Plasmodium* is located (Allen *et al.*, 2015) is highly reducing, with a redox potential of -314 mV (Kasozi *et al.*, 2013). The level of total glutathione in unstressed *Plasmodium* parasites is approximately 2 mM, almost all of it being present as GSH (Becker *et al.*, 2003); however, even 2 mM GSSG did not have a major impact on the G6PD activity in *P. falciparum* and *P. vivax* (Figure 32). This further supports the finding that *S*-glutathionylation most likely does not play a major role in the regulation of the oxidative PPP of *Plasmodium*. *S*-glutathionylation has been shown to inhibit several enzymes of glycolysis; glyceraldehyde 3-phosphate dehydrogenase (GAPDH) is most often considered to be inhibited in various organisms (Barinova *et al.*, 2017; Hildebrandt *et al.*, 2015; Kehr *et al.*, 2011; Zaffagnini *et al.*, 2013). Under oxidative stress, inhibition of glycolysis forces more glucose into the PPP in order to ensure sufficient NADPH production (Ralser *et al.*, 2007; Shenton and Grant, 2003). Since the PPP is the major source of NADPH for *Plasmodium* (1.2.3), it is reasonable that *S*-glutathionylation does not inhibit its enzymes under oxidative stress. To fully exclude *S*-glutathionylation, however, other possibilities for *S*-glutathionylation formation could be tested, e.g. interaction of oxidized proteins with GSH (chapter 1.3.1)

5.4.2 *S*-nitrosation

Protein *S*-nitrosation mediates both physiological and pathophysiological effects of NO, influencing protein conformation, stability, activity, protein-protein interactions, and cellular signal transduction processes (Belcastro *et al.*, 2017; Hess *et al.*, 2005; Jortzik *et al.*, 2012). During their complex life cycle, malaria parasites have to deal with NO from different sources (Ferrari *et al.*, 2011; Jeney *et al.*, 2014; Peterson *et al.*, 2007b). A large-scale proteomic analysis identified 319 potential targets for *S*-nitrosation in *P. falciparum*, many of them located in glycolysis. Interestingly, also *Pf*GluPho and *Pf*6PGD were identified as targets of *S*-nitrosation (Wang *et al.*, 2014). This could be confirmed within this thesis together with *Pf*G6PD and *Pv*G6PD (Figure 35, Figure 36).

<u>GSNO as a nitrosative agent</u>

Within this thesis, *S*-nitrosation was studied by incubating reduced enzymes with the naturally occurring *S*-nitrosoglutathione (GSNO), followed by indirect detection of the modification using the biotin-switch assay (Broniowska *et al.*, 2013; Forrester *et al.*, 2009a). Reactions between reduced glutathione and nitrous acid can synthesize GSNO, which is able to transfer its nitroso group to thiols of other proteins, resulting in *S*-nitrosation. However, GSNO is also able to react with thiols by forming a disulfide bridge, resulting in *S*-glutathionylation instead

of *S*-nitrosation (Broniowska *et al.*, 2013). The indirect detection using the biotin-switch assay is based on replacement of the actual modification by biotin. It has been stated before that ascorbate, used to transform SNOs to free thiols, does not reduce *S*-glutathionylated cysteines (Forrester *et al.*, 2009a). Therefore, *S*-glutathionylation caused by GSNO should in theory not result in a signal using the biotin-switch assay. Moreover, none of the enzymes tested within this thesis were prone to *S*-glutathionylation upon incubation with GSSG (see results in chapter 4.4.1), therefore it is unlikely that GSNO causes *S*-glutathionylation in these enzymes. To fully exclude false negative detection of *S*-nitrosation, experiments could be repeated using *S*-nitrosocysteine instead of GSNO as a nitrosation agent (Grossi and Montevecchi, 2002; Peterson *et al.*, 2007a). Alternatively, potential *S*-glutathionylation of the enzymes by GSNO could be excluded by Western blot analysis using an anti-glutathione antibody.

S-nitrosation of G6PD

So far, *S*-nitrosation of G6PDs in other organisms has not been extensively studied; to our knowledge, there is no information in the literature about *S*-nitrosation in *Homo sapiens* and *Plasmodium* (dbSNO, database of cysteine *S*-nitrosation, http://dbSNO.mbc.nctu.edu.tw). In a proteomic approach performed in *E. coli* (K12), G6PD cysteine residue 10 was identified to be *S*-nitrosated; however, the impact of the modification has not been studied (Forrester *et al.*, 2009b). The C10 found in *E. coli* G6PD is not conserved; however, there are cysteines in close proximity (C315 and C323 of full-length *Pv*GluPho, C346 of *Pf*GluPho) which might be targeted by *S*-nitrosation. In Western blot and kinetic analyses, *Pf*GluPho, *Pf*G6PD, and *Pv*G6PD showed the same results (Figure 35). Therefore, it can be concluded that at least some of the *S*-nitrosation sites of *Pf*GluPho are located in its N-terminal G6PD part.

S-nitrosation of 6PGD

Within this thesis, *Pf*6PGD was found to be reversibly inhibited upon *S*-nitrosation. To test the reversibility, 5 mM DTT was added to the modified enzyme. Under physiological conditions, *Pf*Trx1 – the major cytosolic Trx – might be able to denitrosate *Pf*6PGD (Wang *et al.*, 2014). This needs to be verified.

For 6PGD of other species, *S*-nitrosation has been identified in metabolomic/proteomic studies on mice (Bruegger *et al.*, 2018; Kohr *et al.*, 2011; Qu *et al.*, 2014), and interestingly on recombinant h6PGD. Similar to the findings in this thesis, GSNO downregulated h6PGD activity with an IC_{50} of 556 µM. Using site-directed mutagenesis, cysteine residues 30, 113, 170, 171, 199, 289, 366, 402, and 422 were tested for their susceptibility to *S*-nitrosation (Bruegger *et al.*, 2018). Of these nine residues, only two (170 and 366) are present in *Pf*6PGD. The authors suggest that *S*-nitrosation of C366 is responsible for the inhibition of h6PGD upon GSNO treatment. The residue C366 is located between the two subunits of the dimer and is within hydrogen-bonding distance of the hydroxyl side chains of S129 and S140 (3.3 and 3.6 Å, respectively, Figure 57a). The interaction between the cysteine and the two serines might be important for the structural orientation and rigidity of the subunits. *S*-nitrosation of C366 might disturb this interaction, leading to changes in structural orientations and thereby changes in activity (Bruegger *et al.*, 2018). However, in *P. falciparum*, the distances between C366 and S128 as well as between C366 and S139 seen in our *Pf*6PGD structures are longer: 5.1 and 4.9 Å, respectively (Figure 57b). Movement of the cysteine side chain would shorten the distances to 3.5 Å to S128 and 2.8 Å to S139, which would then in theory enable hydrogen bonding. However, even in case the cysteine side chain moves, the angles between the side chains would still not be favorable to form hydrogen bonds, additional movement of the serine

side chains would be necessary. The orientation of the side chains shown in Figure 57b has been observed in all three *Pf*6PGD structures (apo, in complex with $NADP^+$, in complex with 6PG); movement of all three side chains is possible, however unlikely. A disturbed interaction between the cysteine and the serines most likely does not explain the decreased activity upon *S*-nitrosation in *Pf*6PGD. One hypothesis is that *S*-nitrosation of C366, which is in close proximity to the 6PG binding site, might slightly change the overall conformation of the binding pocket and thereby prevent binding of 6PG. This hypothesis needs to be tested, e.g., by using site-directed mutagenesis or crystallization of *S*-nitrosated protein. Moreover, it has to be considered that *Pf*6PGD has nine cysteine residues that are not conserved in h6PGD and might play a role in the regulation.

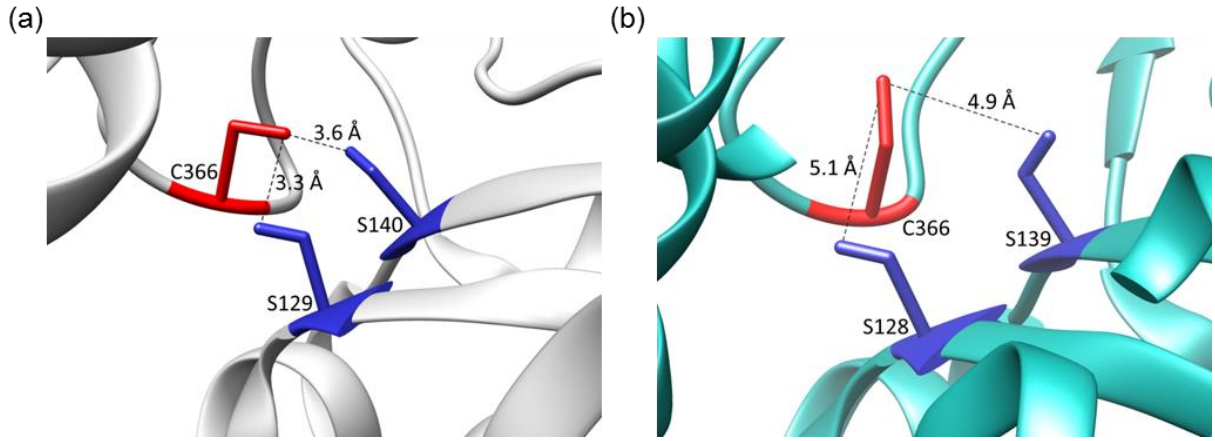

Figure 57. Potential hydrogen bonds of C366 in h6PGD and apo-*Pf*6PGD
(a) In h6PGD (4GWK (Hitosugi *et al.*, 2012)), hydrogen bonds between C366 and S129 or S140 are possible due to the short distances of 3.3 and 3.6 Å, respectively (Bruegger *et al.*, 2018). (b) In apo-*Pf*6PGD (6FQX), the distances between C366 and S128 as well as C366 and S139 are relatively long: 5.1 and 4.9 Å, respectively. Therefore, the formation of hydrogen bonds is unlikely. Cysteine 366 is colored in red, the two serines 129/128 and 140/139 in blue. The distances are indicated with the dashed lines.

Potential explanations for *S*-nitrosation of the PPP in *Plasmodium* parasites

Wang *et al.*, 2014 hypothesized that under nitrosative stress, the inactivation of *Pf*GAPDH via *S*-nitrosation serves as a signaling event that redirects the carbohydrate flux to the PPP. The antioxidative systems of *P. falciparum* can then use NADPH generated in the PPP (see 1.2.3); e.g. the plasmodial thioredoxin system uses NADPH to recover *Pf*GAPDH via denitrosation (Wang *et al.*, 2014). To fight against oxidative stress, it would make sense if the activity of the NADPH-producing PPP would increase or at least remain at the same level. For *Pf*GluPho – shown to be essential for the survival of the parasites, even under physiological conditions (Allen *et al.*, 2015) – downregulation of the activity upon *S*-nitrosation was indeed very moderate (Figure 35b). This is in accordance with the finding from Shenton and Grant, 2003 that oxidative stress does not affect G6PD and 6PGD activities in *Saccharomyces cerevisiae*. However, in this thesis *Pf*6PGD was found to be reversibly downregulated by up to 65%. It might happen that this partial inhibition of *Pf*6PGD leads to the accumulation of substrate, leading to product inhibition of *Pf*GluPho (Jortzik *et al.*, 2011). Moreover, it has been shown for *T. brucei* that high concentrations of 6PG are toxic most likely due to inhibition of phosphoglucose isomerase (Hanau *et al.*, 2004). Therefore, restriction of NADPH production via the PPP upon *S*-nitrosation might lead to severely pathophysiological conditions for the parasite. However, since *Pf*6PGD is not completely inhibited upon *S*-nitrosation, the remaining

activity might be high enough to maintain the flux through the PPP and thereby NADPH production, especially because 65% inhibition is only reached under very high GSNO concentrations. In this case, *S*-nitrosation of the enzymes from the PPP might be used to protect them from irreversible nitrosative damage (Belcastro *et al.*, 2017).

In addition to the downregulation of enzyme activity for signaling purposes by the parasites themselves, the host's immune system might increase the nitrosative stress followed by enzymatic downregulation in order to fight the infection. It has been shown that the production of NO increases upon infection with *Plasmodium* and is involved in the fight against malaria (Akman-Anderson *et al.*, 2007; Jaramillo *et al.*, 2003; Jeney *et al.*, 2014; Ong *et al.*, 2013; Ranjan *et al.*, 2016). In a proteomic approach, glycolytic enzymes of *P. falciparum* were found to be extensively *S*-nitrosated, followed by downregulation of activity – shown, e.g., for *Pf*GAPDH (Wang *et al.*, 2014). The central role of glycolysis in *Plasmodium* parasites is underscored by the finding that there is up to a 100-fold increase in glucose uptake and consumption in parasitized RBCs compared to healthy cells (Roth, 1990). Since inhibition of glycolysis was shown to deteriorate the growth of the parasites (Davis *et al.*, 2016; van Niekerk *et al.*, 2016; van Schalkwyk *et al.*, 2008), *S*-nitrosation and subsequent inactivation of these important enzymes might be part of the antiparasitic defense. As stated above, it has been shown that glycolysis inactivation redirects the carbohydrate flux to the PPP in order to counteract oxidative stress (Ralser *et al.*, 2007; Shenton and Grant, 2003). However, since especially *Pf*6PGD was found to be also *S*-nitrosated, the host's defense might cause this *S*-nitrosation and inhibition of *Pf*6PGD in order to disturb the NADPH supply of the parasites. In addition, there is evidence that the formation of nitroso bonds is not the end-effector mechanism of *S*-nitrosation, but an intermediate state that reacts with thiols to intra- and intermolecular disulfide bonds (Wolhuter and Eaton, 2017). Further research is necessary to find the reason for the downregulation of both – glycolysis and the PPP under nitrosative stress.

5.5 Inhibition of the PPP as a mode of action in new antimalarial drugs

Currently, the WHO recommends ACTs for the treatment of malaria (WHO, 2017b); however, their high failure rates endanger an effective malaria treatment (Ashley *et al.*, 2018; WHO, 2017b). To ensure successful treatment in the future, there is an urgent need for the development of new antimalarial drugs.

A promising mechanism of action of new antimalarial drugs is to disturb the redox homeostasis of *Plasmodium* parasites in order to create a fatal dosage of oxidative stress (Schirmer *et al.*, 1987). There are in principle three ways to reach this situation: (I) application of oxidative drugs that target, e.g., essential parasite components; (II) application of redox-cycling drugs (see discussion for methylene blue below); and (III) inhibition of redox-active enzymes such as NADPH-producing enzymes that ensure the functionality of the antioxidative thioredoxin and glutathione systems (Nepveu and Turrini, 2013). Since the PPP is the major source of NADPH in *Plasmodium* (Preuss *et al.*, 2012b), it is considered a promising target for new antimalarial drugs (Allen *et al.*, 2015; Haeussler *et al.*, 2018); one aim of this thesis was therefore to characterize the effect of potential inhibitors on the important NADPH-producing enzymes *Pf*GluPho, *Pf*6PGD, and *Pv*G6PD.

5.5.1 *Pf*GluPho and *Pv*G6PD as drug targets

Attempted double crossover disruption of the *Pf*GluPho gene showed that this enzyme is essential for the growth of blood stages parasites, validating it as a promising drug target (Allen *et al.*, 2015). So far, it has not been possible to prove the essentiality of *Pv*GluPho, most importantly due to the difficulties in maintaining *P. vivax* in cell culture (Thomson-Luque *et al.*, 2017). However, since *Pf*GluPho and *Pv*GluPho share important features (bifunctional enzyme, central role in the metabolism, similar kinetic behavior of *Pf*GluPho and *Pv*G6PD in response to PTMs and inhibition), it can be assumed that *Pv*GluPho also serves as a potential drug target. The effect of several compounds on *Pf*GluPho and *Pv*G6PD were characterized within this thesis.

5.5.1.1 Structure-based drug design for *Pf*GluPho

Structure-based drug design has already been proved to be a very useful tool in any stage of drug development, including lead identification and lead optimization, but also in the prediction of the pharmacochemical behavior in absorption, distribution, metabolism, excretion, and toxicity (Blundell, 2017; Chen *et al.*, 2012). Although there are already potent, highly selective inhibitors for *Pf*GluPho available (see chapter 4.5.3 and discussion below), it is still necessary to solve the three-dimensional structure, best in the native form and in complex with an inhibitor. Using this approach, the mechanism of inhibition can be fully understood.

Crystallization of *Pf*GluPho and *Pf*G6PD

Despite numerous crystallization trials and several obtained crystals, it has not yet been possible to solve the three-dimensional structure of *Pf*GluPho due to limited size, stability, or diffraction quality of the crystals. In contrast, the structures of G6PDs from several other species have been solved, including *H. sapiens* (5UKW (Ranzani and Cordeiro, 2017), 2BH9, 2BHL (Kotaka *et al.*, 2005), 1QKI (Au *et al.*, 2000)) and *T. cruzi* (6D23, 6D24, 4LSM (to be published), 5AQ1 (Mercaldi *et al.*, 2016)). Interestingly, the structure of *Pv*6PGL has also been solved (3E15 (to be published)). One rational approach of protein crystallization is to initially use the conditions of already known structures of proteins with high sequence similarities (Lu *et al.*, 2012); however, due to the fusion to the bifunctional enzyme, this is not easily applicable to *Pf*GluPho.

So far, crystallization trials have been performed using the vapor diffusion technique as a sitting and hanging drop approach. Besides native *Pf*GluPho/*Pf*G6PD, cocrystallization in complex with inhibitor, substrate, or cofactor has been tested; however, it has not yet been possible to solve the three-dimensional structure of *Pf*GluPho. The following chapter describes several alternative strategies to achieve protein crystallization. (I) Spontaneous formation of protein crystals in living cells has been reported unexpectedly often. Due to continuous improvement of lasers, these small, so-called *in cellulo* grown crystals can nowadays be used to solve the three-dimensional structures of the proteins. There are several physiological reasons for protein crystallization in living cells to appear such as storage, protection and stabilization of cells and proteins, or solid state catalysis (Schönherr *et al.*, 2018). In addition, *in cellulo* crystallization has also been observed for recombinant protein during gene expression in, e.g., plant cells (Stöger *et al.*, 2001), mammalian cells (Baskaran *et al.*, 2015; Hasegawa *et al.*, 2011; Tsutsui *et al.*, 2015), and – most interestingly for this thesis – *E. coli* cells (Oeda *et al.*, 1989). The reason for crystallization during heterologous expression is most

likely the locally high protein concentration that is triggering crystal nucleation. However, further investigations and improvements of this method are required until *in cellulo* crystallization can be used routinely (Schönherr *et al.*, 2018). (II) One more commonly used approach is seeding of crystal fragments into metastable systems. The idea behind this is that conditions enabling nucleation might not be ideal conditions for crystal growth (see Figure 7). Seeding can therefore be used to separate nucleation and growth by introducing previously produced, pulverized crystals into new drops with lower supersaturated levels. It has been shown that this technique can improve the quality of the crystals obtained in the new drop (Bergfors, 2003; Ireton and Stoddard, 2004). (III) As described in 3.4.3, the use of additives such as substrates or inhibitors can improve crystal formation. The tellurium-centered Anderson-Evans polyoxotungstate $[TeW_6O_{24}]^{6-}$ (TEW) has recently been shown to act as an additive that is able to initiate and improve crystallization of several proteins (Bijelic *et al.*, 2015; Mac Sweeney *et al.*, 2018; Molitor *et al.*, 2017). The high negative charge of TEW leads to an interaction with positively charged regions of the protein; in addition, the large size of TEW leads to a distribution of the negative charge over a large area of the protein. This enables TEW to electrostatically interact with many amino acid residues, increasing the probability and strength of TEW-protein interactions. Using this electrostatic cross-linking of protein monomers, TEW is able to initiate and stabilize crystal contacts, thereby facilitating the formation of the crystal lattice (Bijelic and Rompel, 2017). The benefit of TEW for the crystallization of *Pf*GluPho is currently tested in the working group of Prof. Becker. (VI) Besides crystallization trials using wt enzymes, it is a common approach to crystallize mutant proteins that are supposed to be, e.g., more rigid than the wt enzyme. The choice which mutants are reasonable to be used can be based on knowledge of the enzyme mechanism, or on mutants that were successfully used to solve the structure of homologous enzymes. As an example, crystallization of the mutant *Pf*GluPho^{D577N} has been tested based on findings for G6PD from *Leuconostoc mesenteroides* (*Lm*G6PD). In *Lm*G6PD, H240 (corresponding H641 in *Pf*GluPho) most likely accepts protons from G6P, while the carboxylate group of D177 (corresponding D577 in *Pf*GluPho) stabilizes the positive charge that is generated on H240 in the transition state (Cosgrove *et al.*, 1998). Use of the mutant *Lm*G6PD^{D177N} enabled the crystallization of the enzyme in complex with both G6D and NADPH; comparison to the structure of the wt enzyme revealed that the overall structure was not changed in *Lm*G6PD^{D177N} (Cosgrove *et al.*, 2000). Therefore, this approach was tested for the plasmodial enzyme using the mutant *Pf*GluPho^{D577N}; however, in contrast to *Leuconostoc mesenteroides*, it did unfortunately not result in crystals that were suitable for X-ray diffraction analysis. One currently promising looking trial performed in the working group of Prof. Becker uses a modified version of *Pf*G6PD. For the crystallization of *T. cruzi* G6PD, a C-terminally truncated version of the enzyme has been successfully used; the C-terminal end is expected to be flexible, deteriorating the crystal quality (Mercaldi *et al.*, 2016). According to this approach, *Pf*G6PD has been truncated by the C-terminal 27 amino acid residues. Moreover, a Rossmann-like domain starts at amino acid P62 in *T. cruzi* G6PD (Mercaldi *et al.*, 2016), corresponding L333 in *Pf*GluPho. Recombinant *Pf*G6PD used so far started at residue 339 of full-length *Pf*GluPho (Jortzik *et al.*, 2011), potentially interrupting one β-sheet and therewith impair the crystal growth and quality. Accordingly, recombinant *Pf*G6PD was prolonged at the N-terminus by the sequence SLNKEELL ensuring that the potential β-sheet is complete. First crystallization trials using this modified *Pf*G6PD resulted in crystals that are currently subjected to optimization processes. (V) In case these approaches are not successful, nuclear magnetic resonance (NMR) spectroscopy and electron microscopy – methods that are not based on crystal formation of

the protein – can be used to solve the three-dimensional protein structure (Thonghin *et al.*, 2018; Wüthrich, 1989).

Homology model of *Pf*G6PD

Since there is no crystal structure available yet, a homology model of C-terminal *Pf*G6PD has been built by Alencar *et al*., 2018. Comparison of the amino acid sequences of *Pf*G6PD with the sequences of G6PDs from *H. sapiens*, *T. cruzi*, *Mycobacterium avium*, and *Leuconostoc mesenteroides* showed that the residues involved in substrate binding are highly conserved with one exception: the negatively charged D750 in *Pf*G6PD replaces the positively charged R365 in hG6PD. According to the authors, this change in size of the side chain and charge can be used to develop substrate analog-based inhibitors that selectively inhibit *Pf*G6PD. The hypothesis was that replacing the negatively charged phosphate group of G6P with a short side chain ending with a basic functional group that can be protonated at physiological pH could implement the development of a selective inhibitor. The positive charge of the protonated group is supposed to disturb the interaction of the compound with R365 in hG6PD, while it enables an ionic interaction with D750 in *Pf*G6PD and thereby a selective inhibition of the plasmodial enzyme. To test this hypothesis, the authors designed and tested a series of G6P analogs (Alencar *et al.*, 2018). The hypothesis that the replacement of R365 (*H. sapiens*) with D750 (*P. falciparum*) alone is responsible for the selective inhibition has two weaknesses: (I) According to Alencar *et al*., 2018, adding a short side chain containing a basic, protonatable end to G6P should lead to a specific interaction with D750 in *Pf*G6PD. Furthermore, they suggest that amino derivatives have a higher selectivity for the plasmodial enzyme than guanidino derivatives. Four of their nine tested compounds contained a terminal amino group; two of them in fact had a higher affinity for the plasmodial enzyme, while one unexpectedly had a higher affinity for hG6PD. The fourth compound containing an amino group had approximately the same affinity for the two enzymes. (II) The authors stated that in *H. sapiens*, binding the negative charge of G6P is assisted by positively charged residues like R365 which is replaced in *P. falciparum* with the negatively charged D750. One consequence of this would be that binding G6P should be easier in *H. sapiens* than in *P. falciparum*. In contrast, however, the K_M value for G6P of *P. falciparum* is lower than the K_M value of *H. sapiens* (*Pf*G6PD: 11-27 µM (Alencar *et al*., 2018; Jortzik *et al*., 2011); hG6PD: 52-72 µM (Alencar *et al*., 2018), 116 µM (Jortzik *et al*., 2011)). This indicates that there are most likely other amino acid residues that also play a role in selectively binding the compounds and that the important R365 → D750 replacement alone might not be suitable for the development of a selective inhibitor. Site-directed mutagenesis creating the mutants hG6PD^{R365D} and *Pf*GluPho^{D750R} could be used to further investigate the role of the amino acid replacement for selective binding of compounds.

5.5.1.2 Inhibitors of *Pf*GluPho and *Pv*G6PD

Ellagic acid

EA is a polyphenol that can be found in different fruits and vegetables; it was identified to be an active component in plants used in traditional West African medicine for the treatment of malaria (Soh *et al.*, 2009; Verotta *et al.*, 2001). The growth inhibition of *Plasmodium* parasites *in vitro* ranges between 105 nM and 1.3 µM dependent on the strain. Interestingly, EA also inhibits chloroquine-resistant *Plasmodium* strains (Soh *et al.*, 2009; Sturm *et al.*, 2009; Verotta *et al.*, 2001). In combination with commonly used antimalarial drugs, EA is able to potentiate the *in vitro* antiplasmodial activity of the commonly used drugs chloroquine, atovaquone,

mefloquine, and artesunate; however, it acts slightly antagonistically with artemisinin. In addition to the growth inhibition *in vitro*, EA was shown to be active *in vivo* in mice infected with *P. vinckei petteri*; intraperitoneal application of 1 $mg \cdot kg^{-1}$ per day had curative antiplasmodial activity, 10 $mg \cdot kg^{-1}$ per day prophylactic activity. Simultaneously, there was no toxicity observed in the mice. The main targets of EA seem to be the most metabolically active stages: trophozoites and early schizonts (Soh *et al.*, 2009).

The actual mechanism of action of EA has been discussed in several studies. EA, as well as its derivatives CEA and FEA, are known to inhibit various enzymes. Examples are plasmodial GR, G*S*T, and TrxR; however, the IC_{50} values for these enzymes, 7-74 µM, were moderate (Sturm *et al.*, 2009). In accordance with the inhibition of GR, EA is supposed to decrease the glutathione content inside the parasites. In the murine model *P. yoelii*, a strain overproducing GSH, the effect of EA is five times lower than the effect on wt parasites (Njomnang Soh *et al.*, 2012). As stated above, EA is supposed to mainly affect the trophozoites and early schizonts, stages with maximal hemoglobin digestion (Soh *et al.*, 2009; Sturm *et al.*, 2009). As described in 1.2.3, this digestion leads to the release of high amounts of free heme, which needs to be detoxified into hemozoin (Egan *et al.*, 2002; Francis *et al.*, 1997). It has been shown that GSH is able to degrade heme (Atamna and Ginsburg, 1995); however, since EA reduces the GSH pool (Njomnang Soh *et al.*, 2012), this detoxification path is limited under EA. Moreover, EA and its derivatives form soluble complexes with free heme, thereby blocking the hemozoin formation (Sturm *et al.*, 2009). Treatment with EA therefore results in increased oxidative stress due to insufficient detoxification of heme.

In summary, the observations have so far indicated that EA exerts its antiplasmodial effect via a rather broad mechanism of action, thereby affecting the antioxidant balance of the parasites. Interestingly, it was recently shown that EA inhibits *Pf*GluPho with an IC_{50} of 77 ± 22 nM (Allen *et al.*, 2015); e.g., compared to the IC_{50} values on GR, G*S*T, and TrxR stated above (Sturm *et al.*, 2009), the inhibition of *Pf*GluPho is three orders of magnitude higher. This *Pf*GluPho inhibition is likely associated with the GSH depletion due to a lack of NADPH and less efficient glutathione reduction (Allen *et al.*, 2015). Similarly, EA and its derivatives were shown to inhibit *Pv*G6PD in the low nanomolar range; the mixed-type inhibition with respect to both G6P and $NADP^+$, observed for *Pf*GluPho (Allen *et al.*, 2015), was confirmed for *Pv*G6PD. This supports the assumption that *Pf*GluPho and *Pv*GluPho/*Pv*G6PD may structurally be very similar. The inhibition of EA is not selective for plasmodial enzymes; with an IC_{50} of 102 ± 39 nM, it inhibits hG6PD in the same range. Using *in silico* modelling it has been proposed that the region where EA presumably binds is highly conserved between hG6PD and *Pf*GluPho and does not overlap with the substrate/cofactor binding sites. This explains the mixed-type inhibition with similar IC_{50} values in human and plasmodial enzymes (Allen *et al.*, 2015). However, since the overall toxicity in mice is still low and there are no observable hemolytic effects (Soh *et al.*, 2009), the rapidly growing and multiplying parasites might be more susceptible to disturbance of the redox metabolism than human cells.

<u>Novel series of G6PD inhibitors</u>

Based on a compound library screening and subsequent analysis of the structure-activity relationship, a set of new potential G6PD inhibitors has been designed (Figure 51). Although the solubility and stability of several compounds were limited, the approach resulted in two novel compounds with activity against both *Pf*GluPho and *Pv*G6PD in the very low micromolar range. In contrast to the other inhibitors reported in this thesis, compound **4** (vz1732) was

shown to act as a non-competitive inhibitor against both G6P and $NADP^+$. The most promising compounds will be further characterized, e.g., by determining their activity in *P. falciparum* cell culture.

ML304

To identify inhibitors of *Pf*GluPho, a high-throughput screening of various compound libraries, including LOPAC, Spectrum, DIVERSet, and the Molecular Libraries Small Molecule Repository (MLSMR) collection of the NIH, was performed (Preuss *et al.*, 2012a). Within this screening, two compounds of the MLSMR collection could be identified as potent inhibitors of the G6PD reaction of *Pf*GluPho, namely ML276 and ML304. With an IC_{50} of 0.89 µM against *Pf*GluPho and no observable inhibition of hG6PD at 80 µM, ML276 is highly specific for the plasmodial enzyme (Preuss *et al.*, 2012c). As described above (chapter 5.5.1.1), Alencar *et al*., 2018 hypothesized that selective binding of a compound to the plasmodial enzyme might be feasible through the replacement of the negatively charged D750 in *Pf*GluPho with the positively charged R365 in hG6PD. To confirm this hypothesis, they simulated the binding of ML276 to their *Pf*G6PD model. As shown in Figure 58, this simulation in fact showed that the carboxylate group of D750 forms stable hydrogen bonds with the protonated amine and the amide NH groups of ML276. The fluorobenzene ring of ML276 was bound in a hydrophobic pocket that is shaped by V585 and L778 (Alencar *et al.*, 2018). V585 is conserved (corresponding V208 in hG6PD), while the plasmodial leucine L778 is replaced by the similar but shorter amino acid valine V394 in hG6PD. This replacement of a compound binding amino acid supports the hypothesis that D750 alone might not be responsible for the selectivity; most likely, additional amino acid residues of the substrate binding cavity involved in binding ML276 differ between *H. sapiens* and *P. falciparum*, leading to a selective inhibition of the plasmodial enzyme.

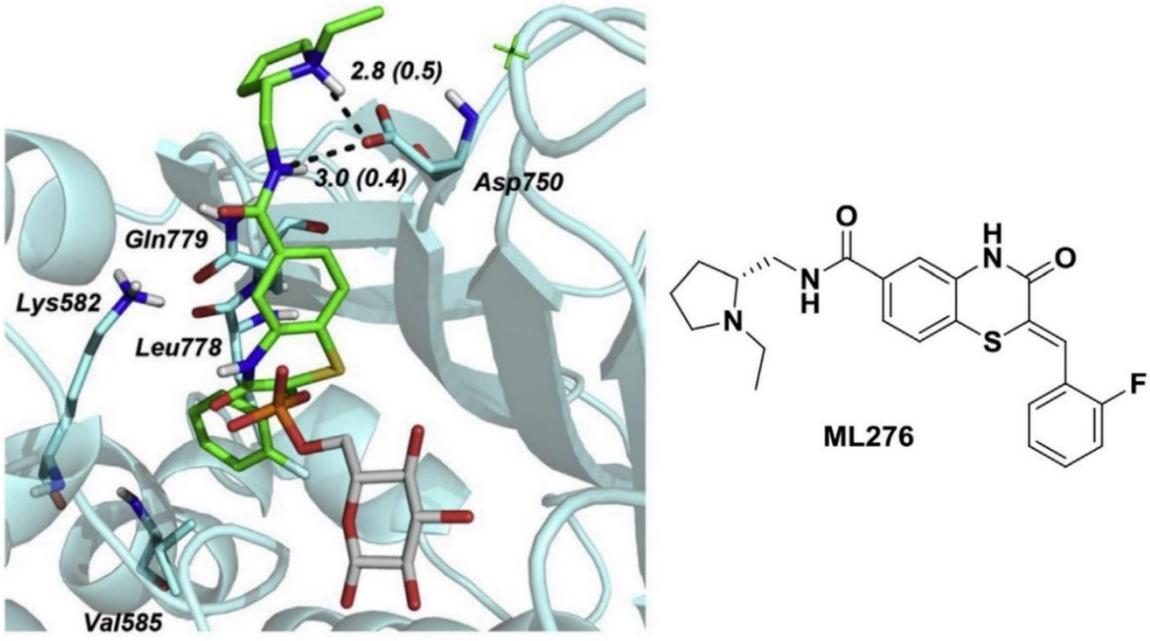

Figure 58. Putative binding mode of ML276 to *Pf*G6PD

Shown is a superposition of the *Pf*G6PD/ML276 complex from Alencar *et al*., 2018 and the X-ray structure of hG6PD in complex with G6P (2BHL (Kotaka *et al.*, 2005)). The protein backbone is colored in light blue, selected amino acid residues are shown as blue sticks. ML276 and G6P are shown as sticks with the carbon atoms in green and gray, respectively. Asp: aspartic acid; Gln: glutamine; Lys: lysine; Leu: leucine; Val: valine. The figure was taken and modified from Alencar *et al*., 2018.

ML304 as the second hit of the high-throughput screening had an IC_{50} for *Pf*GluPho of 190 nM, which was even more potent and was also highly selective for the plasmodial enzyme, with no observable inhibition of hG6PD at 80 µM. The pharmacokinetic characteristics of this promising compound are described in an NIH probe report. ML304 acts on *P. falciparum* 3D7, a chloroquine sensitive strain, at concentrations below 1 µM; on the chloroquine resistant strain Dd2, it is still active at concentrations lower than 5 µM. Interestingly, there was no cytotoxicity against human hepatocytic cells observable; the lethal dose killing 50% of the cells was above 50 µM. To further evaluate the suitability of the compound as a potential antimalarial drug component, an *in vitro* pharmacology screen was used. ML304 was found to have a high passive, transcellular permeability and to be able to cross the blood-brain-barrier. Since *Plasmodium* belongs to the blood-borne parasites, high plasma concentrations of a compound increase the exposure of newly arising parasites. ML304 has been shown to bind efficiently to plasma proteins; therefore, it remains in the plasma and is hardly distributed to other organs or tissues. Even exposure to proteinases and esterases does not significantly change the plasma concentration. In summary, ML304 seems to be stable in the plasma, resulting in a high exposure of the parasites. However, a microsomal stability assay showed that ML304 is completely metabolized in human and mouse liver homogenates within one hour (Maloney *et al.*, 2012).

Within this thesis, ML304 was shown to inhibit *Pv*G6PD in addition to *Pf*GluPho with an IC_{50} in the low micromolar range. Mechanistic studies indicated that it acts as a competitive inhibitor towards G6P in both *Pf*GluPho and *Pv*G6PD; this supports the hypothesis – as discussed above for EA – that the *P. falciparum* and *P. vivax* enzymes are structurally similar. Dr. Mahsa Rahbari investigated within her dissertation the effects of ML304 on the cytosolic glutathione metabolism of *Plasmodium* parasites. There, she used the genetically encoded glutathione redox sensor "human glutaredoxin 1-reduction-oxidation sensitive green fluorescent protein 2" (hGrx1-roGFP2), episomally transfected in *P. falciparum* 3D7 parasites, and stably transfected in NF54-*attB* parasites (Rahbari, 2017). In this sensor, hGrx1 catalyzes the thiol-disulfide exchange between glutathione and roGFP; therewith it is possible to detect alterations in the glutathione redox potential, corresponding to changes in GSSG in the nanomolar range (Gutscher *et al.*, 2008). ML304 was shown to significantly disturb the cytosolic glutathione redox potential of the parasites in a time and concentration-dependent manner (Rahbari, 2017). Moreover, the effects of ML304 on hydrogen peroxide dynamics were determined using the H_2O_2 redox probe roGFP2-Orp1, stably integrated in NF54-*attB* parasites (Rahbari *et al.*, 2017). This sensor is able to detect micromolar H_2O_2 concentrations (Gutscher *et al.*, 2009). It turned out that ML304 significantly increases the cytosolic H_2O_2 levels of the parasites (Rahbari *et al.*, 2017). In addition to the effect on asexual blood stage parasites, ML304 has been shown to have tremendous synergistic effects with methylene blue (MB) on late stage gametocytes, while it was not active alone on gametocytes at a concentration of 20 µM. Interestingly, ML304 was also not able to potentiate the effect of MB when it was only added prior to the addition of MB; simultaneous application of the drugs was necessary (Siciliano *et al.*, 2017). Amongst other effects, MB has been shown to inhibit plasmodial GR, leading to a depletion of GSH (Buchholz *et al.*, 2008; Schirmer *et al.*, 2003). Importantly, MB acts not only as an inhibitor, but also as a so-called redox-cycling substrate of *P. falciparum* reductases; disulfide reductases such as GR and TrxR reduce MB under the consumption of NADPH. The resulting leucoMB is re-oxidized by O_2, followed by another reduction. Each reaction cycle leads to the consumption of NADPH and O_2, accompanied by

the generation of reactive oxygen species (Buchholz *et al.*, 2008). The depletion of NADPH due to MB and the simultaneous prevention of the generation of new NADPH due to inhibition of *Pf*GluPho by ML304 have deleterious effects on the gametocytes (Siciliano *et al.*, 2017). Therefore, this drug combination has a transmission-blocking potential.

In summary, ML304 is able to significantly disturb the overall redox homeostasis of *Plasmodium* parasites via depletion of the important electron donor NADPH. This promising compound is currently followed up as described in the chapter below.

The ML304 derivative SBI-0797750

ML304 had IC_{50} values of 190 nM and 2.6 µM on *Pf*GluPho and *Pv*G6PD, respectively. To further increase the efficiency of the compound, analyses of the structure-activity relationship were performed at the Sanford Burnham Prebys Medical Discovery Institute in La Jolla, CA, USA, followed by synthesis of various derivatives. The most promising compound was SBI-0797750, which was besides the work performed within this thesis characterized by the working group of Prof. Becker and several cooperation partners in yet unpublished experiments. The compound inhibits *Pf*GluPho and *Pv*G6PD with IC_{50} values of 6.7 ± 1.8 and 31.0 ± 3.1 nM, respectively. At the highest tested concentration of 99 µM, inhibition of hG6PD was below 50% (chapter 4.5.3.2); SBI-0797750 is therefore at least 3,200-14,800-fold more effective on the plasmodial enzymes than on the human homolog. Good selectivity of a compound is described as a minimal difference in effect of 10-100, depending on the biological system (Roy, 2018). Therefore, SBI-0797750 is highly selective for the plasmodial enzyme, reducing the risk of adverse side effects when used as an antimalarial drug. Similar to ML304, SBI-0797750 was found to act as a competitive inhibitor with respect to G6P (chapters 4.5.2 and 4.5.3.3), meaning that the compound competes with G6P for the binding site (Bisswanger, 2017). The inhibition of *Pf*GluPho by SBI-0797750 is completely reversible (chapter 4.5.3.4); this competitive, reversible inhibition means that high accumulation of G6P – caused by the inhibition of the G6PD reaction – can potentially displace the inhibitor from the binding site and stop the inhibition. This might be a pitfall when the compound is used in living organisms. It has been shown that oxidative and nitrosative stress situations can lead to the downregulation of the activity of glycolytic enzymes, redirecting the glucose flux towards the PPP to ensure a sufficient production of NADPH (Mullarky and Cantley, 2015; Ralser *et al.*, 2007; Wang *et al.*, 2014). In this case, an inhibition of *Pf*GluPho might lead to an accumulation of high G6P concentrations. However, this seems at least in cell culture not to be problematic since besides inhibition of recombinantly produced *Pf*GluPho and *Pv*G6PD, SBI-0797750 has a growth inhibitory effect on *P. falciparum* parasites; on chloroquine-sensitive *P. falciparum* 3D7 parasites, the compound showed an IC_{50} of 22.5 ± 2.2 nM, and growth of *P. falciparum* NF54-*attB* parasites was inhibited with an IC_{50} of 83.8 ± 17.3 nM (chapter 4.5.3.5). In addition to the effect on asexual blood stage parasites, SBI-0797750 inhibits the gametocyte formation of *P. falciparum* NF54 parasites with an IC_{50} of 74 ± 22 nM, indicating that it might also be able to act as a transmission-blocking agent (personal communication, Dr. Kathrin Buchholz). ML304 has been shown to act synergistically with MB; the redox-cycling activity of MB leads to the consumption of NADPH, while the inhibition of *Pf*GluPho prevents new synthesis (see discussion above; Buchholz *et al.*, 2008; Siciliano *et al.*, 2017). Unexpectedly however, SBI-0797750 tended to act antagonistically towards MB, chloroquine, and artemisinin. One potential explanation for this discrepancy might be found in the different plasmodial stages used; the synergistic effect of ML304 and MB was detected in late stage gametocytes (Siciliano *et al.*, 2017), whereas the antagonistic effect of SBI-0797750 and MB was detected in asexual

blood stage parasites. Stage-dependent differences in metabolism (MacRae *et al.*, 2013) might explain the different results of synergy tests. Further investigations ought to be conducted. Similar to ML304, SBI-0797750 has been shown to significantly disturb the glutathione homeostasis in *P. falciparum* 3D7 and *P. falciparum* NF54-*attB* parasites at the very low concentration of 65 nM and after only 4 h of incubation. Moreover, short term-exposure for 4 h of NF54-*attB* parasites to 65 nM of SBI-0797750 resulted in a significant increase in cytosolic H_2O_2 concentration; long-term exposure for 24 h significantly increased the H_2O_2 concentration in both cytosol and mitochondria. This clearly demonstrates that SBI-0797750 disturbs the maintenance of the cellular redox balance in *Plasmodium* parasites (Rahbari, 2017, SBI-0797750 referred to as "Compound S").

In addition to the effect of a compound on its target organism, one important quality factor of a potential drug component is its effect on the human patient. As summarized in chapter 1.2.1.1, hG6PD deficiency is the most common enzymopathy worldwide (Gomez-Manzo *et al.*, 2016). Since it leads to partial resistance against malaria, G6PD deficiency is mainly distributed in areas where malaria is (or was) endemic (Cappellini and Fiorelli, 2008). Most patients stay asymptomatic during their entire life; however, drug intake can trigger oxidative stress that can manifest as acute hemolysis (Cappellini and Fiorelli, 2008; Luzzatto *et al.*, 2016). To prevent this critical situation for the patient, the effect of SBI-0797750 was tested on healthy and G6PD deficient RBCs. In comparison to untreated cells, exposure to 2 µM SBI-0797750 for 24 h did not change the GSH levels in the cells. Cell lysis was determined by measuring the hemoglobin release in the supernatant; application of up to 2 µM compound did not change the cell lysis in comparison to untreated cells. Moreover, phagocytosis of SBI-0797750-treated RBCs by human phagocytes and monocytes did not increase. In summary, both healthy and G6PD deficient RBCs tolerated treatment with SBI-0797750 well, indicating that using the compound as an antimalarial drug might be nonhazardous (personal communication, Prof. Dr. Paolo Arese). Further characterization of its toxicity on human cells, as well as its behavior in absorption, distribution, metabolism, and excretion needs to be performed.

5.5.2 *Pf*6PGD as a drug target

*Pf*6PGD as the second NADPH-producing enzyme of the PPP contributes to the supply of this important electron donor in the same amounts as *Pf*GluPho (Stincone *et al.*, 2015). For *T. brucei*, 6PGD is already considered a promising target for the treatment of human African trypanosomiasis (Hanau *et al.*, 2004). Therefore, 6PGD is likely to be a promising antimalarial drug target (Haeussler *et al.*, 2018). Currently, there is an ongoing effort in Prof. Becker's group to investigate the role of *Pf*6PGD in parasitic survival using the CRISPR-Cas9 system.

Within this thesis, the MMV Malaria Box was screened to find an initial set of *Pf*6PGD inhibitors. This Box is a collection of 200 drug-like and 200 probe-like compounds with known antimalarial effects and high structural diversity in the compounds. It could be ordered free of charge from MMV until December 2015 (Spangenberg *et al.*, 2013). The MMV Malaria Box was replaced by 'The Pathogen Box', also containing 400 compounds; however, the compounds were not specifically selected based on their known antimalarial effect but should act against a broader range of pathogens causing neglected diseases (malaria (125), tuberculosis (116), kinetoplastids (70), helminths (32), cryptosporidiosis (11), toxoplasmosis (15), dengue (5), reference compounds (26), the number of compounds included against each disease is given in parenthesis) (https://www.pathogenbox.org/). Compounds of the MMV

Malaria Box with promising effect on *Pf*6PGD were tested on h6PGD in parallel in order to study selectivity of the inhibition. Ten compounds were identified to inhibit *Pf*6PGD with IC_{50} values below 5 µM. The best two were MMV011895 and MMV007228, with IC_{50} values of 1.6 ± 0.6 and 1.8 ± 0.1 µM, respectively. Unfortunately, all compounds inhibited h6PGD in the same range. MMV666125 showed a slightly higher preference for the plasmodial enzyme; however, the difference, less than 2-fold, was rather small (2.6 µM on *Pf*6PGD vs. 4.9 µM on h6PGD, Table 19). This similar inhibition is likely due to the highly conserved three-dimensional structure of the 6PGD family. There are some differences between the plasmodial and the human structure: (I) an interaction between the strictly conserved W265 and the *Plasmodium*-specific W104, in *H. sapiens* replaced by a glutamic acid; (II) a disulfide bridge between the *Plasmodium*-specific C281 linking the two subunits of the dimer; (III) the C-terminal end of h6PGD that has twelve additional amino acids covering the active site as soon as the active site loop adopts a closed conformation (Haeussler *et al.*, 2018). However, whether these rather small differences are sufficient for developing a highly selective compound needs to be investigated.

Difficulties in developing selective inhibitors might not exclude *Pf*6PGD as a potential drug target. Currently, h6PGD is considered a promising target for anticancer therapy (Cho *et al.*, 2018; Elf *et al.*, 2017; Guo *et al.*, 2018; Lin *et al.*, 2015). Due to their high metabolic rate, cancer cells have a high demand on nucleic acid biosynthesis and NADPH (Cho *et al.*, 2018; De Santis *et al.*, 2018; Patra and Hay, 2014; Stincone *et al.*, 2015). Inhibition of h6PGD therefore affects cancer cells significantly more than healthy cells. The same effect might be true for *Plasmodium*. During their life cycles, the parasites are continuously exposed to oxidative stress of different sources (see chapter 1.2.3) and are highly susceptible to changes in the cellular redox equilibrium (Becker *et al.*, 2004). This is supported by *experimenta naturae* such as the G6PD deficiency which leads to a tremendously reduced viability of the parasites, while humans can tolerate the deficiency quite well (see chapter 1.2.1.1, Cappellini and Fiorelli, 2008; Luzzatto *et al.*, 2016). One example of a non-selective compound is EA inhibiting *Pf*GluPho and hG6PD in the same range (Allen *et al.*, 2015) but not showing toxic effects on mammalian cells (Soh *et al.*, 2009). Therefore, targeting *Pf*6PGD and simultaneous short-term inhibition of h6PGD might be devastating for the parasites, but not for the humans. Together with knowledge of the three-dimensional structure of *Pf*6PGD, the identified inhibitors are promising starting points for structure-based compound optimizations. In addition, compounds of the MMV Malaria Box found to inhibit h6PGD (Table 19) might be used as a starting point for the development of new anticancer drugs.

6 References

Adams MJ, Ellis GH, Gover S, Naylor CE, and Phillips C (**1994**) Crystallographic study of coenzyme, coenzyme analogue and substrate binding in 6-phosphogluconate dehydrogenase: implications for NADP specificity and the enzyme mechanism. ***Structure*** 2: 651-668.

Adams MJ, Gover S, Leaback R, Phillips C, and Somers DO (**1991**) The structure of 6-phosphogluconate dehydrogenase refined at 2.5 A resolution. ***Acta Crystallogr B*** 47: 817-820.

Akbari OS, Bellen HJ, Bier E, Bullock SL, Burt A, Church GM, Cook KR, Duchek P, Edwards OR, Esvelt KM, Gantz VM, Golic KG, Gratz SJ, Harrison MM, Hayes KR, James AA, Kaufman TC, Knoblich J, Malik HS, Matthews KA, O'Connor-Giles KM, Parks AL, Perrimon N, Port F, Russell S, Ueda R, and Wildonger J (**2015**) BIOSAFETY. Safeguarding gene drive experiments in the laboratory. ***Science*** 349: 927-929.

Akman-Anderson L, Olivier M, and Luckhart S (**2007**) Induction of nitric oxide synthase and activation of signaling proteins in Anopheles mosquitoes by the malaria pigment, hemozoin. ***Infect Immun*** 75: 4012-4019.

Akoachere M, Buchholz K, Fischer E, Burhenne J, Haefeli WE, Schirmer RH, and Becker K (**2005**) *In vitro* assessment of methylene blue on chloroquine-sensitive and -resistant *Plasmodium falciparum* strains reveals synergistic action with artemisinins. ***Antimicrob Agents Chemother*** 49: 4592-4597.

Alencar N, Sola I, Linares M, Juarez-Jimenez J, Pont C, Viayna A, Vilchez D, Sampedro C, Abad P, Perez-Benavente S, Lameira J, Bautista JM, Munoz-Torrero D, and Luque FJ (**2018**) First homology model of *Plasmodium falciparum* glucose-6-phosphate dehydrogenase: discovery of selective substrate analog-based inhibitors as novel antimalarial agents. ***Eur J Med Chem*** 146: 108-122.

Allen SM, Lim EE, Jortzik E, Preuss J, Chua HH, MacRae JI, Rahlfs S, Haeussler K, Downton MT, McConville MJ, Becker K, and Ralph SA (**2015**) *Plasmodium falciparum* glucose-6-phosphate dehydrogenase 6-phosphogluconolactonase is a potential drug target. ***FEBS J*** 282: 3808-3823.

Ashley EA, Pyae Phyo A, and Woodrow CJ (**2018**) Malaria. ***Lancet*** 391: 1608-1621.

Atamna H and Ginsburg H (**1993**) Origin of reactive oxygen species in erythrocytes infected with *Plasmodium falciparum*. ***Mol Biochem Parasitol*** 61: 231-241.

Atamna H and Ginsburg H (**1995**) Heme degradation in the presence of glutathione. A proposed mechanism to account for the high levels of non-heme iron found in the membranes of hemoglobinopathic red blood cells. ***J Biol Chem*** 270: 24876-24883.

Atamna H, Pascarmona G, and Ginsburg H (**1994**) Hexose-monophosphate shunt activity in intact *Plasmodium falciparum*-infected erythrocytes and in free parasites. ***Mol Biochem Parasitol*** 67: 79-89.

Au SW, Gover S, Lam VM, and Adams MJ (**2000**) Human glucose-6-phosphate dehydrogenase: the crystal structure reveals a structural NADP(+) molecule and provides insights into enzyme deficiency. ***Structure*** 8: 293-303.

Bancone G, Chowwiwat N, Somsakchaicharoen R, Poodpanya L, Moo PK, Gornsawun G, Kajeechiwa L, Thwin MM, Rakthinthong S, Nosten S, Thinraow S, Nyo SN, Ling CL, Wiladphaingern J, Kiricharoen NL, Moore KA, White NJ, and Nosten F (**2016**) Single low dose primaquine (0.25 mg/kg) does not cause clinically significant haemolysis in G6PD deficient subjects. ***PLoS One*** 11: e0151898.

Barinova KV, Serebryakova MV, Muronetz VI, and Schmalhausen EV (**2017**) *S*-glutathionylation of glyceraldehyde-3-phosphate dehydrogenase induces formation of C150-C154 intrasubunit disulfide bond in the active site of the enzyme. ***Biochim Biophys Acta*** 1861: 3167-3177.

Baskaran Y, Ang KC, Anekal PV, Chan WL, Grimes JM, Manser E, and Robinson RC (**2015**) An in cellulo-derived structure of PAK4 in complex with its inhibitor Inka1. ***Nat Commun*** 6: 8681.

Becker K, Rahlfs S, Nickel C, and Schirmer RH (**2003**) Glutathione – functions and metabolism in the malarial parasite *Plasmodium falciparum*. ***Biol Chem*** 384: 551-566.

Becker K, Tilley L, Vennerstrom JL, Roberts D, Rogerson S, and Ginsburg H (**2004**) Oxidative stress in malaria parasite-infected erythrocytes: host-parasite interactions. ***Int J Parasitol*** 34: 163-189.

Belcastro E, Gaucher C, Corti A, Leroy P, Lartaud I, and Pompella A (**2017**) Regulation of protein function by *S*-nitrosation and *S*-glutathionylation: processes and targets in cardiovascular pathophysiology. ***Biol Chem*** 398: 1267-1293.

Benhar M, Forrester MT, and Stamler JS (**2009**) Protein denitrosylation: enzymatic mechanisms and cellular functions. ***Nat Rev Mol Cell Biol*** 10: 721-732.

Beppu M, Mizukami A, Nagoya M, and Kikugawa K (**1990**) Binding of anti-band 3 autoantibody to oxidatively damaged erythrocytes. Formation of senescent antigen on erythrocyte surface by an oxidative mechanism. ***J Biol Chem*** 265: 3226-3233.

Bergfors T (**2003**) Seeds to crystals. ***J Struct Biol*** 142: 66-76.

Berneburg I (**2017**) Glucose-6-Phosphat-Dehydrogenase-6-Phosphogluconolactonase aus *Plasmodium vivax* als mögliches *Drug Target*. Master Thesis, Biochemistry and Molecular Biology, Justus Liebig University.

Beutler E (**1984**) Red cell metabolism: a manual of biochemical methods. Grune and Stratton, New York.

Beutler E (**1994**) G6PD deficiency. ***Blood*** 84: 3613-3636.

Bieganowski P, Seidle HF, Wojcik M, and Brenner C (**2006**) Synthetic lethal and biochemical analyses of NAD and NADH kinases in *Saccharomyces cerevisiae* establish separation of cellular functions. ***J Biol Chem*** 281: 22439-22445.

Bienzle U, Ayeni O, Lucas AO, and Luzzatto L (**1972**) Glucose-6-phosphate dehydrogenase and malaria. Greater resistance of females heterozygous for enzyme deficiency and of males with non-deficient variant. ***Lancet*** 1: 107-110.

Bijelic A, Molitor C, Mauracher SG, Al-Oweini R, Kortz U, and Rompel A (**2015**) Hen egg-white lysozyme crystallisation: protein stacking and structure stability enhanced by a Tellurium(VI)-centred polyoxotungstate. ***Chembiochem*** 16: 233-241.

Bijelic A and Rompel A (**2017**) Ten good reasons for the use of the Tellurium-centered Anderson-Evans polyoxotungstate in protein crystallography. ***Acc Chem Res*** 50: 1441-1448.

Bisswanger H (**2017**) Enzyme kinetics principles and methods. WILEY-VCH, Tübingen.

Blundell TL (**2017**) Protein crystallography and drug discovery: recollections of knowledge exchange between academia and industry. ***IUCrJ*** 4: 308-321.

Bourzac K (**2014**) Infectious disease: beating the big three. ***Nature*** 507: S4-7.

Brewer GJ and Dern RJ (**1964**) A new inherited enzymatic deficiency of human erythrocytes: 6-phosphogluconate dehydrogenase deficiency. ***Am J Hum Genet*** 16: 472-476.

Bright GR, Fisher GW, Rogowska J, and Taylor DL (**1987**) Fluorescence ratio imaging microscopy: temporal and spatial measurements of cytoplasmic pH. ***J Cell Biol*** 104: 1019-1033.

Broniowska KA, Diers AR, and Hogg N (**2013**) *S*-nitrosoglutathione. ***Biochim Biophys Acta*** 1830: 3173-3181.

Bruegger JJ, Smith BC, Wynia-Smith SL, and Marletta MA (**2018**) Comparative and integrative metabolomics reveal that *S*-nitrosation inhibits physiologically relevant metabolic enzymes. ***J Biol Chem*** 293: 6282-6296.

Bublitz C and Steavenson S (**1988**) The pentose phosphate pathway in the endoplasmic reticulum. ***J Biol Chem*** 263: 12849-12853.

Buchholz K, Putrianti ED, Rahlfs S, Schirmer RH, Becker K, and Matuschewski K (**2010**) Molecular genetics evidence for the in vivo roles of the two major NADPH-dependent disulfide reductases in the malaria parasite. ***J Biol Chem*** 285: 37388-37395.

Buchholz K, Schirmer RH, Eubel JK, Akoachere MB, Dandekar T, Becker K, and Gromer S (**2008**) Interactions of methylene blue with human disulfide reductases and their orthologues from *Plasmodium falciparum*. ***Antimicrob Agents Chemother*** 52: 183-191.

Bull JJ and Malik HS (**2017**) The gene drive bubble: new realities. ***PLoS Genet*** 13: e1006850.

Burt A (**2003**) Site-specific selfish genes as tools for the control and genetic engineering of natural populations. ***Proc Biol Sci*** 270: 921-928.

Caffrey M and Cherezov V (**2009**) Crystallizing membrane proteins using lipidic mesophases. ***Nat Protoc*** 4: 706-731.

Cameron S, Martini VP, Iulek J, and Hunter WN (**2009**) *Geobacillus stearothermophilus* 6-phosphogluconate dehydrogenase complexed with 6-phosphogluconate. ***Acta Crystallogr Sect F Struct Biol Cryst Commun*** 65: 450-454.

Cappadoro M, Giribaldi G, O'Brien E, Turrini F, Mannu F, Ulliers D, Simula G, Luzzatto L, and Arese P (**1998**) Early phagocytosis of glucose-6-phosphate dehydrogenase (G6PD)-deficient erythrocytes parasitized by *Plasmodium falciparum* may explain malaria protection in G6PD deficiency. ***Blood*** 92: 2527-2534.

Cappellini MD and Fiorelli G (**2008**) Glucose-6-phosphate dehydrogenase deficiency. ***Lancet*** 371: 64-74.

Caprari P, Caforio MP, Cianciulli P, Maffi D, Pasquino MT, Tarzia A, Amadori S, and Salvati AM (**2001**) 6-Phosphogluconate dehydrogenase deficiency in an Italian family. ***Ann Hematol*** 80: 41-44.

Carlton JM, Adams JH, Silva JC, Bidwell SL, Lorenzi H, Caler E, Crabtree J, Angiuoli SV, Merino EF, Amedeo P, Cheng Q, Coulson RM, Crabb BS, Del Portillo HA, Essien K, Feldblyum TV, Fernandez-Becerra C, Gilson PR, Gueye AH, Guo X, Kang'a S, Kooij TW, Korsinczky M, Meyer EV, Nene V, Paulsen I, White O, Ralph SA, Ren Q, Sargeant TJ, Salzberg SL, Stoeckert CJ, Sullivan SA, Yamamoto MM, Hoffman SL, Wortman JR, Gardner MJ, Galinski MR, Barnwell JW, and Fraser-Liggett CM (**2008**) Comparative genomics of the neglected human malaria parasite *Plasmodium vivax*. ***Nature*** 455: 757-763.

Champer J, Reeves R, Oh SY, Liu C, Liu J, Clark AG, and Messer PW (**2017**) Novel CRISPR/Cas9 gene drive constructs reveal insights into mechanisms of resistance allele formation and drive efficiency in genetically diverse populations. ***PLoS Genet*** 13: e1006796.

Chayen NE and Saridakis E (**2008**) Protein crystallization: from purified protein to diffraction-quality crystal. ***Nat Methods*** 5: 147-153.

Chen DS, Locarnini S, and Wallace J (**2015**) From the big three to the big four. ***Lancet Infect Dis*** 15: 626-627.

Chen L, Morrow JK, Tran HT, Phatak SS, Du-Cuny L, and Zhang S (**2012**) From laptop to benchtop to bedside: structure-based drug design on protein targets. ***Curr Pharm Des*** 18: 1217-1239.

Chen YY, Ko TP, Chen WH, Lo LP, Lin CH, and Wang AH (**2010**) Conformational changes associated with cofactor/substrate binding of 6-phosphogluconate dehydrogenase from *Escherichia coli* and *Klebsiella pneumoniae*: implications for enzyme mechanism. ***J Struct Biol*** 169: 25-35.

Cheng Y-C and Prusoff WH (**1973**) Relationship between the inhibition constant (K_I) and the concentration of inhibitior which causes 50 per cent inhibition (I_{50}) of an enzymatic reaction. ***Biochem Pharmacol*** 22: 3099-3108.

Cho ES, Cha YH, Kim HS, Kim NH, and Yook JI (**2018**) The pentose phosphate pathway as a potential target for cancer therapy. ***Biomol Ther (Seoul)*** 26: 29-38.

Cho SW and Joshi JG (**1990**) Characterization of glucose-6-phosphate dehydrogenase isozymes from human and pig brain. ***Neuroscience*** 38: 819-828.

Clark TG, Fry AE, Auburn S, Campino S, Diakite M, Green A, Richardson A, Teo YY, Small K, Wilson J, Jallow M, Sisay-Joof F, Pinder M, Sabeti P, Kwiatkowski DP, and Rockett KA (**2009**) Allelic heterogeneity of G6PD deficiency in West Africa and severe malaria susceptibility. ***Eur J Hum Genet*** 17: 1080-1085.

Clarke JL, Scopes DA, Sodeinde O, and Mason PJ (**2001**) Glucose-6-phosphate dehydrogenase-6-phosphogluconolactonase. A novel bifunctional enzyme in malaria parasites. ***Eur J Biochem*** 268: 2013-2019.

Clarke JL, Sodeinde O, and Mason PJ (**2003**) A unique insertion in *Plasmodium berghei* glucose-6-phosphate dehydrogenase-6-phosphogluconolactonase: evolutionary and functional studies. ***Mol Biochem Parasitol*** 127: 1-8.

Cocco P, Manca P, and Dessi S (**1987**) Preliminary results of a geographic correlation study on G6PD deficiency and cancer. ***Toxicol Pathol*** 15: 106-108.

Cohen J, Nussenzweig V, Nussenzweig R, Vekemans J, and Leach A (**2010**) From the circumsporozoite protein to the RTS, S/AS candidate vaccine. ***Hum Vaccin*** 6: 90-96.

Cohen P and Rosemeyer MA (**1969**) Subunit interactions of glucose-6-phosphate dehydrogenase from human erythrocytes. ***Eur J Biochem*** 8: 8-15.

Cornish-Bowden A (**2004**) Fundamentals of enzyme kinetics. Portland Press Ltd., London.

Cosgrove MS, Gover S, Naylor CE, Vandeputte-Rutten L, Adams MJ, and Levy HR (**2000**) An examination of the role of asp-177 in the His-Asp catalytic dyad of *Leuconostoc mesenteroides* glucose 6-phosphate dehydrogenase: X-ray structure and pH dependence of kinetic parameters of the D177N mutant enzyme. ***Biochemistry*** 39: 15002-15011.

Cosgrove MS, Naylor C, Paludan S, Adams MJ, and Levy HR (**1998**) On the mechanism of the reaction catalyzed by glucose 6-phosphate dehydrogenase. ***Biochemistry*** 37: 2759-2767.

Cowman AF, Healer J, Marapana D, and Marsh K (**2016**) Malaria: biology and disease. ***Cell*** 167: 610-624.

Crooke A, Diez A, Mason PJ, and Bautista JM (**2006**) Transient silencing of *Plasmodium falciparum* bifunctional glucose-6-phosphate dehydrogenase- 6-phosphogluconolactonase. ***FEBS J*** 273: 1537-1546.

Crosnier C, Bustamante LY, Bartholdson SJ, Bei AK, Theron M, Uchikawa M, Mboup S, Ndir O, Kwiatkowski DP, Duraisingh MT, Rayner JC, and Wright GJ (**2011**) Basigin is a receptor essential for erythrocyte invasion by *Plasmodium falciparum*. ***Nature*** 480: 534-537.

Cumming JN, Ploypradith P, and Posner GH (**1997**) Antimalarial activity of artemisinin (qinghaosu) and related trioxanes: mechanism(s) of action. ***Adv Pharmacol*** 37: 253-297.

Dalle-Donne I, Rossi R, Colombo G, Giustarini D, and Milzani A (**2009**) Protein *S*-glutathionylation: a regulatory device from bacteria to humans. ***Trends Biochem Sci*** 34: 85-96.

Davis MI, Patrick SL, Blanding WM, Dwivedi V, Suryadi J, Golden JE, Coussens NP, Lee OW, Shen M, Boxer MB, Hall MD, Sharlow ER, Drew ME, and Morris JC (**2016**) Identification of novel *Plasmodium falciparum* hexokinase inhibitors with antiparasitic activity. ***Antimicrob Agents Chemother*** 60: 6023-6033.

De Santis MC, Porporato PE, Martini M, and Morandi A (**2018**) Signaling pathways regulating redox balance in cancer metabolism. ***Front Oncol*** 8: 126.

Dechant R, Binda M, Lee SS, Pelet S, Winderickx J, and Peter M (**2010**) Cytosolic pH is a second messenger for glucose and regulates the PKA pathway through V-ATPase. ***EMBO J*** 29: 2515-2526.

Desjardins RE, Canfield CJ, Haynes JD, and Chulay JD (**1979**) Quantitative assessment of antimalarial activity *in vitro* by a semiautomated microdilution technique. ***Antimicrob Agents Chemother*** 16: 710-718.

Doerig C, Rayner JC, Scherf A, and Tobin AB (**2015**) Post-translational protein modifications in malaria parasites. ***Nat Rev Microbiol*** 13: 160-172.

Dore MP, Davoli A, Longo N, Marras G, and Pes GM (**2016**) Glucose-6-phosphate dehydrogenase deficiency and risk of colorectal cancer in Northern Sardinia: a retrospective observational study. ***Medicine (Baltimore)*** 95: e5254.

Dore MP, Vidili G, Marras G, Assy S, and Pes GM (**2018**) Inverse association between glucose-6-phosphate dehydrogenase deficiency and hepatocellular carcinoma. ***Asian Pac J Cancer Prev*** 19: 1069-1073.

Drew DR and Beeson JG (**2015**) PfRH5 as a candidate vaccine for *Plasmodium falciparum* malaria. ***Trends Parasitol*** 31: 87-88.

Dutu R, Nedelea M, Veluda G, and Burculet V (**1980**) Cytoenzymologic investigations on carcinomas of the cervix uteri. ***Acta Cytol*** 24: 160-166.

Dyson JE, D'Orazio RE, and Hanson WH (**1973**) Sheep liver 6-phosphogluconate dehydrogenase: isolation procedure and effect of pH, ionic strength, and metal ions on the kinetic parameters. ***Arch Biochem Biophys*** 154: 623-635.

Egan TJ, Combrinck JM, Egan J, Hearne GR, Marques HM, Ntenteni S, Sewell BT, Smith PJ, Taylor D, van Schalkwyk DA, and Walden JC (**2002**) Fate of haem iron in the malaria parasite *Plasmodium falciparum*. ***Biochem J*** 365: 343-347.

Ekland EH, Schneider J, and Fidock DA (**2011**) Identifying apicoplast-targeting antimalarials using high-throughput compatible approaches. ***FASEB J*** 25: 3583-3593.

Elf S, Lin R, Xia S, Pan Y, Shan C, Wu S, Lonial S, Gaddh M, Arellano ML, Khoury HJ, Khuri FR, Lee BH, Boggon TJ, Fan J, and Chen J (**2017**) Targeting 6-phosphogluconate dehydrogenase in the oxidative PPP sensitizes leukemia cells to antimalarial agent dihydroartemisinin. ***Oncogene*** 36: 254-262.

EMA (**2015**) First malaria vaccine receives positive scientific opinion from EMA. http://www.ema.europa.eu/ema/index.jsp?curl=pages/news_and_events/news/2015/07/news_detail_002376.jsp&mid=WC0b01ac058004d5c1. Last access October 29th 2018.

Esteve MI and Cazzulo JJ (**2004**) The 6-phosphogluconate dehydrogenase from *Trypanosoma cruzi*: the absence of two inter-subunit salt bridges as a reason for enzyme instability. ***Mol Biochem Parasitol*** 133: 197-207.

Esvelt KM, Smidler AL, Catteruccia F, and Church GM (**2014**) Concerning RNA-guided gene drives for the alteration of wild populations. ***Elife*** 3: e03401.

Fan J, Ye J, Kamphorst JJ, Shlomi T, Thompson CB, and Rabinowitz JD (**2014**) Quantitative flux analysis reveals folate-dependent NADPH production. ***Nature*** 510: 298-302.

Ferrari CK, Souto PC, Franca EL, and Honorio-Franca AC (**2011**) Oxidative and nitrosative stress on phagocytes' function: from effective defense to immunity evasion mechanisms. ***Arch Immunol Ther Exp (Warsz)*** 59: 441-448.

Fivelman QL, Adagu IS, and Warhurst DC (**2004**) Modified fixed-ratio isobologram method for studying *in vitro* interactions between atovaquone and proguanil or dihydroartemisinin against drug-resistant strains of *Plasmodium falciparum*. ***Antimicrob Agents Chemother*** 48: 4097-4102.

Forrester MT, Foster MW, Benhar M, and Stamler JS (**2009a**) Detection of protein *S*-nitrosylation with the biotin-switch technique. ***Free Radic Biol Med*** 46: 119-126.

Forrester MT, Thompson JW, Foster MW, Nogueira L, Moseley MA, and Stamler JS (**2009b**) Proteomic analysis of *S*-nitrosylation and denitrosylation by resin-assisted capture. ***Nat Biotechnol*** 27: 557-559.

Francis SE, Sullivan DJ, Jr., and Goldberg DE (**1997**) Hemoglobin metabolism in the malaria parasite *Plasmodium falciparum*. ***Annu Rev Microbiol*** 51: 97-123.

Gantz VM, Jasinskiene N, Tatarenkova O, Fazekas A, Macias VM, Bier E, and James AA (**2015**) Highly efficient Cas9-mediated gene drive for population modification of the malaria vector mosquito *Anopheles stephensi*. ***Proc Natl Acad Sci U S A*** 112: E6736-6743.

Gardner MJ, Hall N, Fung E, White O, Berriman M, Hyman RW, Carlton JM, Pain A, Nelson KE, Bowman S, Paulsen IT, James K, Eisen JA, Rutherford K, Salzberg SL, Craig A, Kyes S, Chan MS, Nene V, Shallom SJ, Suh B, Peterson J, Angiuoli S, Pertea M, Allen J, Selengut J, Haft D, Mather MW, Vaidya AB, Martin DM, Fairlamb AH, Fraunholz MJ, Roos DS, Ralph SA, McFadden GI, Cummings LM, Subramanian GM, Mungall C, Venter JC, Carucci DJ, Hoffman SL, Newbold C, Davis RW, Fraser CM, and Barrell B (**2002**) Genome sequence of the human malaria parasite *Plasmodium falciparum*. ***Nature*** 419: 498-511.

Gavira JA (**2016**) Current trends in protein crystallization. ***Arch Biochem Biophys*** 602: 3-11.

Giribaldi G, Ulliers D, Mannu F, Arese P, and Turrini F (**2001**) Growth of *Plasmodium falciparum* induces stage-dependent haemichrome formation, oxidative aggregation of band 3, membrane deposition of complement and antibodies, and phagocytosis of parasitized erythrocytes. ***Br J Haematol*** 113: 492-499.

Gomez-Manzo S, Marcial-Quino J, Vanoye-Carlo A, Serrano-Posada H, Ortega-Cuellar D, Gonzalez-Valdez A, Castillo-Rodriguez RA, Hernandez-Ochoa B, Sierra-Palacios E, Rodriguez-Bustamante E, and Arreguin-Espinosa R (**2016**) Glucose-6-phosphate dehydrogenase: update and analysis of new mutations around the world. ***Int J Mol Sci*** 17.

Gordon G, Mackow MC, and Levy HR (**1995**) On the mechanism of interaction of steroids with human glucose-6-phosphate-dehydrogenase. ***Arch Biochem Biophys*** 318: 25-29.

Gräslund S, Nordlund P, Weigelt J, Hallberg BM, Bray J, Gileadi O, Knapp S, Oppermann U, Arrowsmith C, Hui R, Ming J, dhe-Paganon S, Park HW, Savchenko A, Yee A, Edwards A, Vincentelli R, Cambillau C, Kim R, Kim SH, Rao Z, Shi Y, Terwilliger TC, Kim CY, Hung LW, Waldo GS, Peleg Y, Albeck S, Unger T, Dym O, Prilusky J, Sussman JL, Stevens RC, Lesley SA, Wilson IA, Joachimiak A, Collart F, Dementieva I, Donnelly MI, Eschenfeldt WH, Kim Y, Stols L, Wu R, Zhou M, Burley SK, Emtage JS, Sauder JM, Thompson D, Bain K, Luz J, Gheyi T, Zhang F, Atwell S, Almo SC, Bonanno JB, Fiser A, Swaminathan S, Studier FW, Chance MR, Sali A, Acton TB, Xiao R, Zhao L, Ma LC, Hunt JF, Tong L, Cunningham K, Inouye M, Anderson S, Janjua H, Shastry R, Ho CK, Wang D, Wang H, Jiang M, Montelione GT, Stuart

DI, Owens RJ, Daenke S, Schutz A, Heinemann U, Yokoyama S, Bussow K, and Gunsalus KC (**2008**) Protein production and purification. ***Nat Methods*** 5: 135-146.

Greenwood B, Dicko A, Sagara I, Zongo I, Tinto H, Cairns M, Kuepfer I, Milligan P, Ouedraogo JB, Doumbo O, and Chandramohan D (**2017**) Seasonal vaccination against malaria: a potential use for an imperfect malaria vaccine. ***Malar J*** 16: 182.

Grossi L and Montevecchi PC (**2002**) *S*-nitrosocysteine and cystine from reaction of cysteine with nitrous acid. A kinetic investigation. ***J Org Chem*** 67: 8625-8630.

Guindo A, Fairhurst RM, Doumbo OK, Wellems TE, and Diallo DA (**2007**) X-linked G6PD deficiency protects hemizygous males but not heterozygous females against severe malaria. ***PLoS Med*** 4: e66.

Guo H, Xiang Z, Zhang Y, and Sun D (**2018**) Inhibiting 6-phosphogluconate dehydrogenase enhances chemotherapy efficacy in cervical cancer via AMPK-independent inhibition of RhoA and Rac1. ***Clin Transl Oncol*** doi: 10.1007/s12094-018-1937-x.

Gutscher M, Pauleau AL, Marty L, Brach T, Wabnitz GH, Samstag Y, Meyer AJ, and Dick TP (**2008**) Real-time imaging of the intracellular glutathione redox potential. ***Nat Methods*** 5: 553-559.

Gutscher M, Sobotta MC, Wabnitz GH, Ballikaya S, Meyer AJ, Samstag Y, and Dick TP (**2009**) Proximity-based protein thiol oxidation by H_2O_2-scavenging peroxidases. ***J Biol Chem*** 284: 31532-31540.

Gvozdev VA, Gerasimova TI, Kogan GL, and Braslavskaya O (**1976**) Role of the pentose phosphate pathway in metabolism of *Drosophila melanogaster* elucidated by mutations affecting glucose 6-phosphate and 6-phosphogluconate dehydrogenases. ***FEBS Lett*** 64: 85-88.

Haeussler K (**2015**) Enzymes of the pentose phosphate pathway of *Plasmodium falciparum* and *Plasmodium vivax* as drug targets. Master Thesis, Biochemistry and Molecular Biology, Justus Liebig University.

Haeussler K, Fritz-Wolf K, Reichmann M, Rahlfs S, and Becker K (**2018**) Characterization of *Plasmodium falciparum* 6-phosphogluconate dehydrogenase as an antimalarial drug target. ***J Mol Biol*** 430: 4049-4067.

Haldar K, Bhattacharjee S, and Safeukui I (**2018**) Drug resistance in Plasmodium. ***Nat Rev Microbiol*** 16: 156-170.

Hammond A, Galizi R, Kyrou K, Simoni A, Siniscalchi C, Katsanos D, Gribble M, Baker D, Marois E, Russell S, Burt A, Windbichler N, Crisanti A, and Nolan T (**2016**) A CRISPR-Cas9 gene drive system targeting female reproduction in the malaria mosquito vector *Anopheles gambiae*. ***Nat Biotechnol*** 34: 78-83.

Hanau S, d'Empaire LP, Capone I, Alberighi S, Montioli R, and Dallocchio F (**2013**) Evidence for dimer/tetramer equilibrium in *Trypanosoma brucei* 6-phosphogluconate dehydrogenase. ***Biochim Biophys Acta*** 1834: 2647-2652.

Hanau S, Rinaldi E, Dallocchio F, Gilbert IH, Dardonville C, Adams MJ, Gover S, and Barrett MP (**2004**) 6-Phosphogluconate dehydrogenase: a target for drugs in African trypanosomes. ***Curr Med Chem*** 11: 2639-2650.

Hanau S, Rippa M, Bertelli M, Dallocchio F, and Barrett MP (**1996**) 6-Phosphogluconate dehydrogenase from *Trypanosoma brucei*. Kinetic analysis and inhibition by trypanocidal drugs. ***Eur J Biochem*** 240: 592-599.

Hannaert V, Bringaud F, Opperdoes FR, and Michels PA (**2003**) Evolution of energy metabolism and its compartmentation in Kinetoplastida. ***Kinetoplastid Biol Dis*** 2: 11.

Hasegawa H, Wendling J, He F, Trilisky E, Stevenson R, Franey H, Kinderman F, Li G, Piedmonte DM, Osslund T, Shen M, and Ketchem RR (**2011**) *In vivo* crystallization of human IgG in the endoplasmic reticulum of engineered Chinese hamster ovary (CHO) cells. ***J Biol Chem*** 286: 19917-19931.

He W, Wang Y, Liu W, and Zhou CZ (**2007**) Crystal structure of *Saccharomyces cerevisiae* 6-phosphogluconate dehydrogenase Gnd1. ***BMC Struct Biol*** 7: 38.

Heise N and Opperdoes FR (**1999**) Purification, localisation and characterisation of glucose-6-phosphate dehydrogenase of *Trypanosoma brucei*. ***Mol Biochem Parasitol*** 99: 21-32.

Hess DT, Matsumoto A, Kim SO, Marshall HE, and Stamler JS (**2005**) Protein *S*-nitrosylation: purview and parameters. ***Nat Rev Mol Cell Biol*** 6: 150-166.

Hildebrandt T, Knuesting J, Berndt C, Morgan B, and Scheibe R (**2015**) Cytosolic thiol switches regulating basic cellular functions: GAPDH as an information hub? ***Biol Chem*** 396: 523-537.

Hitosugi T, Zhou L, Elf S, Fan J, Kang HB, Seo JH, Shan C, Dai Q, Zhang L, Xie J, Gu TL, Jin P, Aleckovic M, LeRoy G, Kang Y, Sudderth JA, DeBerardinis RJ, Luan CH, Chen GZ, Muller S, Shin DM, Owonikoko TK, Lonial S, Arellano ML, Khoury HJ, Khuri FR, Lee BH, Ye K, Boggon TJ, Kang S, He C, and Chen J (**2012**) Phosphoglycerate mutase 1 coordinates glycolysis and biosynthesis to promote tumor growth. ***Cancer Cell*** 22: 585-600.

Holcomb J, Spellmon N, Zhang Y, Doughan M, Li C, and Yang Z (**2017**) Protein crystallization: eluding the bottleneck of X-ray crystallography. ***AIMS Biophys*** 4: 557-575.

Hong W, Cai P, Xu C, Cao D, Yu W, Zhao Z, Huang M, and Jin J (**2018**) Inhibition of glucose-6-phosphate dehydrogenase reverses cisplatin resistance in lung cancer cells via the redox system. ***Front Pharmacol*** 9: 43.

Hotez PJ and Kamath A (**2009**) Neglected tropical diseases in sub-saharan Africa: review of their prevalence, distribution, and disease burden. ***PLoS Negl Trop Dis*** 3: e412.

Hung TM, Clapham HE, Bettis AA, Cuong HQ, Thwaites GE, Wills BA, Boni MF, and Turner HC (**2018**) The estimates of the health and economic burden of dengue in Vietnam. ***Trends Parasitol*** 34: 904-918.

Ibrahim MA, Ghazy AH, Salem AM, Ghazy MA, and Abdel-Monsef MM (**2015**) Biochemical characterization of buffalo liver glucose-6-phosphate dehydrogenase isoforms. ***Protein J*** 34: 193-204.

Ireton GC and Stoddard BL (**2004**) Microseed matrix screening to improve crystals of yeast cytosine deaminase. ***Acta Crystallogr D Biol Crystallogr*** 60: 601-605.

Jang M, Cai L, Udeani GO, Slowing KV, Thomas CF, Beecher CW, Fong HH, Farnsworth NR, Kinghorn AD, Mehta RG, Moon RC, and Pezzuto JM (**1997**) Cancer chemopreventive activity of resveratrol, a natural product derived from grapes. ***Science*** 275: 218-220.

Jaramillo M, Gowda DC, Radzioch D, and Olivier M (**2003**) Hemozoin increases IFN-gamma-inducible macrophage nitric oxide generation through extracellular signal-regulated kinase- and NF-kappa B-dependent pathways. ***J Immunol*** 171: 4243-4253.

Jeney V, Ramos S, Bergman ML, Bechmann I, Tischer J, Ferreira A, Oliveira-Marques V, Janse CJ, Rebelo S, Cardoso S, and Soares MP (**2014**) Control of disease tolerance to malaria by nitric oxide and carbon monoxide. ***Cell Rep*** 8: 126-136.

Jonas SK, Benedetto C, Flatman A, Hammond RH, Micheletti L, Riley C, Riley PA, Spargo DJ, Zonca M, and Slater TF (**1992**) Increased activity of 6-phosphogluconate dehydrogenase and glucose-6-phosphate dehydrogenase in purified cell suspensions and single cells from the uterine cervix in cervical intraepithelial neoplasia. ***Br J Cancer*** 66: 185-191.

Jortzik E and Becker K (**2012**) Thioredoxin and glutathione systems in *Plasmodium falciparum*. ***Int J Med Microbiol*** 302: 187-194.

Jortzik E, Mailu BM, Preuss J, Fischer M, Bode L, Rahlfs S, and Becker K (**2011**) Glucose-6-phosphate dehydrogenase-6-phosphogluconolactonase: a unique bifunctional enzyme from *Plasmodium falciparum*. ***Biochem J*** 436: 641-650.

Jortzik E, Wang L, and Becker K (**2012**) Thiol-based posttranslational modifications in parasites. ***Antioxid Redox Signal*** 17: 657-673.

Kabsch W (**2010**) Xds. ***Acta Crystallogr D Biol Crystallogr*** 66: 125-132.

Kane JF (**1995**) Effects of rare codon clusters on high-level expression of heterologous proteins in *Escherichia coli*. ***Curr Opin Biotechnol*** 6: 494-500.

Kanzok SM, Schirmer RH, Turbachova I, Iozef R, and Becker K (**2000**) The thioredoxin system of the malaria parasite *Plasmodium falciparum*. Glutathione reduction revisited. ***J Biol Chem*** 275: 40180-40186.

Kasozi D, Mohring F, Rahlfs S, Meyer AJ, and Becker K (**2013**) Real-time imaging of the intracellular glutathione redox potential in the malaria parasite *Plasmodium falciparum*. ***PLoS Pathog*** 9: e1003782.

Kavishe RA, Koenderink JB, and Alifrangis M (**2017**) Oxidative stress in malaria and artemisinin combination therapy: pros and cons. ***FEBS J*** 284: 2579-2591.

Kay MM (**1984**) Localization of senescent cell antigen on band 3. ***Proc Natl Acad Sci U S A*** 81: 5753-5757.

Kehr S, Jortzik E, Delahunty C, Yates JR, 3rd, Rahlfs S, and Becker K (**2011**) Protein *S*-glutathionylation in malaria parasites. ***Antioxid Redox Signal*** 15: 2855-2865.

Kehr S, Sturm N, Rahlfs S, Przyborski JM, and Becker K (**2010**) Compartmentation of redox metabolism in malaria parasites. ***PLoS Pathog*** 6: e1001242.

Keller MA, Turchyn AV, and Ralser M (**2014**) Non-enzymatic glycolysis and pentose phosphate pathway-like reactions in a plausible Archean ocean. ***Mol Syst Biol*** 10: 725.

Kim KY, Lee HW, Shim YM, Mook-Jung I, Jeon GS, and Sung JJ (**2015**) A phosphomimetic mutant TDP-43 (S409/410E) induces Drosha instability and cytotoxicity in Neuro 2A cells. ***Biochem Biophys Res Commun*** 464: 236-243.

Kirchner S, Power BJ, and Waters AP (**2016**) Recent advances in malaria genomics and epigenomics. ***Genome Med*** 8: 92.

Kohr MJ, Aponte AM, Sun J, Wang G, Murphy E, Gucek M, and Steenbergen C (**2011**) Characterization of potential S-nitrosylation sites in the myocardium. ***Am J Physiol Heart Circ Physiol*** 300: H1327-1335.

Kolifarhood G, Raeisi A, Ranjbar M, Haghdoust AA, Schapira A, Hashemi S, Masoumi-Asl H, Mozafar Saadati H, Azimi S, Khosravi N, and Kondrashin A (**2017**) Prophylactic efficacy of primaquine for preventing *Plasmodium falciparum* and *Plasmodium vivax* parasitaemia in travelers: a meta-analysis and systematic review. ***Travel Med Infect Dis*** 17: 5-18.

Kotaka M, Gover S, Vandeputte-Rutten L, Au SW, Lam VM, and Adams MJ (**2005**) Structural studies of glucose-6-phosphate and NADP+ binding to human glucose-6-phosphate dehydrogenase. ***Acta Crystallogr D Biol Crystallogr*** 61: 495-504.

Krnajski Z, Gilberger TW, Walter RD, Cowman AF, and Müller S (**2002**) Thioredoxin reductase is essential for the survival of *Plasmodium falciparum* erythrocytic stages. ***Journal of Biological Chemistry*** 277: 25970-25975.

Kruger NJ and von Schaewen A (**2003**) The oxidative pentose phosphate pathway: structure and organisation. ***Curr Opin Plant Biol*** 6: 236-246.

Kyrou K, Hammond AM, Galizi R, Kranjc N, Burt A, Beaghton AK, Nolan T, and Crisanti A (**2018**) A CRISPR-Cas9 gene drive targeting doublesex causes complete population suppression in caged *Anopheles gambiae* mosquitoes. ***Nat Biotechnol*** doi: 10.1038/nbt.4245.

Laemmli UK (**1970**) Cleavage of structural proteins during the assembly of the head of bacteriophage T4. ***Nature*** 227: 680-685.

Lambros C and Vanderberg JP (**1979**) Synchronization of *Plasmodium falciparum* erythrocytic stages in culture. ***J Parasitol*** 65: 418-420.

Lasonder E, Green JL, Camarda G, Talabani H, Holder AA, Langsley G, and Alano P (**2012**) The *Plasmodium falciparum* schizont phosphoproteome reveals extensive phosphatidylinositol and cAMP-protein kinase A signaling. ***J Proteome Res*** 11: 5323-5337.

Lee SM, Koh HJ, Park DC, Song BJ, Huh TL, and Park JW (**2002**) Cytosolic NADP(+)-dependent isocitrate dehydrogenase status modulates oxidative damage to cells. ***Free Radic Biol Med*** 32: 1185-1196.

Leibly DJ, Nguyen TN, Kao LT, Hewitt SN, Barrett LK, and Van Voorhis WC (**2012**) Stabilizing additives added during cell lysis aid in the solubilization of recombinant proteins. ***PLoS One*** 7: e52482.

Lin R, Elf S, Shan C, Kang HB, Ji Q, Zhou L, Hitosugi T, Zhang L, Zhang S, Seo JH, Xie J, Tucker M, Gu TL, Sudderth J, Jiang L, Mitsche M, DeBerardinis RJ, Wu S, Li Y, Mao H, Chen PR, Wang D, Chen GZ, Hurwitz SJ, Lonial S, Arellano ML, Khoury HJ, Khuri FR, Lee BH, Lei Q, Brat DJ, Ye K, Boggon TJ, He C, Kang S, Fan J, and Chen J (**2015**) 6-Phosphogluconate dehydrogenase links oxidative PPP, lipogenesis and tumour growth by inhibiting LKB1-AMPK signalling. ***Nat Cell Biol*** 17: 1484-1496.

Ling IT and Wilson RJ (**1988**) Glucose-6-phosphate dehydrogenase activity of the malaria parasite *Plasmodium falciparum*. ***Mol Biochem Parasitol*** 31: 47-56.

Llopis J, McCaffery JM, Miyawaki A, Farquhar MG, and Tsien RY (**1998**) Measurement of cytosolic, mitochondrial, and Golgi pH in single living cells with green fluorescent proteins. ***Proc Natl Acad Sci U S A*** 95: 6803-6808.

Lobo Z and Maitra PK (**1982**) Pentose phosphate pathway mutants of yeast. ***Mol Gen Genet*** 185: 367-368.

Longo L, Vanegas OC, Patel M, Rosti V, Li H, Waka J, Merghoub T, Pandolfi PP, Notaro R, Manova K, and Luzzatto L (**2002**) Maternally transmitted severe glucose 6-phosphate dehydrogenase deficiency is an embryonic lethal. ***EMBO J*** 21: 4229-4239.

Lopez C, Saravia C, Gomez A, Hoebeke J, and Patarroyo MA (**2010**) Mechanisms of genetically-based resistance to malaria. ***Gene*** 467: 1-12.

Louicharoen C, Patin E, Paul R, Nuchprayoon I, Witoonpanich B, Peerapittayamongkol C, Casademont I, Sura T, Laird NM, Singhasivanon P, Quintana-Murci L, and Sakuntabhai A (**2009**) Positively selected G6PD-Mahidol mutation reduces *Plasmodium vivax* density in Southeast Asians. ***Science*** 326: 1546-1549.

Low PS, Waugh SM, Zinke K, and Drenckhahn D (**1985**) The role of hemoglobin denaturation and band 3 clustering in red blood cell aging. ***Science*** 227: 531-533.

Lu HM, Yin DC, Liu YM, Guo WH, and Zhou RB (**2012**) Correlation between protein sequence similarity and crystallization reagents in the biological macromolecule crystallization database. ***Int J Mol Sci*** 13: 9514-9526.

Luckhart S, Vodovotz Y, Cui L, and Rosenberg R (**1998**) The mosquito *Anopheles stephensi* limits malaria parasite development with inducible synthesis of nitric oxide. ***Proc Natl Acad Sci U S A*** 95: 5700-5705.

Lutz HU, Fasler S, Stammler P, Bussolino F, and Arese P (**1988**) Naturally occurring anti-band 3 antibodies and complement in phagocytosis of oxidatively-stressed and in clearance of senescent red cells. ***Blood Cells*** 14: 175-203.

Luzzatto L and Arese P (**2018**) Favism and glucose-6-phosphate dehydrogenase deficiency. ***N Engl J Med*** 378: 60-71.

Luzzatto L, Nannelli C, and Notaro R (**2016**) Glucose-6-phosphate dehydrogenase deficiency. ***Hematol Oncol Clin North Am*** 30: 373-393.

Luzzatto L, Usanga FA, and Reddy S (**1969**) Glucose-6-phosphate dehydrogenase deficient red cells: resistance to infection by malarial parasites. ***Science*** 164: 839-842.

Ma L and Cheng Q (**2018**) Inhibiting 6-phosphogluconate dehydrogenase reverses doxorubicin resistance in anaplastic thyroid cancer via inhibiting NADPH-dependent metabolic reprogramming. ***Biochem Biophys Res Commun*** 498: 912-917.

Mac Sweeney A, Chambovey A, Wicki M, Müller M, Artico N, Lange R, Bijelic A, Breibeck J, and Rompel A (**2018**) The crystallization additive hexatungstotellurate promotes the crystallization of the HSP70 nucleotide binding domain into two different crystal forms. ***PLoS One*** 13: e0199639.

MacRae JI, Dixon MW, Dearnley MK, Chua HH, Chambers JM, Kenny S, Bottova I, Tilley L, and McConville MJ (**2013**) Mitochondrial metabolism of sexual and asexual blood stages of the malaria parasite *Plasmodium falciparum*. ***BMC Biol*** 11: 67.

Maloney P, Hedrick M, Peddibhotla S, Hershberger P, Milewski M, Gosalia P, Li L, Preuss J, Sugarman E, Hood B, Suyama E, Nguyen K, Vasile S, Sergienko E, Salanawil S, Stonich D, Su Y, Dahl R, Mangravita-Novo A, Vicchiarelli M, McAnally D, Smith LH, Roth G, Diwan J, Chung TDY, Pinkerton AB, Bode L, and Becker K (**2012**) A 2nd selective inhibitor of *Plasmodium falciparum* glucose-6-phosphate dehydrogenase (PfG6PDH) - Probe 2. NIH Probe Report, 2010-2012, updated 2013.

Marchand M, Kooystra U, Wierenga RK, Lambeir AM, Van Beeumen J, Opperdoes FR, and Michels PA (**1989**) Glucosephosphate isomerase from *Trypanosoma brucei*. Cloning and characterization of the gene and analysis of the enzyme. ***Eur J Biochem*** 184: 455-464.

Markus MB (**2018**) Biological concepts in recurrent *Plasmodium vivax* malaria. ***Parasitology*** 145: 1765-1771.

McPherson A and Gavira JA (**2014**) Introduction to protein crystallization. ***Acta Crystallogr F Struct Biol Commun*** 70: 2-20.

Mele L, Paino F, Papaccio F, Regad T, Boocock D, Stiuso P, Lombardi A, Liccardo D, Aquino G, Barbieri A, Arra C, Coveney C, La Noce M, Papaccio G, Caraglia M, Tirino V, and Desiderio V (**2018**) A new inhibitor of glucose-6-phosphate dehydrogenase blocks pentose phosphate pathway and suppresses malignant proliferation and metastasis in vivo. ***Cell Death Dis*** 9: 572.

Mercaldi GF, Dawson A, Hunter WN, and Cordeiro AT (**2016**) The structure of a *Trypanosoma cruzi* glucose-6-phosphate dehydrogenase reveals differences from the mammalian enzyme. ***FEBS Lett*** 590: 2776-2786.

Miclet E, Stoven V, Michels PA, Opperdoes FR, Lallemand JY, and Duffieux F (**2001**) NMR spectroscopic analysis of the first two steps of the pentose-phosphate pathway elucidates the role of 6-phosphogluconolactonase. ***J Biol Chem*** 276: 34840-34846.

Miller J, Golenser J, Spira DT, and Kosower NS (**1984**) *Plasmodium falciparum*: thiol status and growth in normal and glucose-6-phosphate dehydrogenase deficient human erythrocytes. ***Exp Parasitol*** 57: 239-247.

Mohring F, Pretzel J, Jortzik E, and Becker K (**2014**) The redox systems of *Plasmodium falciparum* and *Plasmodium vivax*: comparison, in silico analyses and inhibitor studies. ***Curr Med Chem*** 21: 1728-1756.

Molina-Cruz A, DeJong RJ, Charles B, Gupta L, Kumar S, Jaramillo-Gutierrez G, and Barillas-Mury C (**2008**) Reactive oxygen species modulate *Anopheles gambiae* immunity against bacteria and *Plasmodium*. ***J Biol Chem*** 283: 3217-3223.

Molitor C, Bijelic A, and Rompel A (**2017**) The potential of hexatungstotellurate(VI) to induce a significant entropic gain during protein crystallization. ***IUCrJ*** 4: 734-740.

Moritz B, Striegel K, De Graaf AA, and Sahm H (**2000**) Kinetic properties of the glucose-6-phosphate and 6-phosphogluconate dehydrogenases from *Corynebacterium glutamicum* and their application for predicting pentose phosphate pathway flux in vivo. ***Eur J Biochem*** 267: 3442-3452.

Mullarky E and Cantley LC (**2015**) Diverting glycolysis to combat oxidative stress. In: Innovative medicine: basic research and development. Springer, Tokyo.

Müller S (**2004**) Redox and antioxidant systems of the malaria parasite *Plasmodium falciparum*. ***Mol Microbiol*** 53: 1291-1305.

Naing C, Whittaker MA, Nyunt Wai V, and Mak JW (**2014**) Is *Plasmodium vivax* malaria a severe malaria?: A systematic review and meta-analysis. ***PLoS Negl Trop Dis*** 8: e3071.

Neafsey DE, Juraska M, Bedford T, Benkeser D, Valim C, Griggs A, Lievens M, Abdulla S, Adjei S, Agbenyega T, Agnandji ST, Aide P, Anderson S, Ansong D, Aponte JJ, Asante KP, Bejon P, Birkett AJ, Bruls M, Connolly KM, D'Alessandro U, Dobano C, Gesase S, Greenwood B, Grimsby J, Tinto H, Hamel MJ, Hoffman I, Kamthunzi P, Kariuki S, Kremsner PG, Leach A, Lell B, Lennon NJ, Lusingu J, Marsh K, Martinson F, Molel JT, Moss EL, Njuguna P, Ockenhouse CF, Ogutu BR, Otieno W, Otieno L, Otieno K, Owusu-Agyei S, Park DJ, Pelle K, Robbins D, Russ C, Ryan EM, Sacarlal J, Sogoloff B, Sorgho H, Tanner M, Theander T, Valea I, Volkman SK, Yu Q, Lapierre D, Birren BW, Gilbert PB, and Wirth DF (**2015**) Genetic diversity and protective efficacy of the RTS,S/AS01 malaria vaccine. ***N Engl J Med*** 373: 2025-2037.

Neafsey DE, Schaffner SF, Volkman SK, Park D, Montgomery P, Milner DA, Jr., Lukens A, Rosen D, Daniels R, Houde N, Cortese JF, Tyndall E, Gates C, Stange-Thomann N, Sarr O, Ndiaye D, Ndir O, Mboup S, Ferreira MU, Moraes Sdo L, Dash AP, Chitnis CE, Wiegand RC, Hartl DL, Birren BW, Lander ES, Sabeti PC, and Wirth DF (**2008**) Genome-wide SNP genotyping highlights the role of natural selection in *Plasmodium falciparum* population divergence. ***Genome Biol*** 9: R171.

Nepveu F and Turrini F (**2013**) Targeting the redox metabolism of *Plasmodium falciparum*. ***Future Med Chem*** 5: 1993-2006.

Njomnang Soh P, Witkowski B, Gales A, Huyghe E, Berry A, Pipy B, and Benoit-Vical F (**2012**) Implication of glutathione in the *in vitro* antiplasmodial mechanism of action of ellagic acid. ***PLoS One*** 7: e45906.

Notaro R, Afolayan A, and Luzzatto L (**2000**) Human mutations in glucose 6-phosphate dehydrogenase reflect evolutionary history. ***FASEB J*** 14: 485-494.

Novagen (**2004**) Competent Cells User Protocol. https://www.med.unc.edu/pharm/sondeklab/files/resource-files/manuels/novagen_competent_cells2. Last access October 29th 2018.

O'Brien E, Kurdi-Haidar B, Wanachiwanawin W, Carvajal JL, Vulliamy TJ, Cappadoro M, Mason PJ, and Luzzatto L (**1994**) Cloning of the glucose 6-phosphate dehydrogenase gene from *Plasmodium falciparum*. ***Mol Biochem Parasitol*** 64: 313-326.

Oeda K, Inouye K, Ibuchi Y, Oshie K, Shimizu M, Nakamura K, Nishioka R, Takada Y, and Ohkawa H (**1989**) Formation of crystals of the insecticidal proteins of *Bacillus thuringiensis* subsp. *aizawai* IPL7 in *Escherichia coli*. ***J Bacteriol*** 171: 3568-3571.

Olotu A, Fegan G, Wambua J, Nyangweso G, Leach A, Lievens M, Kaslow DC, Njuguna P, Marsh K, and Bejon P (**2016**) Seven-year efficacy of RTS,S/AS01 malaria vaccine among young African children. ***N Engl J Med*** 374: 2519-2529.

Ong PK, Melchior B, Martins YC, Hofer A, Orjuela-Sanchez P, Cabrales P, Zanini GM, Frangos JA, and Carvalho LJ (**2013**) Nitric oxide synthase dysfunction contributes to impaired cerebroarteriolar reactivity in experimental cerebral malaria. ***PLoS Pathog*** 9: e1003444.

Osier FH, Feng G, Boyle MJ, Langer C, Zhou J, Richards JS, McCallum FJ, Reiling L, Jaworowski A, Anders RF, Marsh K, and Beeson JG (**2014**) Opsonic phagocytosis of *Plasmodium falciparum* merozoites: mechanism in human immunity and a correlate of protection against malaria. ***BMC Med*** 12: 108.

Pandolfi PP, Sonati F, Rivi R, Mason P, Grosveld F, and Luzzatto L (**1995**) Targeted disruption of the housekeeping gene encoding glucose 6-phosphate dehydrogenase (G6PD): G6PD is dispensable for pentose synthesis but essential for defense against oxidative stress. ***EMBO J*** 14: 5209-5215.

Parola P (**2013**) The return of the big three killers. ***Clin Microbiol Infect*** 19: 887-888.

RTS,S Clinical Trials Partnership (**2015**) Efficacy and safety of RTS,S/AS01 malaria vaccine with or without a booster dose in infants and children in Africa: final results of a phase 3, individually randomised, controlled trial. ***Lancet*** 386: 31-45.

Pastrana-Mena R, Dinglasan RR, Franke-Fayard B, Vega-Rodriguez J, Fuentes-Caraballo M, Baerga-Ortiz A, Coppens I, Jacobs-Lorena M, Janse CJ, and Serrano AE (**2010**) Glutathione reductase-null malaria parasites have normal blood stage growth but arrest during development in the mosquito. ***J Biol Chem*** 285: 27045-27056.

Patra KC and Hay N (**2014**) The pentose phosphate pathway and cancer. ***Trends Biochem Sci*** 39: 347-354.

Patzewitz EM, Wong EH, and Müller S (**2012**) Dissecting the role of glutathione biosynthesis in *Plasmodium falciparum*. ***Mol Microbiol*** 83: 304-318.

Paul F, Roath S, Melville D, Warhurst DC, and Osisanya JO (**1981**) Separation of malaria-infected erythrocytes from whole blood: use of a selective high-gradient magnetic separation technique. ***Lancet*** 2: 70-71.

Pe'er I, Felder CE, Man O, Silman I, Sussman JL, and Beckmann JS (**2004**) Proteomic signatures: amino acid and oligopeptide compositions differentiate among phyla. ***Proteins*** 54: 20-40.

Pearse BM and Rosemeyer MA (**1974a**) Human 6-phosphogluconate dehydrogenase. Purification of the erythrocyte enzyme and the influence of ions and NADPH on its activity. ***Eur J Biochem*** 42: 213-223.

Pearse BM and Rosemeyer MA (**1974b**) The molecular weight and subunit structure of human erythrocyte 6-phosphogluconate dehydrogenase. ***Eur J Biochem*** 42: 225-235.

Pease BN, Huttlin EL, Jedrychowski MP, Talevich E, Harmon J, Dillman T, Kannan N, Doerig C, Chakrabarti R, Gygi SP, and Chakrabarti D (**2013**) Global analysis of protein expression and phosphorylation of three stages of *Plasmodium falciparum* intraerythrocytic development. ***J Proteome Res*** 12: 4028-4045.

Percario S, Moreira DR, Gomes BA, Ferreira ME, Goncalves AC, Laurindo PS, Vilhena TC, Dolabela MF, and Green MD (**2012**) Oxidative stress in malaria. ***Int J Mol Sci*** 13: 16346-16372.

Peterson LA, Wagener T, Sies H, and Stahl W (**2007a**) Decomposition of *S*-nitrosocysteine via *S*- to N-transnitrosation. ***Chem Res Toxicol*** 20: 721-723.

Peterson TM, Gow AJ, and Luckhart S (**2007b**) Nitric oxide metabolites induced in *Anopheles stephensi* control malaria parasite infection. ***Free Radic Biol Med*** 42: 132-142.

Phillips C, Dohnalek J, Gover S, Barrett MP, and Adams MJ (**1998**) A 2.8 A resolution structure of 6-phosphogluconate dehydrogenase from the protozoan parasite *Trypanosoma brucei*: comparison with the sheep enzyme accounts for differences in activity with coenzyme and substrate analogues. ***J Mol Biol*** 282: 667-681.

Pickl A and Schönheit P (**2015**) The oxidative pentose phosphate pathway in the haloarchaeon *Haloferax volcanii* involves a novel type of glucose-6-phosphate dehydrogenase – The archaeal Zwischenferment. ***FEBS Lett*** 589: 1105-1111.

Poburko D, Santo-Domingo J, and Demaurex N (**2011**) Dynamic regulation of the mitochondrial proton gradient during cytosolic calcium elevations. ***J Biol Chem*** 286: 11672-11684.

Pollak N, Dolle C, and Ziegler M (**2007**) The power to reduce: pyridine nucleotides – small molecules with a multitude of functions. ***Biochem J*** 402: 205-218.

Preuss J, Hedrick M, Sergienko E, Pinkerton A, Mangravita-Novo A, Smith L, Marx C, Fischer E, Jortzik E, Rahlfs S, Becker K, and Bode L (**2012a**) High-throughput screening for small-molecule inhibitors of *Plasmodium falciparum* glucose-6-phosphate dehydrogenase 6-phosphogluconolactonase. ***J Biomol Screen*** 17: 738-751.

Preuss J, Jortzik E, and Becker K (**2012b**) Glucose-6-phosphate metabolism in *Plasmodium falciparum*. ***IUBMB Life*** 64: 603-611.

Preuss J, Maloney P, Peddibhotla S, Hedrick MP, Hershberger P, Gosalia P, Milewski M, Li YL, Sugarman E, Hood B, Suyama E, Nguyen K, Vasile S, Sergienko E, Mangravita-Novo A, Vicchiarelli M, McAnally D, Smith LH, Roth GP, Diwan J, Chung TD, Jortzik E, Rahlfs S, Becker K, Pinkerton AB, and Bode L (**2012c**) Discovery of a *Plasmodium falciparum* glucose-6-phosphate dehydrogenase 6-phosphogluconolactonase inhibitor (R,Z)-N-((1-ethylpyrrolidin-2-yl)methyl)-2-(2-fluorobenzylidene)-3-oxo-3,4-dihydro-2H-benzo[b][1,4] thiazine-6-carboxamide (ML276) that reduces parasite growth in vitro. ***J Med Chem*** 55: 7262-7272.

Preuss J, Richardson AD, Pinkerton A, Hedrick M, Sergienko E, Rahlfs S, Becker K, and Bode L (**2013**) Identification and characterization of novel human glucose-6-phosphate dehydrogenase inhibitors. ***J Biomol Screen*** 18: 286-297.

Price NE and Cook PF (**1996**) Kinetic and chemical mechanisms of the sheep liver 6-phosphogluconate dehydrogenase. ***Arch Biochem Biophys*** 336: 215-223.

Qu Z, Meng F, Bomgarden RD, Viner RI, Li J, Rogers JC, Cheng J, Greenlief CM, Cui J, Lubahn DB, Sun GY, and Gu Z (**2014**) Proteomic quantification and site-mapping of S-nitrosylated proteins using isobaric iodoTMT reagents. ***J Proteome Res*** 13: 3200-3211.

Raab D, Graf M, Notka F, Schodl T, and Wagner R (**2010**) The GeneOptimizer Algorithm: using a sliding window approach to cope with the vast sequence space in multiparameter DNA sequence optimization. ***Syst Synth Biol*** 4: 215-225.

Rahbari M (**2017**) Establishment of genetically encoded H_2O_2 probes and dynamic measurements of H_2O_2 levels in the malaria parasite *Plasmodium falciparum*. Inaugural dissertation, Biochemistry and Molecular Biology, Justus Liebig University.

Rahbari M, Rahlfs S, Przyborski JM, Schuh AK, Hunt NH, Fidock DA, Grau GE, and Becker K (**2017**) Hydrogen peroxide dynamics in subcellular compartments of malaria parasites using genetically encoded redox probes. ***Sci Rep*** 7: 10449.

Rahlfs S, Nickel C, Deponte M, Schirmer RH, and Becker K (**2003**) *Plasmodium falciparum* thioredoxins and glutaredoxins as central players in redox metabolism. ***Redox Rep*** 8: 246-250.

Ralser M, Wamelink MM, Kowald A, Gerisch B, Heeren G, Struys EA, Klipp E, Jakobs C, Breitenbach M, Lehrach H, and Krobitsch S (**2007**) Dynamic rerouting of the carbohydrate flux is key to counteracting oxidative stress. ***J Biol*** 6: 10.

Rammler DH (**1967**) The effect of DMSO on several enzyme systems. ***Ann N Y Acad Sci*** 141: 291-299.

Ranjan R, Karpurapu M, Rani A, Chishti AH, and Christman JW (**2016**) Hemozoin regulates iNOS expression by modulating the transcription factor NF-kappaB in macrophages. ***Biochem Mol Biol J*** 2: pii: 10.

Ranzani AT and Cordeiro AT (**2017**) Mutations in the tetramer interface of human glucose-6-phosphate dehydrogenase reveals kinetic differences between oligomeric states. ***FEBS Lett*** 591: 1278-1284.

Recht J, Ashley EA, and White NJ (**2018**) Use of primaquine and glucose-6-phosphate dehydrogenase deficiency testing: divergent policies and practices in malaria endemic countries. ***PLoS Negl Trop Dis*** 12: e0006230.

Reichmann M (**2018**) Kristallisation von Proteinen des Pentosephosphatweges aus *Plasmodium falciparum*. Master Thesis, Biochemistry and Molecular Biology, Justus Liebig University.

Rendina AR, Hermes JD, and Cleland WW (**1984**) Use of multiple isotope effects to study the mechanism of 6-phosphogluconate dehydrogenase. ***Biochemistry*** 23: 6257-6262.

Richie TL, Billingsley PF, Sim BK, James ER, Chakravarty S, Epstein JE, Lyke KE, Mordmüller B, Alonso P, Duffy PE, Doumbo OK, Sauerwein RW, Tanner M, Abdulla S, Kremsner PG, Seder RA, and Hoffman SL (**2015**) Progress with *Plasmodium falciparum* sporozoite (*Pf*SPZ)-based malaria vaccines. ***Vaccine*** 33: 7452-7461.

Roth E, Jr. (**1990**) *Plasmodium falciparum* carbohydrate metabolism: a connection between host cell and parasite. ***Blood Cells*** 16: 453-460; discussion 461-466.

Roth EF, Jr., Raventos-Suarez C, Rinaldi A, and Nagel RL (**1983**) Glucose-6-phosphate dehydrogenase deficiency inhibits in vitro growth of *Plasmodium falciparum*. ***Proc Natl Acad Sci U S A*** 80: 298-299.

Roy A (**2018**) Early probe and drug discovery in academia: a minireview. ***High Throughput*** 7: pii: E4.

Ruwende C, Khoo SC, Snow RW, Yates SN, Kwiatkowski D, Gupta S, Warn P, Allsopp CE, Gilbert SC, Peschu N, Newbold CI, Greenwood BM, Marsh K, and Hill AVS (**1995**) Natural selection of hemi- and heterozygotes for G6PD deficiency in Africa by resistance to severe malaria. ***Nature*** 376: 246-249.

Schirmer RH, Coulibaly B, Stich A, Scheiwein M, Merkle H, Eubel J, Becker K, Becher H, Müller O, Zich T, Schiek W, and Kouyate B (**2003**) Methylene blue as an antimalarial agent. ***Redox Rep*** 8: 272-275.

Schirmer RH, Schollhammer T, Eisenbrand G, and Krauth-Siegel RL (**1987**) Oxidative stress as a defense mechanism against parasitic infections. ***Free Radic Res Commun*** 3: 3-12.

Schlegel S, Löfblom J, Lee C, Hjelm A, Klepsch M, Strous M, Drew D, Slotboom DJ, and de Gier JW (**2012**) Optimizing membrane protein overexpression in the *Escherichia coli* strain Lemo21(DE3). ***J Mol Biol*** 423: 648-659.

Schönherr R, Rudolph JM, and Redecke L (**2018**) Protein crystallization in living cells. ***Biol Chem*** 399: 751-772.

Schwartz AG, Pashko L, and Whitcomb JM (**1986**) Inhibition of tumor development by dehydroepiandrosterone and related steroids. ***Toxicol Pathol*** 14: 357-362.

Schwartzenberg-Bar-Yoseph F, Armoni M, and Karnieli E (**2004**) The tumor suppressor p53 down-regulates glucose transporters GLUT1 and GLUT4 gene expression. ***Cancer Res*** 64: 2627-2633.

Scopes DA, Bautista JM, Vulliamy TJ, and Mason PJ (**1997**) *Plasmodium falciparum* glucose-6-phosphate dehydrogenase (G6PD)-the N-terminal portion is homologous to a predicted protein encoded near to G6PD in *Haemophilus influenzae*. ***Mol Microbiol*** 23: 847-848.

Senesi S, Csala M, Marcolongo P, Fulceri R, Mandl J, Banhegyi G, and Benedetti A (**2010**) Hexose-6-phosphate dehydrogenase in the endoplasmic reticulum. ***Biol Chem*** 391: 1-8.

Shahabuddin M, Rawlings DJ, and Kaslow DC (**1994**) A novel glucose-6-phosphate dehydrogenase in *Plasmodium falciparum*: cDNA and primary protein structure. ***Biochim Biophys Acta*** 1219: 191-194.

Sharma P, Jha AB, Dubey RS, and Pessarakli M (**2012**) Reactive oxygen species, oxidative damage, and antioxidative defense mechanism in plants under stressful conditions. ***Journal of Botany*** 2012: Article ID 217037.

Shenton D and Grant CM (**2003**) Protein *S*-thiolation targets glycolysis and protein synthesis in response to oxidative stress in the yeast *Saccharomyces cerevisiae*. ***Biochem J*** 374: 513-519.

Siciliano G, Santha Kumar TR, Bona R, Camarda G, Calabretta MM, Cevenini L, Davioud-Charvet E, Becker K, Cara A, Fidock DA, and Alano P (**2017**) A high susceptibility to redox imbalance of the transmissible stages of *Plasmodium falciparum* revealed with a luciferase-based mature gametocyte assay. ***Mol Microbiol*** 104: 306-318.

Sinden RE (**2017**) Developing transmission-blocking strategies for malaria control. ***PLoS Pathog*** 13: e1006336.

Sissoko MS, Healy SA, Katile A, Omaswa F, Zaidi I, Gabriel EE, Kamate B, Samake Y, Guindo MA, Dolo A, Niangaly A, Niare K, Zeguime A, Sissoko K, Diallo H, Thera I, Ding K, Fay MP, O'Connell EM, Nutman TB, Wong-Madden S, Murshedkar T, Ruben AJ, Li M, Abebe Y, Manoj A, Gunasekera A, Chakravarty S, Sim BKL, Billingsley PF, James ER, Walther M, Richie TL, Hoffman SL, Doumbo O, and Duffy PE (**2017**) Safety and efficacy of *Pf*SPZ Vaccine against *Plasmodium falciparum* via direct venous inoculation in healthy malaria-exposed adults in Mali: a randomised, double-blind phase 1 trial. ***Lancet Infect Dis*** 17: 498-509.

Soh PN, Witkowski B, Olagnier D, Nicolau ML, Garcia-Alvarez MC, Berry A, and Benoit-Vical F (**2009**) *In vitro* and *in vivo* properties of ellagic acid in malaria treatment. ***Antimicrob Agents Chemother*** 53: 1100-1106.

Spangenberg T, Burrows JN, Kowalczyk P, McDonald S, Wells TN, and Willis P (**2013**) The open access malaria box: a drug discovery catalyst for neglected diseases. ***PLoS One*** 8: e62906.

Spitzen J and Takken W (**2018**) Keeping track of mosquitoes: a review of tools to track, record and analyse mosquito flight. ***Parasit Vectors*** 11: 123.

Stegmayer A (**2013**) Charakterisierung von Varianten der Glukose-6-Phosphatdehydrogenase-6-Phosphoglukonolactonase aus Malariaparasiten. Master Thesis, Biochemistry and Molecular Biology, Justus Liebig University.

Stincone A, Prigione A, Cramer T, Wamelink MM, Campbell K, Cheung E, Olin-Sandoval V, Gruning NM, Kruger A, Tauqeer Alam M, Keller MA, Breitenbach M, Brindle KM, Rabinowitz JD, and Ralser M (**2015**) The return of metabolism: biochemistry and physiology of the pentose phosphate pathway. ***Biol Rev Camb Philos Soc*** 90: 927-963.

Stöger E, Parker M, Christou P, and Casey R (**2001**) Pea legumin overexpressed in wheat endosperm assembles into an ordered paracrystalline matrix. ***Plant Physiol*** 125: 1732-1742.

Storm J, Perner J, Aparicio I, Patzewitz EM, Olszewski K, Llinas M, Engel PC, and Müller S (**2011**) *Plasmodium falciparum* glutamate dehydrogenase a is dispensable and not a drug target during erythrocytic development. ***Malar J*** 10: 193.

Sturm N, Hu Y, Zimmermann H, Fritz-Wolf K, Wittlin S, Rahlfs S, and Becker K (**2009**) Compounds structurally related to ellagic acid show improved antiplasmodial activity. ***Antimicrob Agents Chemother*** 53: 622-630.

Sundaramoorthy R, Iulek J, Barrett MP, Bidet O, Ruda GF, Gilbert IH, and Hunter WN (**2007**) Crystal structures of a bacterial 6-phosphogluconate dehydrogenase reveal aspects of specificity, mechanism and mode of inhibition by analogues of high-energy reaction intermediates. ***FEBS J*** 274: 275-286.

Tarrado-Castellarnau M, de Atauri P, and Cascante M (**2016**) Oncogenic regulation of tumor metabolic reprogramming. ***Oncotarget*** 7: 62726-62753.

Tetaud E, Hanau S, Wells JM, Le Page RW, Adams MJ, Arkison S, and Barrett MP (**1999**) 6-Phosphogluconate dehydrogenase from *Lactococcus lactis*: a role for arginine residues in binding substrate and coenzyme. ***Biochem J*** 338 (Pt 1): 55-60.

Thomson-Luque R, Shaw Saliba K, Kocken CHM, and Pasini EM (**2017**) A continuous, long-term *Plasmodium vivax in vitro* blood-stage culture: what are we missing? ***Trends Parasitol*** 33: 921-924.

Thonghin N, Kargas V, Clews J, and Ford RC (**2018**) Cryo-electron microscopy of membrane proteins. ***Methods*** 147: 176-186.

Tizifa TA, Kabaghe AN, McCann RS, van den Berg H, Van Vugt M, and Phiri KS (**2018**) Prevention efforts for malaria. ***Curr Trop Med Rep*** 5: 41-50.

Topham CM, Matthews B, and Dalziel K (**1986**) Kinetic studies of 6-phosphogluconate dehydrogenase from sheep liver. ***Eur J Biochem*** 156: 555-567.

Trager W and Jensen JB (**1976**) Human malaria parasites in continuous culture. ***Science*** 193: 673-675.

Treeck M, Sanders JL, Elias JE, and Boothroyd JC (**2011**) The phosphoproteomes of *Plasmodium falciparum* and *Toxoplasma gondii* reveal unusual adaptations within and beyond the parasites' boundaries. ***Cell Host Microbe*** 10: 410-419.

Tsutsui H, Jinno Y, Shoda K, Tomita A, Matsuda M, Yamashita E, Katayama H, Nakagawa A, and Miyawaki A (**2015**) A diffraction-quality protein crystal processed as an autophagic cargo. ***Mol Cell*** 58: 186-193.

Turrini F, Ginsburg H, Bussolino F, Pescarmona GP, Serra MV, and Arese P (**1992**) Phagocytosis of *Plasmodium falciparum*-infected human red blood cells by human monocytes: involvement of immune and nonimmune determinants and dependence on parasite developmental stage. ***Blood*** 80: 801-808.

van Niekerk DD, Penkler GP, du Toit F, and Snoep JL (**2016**) Targeting glycolysis in the malaria parasite *Plasmodium falciparum*. ***FEBS J*** 283: 634-646.

van Schalkwyk DA, Priebe W, and Saliba KJ (**2008**) The inhibitory effect of 2-halo derivatives of D-glucose on glycolysis and on the proliferation of the human malaria parasite *Plasmodium falciparum*. ***J Pharmacol Exp Ther*** 327: 511-517.

Vega-Rodriguez J, Franke-Fayard B, Dinglasan RR, Janse CJ, Pastrana-Mena R, Waters AP, Coppens I, Rodriguez-Orengo JF, Srinivasan P, Jacobs-Lorena M, and Serrano AE (**2009**)

The glutathione biosynthetic pathway of *Plasmodium* is essential for mosquito transmission. ***PLoS Pathog*** 5: e1000302.

Veronese FM, Boccu E, Fontana A, Benassi CA, and Scoffone E (**1974**) Isolation and some properties of 6-phosphogluconate dehydrogenase from *Bacillus stearothermophilus*. ***Biochimica Et Biophysica Acta*** 334: 31-44.

Verotta L, Dell'Agli M, Giolito A, Guerrini M, Cabalion P, and Bosisio E (**2001**) *In vitro* antiplasmodial activity of extracts of Tristaniopsis species and identification of the active constituents: ellagic acid and 3,4,5-trimethoxyphenyl-(6'-O-galloyl)-O-beta-D-glucopyranoside. ***J Nat Prod*** 64: 603-607.

Vives Corrons JL, Colomer D, Pujades A, Rovira A, Aymerich M, Merino A, and Bascompte JLAI (**1996**) Congenital 6-phosphogluconate dehydrogenase (6PGD) deficiency associated with chronic hemolytic anemia in a Spanish family. ***Am J Hematol*** 53: 221-227.

Volkman SK, Sabeti PC, DeCaprio D, Neafsey DE, Schaffner SF, Milner DA, Jr., Daily JP, Sarr O, Ndiaye D, Ndir O, Mboup S, Duraisingh MT, Lukens A, Derr A, Stange-Thomann N, Waggoner S, Onofrio R, Ziaugra L, Mauceli E, Gnerre S, Jaffe DB, Zainoun J, Wiegand RC, Birren BW, Hartl DL, Galagan JE, Lander ES, and Wirth DF (**2007**) A genome-wide map of diversity in *Plasmodium falciparum*. ***Nat Genet*** 39: 113-119.

Wamelink MM, Struys EA, and Jakobs C (**2008**) The biochemistry, metabolism and inherited defects of the pentose phosphate pathway: a review. ***J Inherit Metab Dis*** 31: 703-717.

Wang L, Delahunty C, Prieto JH, Rahlfs S, Jortzik E, Yates JR, 3rd, and Becker K (**2014**) Protein *S*-nitrosylation in *Plasmodium falciparum*. ***Antioxid Redox Signal*** 20: 2923-2935.

Wang XT, Au SW, Lam VM, and Engel PC (**2002**) Recombinant human glucose-6-phosphate dehydrogenase. Evidence for a rapid-equilibrium random-order mechanism. ***Eur J Biochem*** 269: 3417-3424.

Wermuth B, Munch JD, and von Wartburg JP (**1977**) Purification and properties of NADPH-dependent aldehyde reductase from human liver. ***J Biol Chem*** 252: 3821-3828.

Werner C, Stubbs MT, Krauth-Siegel RL, and Klebe G (**2005**) The crystal structure of *Plasmodium falciparum* glutamate dehydrogenase, a putative target for novel antimalarial drugs. ***J Mol Biol*** 349: 597-607.

White N (**1999**) Antimalarial drug resistance and combination chemotherapy. ***Philos Trans R Soc Lond B Biol Sci*** 354: 739-749.

White NJ, Pukrittayakamee S, Hien TT, Faiz MA, Mokuolu OA, and Dondorp AM (**2014**) Malaria. ***Lancet*** 383: 723-735.

WHO (**2012**) WHO policy recommendation: Seasonal malaria chemoprevention (SMC) for *Plasmodium falciparum* malaria control in highly seasonal transmission areas of the Sahel sub-region in Africa. http://www.who.int/malaria/publications/atoz/who_smc_policy_recommendation/en/. Last access October 29th 2018.

WHO (**2015a**) Achieving the malaria MDG target: Reversing the incidence of malaria 2000-2015. http://www.who.int/malaria/publications/atoz/9789241509442/en/. Last access October 29th 2018.

WHO (**2015b**) Investing to overcome the global ompact of neglected tropical diseases: Third WHO report on neglected tropical diseases. http://www.who.int/neglected_diseases/resources/9789241564861/en/. Last access October 29th 2018.

WHO (**2015c**) Policy brief on single-dose primaquine as a gametocytocide in *Plasmodium falciparum* malaria. http://www.who.int/malaria/publications/atoz/policy-brief-single-dose-primaquine-pf/en/. Last access October 29th 2018.

WHO (**2016**) World Malaria Report 2016. http://www.who.int/malaria/publications/world-malaria-report-2016/report/en/. Last access October 29th 2018.

WHO (**2017a**) Global Hepatitis Report 2017. https://www.who.int/hepatitis/publications/global-hepatitis-report2017/en/. Last access October 29th 2018.

WHO (**2017b**) World Malaria Report 2017. http://www.who.int/malaria/publications/world-malaria-report-2017/report/en/. Last access October 29th 2018.

WHO (**2018a**) Global Health Observatory (GHO) data. http://www.who.int/gho/hiv/epidemic_status/deaths/en/. Last access October 29th 2018.

WHO (**2018b**) Global Tuberculosis Report 2018. http://www.who.int/tb/publications/global_report/en/. Last access October 29th 2018.

Wolhuter K and Eaton P (**2017**) How widespread is stable protein *S*-nitrosylation as an end-effector of protein regulation? ***Free Radic Biol Med*** 109: 156-166.

Wrenger C and Müller S (**2003**) Isocitrate dehydrogenase of *Plasmodium falciparum*. ***Eur J Biochem*** 270: 1775-1783.

Wrigley NG, Heather JV, Bonsignore A, and De Flora A (**1972**) Human erythrocyte glucose 6-phosphate dehydrogenase: electron microscope studies on structure and interconversion of tetramers, dimers and monomers. ***J Mol Biol*** 68: 483-499.

Wüthrich K (**1989**) Protein structure determination in solution by nuclear magnetic resonance spectroscopy. ***Science*** 243: 45-50.

Yarlagadda K, Hassani J, Foote IP, and Markowitz J (**2017**) The role of nitric oxide in melanoma. ***Biochim Biophys Acta*** 1868: 500-509.

Zaffagnini M, Fermani S, Costa A, Lemaire SD, and Trost P (**2013**) Plant cytoplasmic GAPDH: redox post-translational modifications and moonlighting properties. ***Front Plant Sci*** 4: 450.

Zamboni N, Fischer E, Laudert D, Aymerich S, Hohmann HP, and Sauer U (**2004**) The *Bacillus subtilis yqjI* gene encodes the NADP+-dependent 6-P-gluconate dehydrogenase in the pentose phosphate pathway. ***J Bacteriol*** 186: 4528-4534.

Zhang J, Ye ZW, Singh S, Townsend DM, and Tew KD (**2018**) An evolving understanding of the *S*-glutathionylation cycle in pathways of redox regulation. ***Free Radic Biol Med*** 120: 204-216.

Zhang N, Diao Y, Hua R, Wang J, Han S, Li J, and Yin Y (**2017**) Nitric oxide-mediated pathways and its role in the degenerative diseases. ***Front Biosci (Landmark Ed)*** 22: 824-834.

Zhang Y, Zheng Y, Qin L, Wang S, Buchko GW, and Garavito RM (**2014**) Structural characterization of a beta-hydroxyacid dehydrogenase from *Geobacter sulfurreducens* and *Geobacter metallireducens* with succinic semialdehyde reductase activity. ***Biochimie*** 104: 61-69.

Zheng W, Feng Q, Liu J, Guo Y, Gao L, Li R, Xu M, Yan G, Yin Z, Zhang S, Liu S, and Shan C (**2017**) Inhibition of 6-phosphogluconate dehydrogenase reverses cisplatin resistance in ovarian and lung cancer. ***Front Pharmacol*** 8: 421.

Appendix

```
PfGluPho       1 MDYENFVKSAEEINNLHNVNYLETKDLNDFNWKAAYYICKEIYDKQQINK     50
                 ||.:...||.|::|:||||.|||.|||.|||.|:|||||.:|.:||...:
PvGluPho       1 MDCQALAKSLEQMNHLHNVKYLEAKDLTDFNQKSAYYICHQIAEKQLSKE     50

PfGluPho      51 DGYVVIGLSGGRTPIDVYKNMCLIKDIKIDKSKLIFFIIDERYKSDDHKF    100
                 .|:||||||||:||||||||:.|:|||||||.||||||||||||.|||||
PvGluPho      51 GGHVVIGLSGGKTPIDVYKNIALVKDIKIDTSKLIFFIIDERYKRDDHKF    100

PfGluPho     101 SNYNNIKFLFHNLNINEKEQLYKPDTTKSIVDCILDYNDKIKIMIEKYKK    150
                 ||||||||||.:|.||||||||:|||:|:||:|:.|||:|||.|::||.|
PvGluPho     101 SNYNNIKFLFESLKINEKEQLYRPDTSKNIVECVRDYNEKIKNMVKKYTK    150

PfGluPho     151 VDIAILGMGSDFHIASLFPNIFYNIYMNNYQNNYIYNEKTLDFINNDQ--    198
                 |||||||||||||||||||||:||||||||:|||:|.::...|::.
PvGluPho     151 VDIAILGMGSDFHIASLFPNIFFNIYMNNYQNSYIYDESSIKVANSNDTS    200

PfGluPho     199 DNDNLKYLKEYVYFTTTNQFDVRKRITVSLNLLANASSKIFLLNSKDKLD    248
                 |||||..||||||||||.||||||||||:||.||||||||||.||||
PvGluPho     201 DNDNLDLLKEYVYFTTTNNFDVRKRITVSLDLLGNASSKIFLLNSTDKLD    250

PfGluPho     249 LWKNMLIKSYIEVNYNLYPATYLIDTSCTNENVNINNNNNNNNNKNKNNYC    298
                 ||||||:|||::|||.||||.||||:.
PvGluPho     251 LWKNMLLKSYVDVNYCLYPAVYLIDSM----------------------    277

PfGluPho     299 YSNTTVISCGYENYTKSIEEIYDSKYALSLYSNSLNKEELLTIIIFGCSG    348
                   ||||::|||.||.:.:|:||.|..:||::|.|||:.|.||||:|||||
PvGluPho     278 --NTTVVTCGYTNYPQMLEDIYVSNSSLSVHSPSLNRRECLTIIVFGCSG    325

PfGluPho     349 DLAKKKIYPALFKLFCNNSLPKDLLIIGFARTVQDFDTFFDKIVIYLKRC    398
                 ||||||||||:||||||..|||||||:||||.|.||:|||||||.|||||
PvGluPho     326 DLAKKKIYPAIFKLFCNKRLPKDLLIVGFARTAQSFDSFFDKIVGYLKRC    375

PfGluPho     399 LLCYEDWSISKKKDLLNGFKNRCRYFVGNYSSSESFENFNKYLTTIEEEE    448
                 |..|||.|:::||||||.|||:||||::|:||||||||.||||||.:|.|.
PvGluPho     376 LHSYEDLSLTQKKDLLNCFKNKCRYYIGDYSSSESFERFNKYLTQLEREN    425

PfGluPho     449 ----AKKKYYATCYKMN-------------------------GSDYNIS    468
                     |...:.|.....:                         |.....:
PvGluPho     426 LIGTAPTSWAAAAGNASFANDTDKVEHHPDEAILAKGTGAATPGEAPGGA    475

PfGluPho     469 NNVAEDNISIDDENKTNEYFQ-MCTPKNCPDNVFSSNYNFPYVINRMLYL    517
                 |..|....:....|..:...| ...|.:...:...|..|.|:.|||:|||
PvGluPho     476 NGPATHGEAHGGANGLSTPMQGKAVPTDDTSDEGHSGANHPFAINRILYL    525

PfGluPho     518 ALPPHIFVSTLKNYKKNCLNSKGTDKILLEKPFGNDLDSFKMLSKQILEN    567
                 ||||||||||||||||.|..||||||||||||.||.:||:||||||||
PvGluPho     526 ALPPHIFVSTLKNYKKNCQNGNGTDKILLEKPFGKDLQTFKVLSKQILEN    575

PfGluPho     568 FNEQQIYRIDHYLGKDMVSGLLKLKFTNTFLLSLMNRHFIKCIKITLKET    617
                 |||:.|||||||||||||||||||||||||||||||||||||||||||||
PvGluPho     576 FNEEHIYRIDHYLGKDMVSGLLKLKFTNTFLLSLMNRHFIKCIKITLKET    625

PfGluPho     618 KGVYGRGQYFDPYGIIRDVMQNHMLQLLTLITMEDPIDLNDESVKNEKIK    667
                 |||||||||||||||||||||||||.||||||||||||||||||||||||
PvGluPho     626 KGVYGRGQYFDPYGIIRDVMQNHMLQLLALITMEDPIDLNDESVKNEKIK    675

PfGluPho     668 ILKSIPSIKLEDTIIGQYEKAENFKEDEN-----NDD----ESKKNHSYH    708
                 |||.|.||||::||||||.|:||::|::|     :||    |||:|||||
PvGluPho     676 ILKCIQSIKLDNTIIGQYVKSENYQEEKNLSAPPSDDHPVDESKRNHSYH    725
```

```
PfGluPho     709 DDPHIDKNSITPTFCTCILYINSINWYGVPIIFKSGKGLNKDICEIRIQF    758
                 ||||||.||||||||||||||||||||||||:||||||||||||:||
PvGluPho     726 DDPHIDSNSITPTFCTCILYINSINWYGVPIIFKAGKGLNKDICEIRLQF    775

PfGluPho     759 HNIMGSSDENMNNNEFVIILQPVEAIYLKMMIKKTGCEEMEEVQLNLTVN    808
                 |||||||||:|.||||||||||||.|||||||||||||||||||||||||
PvGluPho     776 HNIMGSSDESMYNNEFVIILQPVEVIYLKMMIKKTGCEEMEEVQLNLTVN    825

PfGluPho     809 EKNKKINVPEAYETLLLECFKGHKKKFISDEEELYESWRIFTPLLKELQEK    858
                 .|||||..|||||||||||||:|.|||||||||||||||||||.|||||
PvGluPho     826 HKNKKNYVPEAYETLLLECFRGFKKKFISDEELYESWRIFTPLLNELQEK    875

PfGluPho     859 QVKPLKYSFGSSGPKEVFGLVKKYYNYGKNYTHRPEFVRKSSFYEDDLLD    908
                   :|:||||.|||||||||:.||||||||||||.:.|.|||||||||||||
PvGluPho     876 KVQPLKYPFGSSGPKEVYDLVKKYYNYGKNYANTPAFVRKSSFYEDDLLD    925

PfGluPho     909 IN    910
                 ||
PvGluPho     926 IN    927
```

Appendix 1 Amino acid sequence alignment of *Pf*GluPho (PF3D7_1453800) and *Pv*GluPho (PVX_117790)
| Identical residues, : very similar residues, . similar residues.

```
Pv    MTGTCDIGLIGLAVMGQNLSLNIASNGFTIGVYNRTYERTEDTLKKAKEGNLPIQGYETL   60
Pk    MAGTCDIGLIGLAVMGQNLSLNIASNGFTIGVYNRTYERTEDTIKKAKESNLPIYGYETL   60
Pm    MAGVCDIGLVGLAVMGQNLSLNIASKGFKIGVYNRTYARTEVTLKRAKEENLVIYGYKTL   60
Pf    M---CDIGLIGLAVMGQNLSLNISSKGFKIGVYNRTYERTEETMKRAKEENLVVYGYKTV   57
Po    MAEVCDVGLVGLAVMGQNLSLNISSKGFKIGVYNRTYERTEETVKRAKEEKLCIYGYKTL   60
      *   **:**:*************:*:**.******** *** *:*:*** :* : **:*:

Pv    EQLINNLKKPRKIILLIKAGPAVDETIKNILKHFEEGDIIIDGGNEWYLNTERRITLCEE   120
Pk    EQLIKNLKKPRKIILLIKAGPAVDETIKNILKHFEEGDIIIDGGNEWYLNTERRISICEE   120
Pm    EELVNSLKKPKKIILLIKAGPAVDENIKNILNFFEKGDIIIDGGNEWYLNSERRIKLCTE   120
Pf    EELINNLKKPRKVILLIKAGPAVDENISNILKHFEKGDIIIDGGNEWYINSERRIKLCKE   117
Po    EELIQNLKKPKKIILLIKAGPAVDENINNILKYFEKGDIIIDGGNEWYLNSERRIKLCGE   120
      *:*::.****:*:************.*.***:.**:**********:*:*:****.:* *

Pv    HKVEYLAMGVSGGEAGARYGCSFMPGGSKYAYDTIKDILEKCSAKVGTSPCVTYIGPRSS   180
Pk    HKVEYLAMGVSGGEAGARYGCSFMPGGSKYAYDQIKDILEKCSAKVGTSPCVTYIGPRSS   180
Pm    KQVEYLAMGVSGGEAGARYGCSFMPGGSKYAYDCVQDILEKCSAKVGTSPCVTYIGPGSS   180
Pf    KDVEYLAMGVSGGEAGARYGCSFMPGGSKYAYDCVKEILEKCSAQVGNSPCVTYIGPGSS   177
Po    KNVEYLAMGVSGGEAGARYGCSFMPGGSKYAYDCIKDILEKCSAKVGTSPCVTYIGPGSS   180
      :.******************************* :::*******:**.********* **

Pv    GNYVKMVHNGIEYGDMQLISESYLLMKNILNYNNEKLSEVFKKWNEGILNSYLIEITYKI   240
Pk    GNYVKMVHNGIEYGDMQLISESYLLMKHILNYSNEKMSDVFKKWNEGILNSYLIEITYKI   240
Pm    GNYVKMIHNGIEYGDMQLISESYYLMKHILKYDNKKASDVFKKWNEGILNSYLIEITSKI   240
Pf    GNYVKMVHNGIEYGDMQLISESYVIMKHILKYDNQKLSEVFNKWNEGILNSYLIEITANI   237
Po    GNYVKMVHNGIEYGDMQLISESYFIMKHILKYDNKKLSQVFKKWNEGILNSYLIEITANI   240
      ******:**************** :**:**:*.*:* *:**:*************** :*

Pv    LGKKDELT--DNHLVDMILDIAGAKGTGKWTMLEAIERGIPCPTMCAALDARNISAYKQL   298
Pk    LGKKDDLT--DKHLVDMILDIAGAKGTGKWTMLEAIERGIPCPTMCAALDARNISAYKNL   298
Pm    LNKKDNLT--DNYLVDVILDIAGAKGTGKWTMLESIERGIPCPTICAALDSRNISAFKEL   298
Pf    LAKKDDLT--NNYLVDMILDIAGAKGTGKWTMLEATERGIPCPTMCAALDARNISVFKEL   295
Po    LGKTDELTGDNNYLVDMILDIAGAKGTGKWTMMEAIERGIPCPTICAALDARNISTFKQL   300
      * *.*:**  :::***:**********:*: ********:*****:****.:*:*
```

```
Pv    RVKADSHFSNDMKVNKVEGEN-------LINFEDDLLNALYCCKIISYTQGLFLLKQVSE   351
Pk    RIKADSHFCNEMKVRKVEGED-------LSHYEDDLLNALYCCKIISYTQGLFLLKQVSG   351
Pm    RTKADTYFSTVSKVNNLNGDNNLNSNDLMNNFENDLLNALYCCKIISYTQGLFLLRQVSH   358
Pf    RTKAESNFNKDNILI--------DPNEDLNDFENDLLNALYCCKIISYTQGLFLLKQVSE   347
Po    RTKADEHFVTTMKMN--------CTTEKLENLENDLLNALYCCKIISYTQGLFLLKQVSQ   352
      * **:  * .   :             : . *:**********************:***

Pv    EMKWNLNLGEISRIWRGGCIIRAVFLDRITNAYKKNEKLDLLFLDEDFAQEMKNKLPSLR   411
Pk    EMKWNLNLGEISRIWRGGCIIRAVFLDRITNAYKKNENLDLLFLDEDFAKEMKNKLPSLR   411
Pm    EMKWNLDLGEISRIWRGGCIIRAVFLDRITKAYKNNNSLELLFLDDEFAEEMKNKLPSLK   418
Pf    EMNWKLNLGEIARIWRGGCIIRAVFLDRIANAYKNNEKLELLFLDNEFSDDIKNKLPSLR   407
Po    EMKWNLNLGEISRIWRGGCIIRAVFLDRITNAYKNNEKLELLFMANEFSDEMKNKLPSLR   412
      **:*:*:****:******************::***:*:.*:***: ::*:.::*******:

Pv    KVVQVATKSSIPIPAFSASLAYFQMVTSQNLPLNLVQAQRDYFGSHTYKRVDRDGDFHTI   471
Pk    KVVEVATKSSIPIPAFSASLAYFQMVTSKNLPLNLVQAQRDYFGSHTYKRVDRDGDFHTI   471
Pm    KVVHISTMCSIPIPAISASLAYFQMITSKDLPLNLVQAQRDYFGSHTYKRIDREGDYHTV   478
Pf    KIVLMATKYSIPIPAFSASLAYFQMVTSQNLPLNLVQAQRDYFGSHTYRRTDREGNYHTL   467
Po    KIVNLATQCDIPIPAFSASLAYFQMVTSKNLPLNLVQAQRDYFGSHTYQRTDREGSFHTL   472
      *:* ::*  .*****:*********:**::******************:* **:*.:**:

Pv    WE       473
Pk    WE       473
Pm    WD       480
Pf    W-       468
Po    WD       474
      *
```

Appendix 2 Amino acid alignment of 6PGDs from different *Plasmodium* species

R36, W104, C281, as well as the flexible loop close to the active site (255-262) are conversed amongst the different human-pathogenic species (yellow). *Pv*: *Plasmodium vivax*; *Pk*: *Plasmodium knowlesi*; *Pm*: *Plasmodium malariae*; *Pf*: *Plasmodium falciparum*; *Po*: *Plasmodium ovale*. * Identical residues, : very similar residues, . similar residues.

```
                                                    899/900
PfG6PD  LKELQEK-QVKPLKYSFGSSGPKEVFGLVKKYY-NY--GKNYTHRPEFVRKSSFYEDDLL 907
PvG6PD  LNELQEK-KVQPLKYPFGSSGPKEVYDLVKKYY-NY--GKNYANTPAFVRKSSFYEDDLL 924
ScG6PD  LKHIERPDGPTPEIYPYGSRGPKGLKEYMQKHKYVMPEKHPYAWPVTKP----EDTKDN- 505
hG6PD   LHQIELE-KPKPIPYIYGSRGPTEADELMKRVGFQY--EGTYKWVNPHK----L------ 515
AtG6PD  LHRIDKG-EVKSIPYKPGSRGPKEADQLLEKAGYLQ--THGYIWIPPTL---------- 515
        *:.::         *  ** **.     :::          *
```

Appendix 3 Alignment of G6PDs from different species

The serines on positions 899 and 900 were found to be phosphorylated in *P. falciparum* and are specific for malaria parasites. *Pf*: *Plasmodium falciparum* (PlasmoDB PF3D7_1453800); *Pv*: *Plasmodium vivax*, (PlasmoDB PVX_117790); *Sc*: *Saccharomyces cerevisiae* (NCBI CAA93357); h: human (NCBI CAA39089.1); *At*: *Arabidopsis thaliana* (NCBI BAE99888). * Identical residues, : very similar residues, . similar residues.

Acknowledgements

An erster Stelle bedanke ich mich sehr herzlich bei **Prof. Dr. Katja Becker** für die Möglichkeit, in ihrer Arbeitsgruppe zu promovieren und für die Überlassung des spannenden Projektes. Ihre exzellente Betreuung und Unterstützung sowie ihr jederzeit offenes Ohr waren essentiell wichtige Bausteine bei der Anfertigung dieser Arbeit. Herzlichen Dank für das Ermöglichen meines Auslandsforschungsaufenthaltes sowie der Teilnahme an zahlreichen Konferenzen.

Frau **Prof. Dr. Gabriele Klug** möchte ich herzlich für die Übernahme der Zweitbetreuung und ihr Interesse an meiner Arbeit danken. Ebenso danke ich den weiteren Mitgliedern des Prüfungskomitees, Herrn **Prof. Dr. Christoph Grevelding** und Herrn **Prof. Dr. Jörg Fahrer**.

Dr. Karin Fritz-Wolf danke ich herzlich für die Weiterverarbeitung aller erhaltenen Kristalle, für die zahlreichen Anregungen und Tipps sowie für die gute Zusammenarbeit bei der Erstellung unseren Papers.

Ein großes Dankeschön übermittle ich **Dr. Julia Hahn** und **Norma Schulz** für ihre tatkräftige Unterstützung im Labor, insbesondere bei den Experimenten zu den posttranslationalen Modifikationen. **Michaela Stumpf** danke ich für ihre stetige und geduldige Unterstützung, für das Lösen sämtlicher technischer Probleme und für ihr Mitfiebern bei zahlreichen Kristallisationsversuchen. Bei **Marina Fischer** bedanke ich mich für die Hilfe bei kinetischen Fragen und für die Unterstützung verschiedener Messungen. **Dr. Stefan Rahlfs** danke ich für die Beantwortung aller molekularbiologischer Fragen und für die Hilfe bei Klonierungen und Mutagenesen. Ein Dankeschön geht auch an **Stine Weder** für ihre Unterstützung, vor allem im molekularbiologischen Bereich, und für ihre Freundschaft. Meinen Masterstudenten **Isabell Berneburg** und **Max Reichmann** danke ich herzlich für ihr großes Engagement und den wichtigen Beitrag ihrer wissenschaftlichen Ergebnisse zu verschiedensten Projekten. **Siegrid Franke** danke ich für die Charakterisierung der Inhibitoren in Zellkultur. Des Weiteren danke ich **Timothy Bostick** für das schnelle und genaue Korrekturlesen von Papern und dieser Arbeit.

Dr. Christina Brandstädter danke ich sehr herzlich für die Hilfe beim Erstellen der Abbildungen und für das Korrekturlesen dieser Arbeit. Neben Julia und Christina danke ich **Susanne Schipper** für die Unterstützung in allen Lebenslagen, für die kompetente Beantwortung meiner zahlreichen Fragen und für die schöne Zeit, die wir miteinander verbringen konnten. Ein großes Dankeschön geht auch an alle weiteren Mitglieder der **Arbeitsgruppe Becker** für das entspannte Arbeitsklima, das freundliche Miteinander und die immer sehr kollegiale und offene Zusammenarbeit.

I would like to thank **Prof. Dr. Lars Bode** from the University of California San Diego and **Dr. Anthony Pinkerton** from the Sanford Burnham Prebys Medical Discovery Institute for giving me the opportunity to work in their groups. I am thankful to **Dr. Shilpi Khare, Socorro Rodiles**, and **Fusayo Yamamoto** for their patient help, their advice, and the support in the laboratory. I wish to thank **Dr. Michael Hedrick** for sharing his knowledge about the most beautiful places in the USA with me.

Ein ganz besonders liebes Dankeschön geht an meine Familie und Freunde für den Rückhalt und die schönen Ablenkungen. Zuletzt danke ich Marco aus tiefstem Herzen für all die Unterstützung und das große Verständnis während der vergangenen Jahre.

Declaration

I declare that I have completed this dissertation single-handedly without the unauthorized help of a second party and only with the assistance acknowledged therein. I have appropriately acknowledged and cited all text passages that are derived verbatim from or are based on the content of published work of others, and all information relating to verbal communications. I consent to the use of an anti-plagiarism software to check my thesis. I have abided by the principles of good scientific conduct laid down in the charter of the Justus Liebig University Giessen „Satzung der Justus-Liebig-Universität Gießen zur Sicherung guter wissenschaftlicher Praxis“ in carrying out the investigations described in the dissertation

Eidesstattliche Erklärung

Ich erkläre: Ich habe die vorgelegte Dissertation selbständig und ohne unerlaubte fremde Hilfe und nur mit den Hilfen angefertigt, die ich in der Dissertation angegeben habe. Alle Textstellen, die wörtlich oder sinngemäß aus veröffentlichten Schriften entnommen sind, und alle Angaben, die auf mündlichen Auskünften beruhen, sind als solche kenntlich gemacht. Bei den von mir durchgeführten und in der Dissertation erwähnten Untersuchungen habe ich die Grundsätze guter wissenschaftlicher Praxis, wie sie in der „Satzung der Justus-Liebig-Universität Gießen zur Sicherung guter wissenschaftlicher Praxis“ niedergelegt sind, eingehalten.

Gießen, Oktober 2018

_____

Kristina Häußler